TECHNISCHE UNIVERSITÄT MÜNCHEN

Fakultät für Mathematik

Lehrstuhl für Numerische Methoden in der Plasmaphysik

Geometric Particle-in-Cell Methods on Mapped Grids

Benedikt Perse

Vollständiger Abdruck der von der Fakultät für Mathematik der Technischen Universität München zur Erlangung des akademischen Grades eines

Doktors der Naturwissenschaften (Dr. rer. nat.)

genehmigten Dissertation.

Vorsitzender: Prof. Dr. Oliver Junge

Prüfer der Dissertation:

1. Prof. Dr. Eric Sonnendrücker
2. Prof. Dr. Claus-Dieter Munz
3. Prof. Dr. Hong Qin

Die Dissertation wurde am 26.05.2021 bei der Technischen Universität München eingereicht und durch die Fakultät für Mathematik am 05.10.2021 angenommen.

Contents

1 Introduction 9
1.1 Goal 9
1.2 Methods and Challenges in the GEMPIC Framework 9
1.3 Outline 10
1.4 Related Work 11
1.4.1 Structure-preserving Framework 11
1.4.2 Curvilinear PIC Codes 13

I Curvilinear Vlasov–Maxwell System 15

2 The Vlasov–Maxwell System and Curvilinear Coordinates 16
2.1 Conservation Properties 17
2.2 Differential Forms and the Structure of Maxwell's Equations 18
2.3 Curvilinear Coordinates 19
2.3.1 Notation 19
2.3.2 Covariant and Contravariant Basis 20
2.3.3 Transformation of Differential Forms 23
2.4 Curvilinear Vlasov and Maxwell's Equations 25

3 Structure-preserving Discretisation in Curvilinear Geometry 27
3.1 Discrete Particle Distribution Function 27
3.2 Finite Element Discretisation 28
3.2.1 Discrete de Rham Sequence 28
3.2.2 Discretisation of the Curvilinear Maxwell Equations 30

4 Semi-discrete Hamiltonian Structure 33
4.1 Equations of Motion and Poisson Matrix 33
4.2 Discrete Poisson Bracket 35
4.3 Discrete Casimir Invariants 39

5 Lagrangian Formulation of the Vlasov–Maxwell System in Curvilinear Coordinates 41
5.1 Equations of Motion 41
5.2 Poisson Matrix 45
5.3 Logical Particle Velocity 47

6 Time Discretisation of the Equations of Motion 53
6.1 Charge Conserving Splittings 53
6.1.1 GEMPIC Hamiltonian Splitting 53
6.1.2 Alternative Splitting 58
6.2 Energy Conserving Antisymmetric Splitting 59
6.3 Energy and Charge Conserving Antisymmetric Splitting 62

7 Particle and Field Initialisation 65
7.1 Particle Sampling 65
7.2 Poisson's Equation 66

8 Numerical Experiments 68
8.1 Coordinate Transformation 68
8.2 Strong Landau Damping 69
8.3 Weibel Instability 70
8.4 Jean's Instability 73
8.4.1 Introduction Stellar Dynamics 73
8.4.2 Single Species 74
8.4.3 Two Species 75

II Boundary Conditions 78

9 Field Boundary Conditions 79
9.1 Weak Formulation of Maxwell's Equations 79
9.2 Poynting Flux 80
9.3 Spline Boundary Conditions 81
9.4 Boundary Matrices 85
9.5 Perfect Conductor Boundary Conditions 86

10 Particle Boundary Conditions 90
10.1 Introduction 90
10.2 Conservation Properties 90
10.2.1 Charge Monitoring 90
10.2.2 Energy Monitoring 91

11 Challenges with Singular Coordinate Transformations 92

12 Preconditioner 94

13 Numerical Experiments 97
13.1 Coordinate Transformation 97
13.2 Test case 98
13.2.1 Comparison to Periodic Boundary Conditions 99
13.2.2 Domain Deformation 101
13.2.3 Radial Grids 103
13.2.4 Conservation Properties 105

III Quasi-neutral Model 106

14 Introduction 107

15 Time Discretisation 109
15.1 Hamiltonian Splitting 109
15.2 Discrete Gradient Method 110
15.3 Linearised δf Method 111

16 Numerical Experiments 113
16.1 Ion Acoustic Wave 113
16.2 Ion Temperature Gradient Instability 115

IV Physical Units and Dispersion Relation 122

17 Normalisation 123
17.1 Vlasov–Maxwell Equations in SI Units 123
17.2 Physical Parameters of a Plasma 123
17.3 Dimensionless Parameters 124
17.3.1 Vlasov-Maxwell System 126
17.3.2 Quasi-neutral Vlasov System 128

18 Dispersion Relation 130
18.1 Linearised Vlasov Equation 130
18.2 Transformed Field Equations 132
18.3 1D Dispersion Relation 135
18.3.1 Electrostatic Dispersion 135
18.3.2 Electromagnetic Dispersion 138
18.4 2D Dispersion Relation 141
18.4.1 Electrostatic Dispersion 144
18.4.2 Electromagnetic Dispersion 148

19 Summary and Outlook 154

A Appendix 156

List of Figures

Figure 1 Convergence rates for Sobol and random numbers. 66

Figure 2 Orthogonal and distorted grid for distortion parameter $\varepsilon = 0.1$. 68

Figure 3 Landau damping on distorted grid: First component of the electric field energy for various integrators with time step $\Delta t = 0.05$ and distortion parameter $\varepsilon = 0.1$ for the coordinate transformation. 69

Figure 4 Weibel instability: Magnetic field energy for various integrators with time step $\Delta t = 0.05$ and distortion parameter $\varepsilon = 0.1$ for the coordinate transformation. 71

Figure 5 Weibel instability on distorted grid: Third component of the magnetic field energy and energy error for HS with time step $\Delta t = 0.01$ and different values of the distortion parameter ε for the coordinate transformation. 72

Figure 6 Jeans instability: First component of the gravitational energy for various integrators with time step $\Delta t = 0.05$ with analytical growth rates. 74

Figure 7 Two species weak Jeans instability: First component of the gravitational energy for HS with time step $\Delta t = 0.05$ for different values of δ together with the analytical growth rates. 76

Figure 8 Two species weak Jeans instability with $\delta = 0.75$ at time $T = 0, 5$. 77

Figure 9 Two species weak Jeans instability with $\delta = 0.75$ at time $T = 10, 15$. 77

Figure 10 Two species weak Jeans instability with $\delta = 0.75$ at time $T = 20, 25$. 77

Figure 11 Two species weak Jeans instability with $\delta = 0.75$ at time $T = 30, 35$. 77

Figure 12 Analytical eigenvalues of the 1D preconditioned mass matrix for different spline degrees. 95

Figure 13 Distorted grids on different domains for distortion parameter $\varepsilon = 0.05$. 97

Figure 14 Cylindrical grid with $r_0 = 0.5$ and elliptical grid with $r_0 = 0.05$. 98

Figure 15 Weibel instability with $\mathbf{k} = 1.25\hat{\mathbf{e}}_x$: Magnetic field energy for HS with time step $\Delta t = 0.1$ on a Cartesian grid with different boundary conditions. 99

Figure 16 Weibel instability with $\mathbf{k} = 1.25\hat{\mathbf{e}}_y$: Magnetic field energy for HS with time step $\Delta t = 0.1$ on a Cartesian grid with different boundary conditions. 100

Figure 17 Weibel instability with $\mathbf{k} = 1.25\hat{\mathbf{e}}_z$: Magnetic field energy for HS with time step $\Delta t = 0.1$ on a Cartesian grid with different boundary conditions. 100

Figure 18 Weibel instability with $\mathbf{k} = 1.25\hat{\mathbf{e}}_z$ and initialisation of B_2: Different components of the magnetic field energy for HS with time step $\Delta t = 0.1$ on a Cartesian grid with different boundary conditions. 100

Figure 19 Weibel instability with $\mathbf{k} = 1.25\hat{\mathbf{e}}_x$: Magnetic field energy for CEF with time step $\Delta t = 0.1$ on a distorted grid with distortion parameters $\varepsilon = 0, 0.05$ for the coordinate transformation. 101

Figure 20 Weibel instability with $\mathbf{k} = 1.25\hat{\mathbf{e}}_y$: Magnetic field energy for CEF with time step $\Delta t = 0.1$ on a distorted grid with distortion parameters $\varepsilon = 0, 0.05$ for the coordinate transformation. 102

Figure 21 Weibel instability with $\mathbf{k} = 1.25\hat{\mathbf{e}}_z$: Magnetic field energy for CEF with time step $\Delta t = 0.1$ on a distorted grid with distortion parameters $\varepsilon = 0, 0.05$ for the coordinate transformation. 102

Figure 22 Weibel instability with $\mathbf{k} = 1.25\hat{\mathbf{e}}_z$: Magnetic field energy for CEF with time step $\Delta t = 0.1$ on a distorted grid with different values of the distortion parameter ε for the coordinate transformation. 103

Figure 23 Weibel instability with $\mathbf{k} = 1.25\hat{\mathbf{e}}_z$: First component of the magnetic field energy for various integrators with time steps $\Delta t = 0.01, 0.1$ on cylindrical and elliptical grids with $r_0 = 0.01$. 104

Figure 24 Weibel instability with $\mathbf{k} = 1.25\hat{\mathbf{e}}_z$: First component of the magnetic field energy for DisGradE with time step $\Delta t = 0.1$ for various domain deforming mappings. 104

Figure 25 Ion acoustic wave: Scalar potential energy for various integrators with time step $\Delta t = 0.1$ and analytical damping rate. 114

Figure 26 Ion acoustic wave: Energy error for the semi-explicit time integrators with various time steps. 114

Figure 27 Ion acoustic wave: Energy and Gauss' law error for the implicit time integrators with various time steps. 115

Figure 28 Temperature profile and gradient for various values of κ_{T_i} and ω_{Ti} 116

Figure 29 Ion temperature gradient instability in slab geometry: Scalar potential energy for CEF with time step $\Delta t = 0.125$ for various values of κ_{T_i} with approximated temperature profiles and gradients and analytical growth rates. 117

Figure 30 Ion temperature gradient instability in slab geometry: Scalar potential energy for CEF with time step $\Delta t = 0.125$ for various values of κ_{T_i} and ω_{Ti} with varying temperature profiles and gradients and analytical growth rates. 118
Figure 31 Density profile and gradient for the ITG simulation in cylindrical geometry. 120
Figure 32 Temperature profile and gradient for the ITG simulation in cylindrical geometry.120
Figure 33 Ion temperature gradient instability in cylindrical geometry: Scalar potential energy for the semi-explicit time integrators with time step $\Delta t = 0.1$ with approximated density and temperature profiles and gradients.....120

List of Tables

Table 1 Landau damping: Maximum error in Gauss' law and in the total energy until time 500 for the semi-explicit and implicit time integrators with time step $\Delta t = 0.05$ and distortion parameter $\varepsilon = 0.1$ for the coordinate transformation. 70

Table 2 Weibel instability: Maximum error in Gauss' law and in the total energy until time 500 for the semi-explicit and implicit time integrators with time step $\Delta t = 0.05$ and distortion parameter $\varepsilon = 0.05$ for the coordinate transformation. 72

Table 3 Jeans instability: Maximum error in Gauss' law and in the total energy until time 100 for the semi-explicit and implicit time integrators with time step $\Delta t = 0.05$.... 75

Table 4 Weak Jeans instability: Analytical and simulated growth rates for different values of δ. 76

Table 5 Number of iterations for the CG and PCG solver of the mass matrices for spline degree p. 96

Table 6 Weibel instability with perfect conductor boundary conditions: Maximum error in Gauss' law and in the total energy until time 500 for the semi-explicit and implicit time integrators on various grids. 105

Table 7 Ion acoustic wave: Maximum error in Gauss' law and in the total energy until time 1000 for the semi-explicit and implicit time integrators with time step $\Delta t = 0.1$.....113

Table 8 Ion temperature gradient instability in slab geometry: Analytical and simulated growth rates for the approximated and varying temperature profiles and gradients for different values of κ_{Ti}. 117

Table 9 Parameters for different fusion devices.....125

Abstract

The geometric electromagnetic particle-in-cell (GEMPIC) framework provides the foundation for Vlasov–Maxwell solvers that preserve at the discrete level the non-canonical Hamiltonian structure. Preserving the structure of the kinetic equations enables stable numerical methods for long time simulations. In this dissertation, the GEMPIC framework is extended to curvilinear coordinates and perfect conductor boundary conditions. Several semi-implicit time integrators based either on a Hamiltonian splitting or on an antisymmetric splitting of the Poisson matrix are discussed and assessed regarding their conservation properties and computational efficiency.

Zusammenfassung

Das geometrisch elektromagnetische particle-in-cell (GEMPIC) Rahmenkonzept legt die Grundlage für Vlasov–Maxwell Löser, die die nicht kanonische hamiltonische Struktur auf der diskreten Ebene erhalten. Die Erhaltung der Struktur der kinetischen Gleichungen ermöglicht stabile numerische Verfahren für Langzeitsimulationen. In dieser Dissertation wird das GEMPIC Rahmenkonzept um krummlinige Koordinaten und perfekte Leiter Randbedingungen erweitert. Verschiedene semi-implizite Zeitintegratoren, die entweder auf einer Aufteilung des Hamiltonianoperators oder auf einer antisymmetrischen Aufteilung der Poisson Matrix basieren, werden behandelt und bezüglich ihrer Erhaltungseigenschaften und rechnerischen Effizienz eingeschätzt.

1 Introduction

1.1 Goal

Plasma simulation with numerical schemes that preserve the structure of the kinetic equations can provide new insights into the long time behaviour of fusion plasmas. However, there are multiple challenges on the route towards real tokamak simulations such as the handling of the geometry, the boundary conditions or the different time scales. During my doctoral project, I have developed and implemented in the SeLaLib [1] an extension of the geometric electromagnetic particle-in-cell (GEMPIC) framework [56] to curvilinear coordinates and perfect conductor boundary conditions.

1.2 Methods and Challenges in the GEMPIC Framework

The Vlasov-Maxwell (VM) system is a set of partial differential equations, which describe the dynamic behaviour of a collisionless plasma and the coupled self-consistent electromagnetic fields. The Vlasov equation governs the evolution of the plasma particle distribution function whereas Maxwell's equations describe the propagation of the electromagnetic fields with source terms given by the moments of the particle distribution function, namely the charge and the current densities.

The particle-in-cell (PIC) method [51, 8, 23] is a common technique to solve these differential equations. The solution is computed following the trajectories of macro-particles representing the plasma particles. In [40], various PIC methods and their conservation properties are described.

In GEMPIC, the electromagnetic fields are discretised in space with the finite element exterior calculus (FEEC) framework developed by Arnold, Winther & Falk [3]. An important feature of this general approach for the finite element discretisation of partial differential equations is the compatibility with structure-preserving numerical methods. The basis functions for the finite element spaces are constructed from B-splines, since they form a de Rham complex as demonstrated in [12]. This formulation yields a semi-discrete Poisson system that satisfies the Jacobi identity. A review of geometric integration methods for Hamiltonian systems exploiting the Lagrangian and Poisson structure is given in [42].

For the discretisation in time, Poisson integrators as well as energy conserving time-stepping schemes are considered. The former results in two semi-explicit Hamiltonian splittings based on [45] and [21] whereas the latter is based on the discrete gradient method [36, 68] and requires an antisymmetric splitting of the Poisson matrix. The discretisation with the discrete gradient method leads to implicit systems, which have to be solved iteratively. Therefore, the implicit methods are computationally more expensive than the semi-explicit schemes. However, they are more suitable to the multi-scale nature of simulations with magnetohydrodynamic time scales because they do not suffer from the stability constraints that restrict the

semi-explicit schemes to small time steps.

General curvilinear coordinates are introduced into the VM system using the basic notations for the representation of scalar and vector functions in curvilinear coordinates in [79] and [27]. When radial mappings are introduced, real boundary conditions for the fields and particles are required, since periodic boundary conditions are not feasible for the radial direction. For the fields, perfect conductor boundary conditions as described in [41] can be used to model a lossless metallic surface. Compatible particle boundary conditions include reflection and absorption.

The multi-scale dynamics of a plasma occur due to the different magnitudes of the characteristic lengths of the two particle species, the electrons and the ions. The difference in the gyroradii, for example, depends on the square root of the mass ratio between ions and electrons. Therefore, many simulations in realistic fusion devices lay focus on the ion motion considering a quasi-neutral background with adiabatic electrons because this makes it possible to disregard the small time scales of the electrons. However, even in this simplified case, noise reduction techniques have to be applied as proposed in [80, 84] to obtain meaningful results with a reasonable number of particles.

1.3 Outline

The thesis is structured in the following way:

In the first part, a general coordinate transformation is introduced to the VM system. In Chapter 2, the VM system and its Poisson structure and conservation properties are reviewed. Furthermore, the notation for curvilinear coordinate transformations is introduced and applied to the electromagnetic fields. Chapter 3 approaches the structure-preserving semi-discretisation based on the PIC method for the particle distribution function and FEEC for the fields. Here, the discrete de Rham sequence in logical coordinates induces a de Rham sequence on the physical domain. The semi-discrete Hamiltonian structure is presented in Chapter 4, where the equations of motion are derived from the discrete Poisson matrix. Chapter 5 is devoted to the Lagrangian formulation of the VM system in order to examine different representations of the particle trajectories based on the potentials. In Chapter 6, we discretise the equations of motion in time and discuss the advantages and disadvantages of the different discretisation schemes. Chapter 7 comments briefly on our sampling strategy and the initialisation of the electric field. In Chapter 8, the new code is verified in numerical experiments with periodic boundary conditions showing the conservation properties of the respective time discretisation methods.

Part II treats the boundary conditions of the VM system. In Chapter 9, we focus on the field boundary conditions. First, we examine the natural boundary conditions of the variational formulation of Maxwell's equation. Second, the boundary parts are represented in the B-spline

basis and third, we apply the perfect conductor boundary conditions. Chapter 10 comments on the handling of the particle boundary conditions. In Chapter 11, challenges occurring from singular mappings are gathered. Chapter 12 discusses preconditioners for the conjugate gradient solvers of the boundary mass matrices. The implementation of the boundary conditions is verified in a numerical test case with various coordinate transformations in Chapter 13.

Part III presents the quasi-neutral model. In Chapter 14, the quasi-neutral equations with adiabatic electrons are introduced into the GEMPIC framework. Chapter 15 contains the time discretisation of the quasi-neutrality equations, which works analogously to Chapter 6, and reviews the linearised δf method. Concluding, Chapter 16 shows the application of the quasi-neutral model in two numerical test cases, the ion acoustic wave and the ion temperature gradient instabilities.

In Part IV, background information on the physical units and the computation of the dispersion relation is given. The normalisation of the VM system from physical units to dimensionless quantities is presented in Chapter 17. Chapter 18 reviews the linearisation of the VM system in order to compute the dispersion relation of the plasma waves simulated in the numerical experiments.

Chapter 19 concludes the thesis with a short summary of the contributions for the GEMPIC framework and an outlook to related open problems. In the appendix, useful definitions, formulas and integrals are provided.

1.4 Related Work

1.4.1 Structure-preserving Framework

In recent years, various structure-preserving particle-in-cell (PIC) discretisations of the Vlasov–Maxwell (VM) system have been developed as reviewed in [71] and [96]. The preservation of the symmetry in the variational and Hamiltonian structure of the VM system is related to the conservation of physical quantities such as charge, energy or momentum. This leads to algorithms that feature long term accuracy and stability.

Early attempts of structure-preserving PIC codes for the VM system were made by Lewis [61, 62], where a general framework for the semi-discretisation of Low's Lagrangian [64] based on finite differences is given. Similarly, Shadwick, Stamm & Evstatiev described an energy conserving variational semi-discretisation based on finite elements in [31, 77, 82]. For the time discretisation an explicit symplectic integrator is used.

A fully-discrete structure-preserving PIC algorithm for the VM equations was proposed by Squire, Qin & Tang [81] in 2012. Their variational formulation is based on a fully discrete action principle applied to Low's Lagrangian [64], where the electromagnetic fields are discretised using the discrete exterior calculus [26].

In 2015, Crouseilles, Einkemmer & Faou [21] introduced a Hamiltonian splitting (HS) for the continuous Poisson bracket introduced by Morrison in [69]. However, this bracket does not satisfy the Jacobi identity so that the splitting is not Poisson structure conserving. A correction was given by He, Qin, Sun, Xiao, Zhang & Liu [45], who discovered an alternative HS for the corrected Poisson bracket described in [94, 65, 70]. Their HS leads to an explicit time discretisation that preserves the Poisson structure. Using this time discretisation, Xiao, Qin, Liu, He, Zhang & Liu [97] presented a discretisation of the non-canonical Poisson bracket for the VM system. The variational formulation uses Whitney form interpolants [95], which preserve the de Rham complex. Subsequently, He, Sun, Qin & Liu [46] published a structure-preserving PIC method, where the non-canonical VM bracket is discretised based on first order finite elements. In the following, Xiao, Qin, Liu & Zhang showed a local energy conservation law in [98] and derived a fully discrete action principle in [96].

At the same time, Kraus, Kormann, Morrision & Sonnendrücker [56] introduced the systematic mathematical framework GEMPIC, the geometric electromagnetic particle-in-cell method. The framework is based on two main building blocks, the semi-discretisation of the Poisson bracket with finite element exterior calculus (FEEC) [3] and the time discretisation via the HS introduced in [45]. The following work extends or elaborates on parts of this framework:

In 2021, Kormann & Sonnendrücker [55] presented two energy conserving time discretisations based on the discrete gradient method. [72] compared one of these time discretisations in a 1D2V setting to a similar time discretisation proposed by Lapenta [59]. The mathematical framework of GEMPIC coming from the Lagrangian formalism was investigated in [14]. In this paper, Campos Pinto, Kormann & Sonnendrücker consider general basis functions for the finite element spaces in the de Rham complex and investigate the duality of the variational formulation of Maxwell's equations resulting in the choice between a weak or strong formulation of Ampère's, respectively Faraday's equation. The application of this variational framework to spectral methods was described in [13]. The spectral methods feature various conservation properties such as energy, charge or momentum conservation extending the particle-in-Fourier (PIF) ansatz developed by Ameres [2] to the GEMPIC framework.

There exist several possibilities to include collisions into the GEMPIC framework. In the case of energy-preserving time integrators, it is natural to use metriplectic integrators because they share the same time discretisation strategy. Specifically, Kraus, Hirvijoki & Burby [50] examined the extension of the GEMPIC framework with a non-linear Landau collision operator. The metriplectic formulation of the collision operator is employed for a semi-discretisation that conserves density, momentum and energy. Using the discrete gradient method for the time discretisation guarantees energy conservation and a discrete H-theorem, i.e. a monotonic dissipation of entropy and an unique equilibrium state.

In the case of a HS on the other hand, the microscopic description of collisions via stochastic processes is better suited, since metriplectic integrators do not preserve the Hamiltonian

structure. In [88], the variational formulation of the collisional VM system was investigated on the continuous level as a coupling of a partial and a stochastic differential equation. Then, the general formulation of stochastic variational integrators developed in [57] can be used to discretise this formulation in order to include collisional effects in the GEMPIC framework when using Hamiltonian or variational time discretisations.

Associated to the work on this framework, the following publications have been recently released: In 2019, Hirvijoki [48] proposed a drift kinetic PIC code for the VM system, which is based on a discrete action principle and conserves charge. The work on the Landau collision operator in the metriplectic formulation was continued in [49]. However, the new formulation is no longer compatible with the conservation of the Poisson structure in the GEMPIC framework. Holderied, Possaner & Wang [52] presented a hybrid MHD-kinetic code based on the finite element exterior calculus providing an exact de Rham complex. However, the system does not possess a discrete Poisson structure.

1.4.2 Curvilinear PIC Codes

So far, the geometric methods for the VM system have been limited to Cartesian geometry. Yet, on the route to simulations in a fusion device, e.g. a tokamak or a stellarator, a realistic geometry can only be described accurately with a multipatch of coordinate transformations. Therefore, we review the state of the art of PIC codes with curvilinear coordinate transformations.

In 1995, Eastwood, Arter, Brealey & Hockney [30] presented the first electromagnetic PIC code on a non-orthogonal grid based on a body-fitted finite element discretisation that conserves the charge. The equations of motion are derived from an action principle and the particles are pushed in logical coordinates. Proceeding from this work, Wang, Kondrashov, Liewer & Karmesin [90] introduced an electromagnetic PIC code called EMPIC. The code features a finite volume discretisation and a hybrid particle pusher, which means that the velocity is kept in physical coordinates. Simulations are performed on a sinusoidally distorted grid and the energy error is bounded.

Fichtl, Finn & Cartwright [32] proposed an electrostatic 2D2V code in 2012. The fields are discretised with the finite difference method and the particle position and velocity are both pushed in logical coordinates. The code is momentum conserving and applies homogeneous Neumann boundary conditions for the fields. Likewise, Delzanno et al. [25] described an electrostatic 3D PIC code called CPIC with finite difference discretisation. The code uses a hybrid particle pusher and allows for mesh refinement. Absorbing and reflecting particle boundaries are tested on a sinusoidally distorted grid and on an annulus. For the fields Neumann or Dirichlet boundary conditions can be applied.

In 2016, Chen & Chacón [16] published an electromagnetic 2D3V PIC code in curvilinear

coordinates for the Vlasov–Darwin model. The fields are discretised with the finite difference method and the time discretisation is fully implicit featuring charge and energy conservation. While the particle position is pushed in logical coordinates, the velocity is kept in physical coordinates leading to a hybrid particle pusher. A fluid preconditioner is used for acceleration of the field solver and multispecies test cases are simulated on a sinusoidally distorted grid. Complementary, the code was extended to perfect conductor boundary conditions and a reflecting particle boundary in [17].

In 2019, Gonzalez-Herrero, Micera, Boella, Park & Lapenta [37] proposed a semi-implicit PIC code in axially symmetric cylindrical coordinates, which uses a finite volume discretisation. The code is based on the ECSIM code by Lapenta [59] and features energy conservation.

In [73], the GEMPIC framework was extended to general curvilinear coordinate transformations.

More recently, Xiao & Qin [54] extended their geometric PIC code [96] to orthogonal curvilinear coordinate transformations maintaining the explicit time discretisation via a Hamiltonian splitting. The explicit time splitting is obtained by the use of a logical velocity variable but this is only possible for the special case of an orthogonal transformation. They apply perfect electric conductor boundary conditions in two directions and periodicity in the third direction. Particles hitting the boundary are removed from the simulation. A different approach was taken by Wang, Qin, Sturdevant & Chang [91] using the structure-preserving framework to build an electrostatic 2D PIC code on unstructured grids with fully kinetic ions and adiabatic electrons. A de Rham complex is constructed with Whitney forms assuming homogeneous Dirichlet boundary conditions for the fields and a reflecting boundary for the particles. This setup allows for simulations of ion Bernstein waves in a 2D magnetized plasma.

Curvilinear coordinate transformations are also used with a variety of other methods such as semi-Lagrangian [43], gyrokinetic [99] or MHD codes [52]. In 2011, Colella, Dorr, Hittinger & Martin [19] used a finite volume discretisation of the Vlasov–Poisson system with Dirichlet boundary conditions to perform simulations in a D-shaped annular geometry. In [66], this code was extended to mapped multi block grids and tested on a sinusoidally distorted mesh with advection problems. Vogman et al. [89] introduced a continuum code with finite volume discretisation for an electrostatic axisymmetric cylindrical Vlasov–Poisson system using specular reflection as particle boundary conditions and Dirichlet boundary conditions for the fields.

Part I

Curvilinear Vlasov–Maxwell System

2 The Vlasov–Maxwell System and Curvilinear Coordinates

The Vlasov equation in physical phase-space coordinates $(\mathbf{x}, \mathbf{v})$ for a species s with charge q_s and mass m_s reads

$$\frac{\partial f_s(\mathbf{x}, \mathbf{v}, t)}{\partial t} + \mathbf{v} \cdot \nabla_{\mathbf{x}} f_s(\mathbf{x}, \mathbf{v}, t) + \frac{q_s}{m_s}(\mathbf{E}(\mathbf{x}, t) + \mathbf{v} \times \mathbf{B}(\mathbf{x}, t)) \cdot \nabla_{\mathbf{v}} f_s(\mathbf{x}, \mathbf{v}, t) = 0, \quad (2.1)$$

where $\mathbf{E}$ and $\mathbf{B}$ denote the electromagnetic fields, which are evolved according to Maxwell's equations,

$$\frac{\partial \mathbf{E}(\mathbf{x}, t)}{\partial t} = \nabla_{\mathbf{x}} \times \mathbf{B}(\mathbf{x}, t) - \mathbf{J}(\mathbf{x}, t), \quad (2.2a)$$

$$\frac{\partial \mathbf{B}(\mathbf{x}, t)}{\partial t} = -\nabla_{\mathbf{x}} \times \mathbf{E}(\mathbf{x}, t), \quad (2.2b)$$

$$\nabla_{\mathbf{x}} \cdot \mathbf{E}(\mathbf{x}, t) = \rho(\mathbf{x}, t),$$

$$\nabla_{\mathbf{x}} \cdot \mathbf{B}(\mathbf{x}, t) = 0.$$

The system couples through the first two moments of the particle distribution function f_s, the charge and the current densities,

$$\rho(\mathbf{x}, t) = \sum_s q_s \int f_s(\mathbf{x}, \mathbf{v}, t)\, \mathrm{d}\mathbf{v}, \ \mathbf{J}(\mathbf{x}, t) = \sum_s q_s \int f_s(\mathbf{x}, \mathbf{v}, t)\mathbf{v}\, \mathrm{d}\mathbf{v}.$$

The equations (2.1), (2.2a), (2.2b) can be obtained by a bilinear, antisymmetric Poisson bracket that satisfies Leibniz' rule and the Jacobi identity. The following Poisson bracket was introduced in [69] and corrected in [94, 65, 70]:

$$\begin{aligned}\{\mathcal{F}, \mathcal{G}\}[f_s, \mathbf{E}, \mathbf{B}] = &\sum_s \int \left[\frac{\delta \mathcal{F}}{\delta f_s}, \frac{\delta \mathcal{G}}{\delta f_s}\right] \mathrm{d}\mathbf{x}\mathbf{v} \\ &+ \sum_s \frac{q_s}{m_s} \int f_s \left(\nabla_{\mathbf{v}} \frac{\delta \mathcal{F}}{\delta f_s} \cdot \frac{\delta \mathcal{G}}{\delta \mathbf{E}} - \nabla_{\mathbf{v}} \frac{\delta \mathcal{G}}{\delta f_s} \cdot \frac{\delta \mathcal{F}}{\delta \mathbf{E}}\right) \mathrm{d}\mathbf{x}\mathbf{v} \\ &+ \sum_s \frac{q_s}{m_s^2} \int f_s \mathbf{B} \cdot \left(\nabla_{\mathbf{v}} \frac{\delta \mathcal{F}}{\delta f_s} \times \nabla_{\mathbf{v}} \frac{\delta \mathcal{G}}{\delta f_s}\right) \mathrm{d}\mathbf{x}\mathbf{v} \\ &+ \int \left(\mathrm{curl}\, \frac{\delta \mathcal{F}}{\delta \mathbf{E}} \cdot \frac{\delta \mathcal{G}}{\delta \mathbf{B}} - \mathrm{curl}\, \frac{\delta \mathcal{G}}{\delta \mathbf{E}} \cdot \frac{\delta \mathcal{F}}{\delta \mathbf{B}}\right) \mathrm{d}\mathbf{x},\end{aligned}$$

where $[f, g] = \nabla_{\mathbf{x}} f \cdot \nabla_{\mathbf{v}} g - \nabla_{\mathbf{x}} g \cdot \nabla_{\mathbf{v}} f$.

The time evolution of a functional $\mathcal{F}[f_s, \mathbf{E}, \mathbf{B}]$ is expressed by

$$\frac{\mathrm{d}}{\mathrm{d}t} \mathcal{F}[f_s, \mathbf{E}, \mathbf{B}] = \{\mathcal{F}, \mathcal{H}\}, \quad (2.3)$$

where the Hamiltonian $\mathcal{H}$ equals the sum of the kinetic energy of the particles and the electric

and magnetic field energies,

$$\mathcal{H} = \sum_s \frac{m_s}{2} \int |\mathbf{v}|^2 f_s(\mathbf{x}, \mathbf{v}) \ \mathrm{d}\mathbf{x}\, \mathrm{d}\mathbf{v} + \frac{1}{2} \int |\mathbf{E}(\mathbf{x})|^2 + |\mathbf{B}(\mathbf{x})|^2 \, \mathrm{d}\mathbf{x}. \tag{2.4}$$

Equivalently, the equations of motion follow from the Lagrangian introduced by Low [64],

$$\begin{aligned} \mathcal{L}_f = &\sum_s \int f_s(\mathbf{x}, \mathbf{v})[q\mathbf{A}(t, \mathbf{x}) + m\mathbf{v}] \cdot \dot{\mathbf{x}} - \frac{1}{2} m v^2 - q\Phi(t, \mathbf{x})] \, \mathrm{d}\mathbf{x}\, \mathrm{d}\mathbf{v} \\ &+ \frac{1}{2} \int_\Omega \left| -\nabla\Phi(t, \mathbf{x}) - \frac{\partial \mathbf{A}(t, \mathbf{x})}{\partial t} \right|^2 \mathrm{d}\mathbf{x} - \frac{1}{2} \int_\Omega |\nabla \times \mathbf{A}(t, \mathbf{x})|^2 \ \mathrm{d}\mathbf{x}. \end{aligned} \tag{2.5}$$

The Lagrangian is formulated with the scalar potential Φ and the vector potential $\mathbf{A}$. Their relation to the electromagnetic fields is given by

$$\begin{aligned} \mathbf{E}(\mathbf{x}, t) &= -\nabla\Phi(\mathbf{x}, t) - \frac{\partial \mathbf{A}(\mathbf{x}, t)}{\partial t}, \\ \mathbf{B}(\mathbf{x}, t) &= \nabla \times \mathbf{A}(\mathbf{x}, t). \end{aligned}$$

2.1 Conservation Properties

Proposition 2.1. *The Vlasov–Maxwell system features some conservation properties, which are important for long term stability:*

- *Energy conservation*

$$\frac{\mathrm{d}}{\mathrm{d}t}\mathcal{H} = \frac{\mathrm{d}}{\mathrm{d}t} \left(\sum_s \frac{m_s}{2} \int |\mathbf{v}|^2 f_s(\mathbf{x}, \mathbf{v}) \ \mathrm{d}\mathbf{x}\, \mathrm{d}\mathbf{v} + \frac{1}{2} \int |\mathbf{E}(\mathbf{x})|^2 + |\mathbf{B}(\mathbf{x})|^2 \, \mathrm{d}\mathbf{x} \right) = 0,$$

- *Momentum conservation*

$$\frac{\mathrm{d}}{\mathrm{d}t}P = \frac{\mathrm{d}}{\mathrm{d}t} \left(\sum_s \int \int m_s \mathbf{v} f_s \, \mathrm{d}\mathbf{x}\, \mathrm{d}\mathbf{v} + \int_\Omega \mathbf{E} \times \mathbf{B} \, \mathrm{d}\mathbf{x} \right) = 0.$$

Proof. The proof can be found in [78, Sec. 3.4.2]. □

From the Poisson bracket we obtain only Ampère's (2.2a) and Faraday's laws (2.2b) but the conservation of the Gauss laws follows by taking the divergence of Ampère's and Faraday's

laws,

$$\nabla \cdot \frac{\partial \mathbf{E}}{\partial t} = \nabla \cdot \nabla_{\mathbf{x}} \times \mathbf{B} - \nabla \cdot \mathbf{J} \Rightarrow \frac{\mathrm{d}}{\mathrm{d}t}(\nabla \cdot \mathbf{E} - \rho) = 0,$$
$$\nabla \cdot \frac{\partial \mathbf{B}}{\partial t} = -\nabla \cdot \nabla_{\mathbf{x}} \times \mathbf{E} \Rightarrow \frac{\mathrm{d}}{\mathrm{d}t}(\nabla \cdot \mathbf{B}) = 0.$$

The momentum is conserved if Gauss' law is initially satisfied for both particle species and conserved over time, since

$$\frac{\mathrm{d}\mathcal{P}}{\mathrm{d}t} = \{\mathcal{P}, \mathcal{H}\} = \int \mathbf{E}(\rho - \operatorname{div} \mathbf{E})\, \mathrm{d}\mathbf{x}.$$

So, when the conservation of Gauss' law is lost, the conservation of the total momentum is violated, too.

2.2 Differential Forms and the Structure of Maxwell's Equations

Maxwell's equations for the electric and magnetic fields are given as

$$\frac{\partial \mathbf{E}(\mathbf{x},t)}{\partial t} = \nabla_{\mathbf{x}} \times \mathbf{B}(\mathbf{x},t) - \mathbf{J}(\mathbf{x},t), \qquad \frac{\partial \mathbf{B}(\mathbf{x},t)}{\partial t} = -\nabla_{\mathbf{x}} \times \mathbf{E}(\mathbf{x},t),$$
$$\nabla_{\mathbf{x}} \cdot \mathbf{E}(\mathbf{x},t) = \rho(\mathbf{x},t), \qquad \nabla_{\mathbf{x}} \cdot \mathbf{B}(\mathbf{x},t) = 0.$$

The structure of Maxwell's equations can be understood by interpreting the fields as differential forms following [9, 6, 47, 92]. The spaces of electromagnetics form a de Rham complex, which in terms of Sobolev spaces can be expressed as

$$H^1(\Omega) \xrightarrow{\mathrm{grad}} H(\mathrm{curl}, \Omega) \xrightarrow{\mathrm{curl}} H(\mathrm{div}, \Omega) \xrightarrow{\mathrm{div}} L^2(\Omega) \tag{2.6}$$

and is accompanied by the dual de Rham complex

$$L^{2\star}(\Omega) \xrightarrow{\mathrm{grad}} H^\star(\mathrm{div}, \Omega) \xrightarrow{\mathrm{curl}} H^\star(\mathrm{curl}, \Omega) \xrightarrow{\mathrm{div}} H^{1\star}(\Omega) \quad , \tag{2.7}$$

where the notation * is used to denote the dual of the corresponding spaces.

Definition 2.1. *The Sobolev spaces are defined as*

$$H^1(\Omega) := \{\omega \in L^2(\Omega) |\, \mathrm{d}\omega \in L^2(\Omega)^3\},$$
$$H(\mathrm{curl}, \Omega) := \{\boldsymbol{\omega} \in L^2(\Omega)^3 |\, \mathrm{curl}\, \boldsymbol{\omega} \in L^2(\Omega)^3\},$$
$$H(\mathrm{div}, \Omega) := \{\boldsymbol{\omega} \in L^2(\Omega)^3 |\, \mathrm{div}\, \boldsymbol{\omega} \in L^2(\Omega)\},$$
$$L^2(\Omega) := \{\omega \in \Omega | \langle \omega, \omega \rangle_{L^2} < \infty\}.$$

The complex must have the property that in each step the image of the operator is in the kernel of the next operator. This complex property is satisfied, since $\operatorname{curl}\operatorname{grad}\Phi = 0$ for all $\Phi \in H^1(\Omega)$ and $\operatorname{div}\operatorname{curl}\mathbf{A} = 0$ for all $\mathbf{A} \in H(\operatorname{curl}, \Omega)$.

For the interpretation of the field equations, there are two options: Either we choose $\mathbf{E} \in H(\operatorname{curl}, \Omega)$ and $\mathbf{B} \in H(\operatorname{div}, \Omega)$ and then, interpret the two equations of the first column, Ampère's law and the electric Gauss law, in the weak sense, and the two equations of the second column, Faraday's law and the magnetic Gauss law, in the strong sense, or vice versa. We use the first option and consider the following mixed form of Maxwell's equation with the test functions $\boldsymbol{\varphi} \in H(\operatorname{curl}, \Omega)$ and $\psi \in H^1(\Omega)$:

$$\int_\Omega \boldsymbol{\varphi}(\mathbf{x}) \cdot \frac{\partial \mathbf{E}(\mathbf{x}, t)}{\partial t} \,\mathrm{d}\mathbf{x} = \int_\Omega \nabla_{\mathbf{x}} \times \boldsymbol{\varphi}(\mathbf{x}) \cdot \mathbf{B}(\mathbf{x}, t) \,\mathrm{d}\mathbf{x} - \mathbf{J}^\star(\boldsymbol{\varphi})(t), \tag{2.8a}$$

$$\frac{\partial \mathbf{B}(\mathbf{x}, t)}{\partial t} = -\nabla_{\mathbf{x}} \times \mathbf{E}(\mathbf{x}, t), \tag{2.8b}$$

$$-\int_\Omega \nabla_{\mathbf{x}} \psi(\mathbf{x}) \cdot \mathbf{E}(\mathbf{x}, t) = \rho^\star(\psi)(t), \tag{2.8c}$$

$$\nabla_{\mathbf{x}} \cdot \mathbf{B}(\mathbf{x}, t) = 0, \tag{2.8d}$$

where $\mathbf{J}^\star \in H^\star(\operatorname{div}, \Omega)$ and $\rho^\star \in L^{2\star}(\Omega)$ are linear functionals defined as $\mathbf{J}^\star(\boldsymbol{\varphi})(t) = \langle \boldsymbol{\varphi}, \mathbf{J} \rangle_{L^2}, \rho^\star(\psi)(t) = \langle \psi, \rho \rangle_{L^2}$. Note that we have assumed that the boundary terms vanish in (2.8a) and (2.8c). Further investigations regarding the boundary conditions are given in Chapter 9.

2.3 Curvilinear Coordinates

2.3.1 Notation

Let us first introduce our notation for the curvilinear coordinates before discussing how these can be consistently combined with differential forms. We consider a bijective coordinate transformation from the logical space $\tilde{\Omega} := [0, 1]^3$ to the physical space Ω, e.g. a Torus in spherical coordinates. The transformation map is denoted by

$$F \colon \tilde{\Omega} \to \Omega \subset \mathbb{R}^3, \ \boldsymbol{\xi} \mapsto F(\boldsymbol{\xi}) = \mathbf{x},$$

where $\boldsymbol{\xi} = (\xi_1, \xi_2, \xi_3)^\top, \mathbf{x} = (x_1, x_2, x_3)^\top$ are the variables on the logical and physical mesh, respectively.

The matrix of the partial derivatives, the Jacobian matrix, and its determinant are defined as

$$(DF(\boldsymbol{\xi}))_{ij} = \frac{\partial F_i(\boldsymbol{\xi})}{\partial \xi_j} = \frac{\partial x_i}{\partial \xi_j},$$
$$J_F(\boldsymbol{\xi}) = \det(DF(\boldsymbol{\xi})).$$

We assume that the mapping is non-singular, i.e. $J_F(\boldsymbol{\xi}) \neq 0 \ \forall \boldsymbol{\xi} \in \tilde{\Omega}$, and therefore, the Jacobian matrix is invertible. The case of singular mappings is discussed in Chapter 11.

Definition 2.1. *The column vectors of the Jacobian matrix form the so-called covariant basis of the tangent space,*

$$\mathbf{t}_i = \frac{\partial F(\boldsymbol{\xi})}{\partial \xi_i} = \frac{\partial \mathbf{x}}{\partial \xi_i}, \ DF = (\mathbf{t}_1 | \mathbf{t}_2 | \mathbf{t}_3)$$

whereas the columns of the transposed inverse Jacobian matrix form the dual basis, which is called the contravariant basis of the cotangent space,

$$\mathbf{n}_i = \frac{\partial \xi_i}{\partial \mathbf{x}}, \ DF(\boldsymbol{\xi})^{-\top} =: N(\boldsymbol{\xi}) = (\mathbf{n}_1 | \mathbf{n}_2 | \mathbf{n}_3).$$

Proposition 2.2. *The following relations hold between the covariant and the contravariant basis vectors:*

$$\begin{aligned}
\mathbf{n}_1 &= \frac{1}{J_F} \mathbf{t}_2 \times \mathbf{t}_3, & \mathbf{n}_2 \times \mathbf{n}_3 &= \frac{1}{J_F} \mathbf{t}_1, \\
\mathbf{n}_2 &= \frac{1}{J_F} \mathbf{t}_3 \times \mathbf{t}_1, & \mathbf{n}_3 \times \mathbf{n}_1 &= \frac{1}{J_F} \mathbf{t}_2, \\
\mathbf{n}_3 &= \frac{1}{J_F} \mathbf{t}_1 \times \mathbf{t}_2, & \mathbf{n}_1 \times \mathbf{n}_2 &= \frac{1}{J_F} \mathbf{t}_3.
\end{aligned}$$

Proof. The proof can be found in [79]. □

Definition 2.3. *The coefficients of the metric G_m and its inverse are defined in the following symmetric way:*

$$G_m(\boldsymbol{\xi}) = DF(\boldsymbol{\xi})^\top DF(\boldsymbol{\xi}), \qquad G_m^{-1}(\boldsymbol{\xi}) = N(\boldsymbol{\xi})^\top N(\boldsymbol{\xi}),$$

$$G_m = \begin{pmatrix} \mathbf{t}_1 \cdot \mathbf{t}_1 & \mathbf{t}_1 \cdot \mathbf{t}_2 & \mathbf{t}_1 \cdot \mathbf{t}_3 \\ \mathbf{t}_2 \cdot \mathbf{t}_1 & \mathbf{t}_2 \cdot \mathbf{t}_2 & \mathbf{t}_2 \cdot \mathbf{t}_3 \\ \mathbf{t}_3 \cdot \mathbf{t}_1 & \mathbf{t}_3 \cdot \mathbf{t}_2 & \mathbf{t}_3 \cdot \mathbf{t}_3 \end{pmatrix}, \qquad G_m^{-1} = \begin{pmatrix} \mathbf{n}_1 \cdot \mathbf{n}_1 & \mathbf{n}_1 \cdot \mathbf{n}_2 & \mathbf{n}_1 \cdot \mathbf{n}_3 \\ \mathbf{n}_2 \cdot \mathbf{n}_1 & \mathbf{n}_2 \cdot \mathbf{n}_2 & \mathbf{n}_2 \cdot \mathbf{n}_3 \\ \mathbf{n}_3 \cdot \mathbf{n}_1 & \mathbf{n}_3 \cdot \mathbf{n}_2 & \mathbf{n}_3 \cdot \mathbf{n}_3 \end{pmatrix}.$$

2.3.2 Covariant and Contravariant Basis

There is a common notation of the covariant and contravariant basis vectors, which is described in [27, 63].

Definition 2.4. *The basis vectors are defined as*

$$\mathbf{e}_i = \frac{\partial \mathbf{x}}{\partial \xi_i}, \quad \mathbf{e}^i = \nabla \xi_i = \left(\frac{\partial \xi_i}{\partial x_1}, \frac{\partial \xi_i}{\partial x_2}, \frac{\partial \xi_i}{\partial x_3} \right)^\top, \ i = 1, 2, 3$$

so that the vectors $\mathbf{e}_i$ are the columns of the Jacobian matrix DF and the vectors $\mathbf{e}^i$ are the columns of the transposed inverse of the Jacobian matrix $N = DF^{-\top}$.

Definition 2.5. *The entries of the metric, $g_{ij} = (G_m)_{ij}$, and its inverse, $g^{ij} = \left(G_m^{-1}\right)_{ij}$, are represented as*

$$g_{ij} = \mathbf{e}_i \cdot \mathbf{e}_j, \quad g^{ij} = \mathbf{e}^i \cdot \mathbf{e}^j.$$

Proposition 2.6. *The following relation hold between the basis vectors:*

$$\begin{aligned} \mathbf{e}^i \cdot \mathbf{e}_j &= \delta^i_j, \\ \mathbf{e}_i &= g_{ij}\, \mathbf{e}^j, \\ \mathbf{e}^i &= g^{ij}\, \mathbf{e}_j. \end{aligned}$$

Proof. For the differential elements we have the relations

$$\mathrm{d}\xi_i = \nabla \xi_i \cdot \mathrm{d}\mathbf{x} \text{ and } \mathrm{d}\mathbf{x} = \frac{\partial \mathbf{x}}{\partial \xi_1} \mathrm{d}\xi_1 + \frac{\partial \mathbf{x}}{\partial \xi_2} \mathrm{d}\xi_2 + \frac{\partial \mathbf{x}}{\partial \xi_3} \mathrm{d}\xi_3 = \mathbf{e}_j \, \mathrm{d}\xi^j.$$

Then, it follows that

$$\mathrm{d}\xi_i = \nabla \xi_i \cdot \mathbf{e}_j \, \mathrm{d}\xi^j,$$

which leads to

$$\nabla \xi_i \cdot \mathbf{e}_j = \mathbf{e}^i \cdot \mathbf{e}_j = \delta^i_j.$$

When we represent the basis vectors in the respective other basis, we get

$$\begin{aligned} \mathbf{e}_i &= (\mathbf{e}_i \cdot \mathbf{e}_j)\mathbf{e}^j = g_{ij}\mathbf{e}^j, \\ \mathbf{e}^i &= (\mathbf{e}^i \cdot \mathbf{e}^j)\mathbf{e}_j = g^{ij}\mathbf{e}_j. \end{aligned}$$

□

We can represent every vector field either in the contravariant or in the covariant basis,

$$\mathbf{D} = D_1\mathbf{e}^1 + D_2\mathbf{e}^2 + D_3\mathbf{e}^3 = D^1\mathbf{e}_1 + D^2\mathbf{e}_2 + D^3\mathbf{e}_3, \text{ where } D_i = \mathbf{D} \cdot \mathbf{e}_i, D^i = \mathbf{D} \cdot \mathbf{e}^i.$$

However, in the context of differential forms, there is a proper choice, which facilitates the computation of the exterior derivative. Therefore, a differential 1-form, which is for our choice the electric field, is represented in the contravariant basis,

$$\mathbf{E} = E_i \mathbf{e}^i = N\tilde{\mathbf{E}} \Rightarrow E_i = \tilde{E}_i, i = 1, 2, 3$$

whereas the differential 2-form, in this case the magnetic field, is represented in the covariant basis,

$$\mathbf{B} = B^i \mathbf{e}_i = \frac{DF}{J_F}\tilde{\mathbf{B}} \Rightarrow B^i = \frac{\tilde{B}_i}{J_F}, i = 1, 2, 3. \tag{2.9}$$

Note that for the representation in the contravariant basis, we need the covariant components of the vector field and vice versa. We prove this assertions in the next section in Proposition 2.10.

Then, we take a look at the representation of the derivatives.

Proposition 2.7. *With the definitions from above, we state the following relations for the differential operators:*

- *The gradient of a scalar function is given by*

$$\nabla\Phi = N\nabla_{\boldsymbol{\xi}}\tilde{\Phi}. \tag{2.10}$$

- *The curl of a vector field $\mathbf{A}$ is transformed as*

$$\nabla \times \mathbf{A} = \frac{DF}{J_F}\nabla_{\boldsymbol{\xi}} \times \tilde{\mathbf{A}}. \tag{2.11}$$

- *The divergence of a vector field $\mathbf{F}$ is represented in curvilinear coordinates as*

$$\nabla_{\mathbf{x}} \cdot \mathbf{F} = \frac{1}{J_F}\nabla_{\boldsymbol{\xi}} \cdot \left(J_F N^\top \mathbf{F}\right). \tag{2.12}$$

Proof. - We compute the gradient as

$$\nabla\Phi = \nabla\xi_i \frac{\partial\phi}{\partial\xi_i} = \mathbf{e}^i \frac{\partial\phi}{\partial\xi_i} = N\nabla_{\boldsymbol{\xi}}\Phi.$$

- We compute the curl of the vector field as

$$\nabla \times \mathbf{A} = \nabla \times (A_j \mathbf{e}^j) = A_j(\nabla \times \nabla\xi_j) + \nabla A_j \times \mathbf{e}^j = \frac{\partial A_j}{\partial\xi_i}\mathbf{e}^i \times \mathbf{e}^j = \frac{\varepsilon^{ijk}}{J_F}\frac{\partial A_j}{\partial\xi_i}\frac{\partial\mathbf{x}}{\partial\xi_k},$$

  where we used the relation $\mathbf{e}^i \times \mathbf{e}^j = \frac{\varepsilon^{ijk}}{J_F(\boldsymbol{\xi})}\mathbf{e}_k$ from [27]. Then, we prove the claim with

our definition of the vector potential $\mathbf{A} = N\tilde{\mathbf{A}} = A_i \mathbf{e}^i$ as a 1-form,

$$\frac{DF}{J_F} \nabla_{\boldsymbol{\xi}} \times \tilde{\mathbf{A}} = \frac{DF}{J_F} \begin{pmatrix} \frac{\partial \tilde{A}_3}{\partial \xi_2} - \frac{\partial \tilde{A}_2}{\partial \xi_3} \\ \frac{\partial \tilde{A}_1}{\partial \xi_3} - \frac{\partial \tilde{A}_3}{\partial \xi_1} \\ \frac{\partial \tilde{A}_2}{\partial \xi_1} - \frac{\partial \tilde{A}_1}{\partial \xi_2} \end{pmatrix} = \frac{\varepsilon^{ijk}}{J_F} \frac{\partial A_j}{\partial \xi_i} \frac{\partial \mathbf{x}}{\partial \xi_k}.$$

- We compute the divergence of the vector field as

$$\begin{aligned} \nabla_{\mathbf{x}} \cdot \mathbf{F} &= \frac{1}{J_F} \frac{\partial}{\partial \xi^i} \left(J_F F^i \right) = \frac{1}{J_F} \frac{\partial}{\partial \xi^i} \left(J_F \mathbf{e}^i \cdot \mathbf{F} \right) \\ &= \frac{1}{J_F} \nabla_{\boldsymbol{\xi}} \cdot \left(J_F N^\top \mathbf{F} \right). \end{aligned}$$

□

Lemma 2.8. *The cross product between a vector field and a differential 2-form is represented in curvilinear coordinates as*

$$(\mathbf{v} \times \mathbf{B}) = N(N^\top \mathbf{v}) \times \tilde{\mathbf{B}}.$$

Proof. We compute the covariant component of the cross product and obtain

$$\begin{aligned} (\mathbf{v} \times \mathbf{B}) = \mathbf{e}^k (\mathbf{v} \times \mathbf{B})_k &= \mathbf{e}^k \varepsilon_{ijk} J_F v^i B^j = \mathbf{e}^k \varepsilon_{ijk} \mathbf{e}^i \cdot \mathbf{v} J_F B^j \\ &= N(N^\top \mathbf{v}) \times \tilde{\mathbf{B}}, \end{aligned}$$

where we used the Definition 2.4 and the representation of the 2-form in (2.9). □

2.3.3 Transformation of Differential Forms

We introduce curvilinear coordinates to the differential forms and show how they are transformed in a consistent way as can be seen in [58].

Definition 2.9. *For a scalar differential 0-form, $g \in H^1(\Omega)$, we define $\tilde{g} \in H^1(\tilde{\Omega})$ as*

$$\tilde{g}(\boldsymbol{\xi}) := g(F(\boldsymbol{\xi})) = g(\mathbf{x}). \tag{2.13}$$

Next, we consider the transformation of the other differential forms.

Proposition 2.10. *We have the following properties:*

1. *A vector function, $\mathbf{E} \in H(\mathrm{curl}, \Omega)$, corresponding to a differential 1-form, is transformed by the covariant Piola transform,*

$$\mathbf{E}(\mathbf{x}) = N(\boldsymbol{\xi})\tilde{\mathbf{E}}(\boldsymbol{\xi}) \text{ with } \tilde{\mathbf{E}} \in H(\mathrm{curl}, \tilde{\Omega}). \tag{2.14}$$

2. *A vector function, $\mathbf{B} \in H(\mathrm{div}, \Omega)$, corresponding to a differential 2-form, is transformed by the contravariant Piola transform,*

$$\mathbf{B}(\mathbf{x}) = \frac{DF(\boldsymbol{\xi})}{J_F(\boldsymbol{\xi})}\tilde{\mathbf{B}}(\boldsymbol{\xi}) \text{ with } \tilde{\mathbf{B}} \in H(\mathrm{div}, \tilde{\Omega}). \tag{2.15}$$

3. *A scalar differential 3-form, $h \in L^2(\Omega)$, is related to $\tilde{h} \in L^2(\tilde{\Omega})$ via*

$$h(\mathbf{x}) = \frac{1}{J_F(\boldsymbol{\xi})}\tilde{h}(\boldsymbol{\xi}).$$

Proof. 1. Given a scalar function, $\tilde{\Phi}(\boldsymbol{\xi}), \tilde{\Phi}\colon \tilde{\Omega} \to \mathbb{R}$, which is a 0-form, the result follows from the transformation rule for the gradient of a scalar function in Proposition 2.7. Then, the de Rham sequence (2.6) yields a representation of the gradient of a 0-form as a 1-form, $\nabla_{\mathbf{x}}\Phi(\mathbf{x}) = \mathbf{E}(\mathbf{x})$. We compute

$$\nabla_{\mathbf{x}}\Phi(\mathbf{x}) \overset{(2.10)}{=} N(\boldsymbol{\xi})\nabla_{\boldsymbol{\xi}}\tilde{\Phi}(\boldsymbol{\xi})$$

and reformulate the result to get

$$\mathbf{E}(\mathbf{x}) = \nabla_{\mathbf{x}}\Phi(\mathbf{x}) = N(\boldsymbol{\xi})\nabla_{\boldsymbol{\xi}}\tilde{\Phi}(\boldsymbol{\xi}) = N(\boldsymbol{\xi})\tilde{\mathbf{E}}(\boldsymbol{\xi}), \text{ where } \tilde{\mathbf{E}} = \nabla_{\boldsymbol{\xi}}\tilde{\Phi}(\boldsymbol{\xi}).$$

2. A similar proof for differential 2-forms uses the transformation rule for the curl in Proposition 2.7. Given a vector function, $\mathbf{A}\colon \Omega \to \mathbb{R}^3$, which is a 1-form, it follows from the de Rham sequence (2.6) that the curl of the function can be represented as a 2-form, $\nabla_{\mathbf{x}} \times \mathbf{A}(\mathbf{x}) = \mathbf{B}(\mathbf{x})$. So, we obtain

$$\nabla_{\mathbf{x}} \times \mathbf{A}(\mathbf{x}) \overset{(2.11)}{=} \frac{DF(\boldsymbol{\xi})}{J_F(\boldsymbol{\xi})}\nabla_{\boldsymbol{\xi}} \times \tilde{\mathbf{A}}(\boldsymbol{\xi}),$$

which leads to

$$\mathbf{B}(\mathbf{x}) = \frac{DF(\boldsymbol{\xi})}{J_F(\boldsymbol{\xi})}\tilde{\mathbf{B}}(\boldsymbol{\xi}), \text{ where } \nabla_{\boldsymbol{\xi}} \times \tilde{\mathbf{A}}(\boldsymbol{\xi}) = \tilde{\mathbf{B}}(\boldsymbol{\xi}).$$

3. The result for differential 3-forms is proven the same way with the formula for the diver-

gence of a vector field in Proposition 2.7,

$$\nabla_{\mathbf{x}} \cdot \mathbf{B}(\mathbf{x}) \overset{(2.12)}{=} \frac{1}{J_F(\boldsymbol{\xi})} \nabla_{\boldsymbol{\xi}} \cdot \tilde{\mathbf{B}}(\boldsymbol{\xi}).$$

□

For integrals we use the transformation formula

$$\int_{\Omega} g(\mathbf{x}) \, \mathrm{d}\mathbf{x} = \int_{\tilde{\Omega}} g(F(\boldsymbol{\xi})) |J_F(\boldsymbol{\xi})| \, \mathrm{d}\boldsymbol{\xi}. \tag{2.16}$$

2.4 Curvilinear Vlasov and Maxwell's Equations

We transform the Vlasov–Maxwell system using the curvilinear transformation rules for the differential forms.

Proposition 2.1. *Under the coordinate transformation $F(\boldsymbol{\xi}) = \mathbf{x}$,*

1. *the Vlasov equation* (2.1) *transforms to*

$$\begin{aligned} \frac{\partial \tilde{f}_s(\boldsymbol{\xi}, \mathbf{v}, t)}{\partial t} &+ N(\boldsymbol{\xi})^{\top} \mathbf{v} \cdot \nabla_{\boldsymbol{\xi}} \tilde{f}_s(\boldsymbol{\xi}, \mathbf{v}, t) \\ &+ \frac{q_s}{m_s} N(\boldsymbol{\xi}) \left(\tilde{\mathbf{E}}(\boldsymbol{\xi}, t) + (N(\boldsymbol{\xi})^{\top} \mathbf{v}) \times \tilde{\mathbf{B}}(\boldsymbol{\xi}, t) \right) \cdot \nabla_{\mathbf{v}} \tilde{f}_s(\boldsymbol{\xi}, \mathbf{v}, t) = 0; \end{aligned}$$

2. *Faraday's* (2.8b) *and magnetic Gauss' laws* (2.8d) *in strong form do not change, i.e.*

$$\frac{\partial \tilde{\mathbf{B}}(\boldsymbol{\xi}, t)}{\partial t} = -\nabla_{\boldsymbol{\xi}} \times \tilde{\mathbf{E}}(\boldsymbol{\xi}, t), \tag{2.17a}$$

$$\nabla_{\boldsymbol{\xi}} \cdot \tilde{\mathbf{B}}(\boldsymbol{\xi}, t) = 0; \tag{2.17b}$$

3. *the weak formulation of Ampère's* (2.8a) *and Gauss' laws* (2.8c) *is transformed for all $\tilde{\boldsymbol{\varphi}} \in H(\mathrm{curl}, \tilde{\Omega})$, $\tilde{\psi} \in H^1(\tilde{\Omega})$ as*

$$\frac{\partial}{\partial t} \int_{\tilde{\Omega}} N \tilde{\boldsymbol{\varphi}} \cdot N \tilde{\mathbf{E}} |J_F| \, \mathrm{d}\boldsymbol{\xi} = \int_{\tilde{\Omega}} \frac{DF}{J_F} \nabla_{\boldsymbol{\xi}} \times \tilde{\boldsymbol{\varphi}} \cdot \frac{DF}{J_F} \tilde{\mathbf{B}} |J_F| \, \mathrm{d}\boldsymbol{\xi} - \int_{\tilde{\Omega}} N \tilde{\boldsymbol{\varphi}} \cdot N \tilde{\mathbf{J}} |J_F| \, \mathrm{d}\boldsymbol{\xi}, \tag{2.18a}$$

$$- \int_{\tilde{\Omega}} N \nabla_{\boldsymbol{\xi}} \tilde{\psi} \cdot N \tilde{\mathbf{E}} |J_F| \, \mathrm{d}\boldsymbol{\xi} = \int_{\tilde{\Omega}} \tilde{\psi} \tilde{\rho} \, |J_F| \, \mathrm{d}\boldsymbol{\xi}. \tag{2.18b}$$

Proof. The equations are derived by inserting the coordinate transformation into the Vlasov and the Maxwell equations and using Proposition 2.10.

1. We insert the coordinate transformation $\mathbf{x} = F(\boldsymbol{\xi})$ into the Vlasov equation (2.1),

$$\begin{aligned}&\frac{\partial f_s(F(\boldsymbol{\xi}), \mathbf{v}, t)}{\partial t} + \mathbf{v} \cdot \nabla_{\boldsymbol{\xi}} f_s(F(\boldsymbol{\xi}), \mathbf{v}, t) \\ &+ \frac{q_s}{m_s}(\mathbf{E}(F(\boldsymbol{\xi}), t) + \mathbf{v} \times \mathbf{B}(F(\boldsymbol{\xi}), t)) \cdot \nabla_{\mathbf{v}} f_s(F(\boldsymbol{\xi}), \mathbf{v}, t) = 0,\end{aligned}$$

and use the Piola transformations (2.14) and (2.15) to obtain

$$\begin{aligned}&\frac{\partial \tilde{f}_s(\boldsymbol{\xi}, \mathbf{v}, t)}{\partial t} + \mathbf{v} \cdot N(\boldsymbol{\xi}) \nabla_{\boldsymbol{\xi}} \tilde{f}_s(\boldsymbol{\xi}, \mathbf{v}, t) \\ &+ \frac{q}{m}(N(\boldsymbol{\xi})\tilde{\mathbf{E}}(\boldsymbol{\xi}, t) + \mathbf{v} \times \frac{DF(\boldsymbol{\xi})}{J_F(\boldsymbol{\xi})}\tilde{\mathbf{B}}(\boldsymbol{\xi}, t)) \cdot \nabla_{\mathbf{v}} \tilde{f}_s(\boldsymbol{\xi}, \mathbf{v}, t) = 0.\end{aligned}$$

Then, we use the Lemma 2.8 to obtain the proposition.

2. Using the Piola transformation for differential 2-forms (2.15) and the chain rule in Faraday's equation (2.8b) leads to

$$\frac{DF(\boldsymbol{\xi})}{J_F(\boldsymbol{\xi})} \frac{\partial \tilde{\mathbf{B}}(\boldsymbol{\xi}, t)}{\partial t} \overset{(2.15)}{=} \frac{\partial \mathbf{B}(\mathbf{x}, t)}{\partial t} = -\nabla_{\mathbf{x}} \times \mathbf{E}(\mathbf{x}, t) \overset{(2.11)}{=} -\frac{DF(\boldsymbol{\xi})}{J_F(\boldsymbol{\xi})} \nabla_{\boldsymbol{\xi}} \times \tilde{\mathbf{E}}(\boldsymbol{\xi}, t).$$

Since $DF(\boldsymbol{\xi})$ is invertible for any $\boldsymbol{\xi}$, we arrive at (2.17a). With the transformation of the divergence of a 2-form, we obtain for magnetic Gauss' law (2.8d)

$$0 = \nabla_{\mathbf{x}} \cdot \mathbf{B}(\mathbf{x}, t) \overset{(2.12)}{=} \frac{1}{J_F(\boldsymbol{\xi})} \nabla_{\boldsymbol{\xi}} \cdot \tilde{\mathbf{B}}(\boldsymbol{\xi}, t). \tag{2.19}$$

3. We use the transformation formula (2.16), the Piola formulas (2.14) and (2.15) and the curvilinear curl (2.11) to insert the coordinate transformation into the weak formulation of Ampère's law (2.8a) and electric Gauss' law (2.8c).

□

We note that the advection coefficient $N(\boldsymbol{\xi})^\top \mathbf{v}$ for the $\boldsymbol{\xi}$ advection in the curvilinear Vlasov equation depends on ξ. Therefore, $\tilde{f}_s$ is no longer a conserved quantity but instead $J_F \tilde{f}_s$ (cf. [16, 43]) and the curvilinear Vlasov equation in conservative form reads

$$\partial_t(J_F \tilde{f}_s) + \nabla_{\boldsymbol{\xi}} \cdot (N^\top \mathbf{v} J_F \tilde{f}_s) + \nabla_{\mathbf{v}} \cdot \left(\frac{q_s}{m_s} N(\tilde{\mathbf{E}} + (N^\top \mathbf{v}) \times \tilde{\mathbf{B}}) J_F \tilde{f}_s \right) = 0.$$

3 Structure-preserving Discretisation in Curvilinear Geometry

In this section, we will introduce a particle discretisation for the distribution function and a compatible finite element discretisation of the fields extending the discretisation proposed in [56] to the curvilinear case.

3.1 Discrete Particle Distribution Function

In order to define the charge and current densities in Maxwell's equations, we need to define a discrete particle distribution function from the positions $\mathbf{x}_p$ and velocities $\mathbf{v}_p$ of the N_p particles of all species s. We use a definition based on δ-functions in phase space,

$$f_h(\mathbf{x}, \mathbf{v}, t) = \sum_{p=1}^{N_p} \omega_p \delta(\mathbf{x} - \mathbf{x}_p(t)) \delta(\mathbf{v} - \mathbf{v}_p(t)).$$

The δ-function defines the point evaluation in a convolution with another function. Therefore, we need to scale by the inverse Jacobian determinant when the argument is transformed as expressed in the following lemma:

Lemma 3.1. *In curvilinear coordinates the delta distribution transforms with the inverse Jacobian determinant,*

$$\delta(\mathbf{x} - \mathbf{x}_p(t)) = \frac{\delta(\boldsymbol{\xi} - \boldsymbol{\xi}_p(t))}{|J_F(\boldsymbol{\xi})|}.$$

Proof. We choose N_p points $\boldsymbol{\xi}_p \in \tilde{\Omega}$ so that $F(\boldsymbol{\xi}_p) = \mathbf{x}_p \in \Omega \; \forall p \in \{1, ..., N_p\}$ and use the following ansatz:

$$\exists \gamma \in \mathbb{R} : \delta(\mathbf{x} - \mathbf{x}_p) = \gamma \delta(\boldsymbol{\xi} - \boldsymbol{\xi}_p) \quad \forall p \in \{1, ..., N_p\}.$$

Then, we integrate over Ω on both sides and use the transformation rule (2.16) on the right-hand side,

$$\int_\Omega \delta(\mathbf{x} - \mathbf{x}_p) \, \mathrm{d}\mathbf{x} = \int_{\tilde{\Omega}} \gamma \delta(\boldsymbol{\xi} - \boldsymbol{\xi}_p) |J_F(\boldsymbol{\xi})| \, \mathrm{d}\boldsymbol{\xi} \quad \forall p \in \{1, ..., N_p\}.$$

Since the left-hand side equals 1, we get

$$\gamma = \frac{1}{|J_F(\boldsymbol{\xi})|} \Rightarrow \delta(\mathbf{x} - \mathbf{x}_p) = \frac{\delta(\boldsymbol{\xi} - \boldsymbol{\xi}_p)}{|J_F(\boldsymbol{\xi})|} \quad \forall p \in \{1, ..., N_p\}.$$

□

Hence, the discrete distribution function in logical coordinates is defined as

$$\tilde{f}_h(\boldsymbol{\xi}, \mathbf{v}, t) = f_h(F(\boldsymbol{\xi}), \mathbf{v}, t) = \sum_{p=1}^{N_p} \omega_p \frac{\delta(\boldsymbol{\xi} - \boldsymbol{\xi}_p(t))}{|J_F(\boldsymbol{\xi})|} \delta(\mathbf{v} - \mathbf{v}_p(t)). \tag{3.1}$$

Upon inserting the discrete form of the particle distribution function, the current and the charge densities take the following form:

$$\tilde{\mathbf{J}}_h(\boldsymbol{\xi}) = DF^\top(\boldsymbol{\xi}) \sum_s \int q_s \tilde{f}_{hs}(\boldsymbol{\xi}, \mathbf{v}, t)\mathbf{v} \ \mathrm{d}\mathbf{v} = DF^\top(\boldsymbol{\xi}) \sum_{p=1}^{N_p} q_p \omega_p \frac{\delta(\boldsymbol{\xi} - \boldsymbol{\xi}_p)}{|J_F(\boldsymbol{\xi})|} \mathbf{v}_p, \tag{3.2a}$$

$$\tilde{\rho}_h(\boldsymbol{\xi}) = \sum_s \int q_s \tilde{f}_{hs}(\boldsymbol{\xi}, \mathbf{v}, t) \ \mathrm{d}\mathbf{v} = \sum_{p=1}^{N_p} q_p \omega_p \frac{\delta(\boldsymbol{\xi} - \boldsymbol{\xi}_p)}{|J_F(\boldsymbol{\xi})|}.' \tag{3.2b}$$

Note that this representation is smooth enough, since we only consider the densities in weak form and the Jacobian determinant from the transformation rule cancels out the inverse Jacobian determinant.

Let us collect the logical positions of all particles and their velocities in the vectors $\boldsymbol{\Xi} := (\boldsymbol{\xi}_1, ..., \boldsymbol{\xi}_{N_P})^\top, \mathbf{V} := (\mathbf{v}_1, ..., \mathbf{v}_{N_P})^\top$. Moreover, we use use the following notation: $\mathbb{W}_m := \mathrm{diag}(\omega_p m_p) \otimes \mathbb{I}_3, \mathbb{W}_q := \mathrm{diag}(\omega_p q_p) \otimes \mathbb{I}_3, \mathbb{N} := \mathrm{diag}(N(\boldsymbol{\xi}_p)), \mathbb{G} := \mathrm{diag}(G_m(\boldsymbol{\xi}_p)), 1 \leq p \leq N_p$. Hence, the equations for the characteristics of the particles are written as

$$\begin{aligned} \dot{\boldsymbol{\Xi}} &= \mathbb{N}^\top(\boldsymbol{\Xi})\mathbf{V}, \\ \dot{\mathbf{V}} &= \mathbb{W}_{\frac{q}{m}} \mathbb{N}(\boldsymbol{\Xi}) \left(\tilde{\mathbf{E}}(\boldsymbol{\Xi}, t) + (\mathbb{N}^\top(\boldsymbol{\Xi})\mathbf{V}) \times \tilde{\mathbf{B}}(\boldsymbol{\Xi}, t) \right). \end{aligned} \tag{3.3}$$

3.2 Finite Element Discretisation

3.2.1 Discrete de Rham Sequence

Arnold, Falk, and Winther [3] have developed a theoretical framework for the finite element discretisation that respects the sequence properties of the de Rham complex. The idea is to define discrete spaces that form the following commuting diagram with the continuous spaces:

$$\begin{array}{ccccccc} H^1(\tilde{\Omega}) & \xrightarrow{\mathrm{grad}} & H(\mathrm{curl}, \tilde{\Omega}) & \xrightarrow{\mathrm{curl}} & H(\mathrm{div}, \tilde{\Omega}) & \xrightarrow{\mathrm{div}} & L^2(\tilde{\Omega}) \\ \downarrow \Pi_0 & & \downarrow \Pi_1 & & \downarrow \Pi_2 & & \downarrow \Pi_3 \\ \tilde{V}_0 & \xrightarrow{\mathrm{grad}} & \tilde{V}_1 & \xrightarrow{\mathrm{curl}} & \tilde{V}_2 & \xrightarrow{\mathrm{div}} & \tilde{V}_3 \end{array}$$

The operators Π_k, $k = 0, 1, 2, 3$, are projecting the corresponding differential forms to the finite dimensional subspaces $\tilde{V}_k$ with dimension,

$$\dim \tilde{V}_k = \begin{cases} N_k & \text{if } k = 0, 3, \\ 3N_k & \text{if } k = 1, 2, \end{cases} \quad \text{i.e. } \Pi_0\tilde{\Phi} = \tilde{\Phi}_h \in \tilde{V}_0, \Pi_1\tilde{\mathbf{E}} = \tilde{\mathbf{E}}_h \in \tilde{V}_1, \Pi_2\tilde{\mathbf{B}} = \tilde{\mathbf{B}}_h \in \tilde{V}_2.$$

The most common construction of such compatible finite element spaces is based on Lagrange finite elements for V_0, Raviart–Thomas elements for V_1, Nédélec elements for V_2 and discontinuous elements for V_3. Moreover, a compatible sequence can be constructed from splines of mixed order as proposed by Buffa, Sangalli, & Vázquez [12]. In our numerical experiments, we apply the latter elements. We introduce basis functions for the finite dimensional subspaces $\tilde{V}_k$, scalar functions $\tilde{\Lambda}_i^k$ for $k = 0, 3$ and vector valued functions

$$\tilde{\mathbf{\Lambda}}_{i,1}^k = (\tilde{\Lambda}_i^{k,1}, 0, 0)^\top, \tilde{\mathbf{\Lambda}}_{i,2}^k = (0, \tilde{\Lambda}_i^{k,2}, 0)^\top, \tilde{\mathbf{\Lambda}}_{i,3}^k = (0, 0, \tilde{\Lambda}_i^{k,3})^\top \text{ for } k = 1, 2.$$

The de Rham structure can also be expressed on the level of matrices and vectors. For $\boldsymbol{\xi} \in \tilde{\Omega}$, we collect the value of each basis function in a row vector as

$$\begin{aligned} \tilde{\Lambda}^k(\boldsymbol{\xi}) &= \left(\tilde{\Lambda}_1^k(\boldsymbol{\xi}), \tilde{\Lambda}_2^k(\boldsymbol{\xi}), ..., \tilde{\Lambda}_{N_k}^k(\boldsymbol{\xi})\right) \in \mathbb{R}^{1\times N_k} \text{ for } k = 0, 3, \\ \tilde{\mathbf{\Lambda}}^k(\boldsymbol{\xi}) &= \left(\tilde{\mathbf{\Lambda}}_{1,1}^k(\boldsymbol{\xi}), \tilde{\mathbf{\Lambda}}_{2,1}^k(\boldsymbol{\xi}), ..., \tilde{\mathbf{\Lambda}}_{N_k,3}^k(\boldsymbol{\xi})\right) \in \mathbb{R}^{3\times 3N_k} \text{ for } k = 1, 2. \end{aligned}$$

Then, the following relations hold for the basis functions:

$$\begin{aligned} \nabla_{\boldsymbol{\xi}}\tilde{\Lambda}^0(\boldsymbol{\xi}) &= \tilde{\mathbf{\Lambda}}^1(\boldsymbol{\xi})\mathsf{G}, \\ \nabla_{\boldsymbol{\xi}} \times \tilde{\mathbf{\Lambda}}^1(\boldsymbol{\xi}) &= \tilde{\mathbf{\Lambda}}^2(\boldsymbol{\xi})\mathsf{C}, \\ \nabla_{\boldsymbol{\xi}} \cdot \tilde{\mathbf{\Lambda}}^2(\boldsymbol{\xi}) &= \tilde{\Lambda}^3(\boldsymbol{\xi})\mathsf{D} \end{aligned} \tag{3.4}$$

for some matrix $\mathsf{G} \in \mathbb{R}^{3N_1\times N_0}$ denoting the discrete gradient matrix, $\mathsf{C} \in \mathbb{R}^{3N_2\times 3N_1}$ denoting the discrete curl matrix and $\mathsf{D} \in \mathbb{R}^{N_3\times 3N_2}$ denoting the discrete divergence matrix, all independent of $\boldsymbol{\xi}$. These matrices need to satisfy

$$\mathsf{DC} = 0 \text{ and } \mathsf{CG} = 0 \tag{3.5}$$

to mimic the complex properties $\operatorname{div}\operatorname{curl} = 0$ and $\operatorname{curl}\operatorname{grad} = 0$.

Examples of discrete spaces that satisfy these properties have been proposed in the literature and are particularly easy to construct on a Cartesian geometry. Using the transformation rules for differential forms, however, it is straightforward to construct a compatible basis in curvilinear coordinates from a compatible basis on the logical mesh.

Lemma 3.1. *A de Rham sequence on the physical domain can be constructed from the de Rham sequence on the logical mesh by*

$$\Lambda^0(\mathbf{x}) = \tilde{\Lambda}^0(\boldsymbol{\xi}),\ \boldsymbol{\Lambda}^1(\mathbf{x}) = N(\boldsymbol{\xi})\tilde{\boldsymbol{\Lambda}}^1(\boldsymbol{\xi}),\ \boldsymbol{\Lambda}^2(\mathbf{x}) = \frac{DF(\boldsymbol{\xi})}{J_F(\boldsymbol{\xi})}\tilde{\boldsymbol{\Lambda}}^2(\boldsymbol{\xi}),\ \Lambda^3(\mathbf{x}) = \frac{1}{J_F(\boldsymbol{\xi})}\tilde{\Lambda}^3(\boldsymbol{\xi}).$$

Proof. The following computations show the assertions:

$$\begin{aligned}
\nabla_{\mathbf{x}}\Lambda^0(\mathbf{x}) &= N(\boldsymbol{\xi})\nabla_{\boldsymbol{\xi}}\tilde{\Lambda}^0(\boldsymbol{\xi}) = N(\boldsymbol{\xi})\tilde{\boldsymbol{\Lambda}}^1(\boldsymbol{\xi})\mathsf{G} = \boldsymbol{\Lambda}^1(\mathbf{x})\mathsf{G},\\
\nabla_{\mathbf{x}} \times \boldsymbol{\Lambda}^1(\mathbf{x}) &= \frac{DF(\boldsymbol{\xi})}{J_F(\boldsymbol{\xi})}\nabla_{\boldsymbol{\xi}} \times \tilde{\boldsymbol{\Lambda}}^1(\boldsymbol{\xi}) = \frac{DF(\boldsymbol{\xi})}{J_F(\boldsymbol{\xi})}\tilde{\boldsymbol{\Lambda}}^2(\boldsymbol{\xi})\mathsf{C} = \boldsymbol{\Lambda}^2(\mathbf{x})\mathsf{C},\\
\nabla_{\mathbf{x}} \cdot \boldsymbol{\Lambda}^2(\mathbf{x}) &= \frac{1}{J_F(\boldsymbol{\xi})}\nabla_{\boldsymbol{\xi}} \cdot \tilde{\boldsymbol{\Lambda}}^2(\boldsymbol{\xi}) = \frac{1}{J_F(\boldsymbol{\xi})}\tilde{\Lambda}^3(\boldsymbol{\xi})\mathsf{D} = \Lambda^3(\mathbf{x})\mathsf{D}
\end{aligned}$$

for the same matrices G, C and D as on the logical mesh. □

The mass matrices for the differential forms are defined as

$$\begin{aligned}
(\tilde{\mathsf{M}}_0)_{ij} &= \int_{\tilde{\Omega}} \tilde{\Lambda}^0_i(\boldsymbol{\xi})\tilde{\Lambda}^0_j(\boldsymbol{\xi})|J_F(\boldsymbol{\xi})|\ \mathrm{d}\boldsymbol{\xi} \text{ for } 1 \leq i,j \leq N_0,\\
(\tilde{\mathsf{M}}_1)_{IJ} &= \int_{\tilde{\Omega}} \tilde{\boldsymbol{\Lambda}}^1_I(\boldsymbol{\xi})^\top G_m^{-1}(\boldsymbol{\xi})\tilde{\boldsymbol{\Lambda}}^1_J(\boldsymbol{\xi})|J_F(\boldsymbol{\xi})|\ \mathrm{d}\boldsymbol{\xi} \text{ for } 1 \leq I,J \leq 3N_1,\\
(\tilde{\mathsf{M}}_2)_{IJ} &= \int_{\tilde{\Omega}} \tilde{\boldsymbol{\Lambda}}^2_I(\boldsymbol{\xi})^\top G_m(\boldsymbol{\xi})\tilde{\boldsymbol{\Lambda}}^2_J(\boldsymbol{\xi})\frac{1}{|J_F(\boldsymbol{\xi})|}\ \mathrm{d}\boldsymbol{\xi} \text{ for } 1 \leq I,J \leq 3N_2,\\
(\tilde{\mathsf{M}}_3)_{ij} &= \int_{\tilde{\Omega}} \tilde{\Lambda}^3_i(\boldsymbol{\xi})\tilde{\Lambda}^3_j(\boldsymbol{\xi})\frac{1}{|J_F(\boldsymbol{\xi})|}\ \mathrm{d}\boldsymbol{\xi} \text{ for } 1 \leq i,j \leq N_3.
\end{aligned} \tag{3.6}$$

3.2.2 Discretisation of the Curvilinear Maxwell Equations

To discretise Maxwell's equations based on the compatible finite element spaces, we represent the electromagnetic fields with a finite number of degrees of freedom, $\tilde{\mathbf{e}} \in \mathbb{R}^{3N_1\times 1}, \tilde{\mathbf{b}} \in \mathbb{R}^{3N_2\times 1}$, as

$$\tilde{\mathbf{E}}_h(\boldsymbol{\xi},t) = \tilde{\boldsymbol{\Lambda}}^1(\boldsymbol{\xi})\tilde{\mathbf{e}}(t) = \sum_{J=1}^{3N_1} \tilde{\boldsymbol{\Lambda}}^1_J(\boldsymbol{\xi})\tilde{e}_J(t), \tag{3.7a}$$

$$\tilde{\mathbf{B}}_h(\boldsymbol{\xi},t) = \tilde{\boldsymbol{\Lambda}}^2(\boldsymbol{\xi})\tilde{\mathbf{b}}(t) = \sum_{K=1}^{3N_2} \tilde{\boldsymbol{\Lambda}}^2_K(\boldsymbol{\xi})\tilde{b}_K(t). \tag{3.7b}$$

We recapitulate the Piola transforms (2.14) and (2.15) of the electromagnetic fields and introduce the basis representation of the finite-dimensional subspaces,

$$\begin{aligned}
\mathbf{E}_h(\mathbf{x},t) &= \mathbf{E}_h(F(\boldsymbol{\xi}),t) = N(\boldsymbol{\xi})\tilde{\mathbf{E}}_h(\boldsymbol{\xi},t) = N(\boldsymbol{\xi})\tilde{\boldsymbol{\Lambda}}^1(\boldsymbol{\xi})\tilde{\mathbf{e}}(t),\\
\mathbf{B}_h(\mathbf{x},t) &= \mathbf{B}_h(F(\boldsymbol{\xi}),t) = \frac{DF(\boldsymbol{\xi})}{J_F(\boldsymbol{\xi})}\tilde{\mathbf{B}}_h(\boldsymbol{\xi},t) = \frac{DF(\boldsymbol{\xi})}{J_F(\boldsymbol{\xi})}\tilde{\boldsymbol{\Lambda}}^2(\boldsymbol{\xi})\tilde{\mathbf{b}}(t).
\end{aligned}$$

Proposition 3.2. *The transformed discrete versions of Ampère's and electric Gauss' laws take the following form in matrix notation:*

$$\tilde{\mathsf{M}}_1 \dot{\tilde{\mathbf{e}}} = \mathsf{C}^\top \tilde{\mathsf{M}}_2 \tilde{\mathbf{b}} - \mathbb{W}_q \tilde{\mathbb{\Lambda}}^1(\boldsymbol{\Xi})^\top \mathbb{N}^\top(\boldsymbol{\Xi}) \mathbf{V}, \tag{3.8a}$$

$$\mathsf{G}^\top \tilde{\mathsf{M}}_1 \tilde{\mathbf{e}} = -\mathbb{W}_q \tilde{\mathbb{\Lambda}}^0(\boldsymbol{\Xi})^\top \mathbb{1}_{N_p}. \tag{3.8b}$$

Proof. The Maxwell equations in weak formulation are discretised by approximating $(\mathbf{E}, \mathbf{B}) \in H(\mathrm{curl}, \tilde{\Omega}) \times H(\mathrm{div}, \tilde{\Omega})$ with the discrete fields $(\tilde{\mathbf{E}}_h, \tilde{\mathbf{B}}_h) \in \tilde{V}_1 \times \tilde{V}_2$ defined on finite-dimensional subspaces with discrete test functions in $\tilde{V}_0$ and $\tilde{V}_1$.

For Ampère's law, we insert (3.7a) and (3.7b) into (2.18a) and use the basis functions $\tilde{\mathbf{\Lambda}}^1 \in \tilde{V}_1$ as test functions,

$$\begin{aligned}\frac{\partial}{\partial t} \int_{\tilde{\Omega}} N(\boldsymbol{\xi}) \tilde{\mathbf{\Lambda}}^1(\boldsymbol{\xi}) \cdot N(\boldsymbol{\xi}) \tilde{\mathbf{\Lambda}}^1(\boldsymbol{\xi}) \tilde{\mathbf{e}} |J_F(\boldsymbol{\xi})| \, \mathrm{d}\boldsymbol{\xi} &= \int_{\tilde{\Omega}} \frac{DF(\boldsymbol{\xi})}{J_F(\boldsymbol{\xi})} \nabla_{\boldsymbol{\xi}} \times \tilde{\mathbf{\Lambda}}^1(\boldsymbol{\xi}) \cdot \frac{DF(\boldsymbol{\xi})}{J_F(\boldsymbol{\xi})} \tilde{\mathbf{\Lambda}}^2(\boldsymbol{\xi}) \tilde{\mathbf{b}} |J_F(\boldsymbol{\xi})| \, \mathrm{d}\boldsymbol{\xi} \\ &\quad - \int_{\tilde{\Omega}} N(\boldsymbol{\xi}) \tilde{\mathbf{\Lambda}}^1(\boldsymbol{\xi}) \cdot N(\boldsymbol{\xi}) \tilde{\mathbf{J}}_h(\boldsymbol{\xi}) |J_F(\boldsymbol{\xi})| \, \mathrm{d}\boldsymbol{\xi}.\end{aligned}$$

Next, we use the relation (3.4) for the curl and insert the transformed current (3.2a),

$$\begin{aligned}\int_{\tilde{\Omega}} \tilde{\mathbf{\Lambda}}^1(\boldsymbol{\xi})^\top N(\boldsymbol{\xi})^\top N(\boldsymbol{\xi}) \tilde{\mathbf{\Lambda}}^1(\boldsymbol{\xi}) \dot{\tilde{\mathbf{e}}} |J_F(\boldsymbol{\xi})| \, \mathrm{d}\boldsymbol{\xi} &= \int_{\tilde{\Omega}} (\tilde{\mathbf{\Lambda}}^2(\boldsymbol{\xi}) \mathsf{C})^\top DF(\boldsymbol{\xi})^\top DF(\boldsymbol{\xi}) \tilde{\mathbf{\Lambda}}^2(\boldsymbol{\xi}) \tilde{\mathbf{b}} \frac{1}{|J_F(\boldsymbol{\xi})|} \, \mathrm{d}\boldsymbol{\xi} \\ &\quad - \int_{\tilde{\Omega}} \tilde{\mathbf{\Lambda}}^1(\boldsymbol{\xi})^\top N(\boldsymbol{\xi})^\top \sum_{p=1}^{N_p} q_p \omega_p \frac{\delta(\boldsymbol{\xi} - \boldsymbol{\xi}_p)}{|J_F(\boldsymbol{\xi})|} \mathbf{v}_p |J_F(\boldsymbol{\xi})| \, \mathrm{d}\boldsymbol{\xi} \\ \Leftrightarrow \int_{\tilde{\Omega}} \tilde{\mathbf{\Lambda}}^1(\boldsymbol{\xi})^\top G_m^{-1}(\boldsymbol{\xi}) \tilde{\mathbf{\Lambda}}^1(\boldsymbol{\xi}) |J_F(\boldsymbol{\xi})| \, \mathrm{d}\boldsymbol{\xi} \, \dot{\tilde{\mathbf{e}}} &= \mathsf{C}^\top \int_{\tilde{\Omega}} \tilde{\mathbf{\Lambda}}^2(\boldsymbol{\xi})^\top G_m(\boldsymbol{\xi}) \tilde{\mathbf{\Lambda}}^2(\boldsymbol{\xi}) \frac{1}{|J_F(\boldsymbol{\xi})|} \, \mathrm{d}\boldsymbol{\xi} \, \tilde{\mathbf{b}} \\ &\quad - \sum_{p=1}^{N_p} q_p \omega_p \tilde{\mathbf{\Lambda}}^1(\boldsymbol{\xi}_p)^\top N(\boldsymbol{\xi}_p)^\top \mathbf{v}_p.\end{aligned}$$

For Gauss' law, we insert (3.7a) into (2.18b) and choose the basis functions $\tilde{\Lambda}^0 \in \tilde{V}_0$ as test functions,

$$-\int_{\tilde{\Omega}} \Big(N(\boldsymbol{\xi}) \nabla_{\boldsymbol{\xi}} \tilde{\Lambda}^0(\boldsymbol{\xi}) \Big)^\top N(\boldsymbol{\xi}) \tilde{\mathbf{\Lambda}}_1(\boldsymbol{\xi}) \tilde{\mathbf{e}} |J_F(\boldsymbol{\xi})| \, \mathrm{d}\boldsymbol{\xi} = \int_{\tilde{\Omega}} \tilde{\Lambda}^0(\boldsymbol{\xi})^\top \tilde{\boldsymbol{\rho}}_h(\boldsymbol{\xi}) |J_F(\boldsymbol{\xi})| \, \mathrm{d}\boldsymbol{\xi}.$$

Then, we use the relation (3.4) for the gradient and insert the transformed charge (3.2b),

$$\begin{aligned}\int_{\tilde{\Omega}} (\tilde{\mathbf{\Lambda}}^1(\boldsymbol{\xi}) \mathsf{G})^\top N(\boldsymbol{\xi})^\top N(\boldsymbol{\xi}) \tilde{\mathbf{\Lambda}}^1(\boldsymbol{\xi}) \tilde{\mathbf{e}} |J_F(\boldsymbol{\xi})| \, \mathrm{d}\boldsymbol{\xi} &= -\int_{\tilde{\Omega}} \tilde{\Lambda}^0(\boldsymbol{\xi})^\top \sum_{p=1}^{N_p} q_p \omega_p \frac{\delta(\boldsymbol{\xi} - \boldsymbol{\xi}_p)}{|J_F(\boldsymbol{\xi})|} |J_F(\boldsymbol{\xi})| \, \mathrm{d}\boldsymbol{\xi} \\ \Leftrightarrow \mathsf{G}^\top \int_{\tilde{\Omega}} \tilde{\mathbf{\Lambda}}^1(\boldsymbol{\xi})^\top G_m^{-1}(\boldsymbol{\xi}) \tilde{\mathbf{\Lambda}}^1(\boldsymbol{\xi}) |J_F(\boldsymbol{\xi})| \, \mathrm{d}\boldsymbol{\xi} \, \tilde{\mathbf{e}} &= -\sum_{p=1}^{N_p} q_p \omega_p \tilde{\Lambda}^0(\boldsymbol{\xi}_p)^\top.\end{aligned}$$

With the notation of the mass matrices (3.6) we obtain the equations in matrix notation. □

Proposition 3.3. *The transformed discrete versions of Faraday's and magnetic Gauss' laws take the following form in matrix notation:*

$$\dot{\tilde{\mathbf{b}}} = -\mathsf{C}\tilde{\mathbf{e}}, \tag{3.9a}$$

$$\mathsf{D}\tilde{\mathbf{b}} = 0. \tag{3.9b}$$

Proof. For Faraday's law, we insert the discrete transformed fields and their basis representation (3.7a),(3.7b) into (2.17a),

$$\frac{\partial(\tilde{\mathbf{\Lambda}}^2(\boldsymbol{\xi})\tilde{\mathbf{b}}(t))}{\partial t} = -\nabla_{\boldsymbol{\xi}} \times \tilde{\mathbf{\Lambda}}^1(\boldsymbol{\xi})\tilde{\mathbf{e}}(t).$$

Then, we use (3.4) to reformulate the curl,

$$\begin{aligned} \tilde{\mathbf{\Lambda}}^2(\boldsymbol{\xi})\dot{\tilde{\mathbf{b}}}(t) &= -\tilde{\mathbf{\Lambda}}^2(\boldsymbol{\xi})\mathsf{C}\tilde{\mathbf{e}}(t) \\ \Leftrightarrow \dot{\tilde{\mathbf{b}}}(t) &= -\mathsf{C}\tilde{\mathbf{e}}(t). \end{aligned}$$

For the magnetic Gauss law, we insert (3.7b) into (2.17b),

$$\nabla_{\boldsymbol{\xi}} \cdot \tilde{\mathbf{\Lambda}}^2(\boldsymbol{\xi})\tilde{\mathbf{b}}(t) = 0,$$

and use (3.4) to calculate the result,

$$\begin{aligned} \tilde{\Lambda}^3(\boldsymbol{\xi})\mathsf{D}\tilde{\mathbf{b}}(t) &= 0 \\ \Leftrightarrow \mathsf{D}\tilde{\mathbf{b}}(t) &= 0. \end{aligned}$$

□

4 Semi-discrete Hamiltonian Structure

In the previous section, we have obtained a spatial semi-discretisation of the Vlasov–Maxwell system. Let us now analyse the structure of this semi-discretisation.

4.1 Equations of Motion and Poisson Matrix

From the discretisation of the Vlasov–Maxwell system (3.3), (3.8a) and (3.9a) we get the following equations of motion with hybrid particle push:

$$\begin{aligned}
\dot{\boldsymbol{\Xi}} &= \mathbb{N}^\top(\boldsymbol{\Xi})\mathbf{V}, \\
\dot{\mathbf{V}} &= \mathbb{W}_{\substack{q \\ m}}\mathbb{N}(\boldsymbol{\Xi})\left(\tilde{\mathbb{\Lambda}}^1(\boldsymbol{\Xi})\tilde{\mathbf{e}} + (\mathbb{N}^\top(\boldsymbol{\Xi})\mathbf{V}) \times \tilde{\mathbb{\Lambda}}^2(\boldsymbol{\Xi})\tilde{\mathbf{b}}\right), \\
\tilde{\mathsf{M}}_1\dot{\tilde{\mathbf{e}}} &= \mathsf{C}^\top\tilde{\mathsf{M}}_2\tilde{\mathbf{b}} - \tilde{\mathbb{\Lambda}}^1(\boldsymbol{\Xi})^\top\mathbb{N}^\top(\boldsymbol{\Xi})\mathbb{W}_q\mathbf{V}, \\
\dot{\tilde{\mathbf{b}}} &= -\mathsf{C}\tilde{\mathbf{e}},
\end{aligned} \tag{4.1}$$

where we denote by $\tilde{\mathbb{\Lambda}}^1(\boldsymbol{\Xi})$ the $3N_p \times 3N_1$ matrix with generic term $\tilde{\boldsymbol{\Lambda}}^1_I(\boldsymbol{\xi}_p)$ for $1 \leq p \leq N_p$ and $1 \leq I \leq 3N_1$. Furthermore, we introduce the $N_p \times N_0$ matrix $\tilde{\mathbb{\Lambda}}^0(\boldsymbol{\Xi})$ with generic term $\tilde{\Lambda}^0_i(\boldsymbol{\xi}_p)$ for $1 \leq p \leq N_p, 1 \leq i \leq N_0$. $\tilde{\mathbb{\Lambda}}^2(\boldsymbol{\Xi})$ and $\tilde{\mathbb{\Lambda}}^3(\boldsymbol{\Xi})$ are defined accordingly.

The corresponding divergence constraints are discretised in (3.8b) and (3.9b) as

$$\begin{aligned}
\mathsf{G}^\top\tilde{\mathsf{M}}_1\tilde{\mathbf{e}} &= -\mathbb{W}_q\tilde{\mathbb{\Lambda}}^0(\boldsymbol{\Xi})^\top\mathbb{1}_{N_p}, \\
\mathsf{D}\tilde{\mathbf{b}} &= 0.
\end{aligned} \tag{4.2}$$

Let us consider the semi-discrete Hamiltonian for the system (4.1).

Proposition 4.1. *The semi-discrete Hamiltonian can be written in matrix notation as*

$$\tilde{\mathcal{H}}_h = \frac{1}{2}\mathbf{V}^\top\mathbb{W}_m\mathbf{V} + \frac{1}{2}\tilde{\mathbf{e}}^\top\tilde{\mathsf{M}}_1\tilde{\mathbf{e}} + \frac{1}{2}\tilde{\mathbf{b}}^\top\tilde{\mathsf{M}}_2\tilde{\mathbf{b}}. \tag{4.3}$$

Proof. We discretise the Hamiltonian of the Vlasov–Maxwell system (2.4) in curvilinear coordinates,

$$\tilde{\mathcal{H}} = \sum_s \frac{m_s}{2}\int |\mathbf{v}|^2 \tilde{f}_s(\boldsymbol{\xi}, \mathbf{v}, t)|J_F(\boldsymbol{\xi})|\ \mathrm{d}\boldsymbol{\xi}\,\mathrm{d}\mathbf{v} + \frac{1}{2}\int \left(|N(\boldsymbol{\xi})\tilde{\mathbf{E}}(\boldsymbol{\xi})|^2 + \left|\frac{DF(\boldsymbol{\xi})}{J_F(\boldsymbol{\xi})}\tilde{\mathbf{B}}(\boldsymbol{\xi})\right|^2\right)|J_F(\boldsymbol{\xi})|\,\mathrm{d}\boldsymbol{\xi},$$

by inserting the ansatz for the discrete particle distribution function (3.1) and the basis repre-

sentation of the discrete fields (3.7a),(3.7b),

$$\tilde{\mathcal{H}}_h = \sum_{p=1}^{N_p} \frac{m_p}{2}\mathbf{v}_p^2 + \frac{1}{2}\int \tilde{\mathbf{e}}^\top \tilde{\mathbf{\Lambda}}^1(\boldsymbol{\xi})^\top N(\boldsymbol{\xi})^\top N(\boldsymbol{\xi})\tilde{\mathbf{\Lambda}}^1(\boldsymbol{\xi})\tilde{\mathbf{e}}|J_F(\boldsymbol{\xi})|\,\mathrm{d}\boldsymbol{\xi} + \frac{1}{2}\int \tilde{\mathbf{b}}^\top \tilde{\mathbf{\Lambda}}^2(\boldsymbol{\xi})^\top \frac{DF(\boldsymbol{\xi})^\top}{J_F(\boldsymbol{\xi})}\frac{DF(\boldsymbol{\xi})}{J_F(\boldsymbol{\xi})}\tilde{\mathbf{\Lambda}}^2(\boldsymbol{\xi})\tilde{\mathbf{b}}|J_F(\boldsymbol{\xi})|\,\mathrm{d}\boldsymbol{\xi}.$$

Afterwards, we use the definition of the mass matrices (3.6) to obtain the proposition. □

Then, the derivative of the discrete Hamiltonian is computed as

$$D\tilde{\mathcal{H}}_h(\tilde{\mathbf{u}}) = (0, \mathbb{W}_m\mathbf{V}, \tilde{\mathsf{M}}_1\tilde{\mathbf{e}}, \tilde{\mathsf{M}}_2\tilde{\mathbf{b}})^\top.$$

Next, we consider the discretisation of the Poisson bracket, which is expressed as

$$\{\mathcal{F}_h(\tilde{\mathbf{u}}), \mathcal{G}_h(\tilde{\mathbf{u}})\}_d = D\mathcal{F}_h(\tilde{\mathbf{u}})^\top \mathbb{J}(\tilde{\mathbf{u}})D\mathcal{G}_h(\tilde{\mathbf{u}}), \tag{4.4}$$

where $\mathbb{J}$ is the discrete Poisson matrix. In particular, setting $\mathcal{F}_h(\tilde{\mathbf{u}}) = \tilde{\mathbf{u}}$ and $\mathcal{G}_h(\tilde{\mathbf{u}}) = \tilde{\mathcal{H}}_h$, the time evolution of the equations of motion is given by the discrete analogon of (2.3),

$$\frac{\mathrm{d}\tilde{\mathbf{u}}}{\mathrm{d}t} = \mathbb{J}(\tilde{\mathbf{u}})D\tilde{\mathcal{H}}_h. \tag{4.5}$$

This should correspond to the equations of motion (4.1). Therefore, the Poisson matrix needs to have the following form:

$$\mathbb{J} = \begin{pmatrix} 0 & \mathbb{N}^\top(\mathbf{\Xi})\mathbb{W}_m^{-1} & 0 & 0 \\ -\mathbb{W}_m^{-1}\mathbb{N}(\mathbf{\Xi}) & \mathbb{W}_{\frac{q}{m}}\mathbb{N}(\mathbf{\Xi})\tilde{\mathbb{B}}(\mathbf{\Xi}, \tilde{\mathbf{b}})\mathbb{N}^\top(\mathbf{\Xi})\mathbb{W}_m^{-1} & \mathbb{W}_{\frac{q}{m}}\mathbb{N}(\mathbf{\Xi})\tilde{\mathbb{\Lambda}}^1(\mathbf{\Xi})\tilde{\mathsf{M}}_1^{-1} & 0 \\ 0 & -\tilde{\mathsf{M}}_1^{-1}\tilde{\mathbb{\Lambda}}^1(\mathbf{\Xi})^\top\mathbb{N}^\top(\mathbf{\Xi})\mathbb{W}_{\frac{q}{m}} & 0 & \tilde{\mathsf{M}}_1^{-1}\mathsf{C}^\top \\ 0 & 0 & -\mathsf{C}\tilde{\mathsf{M}}_1^{-1} & 0 \end{pmatrix}, \tag{4.6}$$

where $\tilde{\mathbb{B}}(\mathbf{\Xi}, \tilde{\mathbf{b}})$ is a $3N_p \times 3N_p$ block matrix with generic block

$$\hat{\tilde{B}}_h(\boldsymbol{\xi}_p, t) = \sum_{i=1}^{N_2} \begin{pmatrix} 0 & \tilde{b}_{i,3}(t)\tilde{\Lambda}_i^{2,3}(\boldsymbol{\xi}_p) & -\tilde{b}_{i,2}(t)\tilde{\Lambda}_i^{2,2}(\boldsymbol{\xi}_p) \\ -\tilde{b}_{i,3}(t)\tilde{\Lambda}_i^{2,3}(\boldsymbol{\xi}_p) & 0 & \tilde{b}_{i,1}(t)\tilde{\Lambda}_i^{2,1}(\boldsymbol{\xi}_p) \\ \tilde{b}_{i,2}(t)\tilde{\Lambda}_i^{2,2}(\boldsymbol{\xi}_p) & -\tilde{b}_{i,1}(t)\tilde{\Lambda}_i^{2,1}(\boldsymbol{\xi}_p) & 0 \end{pmatrix}. \tag{4.7}$$

4.2 Discrete Poisson Bracket

In this section, we show that, with this form of the Poisson matrix (4.6), (4.4) indeed defines a discrete Poisson bracket.

Theorem 4.1. *The differential operator* $\{f, g\}_d = Df^\top \mathbb{J} Dg$ *forms a discrete Poisson bracket.*

Proof. The Poisson matrix $\mathbb{J}$ is obviously antisymmetric and the bilinearity and Leibniz's rule follow trivially from the form (4.4):

- Bilinearity: $\{c_1 f_1 + c_2 f_2, g\}_d = c_1 Df_1 \mathbb{J} Dg + c_2 Df_2 \mathbb{J} Dg = c_1\{f_1, g\}_d + c_2\{f_2, g\}_d$,
- Leibniz's rule: $\{f, gh\}_d = Df \mathbb{J} D(gh) = Df \mathbb{J} Dgh + Df \mathbb{J} Dhg = \{f, g\}_d h + \{f, h\}_d g$.

So, it is only left to prove that the Poisson matrix satisfies the Jacobi identity.

The matrix $\mathbb{J}$ satisfies the Jacobi identity if and only if the following condition holds:

$$\sum_l \left(\frac{\partial \mathbb{J}_{ij}(\tilde{\mathbf{u}})}{\partial u_l} \mathbb{J}_{lk}(\tilde{\mathbf{u}}) + \frac{\partial \mathbb{J}_{jk}(\tilde{\mathbf{u}})}{\partial u_l} \mathbb{J}_{li}(\tilde{\mathbf{u}}) + \frac{\partial \mathbb{J}_{ki}(\tilde{\mathbf{u}})}{\partial u_l} \mathbb{J}_{ll}(\tilde{\mathbf{u}}) \right) = 0 \quad \forall i, j, k,$$

where i, j, k, l run from 1 to $6N_p + 3N_1 + 3N_2$. The Poisson matrix $\mathbb{J}$ has the following block-structure:

$$\mathbb{J} = \begin{pmatrix} 0 & J_{12}(\boldsymbol{\Xi}) & 0 & 0 \\ J_{21}(\boldsymbol{\Xi}) & J_{22}(\boldsymbol{\Xi}, \tilde{\mathbf{b}}) & J_{23}(\boldsymbol{\Xi}) & 0 \\ 0 & J_{32}(\boldsymbol{\Xi}) & 0 & J_{34} \\ 0 & 0 & J_{43} & 0 \end{pmatrix}.$$

Therefore, many combinations of indices are trivially zero. In particular, the matrix only depends on $\boldsymbol{\Xi}$ and $\tilde{\mathbf{b}}$ and hence the derivatives are only non-zero if $l \in [1, 3N_p]$ or $l \in [6N_p + 3N_1 + 1, 6N_p + 3N_1 + 3N_2]$. Moreover, we need to find combinations of i, j, k (or permutations of these) for which both $\mathcal{J}_{ij}$ and $\mathcal{J}_{l,k}$ are non-vanishing. For $l \in [1, 3N_p]$, this only leaves the options $i, j, k \in [3N_p+1, 6N_p]$ and the option $i \in [1, 3N_p]$ and $j, k \in [3N_p+1, 6N_p]$. However, if $l \in [6N_p + 3N_1 + 1, 6N_p + 3N_1 + 3N_2]$, we only have $i, j \in [3N_p + 1, 6N_p]$ and $k \in [6N_p + 1, 6N_p + 3N_1]$. Let us now consider each of these three non-trivial terms one-by-one.

Let first $i \in [1, 3N_p]$ and $j, k \in [3N_p + 1, 6N_p]$. Then, we obtain the condition

$$\sum_{l=1}^{3N_p} \left(\frac{\partial \mathcal{J}_{12}(\boldsymbol{\Xi})_{ij}}{\partial \Xi_l} (\mathcal{J}_{12})_{lk}(\boldsymbol{\Xi}) + \frac{\partial \mathcal{J}_{21}(\boldsymbol{\Xi})_{ki}}{\partial \Xi_l} (\mathcal{J}_{12})_{lj}(\boldsymbol{\Xi}) \right) = 0.$$

Inserting the expressions of the terms of the Poisson matrix, we get

$$\sum_{l=1}^{3N_p} \left(\frac{\partial (\mathbb{N}^\top(\boldsymbol{\Xi}) \mathbb{W}_m^{-1})_{ij}}{\partial \Xi_l} (\mathbb{N}^\top(\boldsymbol{\Xi}) \mathbb{W}_m^{-1})_{lk} + \frac{\partial (-\mathbb{W}_m^{-1} \mathbb{N}(\boldsymbol{\Xi}))_{ki}}{\partial \Xi_l} (\mathbb{N}^\top(\boldsymbol{\Xi}) \mathbb{W}_m^{-1})_{lj} \right).$$

Since $\mathbb{N}$ is a block diagonal matrix, the terms are only non-zero if all four indices belong to the same particle. Additionally, we can leave out the $\mathbb{W}_m$ term because it is diagonal and has the same entry for each component of one particle. Using the definition of the transpose inverse Jacobian matrix, $\mathbb{N}_{ij} = \frac{\partial \Xi_j}{\partial X_i}$, we are left with the following expression:

$$\sum_{l=1}^{3N_p} \left(\frac{\partial}{\partial \Xi_l} \frac{\partial \Xi_i}{\partial X_j} \frac{\partial \Xi_l}{\partial X_k} - \frac{\partial}{\partial \Xi_l} \frac{\partial \Xi_i}{\partial X_k} \frac{\partial \Xi_l}{\partial X_j} \right) = \frac{\partial^2 \Xi_i}{\partial X_k \partial X_j} - \frac{\partial^2 \Xi_i}{\partial X_j \partial X_k} = 0,$$

where we have used the symmetry of second derivatives by Schwarz's theorem in the last step.

Next, let $i, j, k \in [3N_p + 1, 6N_p]$. This yields the following expression to show:

$$\sum_{l=1}^{3N_p} \left(\frac{\partial \mathcal{J}_{22}(\boldsymbol{\Xi})_{ij}}{\partial \Xi_l} \mathcal{J}_{12}(\boldsymbol{\Xi})_{lk} + \frac{\partial \mathcal{J}_{22}(\boldsymbol{\Xi})_{jk}}{\partial \Xi_l} \mathcal{J}_{12}(\boldsymbol{\Xi})_{li} + \frac{\partial \mathcal{J}_{22}(\boldsymbol{\Xi})_{ki}}{\partial \Xi_l} \mathcal{J}_{12}(\boldsymbol{\Xi})_{lj} \right) = 0.$$

With the expressions of the Poisson matrix we obtain

$$\begin{aligned} \sum_{l=1}^{3N_p} [& \frac{\partial (\mathbb{W}_q \mathbb{N}(\boldsymbol{\Xi}) \tilde{\mathbb{B}}(\boldsymbol{\Xi}, \tilde{\mathbf{b}}) \mathbb{N}^\top(\boldsymbol{\Xi}))_{ij}}{\partial \Xi_l} (\mathbb{N}^\top(\boldsymbol{\Xi}))_{lk} \\ & + \frac{\partial (\mathbb{W}_q \mathbb{N}(\boldsymbol{\Xi}) \tilde{\mathbb{B}}(\boldsymbol{\Xi}, \tilde{\mathbf{b}}) \mathbb{N}^\top(\boldsymbol{\Xi}))_{jk}}{\partial \Xi_l} (\mathbb{N}^\top(\boldsymbol{\Xi}))_{li} \\ & + \frac{\partial (\mathbb{W}_q \mathbb{N}(\boldsymbol{\Xi}) \tilde{\mathbb{B}}(\boldsymbol{\Xi}, \tilde{\mathbf{b}}) \mathbb{N}^\top(\boldsymbol{\Xi}))_{ki}}{\partial \Xi_l} (\mathbb{N}^\top(\boldsymbol{\Xi}))_{lj}]. \end{aligned}$$

Since $\mathbb{W}_m$ is a diagonal matrix, each term contains $(\mathbb{W}_m^{-1})_{ii} (\mathbb{W}_m^{-1})_{jj} (\mathbb{W}_m^{-1})_{kk}$, which therefore is left out. Moreover, both $\mathbb{N}$ and $\tilde{\mathbb{B}}$ are block-diagonal. So, the terms are only non-zero if all four indices belong to the same particle. Let us denote the corresponding particle index by p and introduce $\mu, \nu, \sigma \in \{1, 2, 3\}$ as $i - 3N_p = 3(p-1) + \mu$, $j - 3N_p = 3(p-1) + \nu$, $k - 3N_p = 3(p-1) + \sigma$. In this case, we also have $(\mathbb{W}_q)_{ii} = (\mathbb{W}_q)_{jj} = (\mathbb{W}_q)_{kk}$ so that we can leave out this matrix as well. Then, we use the definition of $\mathbb{N}^\top$ and the following identity for the generic block $\tilde{B}(\boldsymbol{\xi}_p)$ of $\tilde{\mathbb{B}}$:

$$\hat{B}_h = \mathbb{I} \times \mathbf{B}_h = \mathbb{I} \times \frac{DF}{J_F} \tilde{\mathbf{B}}_h = N \left((N^\top) \times \tilde{\mathbf{B}}_h \right) = N \hat{\tilde{B}}_h N^\top.$$

This leaves us with

$$\sum_{\eta=1}^{3}\left(\frac{\partial\hat{B}_h(\mathbf{x}_p)_{\mu\nu}}{\partial\xi_{p,\eta}}\frac{\partial\xi_{p,\eta}}{\partial x_{p,\sigma}}+\frac{\partial\hat{B}_h(\mathbf{x}_p)_{\nu\sigma}}{\partial\xi_{p,\eta}}\frac{\partial\xi_{p,\eta}}{\partial x_{p,\mu}}+\frac{\partial\hat{B}_h(\mathbf{x}_p)_{\sigma\mu}}{\partial\xi_{p,\eta}}\frac{\partial\xi_{p,\eta}}{\partial x_{p,\nu}}\right)$$
$$=\left(\frac{\partial\hat{B}_h(\mathbf{x}_p)_{\mu\nu}}{\partial x_{p,\sigma}}+\frac{\partial\hat{B}_h(\mathbf{x}_p)_{\nu\sigma}}{\partial x_{p,\mu}}+\frac{\partial\hat{B}_h(\mathbf{x}_p)_{\sigma\mu}}{\partial x_{p,\nu}}\right).$$

If $\mu=\nu=\sigma$, we get the diagonal terms that are zero and if two indices are the same, say $\mu=\nu$, we get $\frac{\partial\hat{B}_h(\mathbf{x}_p)_{\mu\sigma}}{\partial x_{p,\mu}}+\frac{\partial\hat{B}_h(\mathbf{x}_p)_{\sigma\mu}}{\partial x_{p,\mu}}=0$ due to the antisymmetry of $\hat{B}_h$. Last, if the three indices are all different, we get

$$\pm\left(\frac{\partial\hat{B}_h(\mathbf{x}_p)_{12}}{\partial x_{p,3}}+\frac{\partial\hat{B}_h(\mathbf{x}_p)_{23}}{\partial x_{p,1}}+\frac{\partial\hat{B}_h(\mathbf{x}_p)_{31}}{\partial x_{p,2}}\right)=\pm\operatorname{div}\mathbf{B}_h(\mathbf{x}_p).$$

Since $\operatorname{div}\mathbf{B}_h=0$ is guaranteed over time by the construction of the discrete de Rham complex when it is initially satisfied, this is also zero.

Finally, we consider the case that $i,j\in[3N_p+1,6N_p]$, $k\in[6N_p+1,6N_p+3N_1]$ yielding

$$\sum_{l=1}^{3N_p}\left(\frac{\partial\mathcal{J}_{23}(\boldsymbol{\Xi})_{ik}}{\partial\Xi_l}\mathcal{J}_{12}(\boldsymbol{\Xi})_{lj}+\frac{\partial\mathcal{J}_{32}(\boldsymbol{\Xi})_{kj}}{\partial\Xi_l}\mathcal{J}_{12}(\Xi)_{li}\right)+\sum_{A=1}^{3N_2}\left(\frac{\partial\mathcal{J}_{22}(\tilde{\mathbf{b}})_{ij}}{\partial\tilde{b}_A}(\mathcal{J}_{43})_{Ak}\right)=0.$$

With the expressions of the Poisson matrix, we obtain

$$\sum_{l=1}^{3N_p}\left(\frac{\partial(\mathbb{W}_{\frac{q}{m}}(\mathbb{N}\tilde{\mathbb{\Lambda}}^1)(\boldsymbol{\Xi})\tilde{\mathsf{M}}_1^{-1})_{ik}}{\partial\Xi_l}(\mathbb{N}^\top(\boldsymbol{\Xi})\mathbb{W}_m^{-1})_{lj}+\frac{\partial(-\tilde{\mathsf{M}}_1^{-1}(\mathbb{N}\tilde{\mathbb{\Lambda}}^1)^\top(\boldsymbol{\Xi})\mathbb{W}_{\frac{q}{m}})_{kj}}{\partial\Xi_l}(\mathbb{N}^\top(\boldsymbol{\Xi})\mathbb{W}_m^{-1})_{li}\right)$$
$$+\sum_{A=1}^{3N_2}\left(\frac{\partial(\mathbb{W}_{\frac{q}{m}}\mathbb{N}(\boldsymbol{\Xi})\tilde{\mathbb{B}}(\boldsymbol{\Xi},\tilde{\mathbf{b}})\mathbb{N}^\top(\boldsymbol{\Xi})\mathbb{W}_m^{-1})_{ij}}{\partial\tilde{b}_A}(-\mathsf{C}\tilde{\mathsf{M}}_1^{-1})_{Ak}\right).$$

We contract this with $\mathbb{W}_m$ for indices i,j, $\tilde{\mathsf{M}}_1$ on index k and $\mathbb{W}_q^{-1}$ on index i,

$$\sum_{l=1}^{3N_p}\frac{\partial((\mathbb{N}\tilde{\mathbb{\Lambda}}^1)(\boldsymbol{\Xi}))_{ik}}{\partial\Xi_l}(\mathbb{N}^\top(\boldsymbol{\Xi}))_{lj}-\frac{\partial((\mathbb{N}\tilde{\mathbb{\Lambda}}^1)^\top(\boldsymbol{\Xi})\mathbb{W}_q)_{kj}}{\partial\Xi_l}(\mathbb{N}^\top(\boldsymbol{\Xi})\mathbb{W}_q^{-1})_{li}$$
$$=\sum_{A=1}^{3N_2}\frac{\partial(\mathbb{N}(\boldsymbol{\Xi})\tilde{\mathbb{B}}(\boldsymbol{\Xi},\tilde{\mathbf{b}})\mathbb{N}^\top(\boldsymbol{\Xi}))_{ij}}{\partial\tilde{b}_A}(\mathsf{C})_{Ak}.$$

This is possible as $\mathbb{W}_m,\mathbb{W}_q^{-1}$ and $\tilde{\mathsf{M}}_1$ are constant, symmetric and positive definite. Moreover, we see again that i and j belong to the same particle due to the block-diagonal structure of the terms. Therefore, we can also contract $\mathbb{W}_q$ on index j and $\mathbb{W}_q^{-1}$ on index i. Let us introduce again the corresponding particle index p and $\mu,\nu\in\{1,2,3\}$ such that $i-3N_p=3(p-1)+\mu$ and $j-3N_p=3(p-1)+\nu$. For these index combinations, the sum over the particle positions

breaks down to

$$\sum_{l=1}^{3N_p}\left(\frac{\partial((\mathbb{N}\tilde{\mathbb{\Lambda}}^1)(\boldsymbol{\Xi}))_{ik}}{\partial\Xi_l}(\mathbb{N}^\top(\boldsymbol{\Xi}))_{lj}-\frac{\partial((\mathbb{N}\tilde{\mathbb{\Lambda}}^1)^\top(\boldsymbol{\Xi})\mathbb{W}_q)_{kj}}{\partial\Xi_l}(\mathbb{N}^\top(\boldsymbol{\Xi})\mathbb{W}_q^{-1})_{li}\right)$$
$$=\frac{\partial\boldsymbol{\Lambda}^1_{k,\mu}(\mathbf{x}_p)}{\partial x_{p,\nu}}-\frac{\partial\boldsymbol{\Lambda}^1_{k,\nu}(\mathbf{x}_p)}{\partial x_{p,\mu}}$$
$$=\begin{cases}0 & \text{if } \mu=\nu,\\ (\operatorname{curl}\boldsymbol{\Lambda}^1(\mathbf{x}_p))_{\sigma k} & \text{if } (\mu,\nu,\sigma) \text{ cyclic permutation of (1,2,3),}\\ -(\operatorname{curl}\boldsymbol{\Lambda}^1(\mathbf{x}_p))_{\sigma k} & \text{if } (\mu,\nu,\sigma) \text{ non-cyclic permutation of (1,2,3),}\end{cases}$$

where we used $\mathbb{N}\tilde{\mathbb{\Lambda}}^1 = \mathbb{\Lambda}^1$ and the chain rule in the first equality. For the derivative with respect to $\tilde{\mathbf{b}}$, we use expression (4.7) for the block of $\tilde{\mathbb{B}}$ belonging to particle p to find

$$\sum_{A=1}^{3N_2}\frac{\partial\hat{\tilde{B}}_h(\boldsymbol{\xi}_p)}{\partial\tilde{b}_A}=\sum_{A=1}^{N_2}\hat{\tilde{\boldsymbol{\Lambda}}}_A(\boldsymbol{\xi}_p),$$

where

$$\hat{\tilde{\boldsymbol{\Lambda}}}_A(\boldsymbol{\xi}_p)=\begin{pmatrix}0 & \tilde{\Lambda}^{2,3}_A(\boldsymbol{\xi}_p) & -\tilde{\Lambda}^{2,2}_A(\boldsymbol{\xi}_p)\\ -\tilde{\Lambda}^{2,3}_A(\boldsymbol{\xi}_p) & 0 & \tilde{\Lambda}^{2,1}_A(\boldsymbol{\xi}_p)\\ \tilde{\Lambda}^{2,2}_A(\boldsymbol{\xi}_p) & -\tilde{\Lambda}^{2,1}_A(\boldsymbol{\xi}_p) & 0\end{pmatrix}.$$

It holds that $\hat{\boldsymbol{\Lambda}}_A = N\hat{\tilde{\boldsymbol{\Lambda}}}_A N^\top$ in the same way as $\hat{\tilde{B}}_h = N\hat{\tilde{B}}_h N^\top$. Hence, we get

$$\sum_{A=1}^{3N_2}\frac{\partial(\mathbb{N}(\boldsymbol{\Xi})\tilde{\mathbb{B}}(\boldsymbol{\Xi},\tilde{\mathbf{b}})\mathbb{N}^\top(\boldsymbol{\Xi}))}{\partial\tilde{b}_A}=\sum_{A=1}^{N_2}\hat{\mathbb{\Lambda}}_A(\mathbf{X}).$$

Now, for $i-3N_p = 3(p-1)+\mu$ and $j-3N_p = 3(p-1)+\nu$, we need the component (μ,ν), which is zero if $\mu=\nu$ and $\boldsymbol{\Lambda}^2_{A,\sigma}$ if (μ,ν,σ) is a cyclic permutation of $(1,2,3)$ (or the negative if the permutation is non-cyclic). This yields

$$\sum_{A=1}^{3N_2}\frac{\partial(\mathbb{N}(\boldsymbol{\Xi})\tilde{\mathbb{B}}(\boldsymbol{\Xi},\tilde{\mathbf{b}})\mathbb{N}^\top(\boldsymbol{\Xi}))_{ij}}{\partial\tilde{b}_A}(\mathsf{C})_{Ak}=\sum_{A=1}^{N_2}\hat{\mathbb{\Lambda}}_A(\mathbf{X})_{ij}(\mathsf{C})_{Ak}$$
$$=\begin{cases}0 & \text{if } \mu=\nu,\\ (\boldsymbol{\Lambda}^2(\mathbf{x}_p)\mathsf{C})_{\sigma k} & \text{if } (\mu,\nu,\sigma) \text{ cyclic permutation of (1,2,3),}\\ -(\boldsymbol{\Lambda}^2(\mathbf{x}_p)\mathsf{C})_{\sigma k} & \text{if } (\mu,\nu,\sigma) \text{ non-cyclic permutation of (1,2,3).}\end{cases}$$

Hence, the term vanishes due to the de Rham sequence properties of the basis. □

Since the conservation properties are tightly connected to the Poisson structure, preserving the Jacobi identity with the numerical approximation results in numerical conservation laws.

4.3 Discrete Casimir Invariants

One class of functionals that are conserved over time in Hamiltonian systems are so-called Casimir invariants, functionals that Poisson commute with all other functionals. In this section, we consider the discrete Casimir invariants of our discrete Poisson structure (4.1), i.e. functions $C(\tilde{\mathbf{u}})$ of our discrete dynamic variables $\tilde{\mathbf{u}} = (\mathbf{\Xi}, \mathbf{V}, \tilde{\mathbf{e}}, \tilde{\mathbf{b}})$ that satisfy

$$\{C, F\} = 0 \Leftrightarrow \mathbb{J}(\tilde{\mathbf{u}})DC(\tilde{\mathbf{u}}) = 0 \quad \forall F(\tilde{\mathbf{u}}).$$

First, we derive a general form for such discrete Casimir invariants and second, we show that the divergence constraints (4.2) are such discrete Casimir invariants and hence, conserved over time in our discretisation.

Proposition 4.1. *Let $C(\tilde{\mathbf{u}})$ be a discrete Poisson invariant of the system* (4.1) *with Poisson matrix* (4.6)*. Then, there exist $\bar{\mathbf{e}} \in \mathbb{R}^{N_0}$ and $\bar{\mathbf{b}} \in \mathbb{R}^{N_3}$ such that*

$$C(\tilde{\mathbf{u}}) = \bar{\mathbf{e}}^\top(\tilde{\Lambda}^0(\mathbf{\Xi})^\top \mathbb{W}_q \mathbb{1}_{N_p} + \mathsf{G}^\top \tilde{\mathsf{M}}_1 \tilde{\mathbf{e}}) + \bar{\mathbf{b}}^\top \mathsf{D}\tilde{\mathbf{b}}. \tag{4.8}$$

Proof. Let us consider the equation $\mathbb{J}(\tilde{\mathbf{u}})DC(\tilde{\mathbf{u}}) = 0$ line by line. The first line reads

$$\mathbb{N}^\top(\mathbf{\Xi})\mathbb{W}_m^{-1} D_{\mathbf{V}} C = 0.$$

Therefore, C must be independent of $\mathbf{V}$. Next, we consider the third line, already assuming $D_{\mathbf{V}}C = 0$, which yields

$$\tilde{\mathsf{M}}_1^{-1}\mathsf{C}^\top D_{\tilde{\mathbf{b}}} C = 0.$$

Hence, it follows that $D_{\tilde{\mathbf{b}}}C \in \ker(\mathsf{C}^\top)$. Due to the complex property of our de Rham sequence, there exist a $\bar{\mathbf{b}} \in \mathbb{R}^{N_3}$ such that $D_{\tilde{\mathbf{b}}}C = \mathsf{D}^\top \bar{\mathbf{b}}$. Analogously, the fourth line,

$$\mathsf{C}\tilde{\mathsf{M}}_1^{-1} D_{\tilde{\mathbf{e}}} C = 0, \text{ i.e. } \tilde{\mathsf{M}}_1^{-1} D_{\tilde{\mathbf{e}}} C \in \ker(\mathsf{C}),$$

yields due to the complex property that there exists a $\bar{\mathbf{e}} \in \mathbb{R}^{N_0}$ such that $D_{\tilde{\mathbf{e}}}C = \tilde{\mathsf{M}}_1 \mathsf{G}\bar{\mathbf{e}}$. Finally, the second line of the Poisson matrix yields the following expression for $D_{\mathbf{\Xi}}C$:

$$D_{\mathbf{\Xi}} C = \mathbb{W}_q \tilde{\Lambda}^1(\mathbf{\Xi})\tilde{\mathsf{M}}_1^{-1} D_{\tilde{\mathbf{e}}} C = \mathbb{W}_q \tilde{\Lambda}^1(\mathbf{\Xi})\mathsf{G}\bar{\mathbf{e}} = \mathbb{W}_q \operatorname{grad} \tilde{\Lambda}^0(\mathbf{\Xi})\bar{\mathbf{e}}, \tag{4.9}$$

where we used again the complex property for the last equality. Putting everything together,

we get the general form (4.8) of a discrete Casimir invariant. □

As a consequence the divergence constraints (4.2) are conserved over time.

Corrolary 4.2. *The discrete electric Gauss law,* $\mathsf{G}^\top \tilde{\mathsf{M}}_1 \tilde{\mathbf{e}} - \mathbb{W}_q \tilde{\mathbb{\Lambda}}^0(\boldsymbol{\Xi})^\top \mathbb{1}_{N_p} = 0$*, is conserved over time if it is satisfied initially.*

Proof. This follows immediately from Proposition 4.1 setting $\bar{\mathbf{e}} = \mathbb{1}_{N_0}$ and $\bar{\mathbf{b}} = \mathbb{0}_{N_3}$, since this leads to the discrete Casimir $\mathsf{G}^\top \tilde{\mathsf{M}}_1 \tilde{\mathbf{e}} - \mathbb{W}_q \tilde{\mathbb{\Lambda}}^0(\boldsymbol{\Xi})^\top \mathbb{1}_{N_p}$. □

Remark 4.3. *The discrete magnetic Gauss law,* $\mathsf{D}\tilde{\mathbf{b}} = 0$*, follows from Proposition 4.1 for* $\bar{\mathbf{e}} = \mathbb{0}_{N_0}$ *and* $\bar{\mathbf{b}} = \mathbb{1}_{N_3}$*. It can be referred to as "pseudo-Casimir", since it satisfies the properties of a Casimir but it is a requirement for the Jacobi identity to hold.*

5 Lagrangian Formulation of the Vlasov–Maxwell System in Curvilinear Coordinates

5.1 Equations of Motion

For this chapter, we consider the Lagrangian (2.5) for one species in discrete form,

$$\begin{aligned}\mathcal{L}_{f_h} = &\int f_h(\mathbf{x},\mathbf{v})[q\mathbf{A}_h(t,\mathbf{x}) + m\mathbf{v}]\cdot\dot{\mathbf{x}} - \frac{1}{2}mv^2 - q\Phi_h(t,\mathbf{x})]\,\mathrm{d}\mathbf{x}\,\mathrm{d}\mathbf{v} \\ &+ \frac{1}{2}\int_\Omega \left|-\nabla\Phi_h(t,\mathbf{x}) - \frac{\partial\mathbf{A}_h(t,\mathbf{x})}{\partial t}\right|^2 \mathrm{d}\mathbf{x} - \frac{1}{2}\int_\Omega |\nabla\times\mathbf{A}_h(t,\mathbf{x})|^2\,\mathrm{d}\mathbf{x}.\end{aligned} \tag{5.1}$$

Theorem 5.1. *The Lagrangian* (5.1) *under coordinate transformation leads to the same equations of motion as in* (4.1) *and* (4.2)*.*

Proof. We start by inserting the coordinate transformation, $F(\boldsymbol{\xi}) = \mathbf{x}$, into the discrete Lagrangian and use the transformation rule (2.16) for the integrals. The scalar potential $\tilde{\Phi}_h$ is described as a 0-form and the vector potential $\tilde{\mathbf{A}}_h$ as a 1-form, for which we use the Piola transform (2.14),

$$\begin{aligned}\mathcal{L}_{\tilde{f}_h} = &\int \tilde{f}_h(\boldsymbol{\xi},\mathbf{v})\left[\Big(qN(\boldsymbol{\xi})\tilde{\mathbf{A}}_h(\boldsymbol{\xi},t) + m\mathbf{v}\Big)\cdot DF(\boldsymbol{\xi})\dot{\boldsymbol{\xi}} - \frac{1}{2}mv^2 - q\tilde{\Phi}_h(\boldsymbol{\xi},t)\right]|J_F(\boldsymbol{\xi})|\,\mathrm{d}\boldsymbol{\xi}\,\mathrm{d}\mathbf{v} \\ &+ \frac{1}{2}\int\left(\left|-N(\boldsymbol{\xi})\nabla_{\boldsymbol{\xi}}\tilde{\Phi}_h(\boldsymbol{\xi},t) - N(\boldsymbol{\xi})\frac{\partial\tilde{\mathbf{A}}_h(\boldsymbol{\xi},t)}{\partial t}\right|^2 - \left|\frac{DF(\boldsymbol{\xi})}{J_F(\boldsymbol{\xi})}\nabla_{\boldsymbol{\xi}}\boldsymbol{\xi}\times\tilde{\mathbf{A}}_h(\xi,t)\right|^2\right)|J_F(\boldsymbol{\xi})|\,\mathrm{d}\boldsymbol{\xi}.\end{aligned}$$

Next, we insert the discrete particle distribution function,

$$\tilde{f}_h(\boldsymbol{\xi},\mathbf{v}) := \sum_{p=1}^{N_p}\omega_p\frac{\delta(\boldsymbol{\xi}-\boldsymbol{\xi}_p)}{|J_F(\boldsymbol{\xi})|}\delta(\mathbf{v}-\mathbf{v}_p),$$

and obtain

$$\begin{aligned}\mathcal{L} = &\sum_{p=1}^{N_p}\omega_p\left[\Big(q_pN(\boldsymbol{\xi}_p)\tilde{\mathbf{A}}_h(\boldsymbol{\xi}_p,t) + m_p\mathbf{v}_p\Big)\cdot DF(\boldsymbol{\xi}_p)\dot{\boldsymbol{\xi}}_p - \frac{1}{2}m_p\mathbf{v}_p^2 - q_p\tilde{\Phi}_h(\boldsymbol{\xi}_p,t)\right] \\ &+ \frac{1}{2}\int\left|-N(\boldsymbol{\xi})\nabla_{\boldsymbol{\xi}}\tilde{\Phi}_h(\boldsymbol{\xi},t) - N(\boldsymbol{\xi})\dot{\tilde{\mathbf{A}}}_h(\boldsymbol{\xi},t)\right|^2|J_F(\boldsymbol{\xi})|\,\mathrm{d}\boldsymbol{\xi} \\ &+ \frac{1}{2}\int -\left|\frac{DF(\boldsymbol{\xi})}{J_F(\boldsymbol{\xi})}\nabla_{\boldsymbol{\xi}}\times\tilde{\mathbf{A}}_h(\boldsymbol{\xi},t)\right|^2|J_F(\boldsymbol{\xi})|\,\mathrm{d}\boldsymbol{\xi}.\end{aligned} \tag{5.2}$$

Then, we use the finite element representation of the potentials in their respective basis,

$$\tilde{\Phi}_h = \tilde{\Lambda}^0(\boldsymbol{\xi})\tilde{\boldsymbol{\phi}}(t), \quad \tilde{\mathbf{A}}_h = \tilde{\boldsymbol{\Lambda}}^1(\boldsymbol{\xi})\tilde{\mathbf{a}}(t),$$

and the discrete derivative matrices from (3.4) to get

$$\begin{aligned}\mathcal{L} =& \sum_{p=1}^{N_p} \omega_p \left[\left(q_p N(\boldsymbol{\xi}_p)\tilde{\boldsymbol{\Lambda}}^1(\boldsymbol{\xi}_p)\tilde{\mathbf{a}}(t) + m_p \mathbf{v}_p \right) \cdot DF(\boldsymbol{\xi}_p)\dot{\boldsymbol{\xi}}_p - \frac{1}{2} m_p \mathbf{v}_p^2 - q_p \tilde{\Lambda}^0(\boldsymbol{\xi}_p)\tilde{\boldsymbol{\phi}}(t) \right] \\ &+ \frac{1}{2} \int \left| -N(\boldsymbol{\xi})\tilde{\boldsymbol{\Lambda}}^1(\boldsymbol{\xi})\mathsf{G}\tilde{\boldsymbol{\phi}}(t) - N(\boldsymbol{\xi})\tilde{\boldsymbol{\Lambda}}^1(\boldsymbol{\xi})\dot{\tilde{\mathbf{a}}}(t) \right|^2 |J_F(\boldsymbol{\xi})| \, \mathrm{d}\boldsymbol{\xi} \\ &+ \frac{1}{2} \int - \left| \frac{DF(\boldsymbol{\xi})}{J_F(\boldsymbol{\xi})} \tilde{\boldsymbol{\Lambda}}^2(\boldsymbol{\xi})\mathsf{C}\tilde{\mathbf{a}}(t) \right|^2 |J_F(\boldsymbol{\xi})| \, \mathrm{d}\boldsymbol{\xi}.\end{aligned}$$

Hence, the Lagrangian consists of three parts, $\mathcal{L} = \mathcal{L}_p(\boldsymbol{\xi}_p, \dot{\boldsymbol{\xi}}_p, \mathbf{v}_p, \tilde{\boldsymbol{\phi}}, \tilde{\mathbf{a}}) + \mathcal{L}_E(\tilde{\boldsymbol{\phi}}, \dot{\tilde{\mathbf{a}}}) + \mathcal{L}_B(\tilde{\mathbf{a}})$.

The equations of motions are given by the Euler–Lagrange equations,

$$\frac{\mathrm{d}}{\mathrm{d}t}\frac{\partial L}{\partial \dot{q}_i} = \frac{\partial L}{\partial q_i},$$

for the particle positions in phase space and the degrees of freedom of the potentials, $q = (\boldsymbol{\Xi}, \mathbf{V}, \tilde{\boldsymbol{\phi}}, \tilde{\mathbf{a}})^\top$.

We start with the particle velocity $\mathbf{v}_p$ for $p = 1, .., N_p$,

$$\begin{aligned}\frac{\partial \mathcal{L}}{\partial \mathbf{v}_p} &= \omega_p m_p DF(\boldsymbol{\xi}_p)\dot{\boldsymbol{\xi}}_p - \omega_p m_p \mathbf{v}_p, \\ \frac{\partial \mathcal{L}}{\partial \dot{\mathbf{v}}_p} &= 0.\end{aligned}$$

Putting these two together yields

$$\dot{\boldsymbol{\xi}}_p = N^\top(\boldsymbol{\xi}_p)\mathbf{v}_p \quad \forall p \in \{1, ..., N_p\}. \tag{5.3}$$

For the particle positions $\boldsymbol{\xi}_p$, we use the Einstein notation for summation over double indices to obtain

$$\begin{aligned}\frac{\mathrm{d}}{\mathrm{d}t}\frac{\partial \mathcal{L}}{\partial \dot{\boldsymbol{\xi}}_p} &= \frac{\mathrm{d}}{\mathrm{d}t}\left(\omega_p (q_p N(\boldsymbol{\xi}_p)\tilde{\boldsymbol{\Lambda}}^1(\boldsymbol{\xi}_p)\tilde{\mathbf{a}}(t) + m_p \mathbf{v}_p) \cdot DF(\boldsymbol{\xi}_p) \right) = \omega_p \frac{\mathrm{d}}{\mathrm{d}t}\left(q_p \tilde{\boldsymbol{\Lambda}}^1(\boldsymbol{\xi}_p)\tilde{\mathbf{a}}(t) + m_p \mathbf{v}_p \cdot DF(\boldsymbol{\xi}_p) \right) \\ &= \omega_p \left(q_p \tilde{\boldsymbol{\Lambda}}^1(\boldsymbol{\xi}_p)\dot{\tilde{\mathbf{a}}} + q_p D\tilde{\boldsymbol{\Lambda}}^1(\boldsymbol{\xi}_p)\tilde{\mathbf{a}}\dot{\boldsymbol{\xi}}_p + m_p DF^\top(\boldsymbol{\xi}_p)\dot{\mathbf{v}}_p + m_p \frac{\partial}{\partial \xi_{p,i}} \mathbf{v}_p^\top DF^\top(\boldsymbol{\xi}_p)\dot{\xi}_{p,i} \right), \\ \frac{\partial \mathcal{L}}{\partial \boldsymbol{\xi}_p} &= \omega_p \left(q_p (D\tilde{\boldsymbol{\Lambda}}^1(\boldsymbol{\xi}_p)\tilde{\mathbf{a}})^\top \dot{\boldsymbol{\xi}}_p - q_p \nabla_{\boldsymbol{\xi}} \tilde{\Lambda}^0(\boldsymbol{\xi}_p)\tilde{\boldsymbol{\phi}} + m_p \nabla_{\boldsymbol{\xi}} \mathbf{v}_p^\top DF(\boldsymbol{\xi}_p)\dot{\boldsymbol{\xi}}_p \right).\end{aligned}$$

Since $\frac{\partial}{\partial \xi_{p,i}} \mathbf{v}_p^\top DF(\boldsymbol{\xi}_p)\dot{\xi}_{p,i} = \nabla_{\boldsymbol{\xi}} \mathbf{v}_p^\top DF(\boldsymbol{\xi}_p)\dot{\boldsymbol{\xi}}_p$, the Euler–Lagrange equation takes the follow-

ing form:

$$q_p\tilde{\mathbf{\Lambda}}^1(\boldsymbol{\xi}_p)\dot{\tilde{\mathbf{a}}} + q_p D\tilde{\mathbf{\Lambda}}^1(\boldsymbol{\xi}_p)\tilde{\mathbf{a}}\dot{\boldsymbol{\xi}}_p + m_p DF^\top(\boldsymbol{\xi}_p)\dot{\mathbf{v}}_p = q_p(D\tilde{\mathbf{\Lambda}}^1(\boldsymbol{\xi}_p)\tilde{\mathbf{a}})^\top\dot{\boldsymbol{\xi}}_p - q_p\nabla_{\boldsymbol{\xi}}\tilde{\Lambda}^0(\boldsymbol{\xi}_p)\tilde{\boldsymbol{\phi}}.$$

We solve for $\dot{\mathbf{v}}_p$ and insert the equation (5.3) for $\dot{\boldsymbol{\xi}}_p$,

$$\dot{\mathbf{v}}_p = \frac{q_p}{m_p}N(\boldsymbol{\xi}_p)\left((D\tilde{\mathbf{\Lambda}}^1(\boldsymbol{\xi}_p)\tilde{\mathbf{a}})^\top N^\top(\boldsymbol{\xi}_p)\mathbf{v}_p - D\tilde{\mathbf{\Lambda}}^1(\boldsymbol{\xi}_p)\tilde{\mathbf{a}}N^\top(\boldsymbol{\xi}_p)\mathbf{v}_p - \nabla_{\boldsymbol{\xi}}\tilde{\Lambda}^0(\boldsymbol{\xi}_p)\tilde{\boldsymbol{\phi}} - \tilde{\mathbf{\Lambda}}^1\dot{\tilde{\mathbf{a}}}\right).$$

Furthermore, we use

$$(N^\top(\boldsymbol{\xi}_p)\mathbf{v}) \times \left(\nabla_{\boldsymbol{\xi}} \times \tilde{\mathbf{\Lambda}}^1(\boldsymbol{\xi}_p)\tilde{\mathbf{a}}\right) = \left((D\tilde{\mathbf{\Lambda}}^1(\boldsymbol{\xi}_p)\tilde{\mathbf{a}})^\top - D\tilde{\mathbf{\Lambda}}^1(\boldsymbol{\xi}_p)\tilde{\mathbf{a}}\right)N^\top(\boldsymbol{\xi}_p)\mathbf{v}$$

and the discrete derivative matrices from (3.4),

$$\begin{aligned}
&\dot{\mathbf{v}}_p = \frac{q_p}{m_p}N(\boldsymbol{\xi}_p)\left((N^\top(\boldsymbol{\xi}_p)\mathbf{v}_p) \times \left(\nabla_{\boldsymbol{\xi}} \times \tilde{\mathbf{\Lambda}}^1(\boldsymbol{\xi}_p)\tilde{\mathbf{a}}\right) - \tilde{\mathbf{\Lambda}}^1(\boldsymbol{\xi}_p)\mathsf{G}\tilde{\boldsymbol{\phi}} - \tilde{\mathbf{\Lambda}}^1(\boldsymbol{\xi}_p)\dot{\tilde{\mathbf{a}}}\right)\right) \\
\Leftrightarrow\ &\dot{\mathbf{v}}_p = \frac{q_p}{m_p}N(\boldsymbol{\xi}_p)\left((N^\top(\boldsymbol{\xi}_p)\mathbf{v}_p) \times \left(\tilde{\mathbf{\Lambda}}^2(\boldsymbol{\xi}_p)\mathsf{C}\tilde{\mathbf{a}}\right) - \tilde{\mathbf{\Lambda}}^1(\boldsymbol{\xi}_p)(\mathsf{G}\tilde{\boldsymbol{\phi}} + \dot{\tilde{\mathbf{a}}})\right).
\end{aligned}$$

Last, we introduce the electromagnetic fields, $\tilde{\mathbf{e}} = -\dot{\tilde{\mathbf{a}}} - \mathsf{G}\tilde{\boldsymbol{\phi}}, \tilde{\mathbf{b}} = \mathsf{C}\tilde{\mathbf{a}}$, to obtain the following form of the Lorentz force:

$$\dot{\mathbf{v}}_p = \frac{q_p}{m_p}N(\boldsymbol{\xi}_p)\left(\tilde{\mathbf{\Lambda}}^1(\boldsymbol{\xi}_p)\tilde{\mathbf{e}}(t) + (N^\top\mathbf{v}_p) \times \tilde{\mathbf{\Lambda}}^2(\boldsymbol{\xi}_p)\tilde{\mathbf{b}}(t)\right) \forall p \in \{1, ..., N_p\}.$$

Next, we compute the Euler–Lagrange equations for $\tilde{\mathbf{a}}_J, J = 1, ..., N_1$. We notice that only $\mathcal{L}_E$ depends on $\dot{\tilde{\mathbf{a}}}_J$,

$$\begin{aligned}
\frac{\mathrm{d}}{\mathrm{d}t}\frac{\partial\mathcal{L}}{\partial\dot{\tilde{\mathbf{a}}}_J} &= \frac{\mathrm{d}}{\mathrm{d}t}\frac{\partial\mathcal{L}_E}{\partial\dot{\tilde{\mathbf{a}}}_J} = \frac{\mathrm{d}}{\mathrm{d}t}\frac{\partial}{\partial\dot{\tilde{\mathbf{a}}}_J}\left[\frac{1}{2}\int(-N(\boldsymbol{\xi})\tilde{\mathbf{\Lambda}}^1(\boldsymbol{\xi})\mathsf{G}\tilde{\boldsymbol{\phi}}(t) - N(\boldsymbol{\xi})\tilde{\mathbf{\Lambda}}^1(\boldsymbol{\xi})\dot{\tilde{\mathbf{a}}}(t))^2\,|J_F(\boldsymbol{\xi})|\,\mathrm{d}\boldsymbol{\xi}\right] \\
&= -\frac{\mathrm{d}}{\mathrm{d}t}\int\left(N(\boldsymbol{\xi})\tilde{\mathbf{\Lambda}}^1_J(\boldsymbol{\xi})\right)\cdot N(\boldsymbol{\xi})\tilde{\mathbf{\Lambda}}^1(\boldsymbol{\xi})(-\mathsf{G}\tilde{\boldsymbol{\phi}} - \dot{\tilde{\mathbf{a}}})\,|J_F(\boldsymbol{\xi})|\,\mathrm{d}\boldsymbol{\xi} \\
&= -\int(\tilde{\mathbf{\Lambda}}^1(\boldsymbol{\xi}))^\top N^\top(\boldsymbol{\xi})N(\boldsymbol{\xi})\tilde{\mathbf{\Lambda}}^1_J(\boldsymbol{\xi})\dot{\tilde{\mathbf{e}}}\,|J_F(\boldsymbol{\xi})|\,\mathrm{d}\boldsymbol{\xi} \quad \forall J \in \{1, ..., N_1\}.
\end{aligned}$$

We write this in matrix form with the help of the mass matrix from (3.6),

$$\frac{\mathrm{d}}{\mathrm{d}t}\frac{\partial\mathcal{L}}{\partial\dot{\tilde{\mathbf{a}}}} = -\tilde{\mathsf{M}}_1\dot{\tilde{\mathbf{e}}}.$$

Then, we see that only $\mathcal{L}_B$ and $\mathcal{L}_p$ depend on $\tilde{\mathbf{a}}_J$. Let us start with $\mathcal{L}_p$,

$$\begin{aligned}\frac{\partial \mathcal{L}_p}{\partial \tilde{\mathbf{a}}_J} &= \frac{\partial}{\partial \tilde{\mathbf{a}}_J}\left[\sum_p \omega_p \left(\left(q_p N(\boldsymbol{\xi}_p)\tilde{\boldsymbol{\Lambda}}^1(\boldsymbol{\xi}_p)\tilde{\mathbf{a}}(t) + m_p \mathbf{v}_p\right)\cdot DF(\boldsymbol{\xi}_p)\dot{\boldsymbol{\xi}}_p - \frac{1}{2}m_p \mathbf{v}_p^2 - q_p \tilde{\Lambda}^0(\boldsymbol{\xi}_p)\tilde{\boldsymbol{\phi}}\right)\right] \\ &= \sum_p \omega_p q_p N(\boldsymbol{\xi}_p)\tilde{\boldsymbol{\Lambda}}^1_J(\boldsymbol{\xi}_p)\cdot DF(\boldsymbol{\xi}_p)\dot{\boldsymbol{\xi}}_p = \sum_p \omega_p q_p \tilde{\boldsymbol{\Lambda}}^1_J(\boldsymbol{\xi}_p)^\top N^\top(\boldsymbol{\xi}_p)\mathbf{v}_p \quad \forall J \in \{1, ..., N_1\}.\end{aligned}$$

From the particle part of the Lagrangian we got the discrete current. Now, we look at the magnetic field part of the Lagrangian,

$$\begin{aligned}\frac{\partial \mathcal{L}_B}{\partial \tilde{\mathbf{a}}_J} &= \frac{\partial}{\partial \tilde{\mathbf{a}}_J}\left[\frac{1}{2}\int -\left|\frac{DF(\boldsymbol{\xi})}{J_F(\boldsymbol{\xi})}\tilde{\boldsymbol{\Lambda}}^2(\boldsymbol{\xi})\mathsf{C}\tilde{\mathbf{a}}(t)\right|^2 |J_F(\boldsymbol{\xi})|\,\mathrm{d}\boldsymbol{\xi}\right] \\ &= -\int \left(\frac{DF(\boldsymbol{\xi})}{J_F(\boldsymbol{\xi})}\nabla_{\boldsymbol{\xi}} \times \tilde{\boldsymbol{\Lambda}}^2_J(\boldsymbol{\xi})\right)\cdot \frac{DF(\boldsymbol{\xi})}{J_F(\boldsymbol{\xi})}\tilde{\boldsymbol{\Lambda}}^2(\boldsymbol{\xi})\mathsf{C}\tilde{\mathbf{a}}\,|J_F(\boldsymbol{\xi})|\,\mathrm{d}\boldsymbol{\xi} \quad \forall J \in \{1, ..., N_1\} \\ &= -\int \mathsf{C}^\top \tilde{\boldsymbol{\Lambda}}^2_K(\boldsymbol{\xi})^\top \frac{DF^\top(\boldsymbol{\xi})}{J_F(\boldsymbol{\xi})}\cdot \frac{DF(\boldsymbol{\xi})}{J_F(\boldsymbol{\xi})}\tilde{\boldsymbol{\Lambda}}^2(\boldsymbol{\xi})\tilde{\mathbf{b}}\,|J_F(\boldsymbol{\xi})|\,\mathrm{d}\boldsymbol{\xi} \quad \forall K \in \{1, ..., N_2\}.\end{aligned}$$

Introducing the mass matrix (3.6), this becomes in matrix notation

$$\frac{\partial \mathcal{L}_B}{\partial \tilde{\mathbf{a}}} = -\mathsf{C}^\top \tilde{\mathsf{M}}_2 \tilde{\mathbf{b}}.$$

Finally, we put the three parts together to get the weak form of Ampère's law (3.8a),

$$\tilde{\mathsf{M}}_1 \dot{\tilde{\mathbf{e}}} = \mathsf{C}^\top \tilde{\mathsf{M}}_2 \tilde{\mathbf{b}} - \sum_p \omega_p q_p \tilde{\boldsymbol{\Lambda}}^1(\boldsymbol{\xi}_p)^\top N^\top(\boldsymbol{\xi}_p)\mathbf{v}_p.$$

Last, we look at the equations for $\tilde{\phi}_I, I = 1, ..., N_0$. Since the Lagrangian has no dependency on $\dot{\tilde{\phi}}_I$, the right-hand side of the Euler–Lagrange equations equals zero. Observing that $\mathcal{L}_B$ does not depend on $\tilde{\phi}$, the left-hand side reduces to $\frac{\partial \mathcal{L}_p}{\partial \tilde{\phi}_I} + \frac{\partial \mathcal{L}_E}{\partial \tilde{\phi}_I}$. From $\mathcal{L}_p$ we obtain the discrete charge,

$$\begin{aligned}\frac{\partial \mathcal{L}_p}{\partial \tilde{\phi}_I} &= \frac{\partial}{\partial \tilde{\phi}_I}\left[\sum_p \omega_p \left(\left(q_p N(\boldsymbol{\xi}_p)\tilde{\boldsymbol{\Lambda}}^1(\boldsymbol{\xi}_p)\tilde{\mathbf{a}}(t) + m_p \mathbf{v}_p\right)\cdot DF(\boldsymbol{\xi}_p)\dot{\boldsymbol{\xi}}_p - \frac{1}{2}m_p \mathbf{v}_p^2 - q_p \tilde{\Lambda}^0(\boldsymbol{\xi}_p)\tilde{\boldsymbol{\phi}}(t)\right)\right] \\ &= -\sum_p \omega_p q_p \tilde{\Lambda}^0_I(\boldsymbol{\xi}_p) \quad \forall I \in \{1, ..., N_0\},\end{aligned}$$

whereas the equation for $\mathcal{L}_E$ leads to

$$\begin{aligned}\frac{\partial \mathcal{L}_E}{\partial \tilde{\phi}_I} &= \frac{\partial}{\partial \tilde{\phi}_I}\left[\frac{1}{2}\int (-N(\boldsymbol{\xi})\tilde{\boldsymbol{\Lambda}}^1(\boldsymbol{\xi})\mathsf{G}\tilde{\boldsymbol{\phi}}(t) - N(\boldsymbol{\xi})\tilde{\boldsymbol{\Lambda}}^1(\boldsymbol{\xi})\dot{\tilde{\mathbf{a}}}(t))^2\,|J_F(\boldsymbol{\xi})|\,\mathrm{d}\boldsymbol{\xi}\right] \\ &= -\int (N(\boldsymbol{\xi})\nabla_{\boldsymbol{\xi}}\tilde{\Lambda}^0_I(\boldsymbol{\xi}))\cdot N(\boldsymbol{\xi})\tilde{\boldsymbol{\Lambda}}^1(\boldsymbol{\xi})(-\mathsf{G}\tilde{\boldsymbol{\phi}} - \dot{\tilde{\mathbf{a}}})\,|J_F(\boldsymbol{\xi})|\,\mathrm{d}\boldsymbol{\xi} \quad \forall I \in \{1, ..., N_0\} \\ &= -\int \mathsf{G}^\top \tilde{\boldsymbol{\Lambda}}^1_J(\boldsymbol{\xi})^\top N^\top(\boldsymbol{\xi})N(\boldsymbol{\xi})\tilde{\boldsymbol{\Lambda}}^1(\boldsymbol{\xi})\,|J_F(\boldsymbol{\xi})|\,\mathrm{d}\boldsymbol{\xi}\tilde{\mathbf{e}} \quad \forall J \in \{1, ..., N_1\}.\end{aligned}$$

We put this two parts together and use the mass matrix (3.6) to end up with the weak formu-

lation of the electric Gauss law (3.8b),

$$\mathsf{G}^\top \tilde{\mathsf{M}}_1 \mathbf{e} = -\sum_p \omega_p q_p \tilde{\Lambda}^0(\boldsymbol{\xi}_p).$$

In conclusion, we obtained the following equations of motion from the Euler–Lagrange equations with the particle positions and velocities, $\boldsymbol{\Xi} = (\boldsymbol{\xi}_1, ..., \boldsymbol{\xi}_{N_p})^\top, \mathbf{V} = (\mathbf{v}_1, ..., \mathbf{v}_{N_p})^\top$, and the degrees of freedom of the electromagnetic fields, $\tilde{\mathbf{e}}, \tilde{\mathbf{b}}$:

$$\begin{aligned}
\dot{\boldsymbol{\Xi}} &= \mathbb{N}^\top(\boldsymbol{\Xi})\mathbf{V}, \\
\dot{\mathbf{V}} &= \mathbb{W}_{\frac{q}{m}} \mathbb{N}(\boldsymbol{\Xi}) \left(\tilde{\boldsymbol{\Lambda}}^1 \tilde{\mathbf{e}} + \mathbb{N}^\top(\boldsymbol{\Xi})\mathbf{V} \times \tilde{\boldsymbol{\Lambda}}^2(\boldsymbol{\Xi})\tilde{\mathbf{b}} \right), \\
\tilde{\mathsf{M}}_1 \dot{\tilde{\mathbf{e}}} &= \mathsf{C}^\top \tilde{\mathsf{M}}_2 \tilde{\mathbf{b}} - \mathbb{W}_q \tilde{\mathbb{\Lambda}}^1(\boldsymbol{\Xi})^\top \mathbb{N}^\top(\boldsymbol{\Xi})\mathbf{V}, \\
\mathsf{G}^\top \tilde{\mathsf{M}}_1 \tilde{\mathbf{e}} &= -\mathbb{W}_q \tilde{\mathbb{\Lambda}}^0(\boldsymbol{\Xi})^\top \mathbb{1}_{N_p}.
\end{aligned}$$

Additionally, the relation between the potentials and the electromagnetic fields gives us the missing two Maxwell equations

$$\begin{aligned}
&\tilde{\mathbf{e}} = -\mathsf{G}\tilde{\boldsymbol{\phi}} - \dot{\tilde{\mathbf{a}}} \Rightarrow -\mathsf{C}\tilde{\mathbf{e}} = \mathsf{C}\dot{\tilde{\mathbf{a}}} = \dot{\tilde{\mathbf{b}}}, \\
&\tilde{\mathbf{b}} = \mathsf{C}\tilde{\mathbf{a}} \Rightarrow \mathsf{D}\tilde{\mathbf{b}} = 0.
\end{aligned}$$

□

5.2 Poisson Matrix

In this section, we introduce a generalised notation of the Lagrangian formalism by using the general coordinate $\mathbf{z} = (\boldsymbol{\Xi}, \mathbf{V}, \tilde{\mathbf{e}}, \tilde{\mathbf{a}})^\top$ with $\tilde{\mathbf{e}} = -\dot{\tilde{\mathbf{a}}}$. Therefore, we use the temporal gauge setting the scalar potential $\tilde{\phi}$ to zero in order to simplify the scheme.

Then, the Lagrangian from (5.2) takes the following form:

$$\mathcal{L} = \gamma(\mathbf{z}) \cdot \dot{\mathbf{z}} - h(\mathbf{z})$$

with

$$\begin{aligned}
\gamma(\mathbf{z}) =& \left(\mathbb{W}_q \tilde{\boldsymbol{\Lambda}}^1(\boldsymbol{\Xi})\tilde{\mathbf{a}} + \mathbb{W}_m \mathbb{DF}^\top(\boldsymbol{\Xi})\mathbf{V}, 0, 0, -\tilde{\mathsf{M}}_1 \tilde{\mathbf{e}} \right)^\top, \\
h(\mathbf{z}) =& \frac{1}{2} \tilde{\mathbf{V}}^\top \mathbb{W}_m \tilde{\mathbf{V}} + \frac{1}{2} \tilde{\mathbf{e}}^\top \tilde{\mathsf{M}}_1 \tilde{\mathbf{e}} + \frac{1}{2} (\mathsf{C}\tilde{\mathbf{a}})^\top \tilde{\mathsf{M}}_2 \mathsf{C}\tilde{\mathbf{a}}.
\end{aligned}$$

Definition 5.1. *We define the Lagrangian matrix as* $\mathbb{L}_{ij} := \frac{\partial \gamma_j}{\partial \mathbf{z}_i} - \frac{\partial \gamma_i}{\partial \mathbf{z}_j}$.

Then, we review the following proposition taken from [10]:

Proposition 5.2. *The discrete Poisson matrix can be computed as the inverse of the Lagrangian matrix.*

Proof. We take a look at the Euler–Lagrange equations, $\frac{\mathrm{d}}{\mathrm{d}t}\frac{\partial \mathcal{L}}{\partial \dot{\mathbf{z}}} = \frac{\partial \mathcal{L}}{\partial \mathbf{z}}$, and note that the derivatives can be written in general form with Einstein summation as

$$\begin{aligned}\frac{\mathrm{d}}{\mathrm{d}t}\frac{\partial \mathcal{L}(\mathbf{z})}{\partial \dot{z}_i} &= \frac{\mathrm{d}}{\mathrm{d}t}\gamma_i(\mathbf{z}) = \frac{\partial \gamma_i(\mathbf{z})}{\partial z_j}\dot{z}_j,\\ \frac{\partial \mathcal{L}(\mathbf{z})}{\partial z_i} &= \frac{\partial \gamma_j(\mathbf{z})}{\partial z_i}\dot{z}_j - \frac{\partial h(\mathbf{z})}{\partial z_i}.\end{aligned}$$

So, the Euler–Lagrange equations are denoted by

$$\frac{\partial \gamma_i}{\partial z_j}\dot{z}_j = \frac{\partial \gamma_j}{\partial z_i}\dot{z}_j - \frac{\partial h}{\partial z_i}.$$

Solving this equation for $\frac{\partial h}{\partial z_i}$ leads to

$$\left(\frac{\partial \gamma_j}{\partial z_i} - \frac{\partial \gamma_i}{\partial z_j}\right)\dot{z}_j = \mathbb{L}_{ij}\dot{z}_j = \frac{\partial h}{\partial z_i}.$$

With a Legendre transformation we realise that the Hamiltonian of this system is given by

$$\mathcal{H}_h = \frac{\partial \mathcal{L}}{\partial \dot{\mathbf{z}}}\cdot\dot{\mathbf{z}} - \mathcal{L} = \gamma(\mathbf{z})\cdot\dot{\mathbf{z}} - \mathcal{L} = h(\mathbf{z}).$$

Therefore, we write this equation as

$$\mathbb{L}(\mathbf{z})\frac{\mathrm{d}\mathbf{z}}{\mathrm{d}t} = D\mathcal{H}_h(\mathbf{z}).$$

Assuming that the Lagrangian matrix is invertible, we see that its inverse is the discrete Poisson matrix as inverting the matrix leads to the same system as in (4.5),

$$\frac{\mathrm{d}\mathbf{z}}{\mathrm{d}t} = \mathbb{L}^{-1}(\mathbf{z})D\mathcal{H}_h.$$

□

For the Lagrangian (5.2), the Lagrangian matrix is a 4×4 block matrix with the following

form:

$$\mathbb{L} = \begin{pmatrix} \mathbb{L}_1 & -\mathbb{L}_2 & 0 & -\mathbb{L}_3 \\ \mathbb{L}_2^\top & 0 & 0 & 0 \\ 0 & 0 & 0 & -\mathbb{L}_4 \\ \mathbb{L}_3^\top & 0 & \mathbb{L}_4^\top & 0 \end{pmatrix}. \tag{5.4}$$

Hence, the inverse is computed as

$$\mathbb{L}^{-1} = \begin{pmatrix} 0 & \mathbb{L}_2^{-\top} & 0 & 0 \\ -\mathbb{L}_2^{-1} & \mathbb{L}_2^{-1}\mathbb{L}_1\mathbb{L}_2^{-\top} & \mathbb{L}_2^{-1}\mathbb{L}_3\mathbb{L}_4^{-1} & 0 \\ 0 & -\mathbb{L}_4^{-\top}\mathbb{L}_3^\top\mathbb{L}_2^{-\top} & 0 & \mathbb{L}_4^{-\top} \\ 0 & 0 & -\mathbb{L}_4^{-1} & 0 \end{pmatrix}.$$

In this case, we have

$$\begin{aligned} \mathbb{L}_1 &= \mathbb{W}_q\tilde{\mathbb{B}}(\boldsymbol{\Xi}, \tilde{\mathbf{a}}), \\ \mathbb{L}_2 &= \mathbb{D}\mathbb{F}^\top(\boldsymbol{\Xi})\mathbb{W}_m, \\ \mathbb{L}_3 &= \mathbb{W}_q\tilde{\mathbb{\Lambda}}^1(\boldsymbol{\Xi}), \\ \mathbb{L}_4 &= \tilde{\mathsf{M}}_1, \end{aligned}$$

which leads to an equivalent Poisson matrix to (4.6) considering $\tilde{\mathbf{b}} = \mathsf{C}\tilde{\mathbf{a}}$,

$$\mathbb{J} = \begin{pmatrix} 0 & \mathbb{N}^\top(\boldsymbol{\Xi})\mathbb{W}_m^{-1} & 0 & 0 \\ -\mathbb{W}_m^{-1}\mathbb{N}(\boldsymbol{\Xi}) & \mathbb{W}_{\frac{q}{m}}\mathbb{N}(\boldsymbol{\Xi})\tilde{\mathbb{B}}(\boldsymbol{\Xi}, \tilde{\mathbf{a}})\mathbb{N}^\top(\boldsymbol{\Xi})\mathbb{W}_m^{-1} & \mathbb{W}_{\frac{q}{m}}\mathbb{N}(\boldsymbol{\Xi})\tilde{\mathbb{\Lambda}}^1\tilde{\mathsf{M}}_1^{-1} & 0 \\ 0 & -\tilde{\mathsf{M}}_1^{-1}(\tilde{\mathbb{\Lambda}}^1)^\top\mathbb{N}^\top(\boldsymbol{\Xi})\mathbb{W}_{\frac{q}{m}} & 0 & \tilde{\mathsf{M}}_1^{-1} \\ 0 & 0 & -\tilde{\mathsf{M}}_1^{-1} & 0 \end{pmatrix}.$$

5.3 Logical Particle Velocity

Up to this point, we only considered a hybrid particle push as given in (4.1). Now, let us look at the particle velocity in curvilinear coordinates. We note that there are two options for transforming the particle velocity. Either we represent it in the covariant basis with contravariant

components or vice versa,

$$\mathbf{v} = \mathbf{e}_i v^i = DF(\boldsymbol{\xi})\tilde{\mathbf{v}},$$
$$\mathbf{v} = \mathbf{e}^i v_i = N(\boldsymbol{\xi})\hat{\mathbf{v}}.$$

Naturally, we have $\mathbf{v} = \dot{\mathbf{x}} = DF(\boldsymbol{\xi})\dot{\boldsymbol{\xi}} = \mathbf{e}_i \dot{x}^i$. So, if we choose the contravariant components of the velocity, we get $\dot{\boldsymbol{\xi}} = \tilde{\mathbf{v}}$ whereas for the covariant components, we get $\dot{\boldsymbol{\xi}} = G_m^{-1}(\boldsymbol{\xi})\hat{\mathbf{v}}$.

For the contravariant velocity components $\tilde{\mathbf{v}}$, we obtain

$$\begin{aligned}
\mathbf{z}_1 = \boldsymbol{\Xi}, \mathbf{z}_2 = \tilde{\mathbf{V}}, \mathbf{z}_3 = \tilde{\mathbf{e}}, \mathbf{z}_4 = \tilde{\mathbf{a}},\\
\gamma_1(\boldsymbol{\Xi}, \tilde{\mathbf{V}}, \tilde{\mathbf{a}}) = \mathbb{W}_q \tilde{\mathbb{\Lambda}}^1(\boldsymbol{\Xi})\tilde{\mathbf{a}} + \mathbb{W}_m \mathbb{G}_m(\boldsymbol{\Xi})\tilde{\mathbf{V}},\\
\gamma_2 = \gamma_3 = 0,\\
\gamma_4(\tilde{\mathbf{e}}) = \tilde{\mathsf{M}}_1 \tilde{\mathbf{e}},\\
h(\mathbf{z}) = \frac{1}{2}\mathbb{W}_m \tilde{\mathbf{V}}^\top \mathbb{G}_m(\boldsymbol{\Xi})\tilde{\mathbf{V}} + \frac{1}{2}, \tilde{\mathbf{e}}^\top \tilde{\mathsf{M}}_1 \tilde{\mathbf{e}} + \frac{1}{2}(\mathsf{C}\tilde{\mathbf{a}})^\top \tilde{\mathsf{M}}_2 \mathsf{C}\tilde{\mathbf{a}}.
\end{aligned}$$

For the covariant velocity components $\hat{\mathbf{v}}$, we get

$$\begin{aligned}
\mathbf{z}_1 = \boldsymbol{\Xi}, \mathbf{z}_2 = \hat{\mathbf{V}}, \mathbf{z}_3 = \tilde{\mathbf{e}}, \mathbf{z}_4 = \tilde{\mathbf{a}},\\
\gamma_1(\boldsymbol{\Xi}, \hat{\mathbf{V}}, \tilde{\mathbf{a}}) = \mathbb{W}_q \tilde{\mathbb{\Lambda}}^1(\boldsymbol{\Xi})\tilde{\mathbf{a}} + \mathbb{W}_m \hat{\mathbf{V}},\\
\gamma_2 = \gamma_3 = 0,\\
\gamma_4(\tilde{\mathbf{e}}) = \tilde{\mathsf{M}}_1 \tilde{\mathbf{e}},\\
h(\mathbf{z}) = \frac{1}{2}\mathbb{W}_m \hat{\mathbf{V}}^\top \mathbb{G}_m^{-1}(\boldsymbol{\Xi})\hat{\mathbf{V}}_p + \frac{1}{2}\tilde{\mathbf{e}}^\top \tilde{\mathsf{M}}_1 \tilde{\mathbf{e}} + \frac{1}{2}\tilde{\mathbf{a}}^\top \mathsf{C}^\top \tilde{\mathsf{M}}_2 \mathsf{C}\tilde{\mathbf{a}}.
\end{aligned}$$

We divide the Lagrange matrix in the block matrices $\mathbb{L}_{IJ} = \frac{\partial \gamma_J}{\partial \mathbf{z}_I} - \frac{\partial \gamma_I}{\partial \mathbf{z}_J}, I = 1, ..4, J = 1, .., 4$. Since γ_1 does not depend on $\tilde{\mathbf{e}}$ and γ_2 and γ_3 equal zero, we get $\mathbb{L}_{13} = \mathbb{L}_{31} = \mathbb{L}_{22} = \mathbb{L}_{23} = \mathbb{L}_{32} = \mathbb{L}_{33} = 0$ and since γ_4 only depends on $\tilde{\mathbf{e}}$, we obtain $\mathbb{L}_{24} = \mathbb{L}_{42} = \mathbb{L}_{44} = 0$. Hence, the only non-zero blocks are $\mathbb{L}_{11}, \mathbb{L}_{12}, \mathbb{L}_{21}, \mathbb{L}_{14}, \mathbb{L}_{41}, \mathbb{L}_{34}$ and $\mathbb{L}_{43}$. Let us begin with the parts that are identical for both choices,

$$\mathbb{L}_{14} = -\mathbb{L}_{41}^\top = -\frac{\partial \gamma_1}{\partial \tilde{\mathbf{a}}} = -\mathbb{W}_q \tilde{\mathbb{\Lambda}}^1(\boldsymbol{\Xi}),$$
$$\mathbb{L}_{43} = -\mathbb{L}_{34}^\top = -\frac{\partial \gamma_4}{\partial \tilde{\mathbf{e}}} = -\tilde{\mathsf{M}}_1.$$

Now, we look at the parts that are different. For the velocity $\tilde{\mathbf{v}}$, we get

$$\mathbb{L}_{12} = -\mathbb{L}_{21}^\top = -\frac{\partial \gamma_1}{\partial \tilde{\mathbf{V}}} = -\mathbb{W}_m \mathbb{G}_m(\boldsymbol{\Xi})$$

whereas for $\hat{\mathbf{v}}$, we obtain

$$\mathbb{L}_{12} = -\mathbb{L}_{21}^{\top} = -\frac{\partial \gamma_1}{\partial \hat{\mathbf{V}}} = -\mathbb{W}_m.$$

Since term $\mathbb{L}_{11}$ is more complicated to compute, we look at it componentwise for each particle,

$$(\mathbb{L}_{11})_{ij}\dot{\xi}_j = \left(\frac{\partial \gamma_{1,j}}{\partial \xi_i} - \frac{\partial \gamma_{1,i}}{\partial \xi_j}\right)\dot{\xi}_j, \quad i,j = 1,...,3N_p.$$

For the contravariant components of the velocity, $\tilde{\mathbf{v}}$, we obtain

$$\begin{aligned}\left(\frac{\partial \gamma_{1,j}}{\partial \xi_i} - \frac{\partial \gamma_{1,i}}{\partial \xi_j}\right)\dot{\xi}_j &= q\left(\partial_{\xi_i}\tilde{A}_j - \partial_{\xi_j}\tilde{A}_i\right)\dot{\xi}_j + m\left(\partial_{\xi_i}(G_m(\boldsymbol{\xi})\tilde{\mathbf{v}})_j - \partial_{\xi_j}(G_m(\boldsymbol{\xi})\tilde{\mathbf{v}})_i\right)\dot{\xi}_j \\ &= q\left(\dot{\boldsymbol{\xi}} \times (\nabla_{\boldsymbol{\xi}} \times \tilde{\mathbf{A}})\right)_i + m\left(\dot{\boldsymbol{\xi}} \times (\nabla_{\boldsymbol{\xi}} \times G_m\tilde{\mathbf{v}})\right)_i.\end{aligned}$$

Next, we introduce the matrix $\tilde{\mathbb{B}}(\boldsymbol{\Xi}, \tilde{\mathbf{a}})$ via

$$\tilde{\mathbb{B}}(\boldsymbol{\Xi}, \tilde{\mathbf{a}})\dot{\boldsymbol{\Xi}} = \left(\dot{\boldsymbol{\Xi}} \times (\tilde{\mathbb{\Lambda}}^2(\boldsymbol{\Xi})\mathsf{C}\tilde{\mathbf{a}})\right) = \left(\dot{\boldsymbol{\Xi}} \times (\nabla_{\boldsymbol{\Xi}} \times \tilde{\mathbb{\Lambda}}^1(\boldsymbol{\Xi})\tilde{\mathbf{a}})\right).$$

Using $\dot{\boldsymbol{\Xi}} = \tilde{\mathbf{V}}$, this leads to

$$\mathbb{L}_{11} = \mathbb{W}_q\tilde{\mathbb{B}}(\boldsymbol{\Xi}, \tilde{\mathbf{a}}) + \mathbb{W}_m\left(\nabla_{\boldsymbol{\Xi}}\tilde{\mathbf{V}}^{\top}\mathbb{G}_m(\boldsymbol{\Xi}) - \tilde{V}_j\partial_{\Xi_j}\mathbb{G}_m(\boldsymbol{\Xi})\right).$$

On the other hand, for the covariant components of the velocity, $\hat{\mathbf{v}}$, we get

$$\left(\frac{\partial \gamma_{1,j}}{\partial \xi_i} - \frac{\partial \gamma_{1,i}}{\partial \xi_j}\right)\dot{\xi}_j = q\left(\partial_{\xi_i}\tilde{A}_j - \partial_{\xi_j}\tilde{A}_i\right)\dot{\xi}_j = q\left(\dot{\boldsymbol{\xi}} \times (\nabla_{\boldsymbol{\xi}} \times \tilde{\mathbf{A}})\right)_i.$$

We can write this part of the Lagrangian matrix as

$$\mathbb{L}_{11} = \mathbb{W}_q\tilde{\mathbb{B}}(\boldsymbol{\Xi}, \tilde{\mathbf{a}}).$$

Now, we can build the Lagrangian matrix for $\tilde{\mathbf{v}}$ and $\hat{\mathbf{v}}$ using the same structure as in (5.4).

For $\tilde{\mathbf{v}}$, we get

$$\begin{aligned}
\mathbb{L}_1 &= \mathbb{W}_q \tilde{\mathbb{B}}(\boldsymbol{\Xi}, \tilde{\mathbf{a}}) + \mathbb{W}_m \left(\nabla_{\boldsymbol{\Xi}} \tilde{\mathbf{V}}^\top \mathbb{G}_m - \tilde{V}_j \partial_{\Xi_j} \mathbb{G}_m \right), \\
\mathbb{L}_2 &= \mathbb{G}(\boldsymbol{\Xi}) \mathbb{W}_m, \\
\mathbb{L}_3 &= \mathbb{W}_q \tilde{\mathbb{\Lambda}}^1(\boldsymbol{\Xi}), \\
\mathbb{L}_4 &= \tilde{\mathsf{M}}_1,
\end{aligned}$$

which leads to the Lagrangian matrix,

$$\mathbb{L} = \begin{pmatrix}
\mathbb{W}_q \tilde{\mathbb{B}}(\boldsymbol{\Xi}, \tilde{\mathbf{a}}) + \mathbb{W}_m \nabla_{\boldsymbol{\Xi}} \tilde{\mathbf{V}}^\top \mathbb{G}_m - \mathbb{W}_m \partial_{\Xi_j} \mathbb{G}_m \tilde{V}_j & -\mathbb{G}_m(\boldsymbol{\Xi}) \mathbb{W}_m & 0 & -\mathbb{W}_q \tilde{\mathbb{\Lambda}}^1(\boldsymbol{\Xi}) \\
\mathbb{W}_m \mathbb{G}_m(\boldsymbol{\Xi}) & 0 & 0 & 0 \\
0 & 0 & 0 & -\tilde{\mathsf{M}}_1 \\
\tilde{\mathbb{\Lambda}}^1(\boldsymbol{\Xi})^\top \mathbb{W}_q & 0 & \tilde{\mathsf{M}}_1 & 0
\end{pmatrix}.$$

Then, we compute the Poisson matrix as

$$\mathbb{J} = \begin{pmatrix}
0 & \mathbb{G}_m^{-1} \mathbb{W}_m^{-1} & 0 & 0 \\
-\mathbb{W}_m^{-1} \mathbb{G}_m^{-1} & \mathbb{G}_m^{-1} \left(\mathbb{W}_{\frac{q}{m}} \tilde{\mathbb{B}}(\boldsymbol{\Xi}, \tilde{\mathbf{a}}) + \nabla_{\boldsymbol{\Xi}} \tilde{\mathbf{V}}^\top \mathbb{G}_m - \partial_{\Xi_j} \mathbb{G}_m \tilde{V}_j \right) \mathbb{G}_m^{-1} \mathbb{W}_m^{-1} & \mathbb{W}_{\frac{q}{m}} \mathbb{G}_m^{-1} \tilde{\mathbb{\Lambda}}^1 \tilde{\mathsf{M}}_1^{-1} & 0 \\
0 & -\tilde{\mathsf{M}}_1^{-1} (\tilde{\mathbb{\Lambda}}^1)^\top \mathbb{G}_m^{-1} \mathbb{W}_{\frac{q}{m}} & 0 & \tilde{\mathsf{M}}_1^{-1} \\
0 & 0 & -\tilde{\mathsf{M}}_1^{-1} & 0
\end{pmatrix}.$$

With the derivative of the Hamiltonian,

$$D\mathcal{H} = \left(\frac{1}{2} \nabla_{\boldsymbol{\Xi}} \tilde{\mathbf{V}}^\top \mathbb{W}_m \mathbb{G}_m(\boldsymbol{\Xi}) \tilde{\mathbf{V}}, \mathbb{W}_m \mathbb{G}_m \tilde{\mathbf{V}}, \tilde{\mathsf{M}}_1 \tilde{\mathbf{e}}, \mathsf{C}^\top \tilde{\mathsf{M}}_2 \mathsf{C} \tilde{\mathbf{a}} \right)^\top,$$

the equations of motion are given by

$$\begin{aligned}
\dot{\boldsymbol{\Xi}} =& \tilde{\mathbf{V}}, \\
\dot{\tilde{\mathbf{V}}} =& \mathbb{G}_m^{-1}(\boldsymbol{\Xi}) \left(\mathbb{W}_{\frac{q}{m}} \tilde{\mathbb{B}}(\boldsymbol{\Xi}, \tilde{\mathbf{a}}) + \frac{1}{2} \nabla_{\boldsymbol{\Xi}} (\tilde{\mathbf{V}}^\top \mathbb{G}_m(\boldsymbol{\Xi})) - \tilde{V}_j \partial_{\Xi_j} G M_m(\boldsymbol{\Xi}) \right) \tilde{\mathbf{V}} \\
& + \mathbb{G}_m^{-1}(\boldsymbol{\Xi}) \mathbb{W}_{\frac{q}{m}} \tilde{\mathbb{\Lambda}}^1(\boldsymbol{\Xi}) \tilde{\mathbf{e}}, \\
\dot{\tilde{\mathbf{e}}} =& -\tilde{\mathsf{M}}_1^{-1} \tilde{\mathbb{\Lambda}}^1(\boldsymbol{\Xi})^\top \mathbb{W}_q \tilde{\mathbf{V}} + \tilde{\mathsf{M}}^{-1} \mathsf{C}^\top \tilde{\mathsf{M}}_2 \mathsf{C} \tilde{\mathbf{a}}, \\
\mathsf{C} \dot{\tilde{\mathbf{a}}} =& -\mathsf{C} \tilde{\mathbf{e}}.
\end{aligned} \tag{5.5}$$

For $\hat{\mathbf{v}}$, we obtain

$$\begin{aligned}\mathbb{L}_1 &= \mathbb{W}_q\tilde{\mathbb{B}}(\boldsymbol{\Xi},\tilde{\mathbf{a}}),\\ \mathbb{L}_2 &= \mathbb{W}_m,\\ \mathbb{L}_3 &= \mathbb{W}_q\tilde{\mathbb{\Lambda}}^1(\boldsymbol{\Xi}),\\ \mathbb{L}_4 &= \tilde{\mathsf{M}}_1.\end{aligned}$$

So, the Lagrangian matrix has the following form:

$$\mathbb{L} = \begin{pmatrix} \mathbb{W}_q\tilde{\mathbb{B}}(\boldsymbol{\Xi},\tilde{\mathbf{a}}) & -\mathbb{W}_m & 0 & -\mathbb{W}_q\tilde{\mathbb{\Lambda}}^1(\boldsymbol{\Xi}) \\ \mathbb{W}_m & 0 & 0 & 0 \\ 0 & 0 & 0 & -\tilde{\mathsf{M}}_1 \\ \tilde{\mathbb{\Lambda}}^1(\boldsymbol{\Xi})^\top\mathbb{W}_q & 0 & \tilde{\mathsf{M}}_1 & 0 \end{pmatrix}$$

and the Poisson matrix is computed as the inverse of the Lagrangian matrix,

$$\mathbb{J} = \begin{pmatrix} 0 & \mathbb{W}_m^{-1} & 0 & 0 \\ -\mathbb{W}_m^{-1} & \mathbb{W}_{\frac{q}{m}}\tilde{\mathbb{B}}(\boldsymbol{\Xi},\tilde{\mathbf{a}})\mathbb{W}_m^{-1} & \mathbb{W}_{\frac{q}{m}}\tilde{\mathbb{\Lambda}}^1\tilde{\mathsf{M}}_1^{-1} & 0 \\ 0 & -\tilde{\mathsf{M}}_1^{-1}(\tilde{\mathbb{\Lambda}}^1)^\top\mathbb{W}_{\frac{q}{m}} & 0 & \tilde{\mathsf{M}}_1^{-1} \\ 0 & 0 & -\tilde{\mathsf{M}}_1^{-1} & 0 \end{pmatrix}.$$

With the derivative of the Hamiltonian,

$$D\mathcal{H} = \left(\frac{1}{2}\nabla_{\boldsymbol{\Xi}}\hat{\mathbf{V}}^\top\mathbb{W}_m\mathbb{G}_m^{-1}(\boldsymbol{\Xi})\hat{\mathbf{V}}, \mathbb{W}_m\mathbb{G}_m^{-1}\hat{\mathbf{V}}, \tilde{\mathsf{M}}_1\tilde{\mathbf{e}}, \mathsf{C}^\top\tilde{\mathsf{M}}_2\mathsf{C}\tilde{\mathbf{a}}\right)^\top,$$

we obtain the following equations of motion:

$$\begin{aligned}\dot{\boldsymbol{\Xi}} &= \mathbb{G}_m^{-1}(\boldsymbol{\Xi})\hat{\mathbf{V}},\\ \dot{\hat{\mathbf{V}}} &= -\frac{1}{2}\nabla_{\boldsymbol{\Xi}}\hat{\mathbf{V}}^\top\mathbb{G}_m^{-1}(\boldsymbol{\Xi})\hat{\mathbf{V}} + \mathbb{W}_{\frac{q}{m}}\tilde{\mathbb{B}}(\boldsymbol{\Xi},\tilde{\mathbf{a}})\mathbb{G}_m^{-1}(\boldsymbol{\Xi})\hat{\mathbf{V}} + \mathbb{W}_{\frac{q}{m}}\tilde{\mathbb{\Lambda}}^1\tilde{\mathbf{e}},\\ \dot{\tilde{\mathbf{e}}} &= -\tilde{\mathsf{M}}_1^{-1}(\tilde{\mathbb{\Lambda}}^1)^\top\mathbb{W}_q\mathbb{G}_m^{-1}(\boldsymbol{\Xi})\hat{\mathbf{V}} + \tilde{\mathsf{M}}^{-1}\mathsf{C}^\top\tilde{\mathsf{M}}_2\mathsf{C}\tilde{\mathbf{a}},\\ \mathsf{C}\dot{\tilde{\mathbf{a}}} &= -\mathsf{C}\tilde{\mathbf{e}}.\end{aligned} \tag{5.6}$$

Remark 5.1. *When we compare the particle characteristics for the hybrid ansatz and the two representations in logical coordinates, we see that for a non-orthogonal mapping the equations of motion are non-linear. Only for the representation of the velocity in contravariant*

coordinates $\tilde{\mathbf{V}}$, the position update can be solved explicitly, since

$$\dot{\boldsymbol{\Xi}} = \tilde{\mathbf{V}} = \mathbb{G}_m^{-1}(\boldsymbol{\Xi})\hat{\mathbf{V}} = \mathbb{N}^\top(\boldsymbol{\Xi})\mathbf{V}.$$

However, for the velocity in logical coordinates, we get an additional part compared to the hybrid case because the Hamiltonian is dependent on $\boldsymbol{\Xi}$,

$$\begin{aligned}
\dot{\mathbf{V}} &= \mathbb{W}_{\frac{q}{m}}\mathbb{N}(\boldsymbol{\Xi})\left(\tilde{\mathbb{\Lambda}}^1(\boldsymbol{\Xi})\tilde{\mathbf{e}} + (\mathbb{N}^\top(\boldsymbol{\Xi})\mathbf{V}) \times \tilde{\mathbb{\Lambda}}^2(\boldsymbol{\Xi})\tilde{\mathbf{b}}\right), \\
\dot{\tilde{\mathbf{V}}} &= \mathbb{W}_{\frac{q}{m}}\mathbb{G}_m^{-1}(\boldsymbol{\Xi})\left(\tilde{\mathbb{\Lambda}}^1(\boldsymbol{\Xi})\tilde{\mathbf{e}} + \tilde{\mathbf{V}} \times \tilde{\mathbb{\Lambda}}^2(\boldsymbol{\Xi})\tilde{\mathbf{b}}\right) + \mathbb{G}_m^{-1}(\boldsymbol{\Xi})\left(\frac{1}{2}\nabla_{\boldsymbol{\Xi}}(\tilde{\mathbf{V}}^\top\mathbb{G}_m(\boldsymbol{\Xi})\tilde{\mathbf{V}}) - \tilde{V}_j\partial_{\Xi_j}\mathbb{G}_m(\boldsymbol{\Xi})\tilde{\mathbf{V}}\right), \\
\dot{\hat{\mathbf{V}}} &= \mathbb{W}_{\frac{q}{m}}\left(\tilde{\mathbb{\Lambda}}^1(\boldsymbol{\Xi})\tilde{\mathbf{e}} + (\mathbb{G}_m^{-1}(\boldsymbol{\Xi})\hat{\mathbf{V}}) \times \tilde{\mathbb{\Lambda}}^2(\boldsymbol{\Xi})\tilde{\mathbf{b}}\right) - \frac{1}{2}\nabla_{\boldsymbol{\Xi}}\hat{\mathbf{V}}^\top\mathbb{G}_m^{-1}(\boldsymbol{\Xi})\hat{\mathbf{V}}.
\end{aligned}$$

Generally, this leads to a non-linear velocity update with a quadratic velocity. Therefore, we have chosen the hybrid particle push for our implementation.

6 Time Discretisation of the Equations of Motion

For the GEMPIC method on Cartesian grids, two approaches for structure-preserving time propagation schemes that exploit the form (4.5) have been proposed: In [56], the discrete Hamiltonian (4.3) is split into five parts $\tilde{\mathcal{H}}_{h,i}$, $i = 1, \ldots, 5$ so that each part of the equations $\dot{\tilde{\mathbf{u}}} = \{\tilde{\mathbf{u}}, \tilde{\mathcal{H}}_{h,i}\}$ yields explicit equations of motion and the discretisation preserves Gauss' law. This splitting was first proposed in [45, 97]. A second ansatz is to decouple system (4.5) with an antisymmetric splitting of the Poisson matrix $\mathbb{J}$. Then, the resulting subsystems can be solved by a discrete gradient method yielding an energy-preserving time stepping scheme. In [55], two schemes are constructed this way: a semi-implicit scheme that does not preserve the electric Gauss law and a fully implicit scheme that preserves Gauss' law. The discrete gradient methods readily extend to the curvilinear case as we will show in Sections 6.2 and 6.3. However, for a general coordinate transformation an explicit Hamiltonian splitting (HS) can no longer be constructed, since the coordinate directions do not decouple for non-orthogonal mappings. Instead, we will construct two semi-explicit splittings that preserve Gauss' law in Section 6.1.

6.1 Charge Conserving Splittings

6.1.1 GEMPIC Hamiltonian Splitting

In this section, we consider an HS as in [56]; however, we only split into three parts,

$$\tilde{\mathcal{H}}_h = \tilde{\mathcal{H}}_p + \tilde{\mathcal{H}}_E + \tilde{\mathcal{H}}_B$$

with

$$\tilde{\mathcal{H}}_p = \frac{1}{2}\mathbf{V}^\top \mathbb{W}_m \mathbf{V},\ \tilde{\mathcal{H}}_E = \frac{1}{2}\tilde{\mathbf{e}}^\top \tilde{\mathsf{M}}_1 \tilde{\mathbf{e}},\ \tilde{\mathcal{H}}_B = \frac{1}{2}\tilde{\mathbf{b}}^\top \tilde{\mathsf{M}}_2 \tilde{\mathbf{b}}.$$

Thus, we obtain the three subsystems

$$\dot{\mathbf{u}} = \{\mathbf{u}, \tilde{\mathcal{H}}_p\},\ \dot{\mathbf{u}} = \{\mathbf{u}, \tilde{\mathcal{H}}_E\},\ \dot{\mathbf{u}} = \{\mathbf{u}, \tilde{\mathcal{H}}_B\}.$$

The subsystems for $\tilde{\mathcal{H}}_E$ and $\tilde{\mathcal{H}}_B$ are solved exactly and then, evaluated at the discrete time steps $t^n = n\Delta t$. Let us denote $\tilde{\mathbf{u}}(t^n) =: \tilde{\mathbf{u}}^n$.

For $\tilde{\mathcal{H}}_E$, the equations of motion are

$$\begin{aligned}\dot{\boldsymbol{\Xi}} &= 0,\\ \dot{\mathbf{V}} &= \mathbb{W}_{\frac{q}{m}}\mathbb{N}(\boldsymbol{\Xi})\tilde{\mathbb{\Lambda}}^1(\boldsymbol{\Xi})\tilde{\mathbf{e}},\\ \dot{\tilde{\mathbf{e}}} &= 0,\\ \dot{\tilde{\mathbf{b}}} &= -\mathsf{C}\tilde{\mathbf{e}}\end{aligned} \tag{6.1}$$

and the time discrete version reads

$$\begin{aligned}\boldsymbol{\Xi}^{n+1} &= \boldsymbol{\Xi}^n,\\ \mathbf{V}^{n+1} &= \mathbf{V}^n + \Delta t\mathbb{W}_{\frac{q}{m}}\mathbb{N}(\boldsymbol{\Xi}^n)\tilde{\mathbb{\Lambda}}^1(\boldsymbol{\Xi}^n)\tilde{\mathbf{e}}^n,\\ \tilde{\mathbf{e}}^{n+1} &= \tilde{\mathbf{e}}^n,\\ \tilde{\mathbf{b}}^{n+1} &= \tilde{\mathbf{b}}^n - \Delta t\mathsf{C}\tilde{\mathbf{e}}^n.\end{aligned}$$

For $\tilde{\mathcal{H}}_B$, we get

$$\begin{aligned}\dot{\boldsymbol{\Xi}} &= 0,\\ \dot{\mathbf{V}} &= 0,\\ \tilde{\mathsf{M}}_1\dot{\tilde{\mathbf{e}}} &= \mathsf{C}^\top\tilde{\mathsf{M}}_2\tilde{\mathbf{b}},\\ \dot{\tilde{\mathbf{b}}} &= 0,\end{aligned} \tag{6.2}$$

which leads to the discretisation

$$\begin{aligned}\boldsymbol{\Xi}^{n+1} &= \boldsymbol{\Xi}^n,\\ \mathbf{V}^{n+1} &= \mathbf{V}^n,\\ \tilde{\mathsf{M}}_1\tilde{\mathbf{e}}^{n+1} &= \tilde{\mathsf{M}}_1\tilde{\mathbf{e}}^n + \Delta t\mathsf{C}^\top\tilde{\mathsf{M}}_2\tilde{\mathbf{b}}^n,\\ \tilde{\mathbf{b}}^{n+1} &= \tilde{\mathbf{b}}^n.\end{aligned}$$

For $\tilde{\mathcal{H}}_p$, we obtain the following equations:

$$\begin{aligned}\dot{\boldsymbol{\Xi}} &= \mathbb{N}^\top(\boldsymbol{\Xi})\mathbf{V},\\ \dot{\mathbf{V}} &= \mathbb{W}_{\frac{q}{m}}\mathbb{N}(\boldsymbol{\Xi})\tilde{\mathbb{B}}(\boldsymbol{\Xi},\tilde{\mathbf{b}})\mathbb{N}^\top(\boldsymbol{\Xi})\mathbf{V},\\ \tilde{\mathsf{M}}_1\dot{\tilde{\mathbf{e}}} &= -\tilde{\mathbb{\Lambda}}^1(\boldsymbol{\Xi})^\top\mathbb{N}^\top(\boldsymbol{\Xi})\mathbb{W}_q\mathbf{V},\\ \dot{\tilde{\mathbf{b}}} &= 0.\end{aligned} \tag{6.3}$$

Here, we get the analytic solution

$$\begin{aligned}
\boldsymbol{\Xi}(\Delta t) &= \boldsymbol{\Xi}(0) + \int_0^{\Delta t} \mathbb{N}^\top(\boldsymbol{\Xi}(t))\mathbf{V}(t)\ \mathrm{d}t,\\
\mathbf{V}(\Delta t) &= \mathbf{V}(0) + \mathbb{W}_{\frac{q}{m}} \int_0^{\Delta t} \mathbb{N}(\boldsymbol{\Xi}(t))\tilde{\mathbb{B}}(\boldsymbol{\Xi}(t), \tilde{\mathbf{b}}(0))\mathbb{N}^\top(\boldsymbol{\Xi}(t))\mathbf{V}(t)\ \mathrm{d}t,\\
\tilde{\mathsf{M}}_1\tilde{\mathbf{e}}(\Delta t) &= \tilde{\mathsf{M}}_1\tilde{\mathbf{e}}(0) - \int_0^{\Delta t} \tilde{\mathbb{\Lambda}}^1(\boldsymbol{\Xi}(t))^\top \mathbb{N}^\top(\boldsymbol{\Xi}(t))\mathbb{W}_q\mathbf{V}(t)\ \mathrm{d}t,\\
\tilde{\mathbf{b}}(\Delta t) &= \tilde{\mathbf{b}}(0).
\end{aligned}$$

This system is implicit in the particle coordinates $(\boldsymbol{\Xi}, \mathbf{V})$ but decouples between different particles. It is not possible to solve the resulting 6×6 systems explicitly. Therefore, the kinetic energy part was further split into the three directions in [56]. Such a splitting yields explicit equations only if the Jacobian matrix of the coordinate transformation is diagonal and constant. Since this is generally not true, we keep the kinetic part together.

In order to solve the non-linearity caused by the dependence of $\mathbb{N}$ on $\boldsymbol{\Xi}$, we need to introduce an approximation that conserves the Poisson structure. In [55], it has been shown that a Gauss-conserving discretisation can be obtained using the same constant velocity for both the position and the current update. We solve the particle equations with the symplectic midpoint method in a fixpoint iteration using a predictor-corrector scheme. Then, the current for the update of the electric field is computed with a line integral for $\tilde{\mathbb{\Lambda}}^1(\boldsymbol{\Xi}(t))$ and the velocity from the position update. This results in the following system:

$$\begin{aligned}
\boldsymbol{\Xi}^{n+1} &= \boldsymbol{\Xi}^n + \Delta t \mathbb{N}^\top\left(\overline{\boldsymbol{\Xi}}\right)\overline{\mathbf{V}}, && \text{(6.4a)}\\
\mathbf{V}^{n+1} &= \mathbf{V}^n + \Delta t \mathbb{W}_{\frac{q}{m}}\mathbb{N}\left(\overline{\boldsymbol{\Xi}}\right)\tilde{\mathbb{B}}\left(\overline{\boldsymbol{\Xi}}, \tilde{\mathbf{b}}^n\right)\mathbb{N}^\top\left(\overline{\boldsymbol{\Xi}}\right)\overline{\mathbf{V}},\\
\tilde{\mathsf{M}}_1\tilde{\mathbf{e}}^{n+1} &= \tilde{\mathsf{M}}_1\tilde{\mathbf{e}}^n - \int_{t^n}^{t^{n+1}} \tilde{\mathbb{\Lambda}}^1(\boldsymbol{\Xi}(\tau))^\top \mathrm{d}\tau \mathbb{W}_q\mathbb{N}^\top\left(\overline{\boldsymbol{\Xi}}\right)\overline{\mathbf{V}}, && \text{(6.4b)}\\
\tilde{\mathbf{b}}^{n+1} &= \tilde{\mathbf{b}}^n,
\end{aligned}$$

where $\overline{\boldsymbol{\Xi}} = \frac{\boldsymbol{\Xi}^{n+1}+\boldsymbol{\Xi}^n}{2}$, $\overline{\mathbf{V}} = \frac{\mathbf{V}^{n+1}+\mathbf{V}^n}{2}$ and $\boldsymbol{\Xi}(\tau) = \frac{(t^{n+1}-\tau)\boldsymbol{\Xi}^n+(\tau-t^n)\boldsymbol{\Xi}^{n+1}}{\Delta t}$.

Proposition 6.1. *For the proposed splitting, Gauss' law is preserved over time if it is satisfied initially and* (6.3) *is discretised as in* (6.4)*.*

Proof. First, we identify the two splitting steps in which the electric field is changed. In $\tilde{\mathcal{H}}_B$, the update of the electric field (6.2) multiplied by $\mathsf{G}^\top$ stays constant due to the discrete complex property (3.5). For $\tilde{\mathcal{H}}_p$, we multiply (6.4b) with $\mathsf{G}^\top$, plug in the position formula (6.4a)

and use that $\frac{\mathrm{d}\boldsymbol{\Xi}}{\mathrm{d}\tau} = \frac{\boldsymbol{\Xi}^{n+1}-\boldsymbol{\Xi}^n}{\Delta t}$ is constant in time,

$$\begin{aligned}
&\mathsf{G}^\top \tilde{\mathsf{M}}_1 \tilde{\mathbf{e}}^{n+1} - \mathsf{G}^\top \tilde{\mathsf{M}}_1 \tilde{\mathbf{e}}^{n} = -\int_{t^n}^{t^{n+1}} \mathsf{G}^\top \tilde{\mathbb{\Lambda}}^1(\boldsymbol{\Xi}(\tau))^\top \,\mathrm{d}\tau \mathbb{W}_q \frac{\boldsymbol{\Xi}^{n+1}-\boldsymbol{\Xi}^n}{\Delta t} \\
\Leftrightarrow\ &\mathsf{G}^\top \tilde{\mathsf{M}}_1 \tilde{\mathbf{e}}^{n+1} - \mathsf{G}^\top \tilde{\mathsf{M}}_1 \tilde{\mathbf{e}}^{n} = -\int_{t^n}^{t^{n+1}} \mathbb{W}_q \mathsf{G}^\top \tilde{\mathbb{\Lambda}}^1(\boldsymbol{\Xi}(\tau))^\top \frac{\mathrm{d}\boldsymbol{\xi}(\tau)}{\mathrm{d}\tau} \,\mathrm{d}\tau.
\end{aligned}$$

Last, we use the chain rule, $\frac{\mathrm{d}\tilde{\mathbb{\Lambda}}^0(\boldsymbol{\Xi}(\tau))^\top}{\mathrm{d}\tau}\mathbb{1}_{N_p} = \mathsf{G}^\top \tilde{\mathbb{\Lambda}}^1(\boldsymbol{\Xi}(\tau))^\top \frac{\mathrm{d}\boldsymbol{\xi}(\tau)}{\mathrm{d}\tau}$, and obtain

$$\begin{aligned}
&\mathsf{G}^\top \tilde{\mathsf{M}}_1 \tilde{\mathbf{e}}^{n+1} - \mathsf{G}^\top \tilde{\mathsf{M}}_1 \tilde{\mathbf{e}}^{n} = -\int_{t^n}^{t^{n+1}} \mathbb{W}_q \frac{\mathrm{d}\tilde{\mathbb{\Lambda}}^0(\boldsymbol{\Xi}(\tau))^\top}{\mathrm{d}\tau}\mathbb{1}_{N_p} \,\mathrm{d}\tau \\
\Leftrightarrow\ &\mathsf{G}^\top \tilde{\mathsf{M}}_1 \tilde{\mathbf{e}}^{n+1} - \mathsf{G}^\top \tilde{\mathsf{M}}_1 \tilde{\mathbf{e}}^{n} = -\left(\mathbb{W}_q \tilde{\mathbb{\Lambda}}^0(\boldsymbol{\Xi}^{n+1})^\top \mathbb{1}_{N_p} - \mathbb{W}_q \tilde{\mathbb{\Lambda}}^0(\boldsymbol{\Xi}^{n})^\top \mathbb{1}_{N_p}\right).
\end{aligned}$$

□

Note that the source-free part of Maxwell's equations is solved in separate splitting steps, which causes a restriction on the time step (cf. [55, Appendix A.2]. Using the stability condition for $\frac{\Delta t}{\Delta x}$ on Cartesian grids with the minimal cell size of the mapped grid provides a rough estimate for the maximal time step. For the simulation results of this Hamiltonian splitting we use the acronym HS.

In [54], the original explicit Hamiltonian splitting into five parts from [45] was constructed for curvilinear coordinates with the velocity represented in covariant coordinates $\hat{\mathbf{v}}$ (5.6). However, this works only for orthogonal mappings, where the partial derivatives of the diagonal entries of the inverse metric equal zero, i.e. $\partial_{\xi_i} g^{ii} = 0, i = 1,2,3$. In this case, the particle update is componentwise independent, meaning $\dot{\xi}_i$ does not depend on ξ_i and $\dot{\hat{v}}_i$ does not depend on $\hat{v}_i$ for $i = 1,2,3$, which yields the following splitting:

$$\tilde{\mathcal{H}}_h = \tilde{\mathcal{H}}_{p1} + \tilde{\mathcal{H}}_{p2} + \tilde{\mathcal{H}}_{p3} + \tilde{\mathcal{H}}_E + \tilde{\mathcal{H}}_B$$

with $\tilde{\mathcal{H}}_{pi} = \frac{1}{2} m_p \hat{v}_i g^{ii} \hat{v}_i, i = 1,2,3, \tilde{\mathcal{H}}_E = \frac{1}{2}\tilde{\mathbf{e}}^\top \tilde{\mathsf{M}}_1 \tilde{\mathbf{e}}, \tilde{\mathcal{H}}_B = \frac{1}{2}\mathsf{C}^\top \tilde{\mathbf{a}}^\top \tilde{\mathsf{M}}_2 \mathsf{C}\tilde{\mathbf{a}}$.

Then, with the notation from [27], $g^{ii} = (G_m)^{-1}_{ii}$, the five operators are given by

$$\begin{aligned}
&\tilde{\mathcal{H}}_{p1}: \\
&\quad \dot{\xi}_1 = g^{11}(\xi_2,\xi_3)\hat{v}_1, \\
&\quad \dot{\hat{v}}_2 = -\frac{q}{m} g^{11}(\xi_2,\xi_3)\hat{v}_1 \tilde{\Lambda}^2_3 \tilde{b}_3 - \frac{1}{2}\partial_{\xi_2} g^{11}(\xi_2,\xi_3)\hat{v}_1, \\
&\quad \dot{\hat{v}}_3 = \frac{q}{m} g^{11}(\xi_2,\xi_3)\hat{v}_1 \tilde{\Lambda}^2_2 \tilde{b}_2 - \frac{1}{2}\partial_{\xi_3} g^{11}(\xi_2,\xi_3)\hat{v}_1^2, \\
&\quad \dot{\tilde{e}}_1 = -q\tilde{\mathsf{M}}^{-1}_{11} \tilde{\mathbf{\Lambda}}^1_1(\boldsymbol{\xi})^\top g^{11}(\xi_2,\xi_3)\hat{v}_1^2.
\end{aligned}$$

$$
\begin{aligned}
&\tilde{\mathcal{H}}_{p2}: \\
&\quad \dot{\xi}_2 = g^{22}(\xi_1, \xi_3)\hat{v}_2, \\
&\quad \dot{\hat{v}}_1 = \frac{q}{m} g^{22}(\xi_1, \xi_3)\hat{v}_2 \tilde{\Lambda}_3^2 \tilde{b}_3 - \frac{1}{2}\partial_{\xi_1} g^{22}(\xi_1, \xi_3)\hat{v}_2^2, \\
&\quad \dot{\hat{v}}_3 = -\frac{q}{m} g^{22}(\xi_1, \xi_3)\tilde{\Lambda}_1^2 \tilde{b}_1 - \frac{1}{2}\partial_{\xi_3} g^{22}(\xi_1, \xi_3)\hat{v}_2^2, \\
&\quad \dot{\tilde{e}}_2 = -q\tilde{\mathsf{M}}_{12}^{-1} \tilde{\mathbf{\Lambda}}_2^1(\boldsymbol{\xi})^\top g^{22}(\xi_1, \xi_3)\hat{v}_2.
\end{aligned}
$$

$$
\begin{aligned}
&\tilde{\mathcal{H}}_{p3}: \\
&\quad \dot{\xi}_3 = g^{33}(\xi_1, \xi_2)\hat{v}_3, \\
&\quad \dot{\hat{v}}_1 = -\frac{q}{m} g^{33}(\xi_1, \xi_2)\hat{v}_3 \tilde{\Lambda}_2^2 \tilde{b}_2 - \frac{1}{2}\partial_{\xi_1} g^{33}(\xi_1, \xi_2)\hat{v}_3^2, \\
&\quad \dot{\hat{v}}_2 = \frac{q}{m} g^{33}(\xi_1, \xi_2)\hat{v}_3 \tilde{\Lambda}_1^2 \tilde{b}_1 - \frac{1}{2}\partial_{\xi_2} g^{33}(\xi_1, \xi_2)\hat{v}_3^2, \\
&\quad \dot{\tilde{e}}_3 = -q\tilde{\mathsf{M}}_{13}^{-1} \tilde{\mathbf{\Lambda}}_3^1(\boldsymbol{\xi})^\top g^{33}(\xi_1, \xi_2)\hat{v}_3.
\end{aligned}
$$

$$
\begin{aligned}
&\tilde{\mathcal{H}}_E: \\
&\quad \dot{\hat{\mathbf{v}}} = \frac{q}{m} \tilde{\mathbf{\Lambda}}^1 \tilde{\mathbf{e}}, \\
&\quad \dot{\tilde{\mathbf{b}}} = -\mathsf{C}\tilde{\mathbf{e}}. \\
&\tilde{\mathcal{H}}_B: \\
&\quad \dot{\tilde{\mathbf{e}}} = \tilde{\mathsf{M}}_1^{-1} \mathsf{C}^\top \tilde{\mathsf{M}}_2 \tilde{\mathbf{b}}.
\end{aligned}
$$

Remark 6.2. *Examples for orthogonal mappings that satisfy the additional condition are cylindrical and spherical coordinates,*

$$
\mathbf{x} = (\xi_1 \cos(\xi_2), \xi_1 \sin(\xi_2), \xi_3)^\top, \mathbf{x} = (\xi_1 \sin(\xi_2)\cos(\xi_3), \xi_1 \sin(\xi_2)\sin(\xi_3), \xi_1 \cos(\xi_2))^\top.
$$

Examples for mappings that are orthogonal but do not satisfy the additional condition are the cylindrical mapping with a square root of the radial direction,

$$
\mathbf{x} = (\sqrt{\xi_1}\cos(\xi_2), \sqrt{\xi_1}\sin(\xi_2), \xi_3)^\top,
$$

or an elliptical mapping,

$$
\mathbf{x} = (R\cosh(\xi_1)\cos(\xi_2), R\sinh(\xi_1)\sin(\xi_2), \xi_3)^\top.
$$

Other mappings such as the sinusoidally distorted mapping,

$$
\mathbf{x} = (\xi_1 + \alpha\sin(\xi_1)\sin(\xi_2), \xi_2 + \alpha\sin(\xi_1)\sin(\xi_2), \xi_3)^\top,
$$

are not even orthogonal so that the metric has non-diagonal entries. This prevents an explicit time discretisation in form of a Hamiltonian splitting. In summary, we see that the explicit

Hamiltonian splitting can only be constructed for a limited number of mappings. Therefore, on the route towards realistic tokamak geometry, we focus on the semi-implicit time stepping methods based on a hybrid particle push.

6.1.2 Alternative Splitting

The following splitting in three parts is taken from the paper of Crouseilles, Einkemmer & Faou [21], where another bracket is used, which does not satisfy the Jacobi identity. The discretisation of this bracket yields a different matrix, which together with a Hamiltonian splitting results in slightly different subsystems. In this splitting, the first subsystem takes the same form as (6.1) in the GEMPIC splitting but the second subsystem is given as

$$\begin{aligned}
\dot{\boldsymbol{\Xi}} &= 0, \\
\dot{\mathbf{V}} &= \mathbb{W}_{\frac{q}{m}} \mathbb{N}(\boldsymbol{\Xi}) \tilde{\mathbb{B}}(\boldsymbol{\Xi}, \tilde{\mathbf{b}}) \mathbb{N}^\top(\boldsymbol{\Xi}) \mathbf{V}, \\
\tilde{\mathsf{M}}_1 \dot{\tilde{\mathbf{e}}} &= \mathsf{C}^\top \tilde{\mathsf{M}}_2 \tilde{\mathbf{b}}, \\
\dot{\tilde{\mathbf{b}}} &= 0.
\end{aligned}$$

Thus, only the update of the electric field can be solved exactly whereas the velocity equation must be solved implicitly because the velocity directions cannot be decoupled. For the discretisation, the symplectic midpoint method is used. However, as this is only a 3×3 system particle-wise, the direct computation of the inverse of $\left(\mathbb{I} - \frac{\Delta t}{2} \mathbb{W}_{\frac{q}{m}} \mathbb{N}(\boldsymbol{\Xi}^n) \tilde{\mathbb{B}}(\boldsymbol{\Xi}^n, \tilde{\mathbf{b}}^n) \mathbb{N}^\top(\boldsymbol{\Xi}^n)\right)$ is most suitable. This leads to the following discrete equations:

$$\begin{aligned}
\boldsymbol{\Xi}^{n+1} &= \boldsymbol{\Xi}^n, \\
\left(\mathbb{I} - \frac{\Delta t}{2} \mathbb{W}_{\frac{q}{m}} \mathbb{N}(\boldsymbol{\Xi}^n) \tilde{\mathbb{B}}(\boldsymbol{\Xi}^n, \tilde{\mathbf{b}}^n) \mathbb{N}^\top(\boldsymbol{\Xi}^n)\right) \mathbf{V}^{n+1} &= \left(\mathbb{I} + \frac{\Delta t}{2} \mathbb{W}_{\frac{q}{m}} \mathbb{N}(\boldsymbol{\Xi}^n) \tilde{\mathbb{B}}(\boldsymbol{\Xi}^n, \tilde{\mathbf{b}}^n) \mathbb{N}^\top(\boldsymbol{\Xi}^n)\right) \mathbf{V}^n, \\
\tilde{\mathsf{M}}_1 \tilde{\mathbf{e}}^{n+1} &= \tilde{\mathsf{M}}_1 \tilde{\mathbf{e}}^n + \Delta t \mathsf{C}^\top \tilde{\mathsf{M}}_2 \tilde{\mathbf{b}}^n, \\
\tilde{\mathbf{b}}^{n+1} &= \tilde{\mathbf{b}}^n.
\end{aligned} \tag{6.5}$$

For the third subsystem, the equations of motion read

$$\begin{aligned}
\dot{\boldsymbol{\Xi}} &= \mathbb{N}^\top(\boldsymbol{\Xi}) \mathbf{V}, \\
\dot{\mathbf{V}} &= 0, \\
\tilde{\mathsf{M}}_1 \dot{\tilde{\mathbf{e}}} &= -\tilde{\mathbb{\Lambda}}^1(\boldsymbol{\Xi})^\top \mathbb{N}^\top(\boldsymbol{\Xi}) \mathbb{W}_q \mathbf{V}, \\
\dot{\tilde{\mathbf{b}}} &= 0.
\end{aligned}$$

As in the GEMPIC splitting (6.4a),(6.4b), we solve the position update iteratively with the symplectic midpoint method in a predictor-corrector scheme. Then, we compute the current

with the same velocity and an exact line integral for $\tilde{\Lambda}^1(\boldsymbol{\Xi}(t))$,

$$\begin{aligned}
\boldsymbol{\Xi}^{n+1} &= \boldsymbol{\Xi}^n + \Delta t \mathbb{N}^\top \left(\frac{\boldsymbol{\Xi}^{n+1} + \boldsymbol{\Xi}^n}{2} \right) \mathbf{V}^n, \\
\mathbf{V}^{n+1} &= \mathbf{V}^n, \\
\tilde{\mathsf{M}}_1 \tilde{\mathbf{e}}^n &= \tilde{\mathsf{M}}_1 \tilde{\mathbf{e}}^n - \int_{t^n}^{t^{n+1}} \tilde{\Lambda}^1(\boldsymbol{\Xi}(\tau))^\top \, \mathrm{d}\tau \mathbb{W}_q \mathbb{N}^\top \left(\frac{\boldsymbol{\Xi}^{n+1} + \boldsymbol{\Xi}^n}{2} \right) \mathbf{V}^n, \\
\tilde{\mathbf{b}}^{n+1} &= \tilde{\mathbf{b}}^n.
\end{aligned} \tag{6.6}$$

Proposition 6.3. *For the proposed splitting, Gauss' law is preserved over time if it is satisfied initially and the third system is discretised as in* (6.6)*.*

Proof. It applies the same proof of Proposition 6.1 with $\frac{\boldsymbol{\Xi}^{n+1} - \boldsymbol{\Xi}^n}{\Delta t} = \mathbb{N}^\top \left(\frac{\boldsymbol{\Xi}^{n+1} + \boldsymbol{\Xi}^n}{2} \right) \mathbf{V}^n$. □

Although this splitting is not derived from our Poisson structure, it still conserves Gauss' law and is quite fast as we do not need to deal with the non-linear dependency of $\boldsymbol{\Xi}$ and $\mathbf{V}$ in the $\tilde{\mathcal{H}}_p$ step. Again the curl-part of Maxwell's equations is split so that the scheme is subject to a time step restriction. For the simulation results of this method, we use the acronym CEF.

6.2 Energy Conserving Antisymmetric Splitting

Next, we consider energy conserving time discretisations constructed as discrete gradients [75]. First, we revise the idea of the discrete gradient method following [67].

Theorem 6.1. *Let us consider a system of ordinary differential equations of the form*

$$\dot{\tilde{\mathbf{u}}} = \mathcal{J}(\tilde{\mathbf{u}}) D\tilde{\mathcal{H}}(\tilde{\mathbf{u}})$$

with a skew-symmetric matrix $\mathcal{J}$. Then, the discrete gradient discretisation of the form

$$\frac{\tilde{\mathbf{u}}^{n+1} - \tilde{\mathbf{u}}^n}{\Delta t} = \bar{\mathcal{J}}(\tilde{\mathbf{u}}^{n+1}, \tilde{\mathbf{u}}^n) D\tilde{\mathcal{H}}_h(\tilde{\mathbf{u}}^{n+1}, \tilde{\mathbf{u}}^n)$$

is energy conserving if $\bar{\mathcal{J}}(\tilde{\mathbf{u}}^{n+1}, \tilde{\mathbf{u}}^n)$ is skew-symmetric.

Proof. The energy variation in one time step is defined as

$$\tilde{\mathcal{H}}_h^{n+1} - \tilde{\mathcal{H}}_h^n = D\tilde{\mathcal{H}}_h(\tilde{\mathbf{u}}^{n+1}, \tilde{\mathbf{u}}^n)^\top \left(\tilde{\mathbf{u}}^{n+1} - \tilde{\mathbf{u}}^n \right).$$

Now, we insert the discretisation from above and use the skew-symmetry of $\bar{\mathcal{J}}(\tilde{\mathbf{u}}^{n+1}, \tilde{\mathbf{u}}^n)$,

$$\begin{aligned}\tilde{\mathcal{H}}_h^{n+1} - \tilde{\mathcal{H}}_h^n &= D\tilde{\mathcal{H}}_h(\tilde{\mathbf{u}}^{n+1}, \tilde{\mathbf{u}}^n)^\top \left(\Delta t \bar{\mathcal{J}}(\tilde{\mathbf{u}}^{n+1}, \tilde{\mathbf{u}}^n) D\tilde{\mathcal{H}}_h(\tilde{\mathbf{u}}^{n+1}, \tilde{\mathbf{u}}^n)\right) \\ &= -\Delta t D\tilde{\mathcal{H}}_h(\tilde{\mathbf{u}}^{n+1}, \tilde{\mathbf{u}}^n)^\top \bar{\mathcal{J}}(\tilde{\mathbf{u}}^{n+1}, \tilde{\mathbf{u}}^n) D\tilde{\mathcal{H}}_h(\tilde{\mathbf{u}}^{n+1}, \tilde{\mathbf{u}}^n) = 0.\end{aligned}$$

□

Several ways to construct discrete gradients have been proposed in the literature [53, 36, 15]. However, in our case the Hamiltonian is quadratic—and $D\tilde{\mathcal{H}}_h$ linear—so that all methods simplify to the second order midpoint rule. Hence, this leaves us with the choice of how to discretise $\mathcal{J}$. Moreover, we follow [55] and split the discrete Poisson matrix $\mathbb{J}$, keeping its skew-symmetry in each subsystem. So, we obtain the following four subsystems:

$$\begin{aligned}&\text{system 1: } \dot{\boldsymbol{\Xi}} = \mathbb{N}^\top(\boldsymbol{\Xi})\mathbf{V}, \\ &\text{system 2: } \dot{\mathbf{V}} = \mathbb{W}_{\frac{q}{m}} \mathbb{N}(\boldsymbol{\Xi}) \tilde{\mathbb{B}}(\boldsymbol{\Xi}, \tilde{\mathbf{b}}) \mathbb{N}^\top(\boldsymbol{\Xi}) \mathbf{V}, \\ &\text{system 3: } \dot{\tilde{\mathbf{b}}} = -\mathsf{C}\tilde{\mathbf{e}},\ \tilde{\mathsf{M}}_1 \dot{\tilde{\mathbf{e}}} = \mathsf{C}^\top \tilde{\mathsf{M}}_2 \tilde{\mathbf{b}}, \\ &\text{system 4: } \dot{\mathbf{V}} = \mathbb{W}_{\frac{q}{m}} \mathbb{N}(\boldsymbol{\Xi}) \tilde{\mathbb{\Lambda}}^1(\boldsymbol{\Xi}) \tilde{\mathbf{e}},\ \tilde{\mathsf{M}}_1 \dot{\tilde{\mathbf{e}}} = -\tilde{\mathbb{\Lambda}}^1(\boldsymbol{\Xi})^\top \mathbb{N}^\top(\boldsymbol{\Xi}) \mathbb{W}_q \mathbf{V}.\end{aligned} \tag{6.7}$$

In the first system, the element of the Poisson matrix $\mathbb{N}(\boldsymbol{\Xi})^\top$ is changing over time and needs to be approximated. We use a Crank-Nicolson method to maintain second order accuracy and solve the system iteratively with a predictor-corrector scheme,

$$\boldsymbol{\Xi}^{n+1} = \boldsymbol{\Xi}^n + \Delta t \frac{\mathbb{N}^\top(\boldsymbol{\Xi}^{n+1}) + \mathbb{N}^\top(\boldsymbol{\Xi}^n)}{2} \mathbf{V}^n.$$

Note that the system is block-diagonal and hence, only couples the position of one particle at a time.

In the other three systems, the Poisson matrix is constant over time and we use the midpoint rule to discretise the $D\tilde{\mathcal{H}}_h$ part. Then, the equation for the second system reads

$$\begin{aligned}\frac{\mathbf{V}^{n+1} - \mathbf{V}^n}{\Delta t} &= \mathbb{W}_{\frac{q}{m}} \mathbb{N} \tilde{\mathbb{B}} \mathbb{N}^\top \frac{\mathbf{V}^{n+1} + \mathbf{V}^n}{2} \\ \Leftrightarrow \left(\mathbb{I} - \frac{\Delta t}{2} \mathbb{W}_{\frac{q}{m}} \mathbb{N} \tilde{\mathbb{B}} \mathbb{N}^\top\right) \mathbf{V}^{n+1} &= \left(\mathbb{I} + \frac{\Delta t}{2} \mathbb{W}_{\frac{q}{m}} \mathbb{N} \tilde{\mathbb{B}} \mathbb{N}^\top\right) \mathbf{V}^n,\end{aligned} \tag{6.8}$$

where for every particle the inverse of the 3×3 matrix on the left-hand side can be exactly calculated.

With the same method, system 3 becomes

$$\tilde{\mathsf{M}}_1 \frac{\tilde{\mathbf{e}}^{n+1} - \tilde{\mathbf{e}}^n}{\Delta t} = \mathsf{C}^\top \tilde{\mathsf{M}}_2 \frac{\tilde{\mathbf{b}}^{n+1} + \tilde{\mathbf{b}}^n}{2},$$
$$\frac{\tilde{\mathbf{b}}^{n+1} - \tilde{\mathbf{b}}^n}{\Delta t} = -\mathsf{C} \frac{\tilde{\mathbf{e}}^{n+1} + \tilde{\mathbf{e}}^n}{2}.$$

We write this in matrix form as

$$\begin{pmatrix} \tilde{\mathsf{M}}_1 & -\frac{\Delta t}{2}\mathsf{C}^\top \tilde{\mathsf{M}}_2 \\ \frac{\Delta t}{2}\mathsf{C} & \mathbb{I} \end{pmatrix} \begin{pmatrix} \tilde{\mathbf{e}}^{n+1} \\ \tilde{\mathbf{b}}^{n+1} \end{pmatrix} = \begin{pmatrix} \tilde{\mathsf{M}}_1 & \frac{\Delta t}{2}\mathsf{C}^\top \tilde{\mathsf{M}}_2 \\ -\frac{\Delta t}{2}\mathsf{C} & \mathbb{I} \end{pmatrix} \begin{pmatrix} \tilde{\mathbf{e}}^{n} \\ \tilde{\mathbf{b}}^{n} \end{pmatrix}$$

and decouple the equation with the Schur complement $S = \tilde{\mathsf{M}}_1 + \frac{\Delta t^2}{4}\mathsf{C}^\top \tilde{\mathsf{M}}_2 \mathsf{C}$,

$$\begin{pmatrix} \tilde{\mathsf{M}}_1 & -\frac{\Delta t}{2}\mathsf{C}^\top \tilde{\mathsf{M}}_2 \\ \frac{\Delta t}{2}\mathsf{C} & \mathbb{I} \end{pmatrix}^{-1} = \begin{pmatrix} \mathbb{I} & 0 \\ -\frac{\Delta t}{2}\mathsf{C} & \mathbb{I} \end{pmatrix} \begin{pmatrix} S^{-1} & 0 \\ 0 & \mathbb{I} \end{pmatrix} \begin{pmatrix} \mathbb{I} & \frac{\Delta t}{2}\mathsf{C}^\top M_2 \\ 0 & \mathbb{I} \end{pmatrix}.$$

So, we get

$$\begin{aligned} \tilde{\mathbf{e}}^{n+1} &= S^{-1}\left((\tilde{\mathsf{M}}_1 - \frac{\Delta t^2}{4}\mathsf{C}^\top \tilde{\mathsf{M}}_2 \mathsf{C})\tilde{\mathbf{e}}^n + \Delta t \mathsf{C}^\top \tilde{\mathsf{M}}_2 \tilde{\mathbf{b}}^n \right), \\ \tilde{\mathbf{b}}^{n+1} &= \tilde{\mathbf{b}}^n - \frac{\Delta t}{2}\mathsf{C}(\tilde{\mathbf{e}}^{n+1} + \tilde{\mathbf{e}}^n). \end{aligned} \tag{6.9}$$

Finally, system 4 is discretised as

$$\frac{\mathbf{V}^{n+1} - \mathbf{V}^n}{\Delta t} = \mathbb{W}_{\frac{q}{m}} \mathbb{N} \tilde{\mathbb{\Lambda}}^1 \frac{\tilde{\mathbf{e}}^{n+1} + \tilde{\mathbf{e}}^n}{2},$$
$$\tilde{\mathsf{M}}_1 \frac{\tilde{\mathbf{e}}^{n+1} - \tilde{\mathbf{e}}^n}{\Delta t} = -(\tilde{\mathbb{\Lambda}}^1)^\top \mathbb{N}^\top \mathbb{W}_q \frac{\mathbf{V}^{n+1} + \mathbf{V}^n}{2}$$

and we use again the Schur complement to decouple the matrix form of the system,

$$\begin{pmatrix} \mathbb{I} & -\frac{\Delta t}{2}\mathbb{W}_{\frac{q}{m}} \mathbb{N} \tilde{\mathbb{\Lambda}}^1 \\ \frac{\Delta t}{2}(\tilde{\mathbb{\Lambda}}^1)^\top \mathbb{N}^\top \mathbb{W}_q & \tilde{\mathsf{M}}_1 \end{pmatrix} \begin{pmatrix} \mathbf{V}^{n+1} \\ \tilde{\mathbf{e}}^{n+1} \end{pmatrix} = \begin{pmatrix} \mathbb{I} & \frac{\Delta t}{2}\mathbb{W}_{\frac{q}{m}} \mathbb{N} \tilde{\mathbb{\Lambda}}^1 \\ -\frac{\Delta t}{2}(\tilde{\mathbb{\Lambda}}^1)^\top \mathbb{N}^\top \mathbb{W}_q & \tilde{\mathsf{M}}_1 \end{pmatrix} \begin{pmatrix} \mathbf{V}^{n} \\ \tilde{\mathbf{e}}^{n} \end{pmatrix}.$$

Then, the Schur complement has the following form: $S = \tilde{\mathsf{M}}_1 + \frac{\Delta t^2}{4}\mathbb{W}_q \mathbb{W}_{\frac{q}{m}} (\tilde{\mathbb{\Lambda}}^1)^\top \mathbb{N}^\top \mathbb{N} \tilde{\mathbb{\Lambda}}^1$, which leads to the inverse

$$\begin{pmatrix} \mathbb{I} & -\frac{\Delta t}{2}\mathbb{W}_{\frac{q}{m}} \mathbb{N} \tilde{\mathbb{\Lambda}}^1 \\ \frac{\Delta t}{2}(\tilde{\mathbb{\Lambda}}^1)^\top \mathbb{N}^\top \mathbb{W}_q & \tilde{\mathsf{M}}_1 \end{pmatrix}^{-1} = \begin{pmatrix} \mathbb{I} & \frac{\Delta t}{2}\mathbb{W}_{\frac{q}{m}} \mathbb{N} \tilde{\mathbb{\Lambda}}^1 \\ 0 & \mathbb{I} \end{pmatrix} \begin{pmatrix} \mathbb{I} & 0 \\ 0 & S^{-1} \end{pmatrix} \begin{pmatrix} \mathbb{I} & 0 \\ -\frac{\Delta t}{2}(\tilde{\mathbb{\Lambda}}^1)^\top \mathbb{N}^\top \mathbb{W}_q & \mathbb{I} \end{pmatrix}.$$

Hence, we obtain the decoupled equations

$$\tilde{\mathbf{e}}^{n+1} = S^{-1}\left((\tilde{\mathsf{M}}_1 - \frac{\Delta t^2}{4}\mathbb{W}_q\mathbb{W}_{\frac{q}{m}}\mathbb{M}^\star)\tilde{\mathbf{e}}^n - \Delta t(\tilde{\mathbb{\Lambda}}^1)^\top\mathbb{N}^\top\mathbb{W}_q\mathbf{V}^n\right),$$
$$\mathbf{V}^{n+1} = \mathbf{V}^n + \frac{\Delta t}{2}\mathbb{W}_{\frac{q}{m}}\mathbb{N}\tilde{\mathbb{\Lambda}}^1(\tilde{\mathbf{e}}^{n+1} + \tilde{\mathbf{e}}^n),$$

where we introduced the particle mass matrix, $\mathbb{M}^\star := (\tilde{\mathbb{\Lambda}}^1)^\top\mathbb{N}^\top\mathbb{N}\tilde{\mathbb{\Lambda}}^1$, which is calculated componentwise for one particle as

$$(M^\star)_{ij} := \begin{pmatrix} \tilde{\Lambda}_i^{1,1} & 0 & 0 \\ 0 & \tilde{\Lambda}_i^{1,2} & 0 \\ 0 & 0 & \tilde{\Lambda}_i^{1,3} \end{pmatrix} G_m^{-1} \begin{pmatrix} \tilde{\Lambda}_j^{1,1} & 0 & 0 \\ 0 & \tilde{\Lambda}_j^{1,2} & 0 \\ 0 & 0 & \tilde{\Lambda}_j^{1,3} \end{pmatrix} = \begin{pmatrix} \tilde{\Lambda}_i^{1,1} g^{11} \tilde{\Lambda}_j^{1,1} & \tilde{\Lambda}_i^{1,1} g^{12} \tilde{\Lambda}_j^{1,2} & \tilde{\Lambda}_i^{1,1} g^{13} \tilde{\Lambda}_j^{1,3} \\ \tilde{\Lambda}_i^{1,2} g^{21} \tilde{\Lambda}_j^{1,1} & \tilde{\Lambda}_i^{1,2} g^{22} \tilde{\Lambda}_j^{1,2} & \tilde{\Lambda}_i^{1,2} g^{23} \tilde{\Lambda}_j^{1,3} \\ \tilde{\Lambda}_i^{1,3} g^{31} \tilde{\Lambda}_j^{1,1} & \tilde{\Lambda}_i^{1,3} g^{32} \tilde{\Lambda}_j^{1,2} & \tilde{\Lambda}_i^{1,3} g^{33} \tilde{\Lambda}_j^{1,3} \end{pmatrix}$$

for $1 \leq i, j \leq N_1$.

When we look at the charge conservation of the system, we notice that the conservation of Gauss' law gets lost if the current is not computed in the same splitting step as the position update, which is pointed out in [55]. The simulation results of this energy conserving discrete gradient method are labeled as DisGradE.

6.3 Energy and Charge Conserving Antisymmetric Splitting

In this section, we change the splitting and solve the systems 1 and 4 from the antisymmetric splitting (6.7) together. Our goal is to devise a discrete gradient method that also preserves Gauss' law. The three subsystems are given as

$$\text{system 1: } \dot{\mathbf{\Xi}} = \mathbb{N}(\mathbf{\Xi})^\top\mathbf{V}, \dot{\mathbf{V}} = \mathbb{W}_{\frac{q}{m}}\mathbb{N}(\mathbf{\Xi})\tilde{\mathbb{\Lambda}}^1(\mathbf{\Xi})\tilde{\mathbf{e}},\ \tilde{\mathsf{M}}_1\dot{\tilde{\mathbf{e}}} = -\tilde{\mathbb{\Lambda}}^1(\mathbf{\Xi})^\top\mathbb{N}(\mathbf{\Xi})^\top\mathbb{W}_q\mathbf{V},$$
$$\text{system 2: } \dot{\mathbf{V}} = \mathbb{W}_{\frac{q}{m}}\mathbb{N}(\mathbf{\Xi})\tilde{\mathbb{B}}(\mathbf{\Xi}, \tilde{\mathbf{b}})\mathbb{N}(\mathbf{\Xi})^\top\mathbf{V},$$
$$\text{system 3: } \dot{\tilde{\mathbf{b}}} = -\mathsf{C}\tilde{\mathbf{e}},\ \tilde{\mathsf{M}}_1\dot{\tilde{\mathbf{e}}} = \mathsf{C}^\top\tilde{\mathsf{M}}_2\tilde{\mathbf{b}}.$$

For the first system, we have to construct a discretisation of the partial Poisson matrix that is antisymmetric to maintain the energy conservation. Moreover, we are aiming at an approximation that preserves Gauss' law. Both goals are achieved with the following discretisation:

$$\frac{\mathbf{\Xi}^{n+1} - \mathbf{\Xi}^n}{\Delta t} = \frac{\mathbb{N}^\top(\mathbf{\Xi}^{n+1}) + \mathbb{N}^\top(\mathbf{\Xi}^n)}{2}\frac{\mathbf{V}^{n+1} + \mathbf{V}^n}{2},$$
$$\frac{\mathbf{V}^{n+1} - \mathbf{V}^n}{\Delta t} = \mathbb{W}_{\frac{q}{m}}\frac{\mathbb{N}(\mathbf{\Xi}^{n+1}) + \mathbb{N}(\mathbf{\Xi}^n)}{2}\frac{1}{\Delta t}\int_{t^n}^{t^{n+1}}\tilde{\mathbb{\Lambda}}^1(\mathbf{\Xi}(\tau))\,\mathrm{d}\tau\frac{\tilde{\mathbf{e}}^{n+1} + \tilde{\mathbf{e}}^n}{2}, \tag{6.10a}$$
$$\frac{\tilde{\mathsf{M}}_1\tilde{\mathbf{e}}^{n+1} - \tilde{\mathsf{M}}_1\tilde{\mathbf{e}}^n}{\Delta t} = -\frac{1}{\Delta t}\int_{t^n}^{t^{n+1}}\tilde{\mathbb{\Lambda}}^1(\mathbf{\Xi}(\tau))^\top\,\mathrm{d}\tau\frac{\mathbb{N}^\top(\mathbf{\Xi}^{n+1}) + \mathbb{N}^\top(\mathbf{\Xi}^n)}{2}\mathbb{W}_q\frac{\mathbf{V}^{n+1} + \mathbf{V}^n}{2}, \tag{6.10b}$$
$$\tilde{\mathbf{b}}^{n+1} = \tilde{\mathbf{b}}^n.$$

Since the system (6.10) is implicit, it has to be solved iteratively: First, we loop over the particle position and velocity and second, update the electric field with the computed current. Last, the whole system is looped over in a fixpoint iteration for the electric field.

The last two systems are still solved as in (6.8) and (6.9). Let us take a look at the conservation properties of this splitting.

Proposition 6.1. *The splitting defined by* (6.10)*,* (6.8) *and* (6.9) *conserves the discrete energy.*

Proof. Since system 2 and 3 are still discretised with the discrete gradient method, they trivially conserve the discrete energy. Therefore, we only have to check the discretisation of the first system (6.10). The variation of the discrete energy in this splitting step is given by

$$\begin{aligned}\tilde{\mathcal{H}}_h^{n+1} - \tilde{\mathcal{H}}_h^n &= \frac{1}{2}\left((\mathbf{V}^{n+1})^\top \mathbb{W}_m \mathbf{V}^{n+1} + (\tilde{\mathbf{e}}^{n+1})^\top \tilde{\mathsf{M}}_1 \tilde{\mathbf{e}}^{n+1}\right) - \frac{1}{2}\left((\mathbf{V}^n)^\top \mathbb{W}_m \mathbf{V}^n + (\tilde{\mathbf{e}}^n)^\top \tilde{\mathsf{M}}_1 \tilde{\mathbf{e}}^n\right) \\ &= \frac{1}{2}\left((\mathbf{V}^{n+1})^\top \mathbb{W}_m \mathbf{V}^{n+1} - (\mathbf{V}^n)^\top \mathbb{W}_m \mathbf{V}^n + (\tilde{\mathbf{e}}^{n+1})^\top \tilde{\mathsf{M}}_1 \tilde{\mathbf{e}}^{n+1} - (\tilde{\mathbf{e}}^n)^\top \tilde{\mathsf{M}}_1 \tilde{\mathbf{e}}^n\right).\end{aligned}$$

We multiply (6.10a) with $(\mathbf{V}^{n+1} + \mathbf{V}^n)^\top \mathbb{W}_m$ to find after some reordering,

$$\begin{aligned}&(\mathbf{V}^{n+1})^\top \mathbb{W}_m \mathbf{V}^{n+1} - (\mathbf{V}^n)^\top \mathbb{W}_m \mathbf{V}^n = \\ &\left(\int_{t^n}^{t^{n+1}} \tilde{\mathbb{\Lambda}}^1(\boldsymbol{\Xi}(\tau))^\top \,\mathrm{d}\tau \frac{\mathbb{N}^\top(\boldsymbol{\Xi}^{n+1}) + \mathbb{N}^\top(\boldsymbol{\Xi}^n)}{2} \mathbb{W}_q \frac{\mathbf{V}^{n+1} + \mathbf{V}^n}{2}\right)^\top (\tilde{\mathbf{e}}^{n+1} + \tilde{\mathbf{e}}^n).\end{aligned}$$

Using (6.10b) to express the right-hand side yields

$$\begin{aligned}&(\mathbf{V}^{n+1})^\top \mathbb{W}_m \mathbf{V}^{n+1} - (\mathbf{V}^n)^\top \mathbb{W}\mathbb{W}_m \mathbf{V}^n = -\left(\tilde{\mathsf{M}}_1 \tilde{\mathbf{e}}^{n+1} - \tilde{\mathsf{M}}_1 \tilde{\mathbf{e}}^n\right)^\top (\tilde{\mathbf{e}}^{n+1} + \tilde{\mathbf{e}}^n) \\ &= -\left((\tilde{\mathbf{e}}^{n+1})^\top \tilde{\mathsf{M}}_1 \tilde{\mathbf{e}}^{n+1} - (\tilde{\mathbf{e}}^n)^\top \tilde{\mathsf{M}}_1 \tilde{\mathbf{e}}^n\right).\end{aligned}$$

□

Proposition 6.2. *The splitting defined by* (6.10)*,* (6.8) *and* (6.9) *preserves Gauss' law over time if it is satisfied initially and system 1 is discretised as in* (6.10)*.*

Proof. This is proven in the same way as Proposition 6.1 with a constant term $\frac{\boldsymbol{\Xi}^{n+1} - \boldsymbol{\Xi}^n}{\Delta t} = \frac{\mathbb{N}^\top(\boldsymbol{\Xi}^{n+1}) + \mathbb{N}^\top(\boldsymbol{\Xi}^n)}{2} \frac{\mathbf{V}^{n+1} + \mathbf{V}^n}{2}$ in this step. □

The simulation results of this charge and energy conserving discrete gradient method are labeled as DisGradEC.

Let us compare the building blocks of the DisGradEC method to the HS in terms of complexity. Usually, the number of particles is much larger than the number of degrees of freedom for the fields so that the most expensive step is the evaluation of the line integral for the current deposition (cf. [55, Sec. 5.2.2.]). However, for DisGradEC, this evaluation needs to be repeated in each non-linear iteration. Moreover, for the source-free Maxwell equations, the computation of the Schur complement for DisGradEC is more expensive than the explicit solution for HS.

The DisGradE scheme treats the source-free Maxwell equations in the same way as DisGradEC. Computationally, the most expensive part is the assembly of the particle mass matrix. Both the evaluation of the line integral and the particle mass matrix depend to the sixth power on the order of the basis functions (cf. the discussion in [55]). In the case of DisGradEC however, the constant depends both on the number of cells crossed by the particles in the line integral and on the number of non-linear iterations. Therefore, a general comparison is not possible.

7 Particle and Field Initialisation

7.1 Particle Sampling

Proposition 7.1. *When we sample uniformly in logical coordinates, the weights of the particle distribution function are scaled with the Jacobian determinant.*

Proof. The particle weights are defined as $\omega_p = \frac{\tilde{f}}{\tilde{g}}$, where $\tilde{f}$ is the distribution function and $\tilde{g}$ the particle density function from which we sample. For the particle distribution function we assume a small perturbation of an equilibrium function f_0,

$$\begin{aligned} f(\mathbf{x}, \mathbf{v}, t=0) =& \tilde{f}(\boldsymbol{\xi}, \mathbf{v}, t=0) = (1 + \alpha \cos(\mathbf{k} \cdot F(\boldsymbol{\xi}))) \, f_0(\mathbf{v}), \\ f_0(\mathbf{v}) =& \frac{1}{(\sqrt{2\pi} v_{Tx})^3} \exp\left(-\frac{1}{2} \frac{(\mathbf{v} - \mathbf{v}_0)^2}{v_{Tx}^2} \right), \boldsymbol{\xi} \in [0,1)^3 = \tilde{\Omega}, \mathbf{v} \in \mathbb{R}^3. \end{aligned}$$

When sampling uniformly in $\mathbf{x}$, the particle density function $g(\mathbf{x}, \mathbf{v})$ is characterised via

$$\int_{\mathbb{R}^3} \int_{\Omega} g(\mathbf{x}, \mathbf{v}) \, \mathrm{d}\mathbf{x} \, \mathrm{d}\mathbf{v} = 1.$$

So, we choose

$$\tilde{g}(\mathbf{v}) = g(\mathbf{v}) = \frac{1}{\mathrm{vol}(\Omega)} \frac{1}{(\sqrt{2\pi} v_{Tx})^3} \exp\left(-\frac{1}{2} \frac{(\mathbf{v} - \mathbf{v}_0)^2}{v_{Tx}^2} \right).$$

However, when we sample directly in $\boldsymbol{\xi}$, the normalisation is transformed to

$$\int_{\mathbb{R}^3} \int_{\Omega} g(\mathbf{x}, \mathbf{v}) \, \mathrm{d}\mathbf{x} \, \mathrm{d}\mathbf{v} = \int_{\mathbb{R}^3} \int_{\tilde{\Omega}} \tilde{g}(\boldsymbol{\xi}, \mathbf{v}) |J_F(\boldsymbol{\xi})| \, \mathrm{d}\boldsymbol{\xi} \, \mathrm{d}\mathbf{v} = 1.$$

This leads to the choice

$$\tilde{g}(\boldsymbol{\xi}, \mathbf{v}) = \frac{1}{\mathrm{vol}(\tilde{\Omega}) |J_F(\boldsymbol{\xi})|} \frac{1}{(\sqrt{2\pi} v_{Tx})^3} \exp\left(-\frac{1}{2} \frac{(\mathbf{v} - \mathbf{v}_0)^2}{v_{Tx}^2} \right).$$

Since we defined the logical domain as $\tilde{\Omega} = [0,1]^3$, we obtain $\mathrm{vol}(\tilde{\Omega}) = 1$ and the weights are computed as

$$\omega_p = \frac{\tilde{f}(\boldsymbol{\xi}_p, \mathbf{v}_p)}{\tilde{g}(\boldsymbol{\xi}_p, \mathbf{v}_p)} = \left(1 + \alpha \cos(\mathbf{k} \cdot F(\boldsymbol{\xi}_p))\right) |J_F(\boldsymbol{\xi}_p)|.$$

□

Remark 7.2. *If we sample uniformly in the physical domain, the inverse of the coordinate transformation is needed to compute the logical coordinates. Therefore, this sampling strat-*

egy is only feasible if the inverse transformation can be computed analytically.

7.2 Poisson's Equation

For the initial electric field we solve Poisson's equation:

$$\begin{aligned} \mathsf{G}^T \tilde{\mathsf{M}}_1 \mathsf{G} \tilde{\boldsymbol{\phi}} &= \tilde{\boldsymbol{\rho}}, \\ \tilde{\mathbf{e}} &= -\mathsf{G}\tilde{\boldsymbol{\phi}}. \end{aligned}$$

When the kernel of the Poisson matrix is not equal to the zero vector, we have to compute the whole nullspace in order to use a linear solver. The condition for the nullspace is given by

$$\int \mathbf{E}(\mathbf{x}) \, \mathrm{d}\mathbf{x} = \vec{0} \Leftrightarrow \int N(\boldsymbol{\xi}) \tilde{\mathbf{E}}(\boldsymbol{\xi}) J_F(\boldsymbol{\xi}) \, \mathrm{d}\boldsymbol{\xi} = \vec{0} \Leftrightarrow \int N(\boldsymbol{\xi}) \tilde{\boldsymbol{\Lambda}}^1(\boldsymbol{\xi}) J_F(\boldsymbol{\xi}) \, \mathrm{d}\boldsymbol{\xi} \tilde{\mathbf{e}} = \vec{0}.$$

The initial charge for the weak formulation of Poisson's equation is accumulated as $\tilde{\boldsymbol{\rho}} = \tilde{\boldsymbol{\rho}}_{electron} + \tilde{\boldsymbol{\rho}}_{ion}$, where

$$\tilde{\boldsymbol{\rho}}_e = \int_{\tilde{\Omega}} \tilde{\rho}(\boldsymbol{\xi}) \cdot \tilde{\Lambda}^0(\boldsymbol{\xi}) |J_F(\boldsymbol{\xi})| \, \mathrm{d}\boldsymbol{\xi} = q_e \sum_p \omega_p \tilde{\Lambda}^0(\boldsymbol{\xi}_p).$$

In this case, we use a constant ion background represented by

$$\tilde{f}_i \equiv 1 \Rightarrow \tilde{\boldsymbol{\rho}}_i = \int_{\tilde{\Omega}} \tilde{\Lambda}^0(\boldsymbol{\xi}) |J_F(\boldsymbol{\xi})| \, \mathrm{d}\boldsymbol{\xi}.$$

The integral is solved with Gauss quadrature points $\boldsymbol{\xi}_q$ and quadrature weights ω_q as

$$\tilde{\boldsymbol{\rho}}_i = q_i \sum_q \omega_q \Delta\xi \tilde{\Lambda}^0(\boldsymbol{\xi}_q) |J_F(\boldsymbol{\xi}_q)|.$$

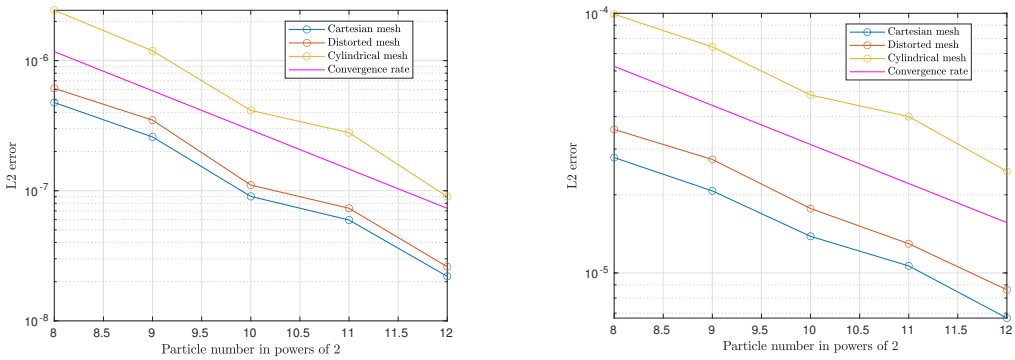

(a) Sobol numbers

(b) Random numbers

Figure 1 Convergence rates for Sobol and random numbers.

To check the convergence of our sampling strategy in different domains, we sample a constant

particle distribution function in $\boldsymbol{\xi}$ and measure the value of $\tilde{\boldsymbol{\rho}}_{electron} + \tilde{\boldsymbol{\rho}}_{ion}$ in the L^2 norm for different numbers N_p of particles. We use Sobol and random numbers on a Cartesian, distorted and cylindrical grid and obtain the expected convergence rate of $\frac{1}{N_p}$ for Sobol and $\frac{1}{\sqrt{N_p}}$ for random numbers [5]. In Figure 1, we see the L^2 error for the different grids together with the expected convergence rate for Sobol and random numbers.

8 Numerical Experiments

We have implemented the 3D3V propagators in curvilinear coordinates as part of the SeLaLib library [1] with a finite element solver based on compatible splines (see [4, Appendix A] for some details on the implementation). In this section, we reproduce two numerical test cases from [56] in a three dimensional setting to validate the code. Additionally, we perform an actual three dimensional (3D) simulation and compare the conservation properties of the different schemes. All numerical simulations are performed for electrons with a neutralising ion background. The particles are loaded with Sobol numbers and sampled uniformly in logical configuration space. In the absence of a coordinate transformation, the mass matrices are block-diagonal and can thus be inverted in Fourier space (cf. [55]). With a coordinate transformation, this is no longer the case. Therefore, we use a conjugate gradient solver that we precondition with the Fourier solver for the Cartesian case to invert the mass matrices. The idea to use a direct solver on the Cartesian mesh as preconditioner for an iterative solver on the curvilinear mesh was borrowed from [29]. Note that this yields a solution to machine accuracy for the Cartesian case. Therefore, we switch off the preconditioner in this case to show comparable accuracy in the conservation properties, which depends on the solver tolerance.

8.1 Coordinate Transformation

We use two periodic coordinate transformations for our test cases, an orthogonal non-uniform transformation and a sinusoidal transformation as defined in [19], which leads to a distorted grid. The transformations are defined by the following functions:

$$F_{\text{orth}}(\boldsymbol{\xi}) = \begin{pmatrix} L\left(\xi_1 + \varepsilon \sin(2\pi\xi_1)\right) \\ L\left(\xi_2 + \varepsilon \sin(2\pi\xi_2)\right) \\ L\xi_3 \end{pmatrix}, \quad F_{\text{dist}}(\boldsymbol{\xi}) = \begin{pmatrix} L\left(\xi_1 + \varepsilon \sin(2\pi\xi_1)\sin(2\pi\xi_2)\right) \\ L\left(\xi_2 + \varepsilon \sin(2\pi\xi_1)\sin(2\pi\xi_2)\right) \\ L\xi_3 \end{pmatrix}.$$

We choose $\varepsilon < \frac{1}{2\pi}$ so that the inverse Jacobian matrix does not become singular. Figure 2 visualises the (x, y)-part of the corresponding grids for the distortion parameter $\varepsilon = 0.1$.

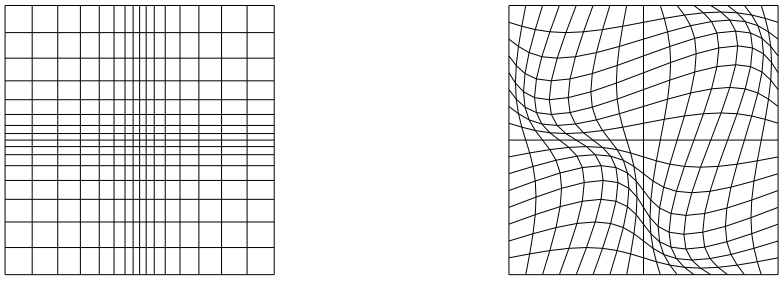

(a) Orthogonal non-uniform grid (b) Distorted grid

Figure 2 Orthogonal and distorted grid for distortion parameter $\varepsilon = 0.1$.

8.2 Strong Landau Damping

First, we consider an electrostatic test case so that the equations of motion (4.1) simplify to

$$\begin{aligned}
\dot{\boldsymbol{\Xi}} &= \mathbb{N}^T(\boldsymbol{\Xi})\mathbf{V}, \\
\dot{\mathbf{V}} &= \mathbb{W}_{\frac{q}{m}}\mathbb{N}(\boldsymbol{\Xi})\tilde{\mathbb{\Lambda}}^1(\boldsymbol{\Xi})\tilde{\mathbf{e}}, \\
\mathbb{M}_1\dot{\tilde{\mathbf{e}}} &= -\tilde{\mathbb{\Lambda}}^1(\boldsymbol{\Xi})^\top\mathbb{N}^\top(\boldsymbol{\Xi})\mathbb{W}_q\mathbf{V}, && \text{(8.1a)} \\
\mathsf{G}^\top\tilde{\mathsf{M}}_1\tilde{\mathbf{e}} &= \tilde{\boldsymbol{\rho}}. && \text{(8.1b)}
\end{aligned}$$

In the electrostatic case, the magnetic field is set to zero and Faraday's law is excluded. The electric field at initial time, $\mathbf{E}(\mathbf{x}, t=0)$, is calculated using Gauss' law (8.1b) with the scalar potential $\tilde{\mathbf{e}} = -\mathsf{G}\tilde{\boldsymbol{\phi}}$ and the propagation of the electric field is determined by Ampère's law (8.1a).

The initial distribution for the electrostatic Landau damping is given by

$$f_e(\mathbf{x}, \mathbf{v}, t=0) = (1 + \alpha\cos(\mathbf{k}\cdot\mathbf{x}))\,\frac{1}{(2\pi)^{\frac{3}{2}}v_{Tx}^3}\exp\left(-\frac{1}{2}\left(\frac{v^2}{v_{Tx}^2}\right)\right), \mathbf{x}\in[0,L]^3, \mathbf{v}\in\mathbb{R}^3.$$

We choose the parameter as $v_{Tx} = 1, \mathbf{k} = (0.5, 0, 0)^\top, \alpha = 0.5$ and $L = \frac{2\pi}{0.5}$. For the numerical resolution, we take $3{,}200{,}000$ particles, $16\times16\times2$ grid cells, spline degrees $(3, 3, 1)$ and a time step of $\Delta t = 0.05$ and for the iterative solver a tolerance of 10^{-13}. The tolerance for the non-linear iteration in DisGradEC is set to 10^{-12}, which leads on average to 6 iterations per time step on the Cartesian grid and 13 on the distorted grid. Note that we normalised to dimensionless quantities in terms of the electron Debye length λ_{De} and the plasma frequency ω_{pe}.

These parameters embed the 1D2V setup from [56] in the 3D3V phase space.

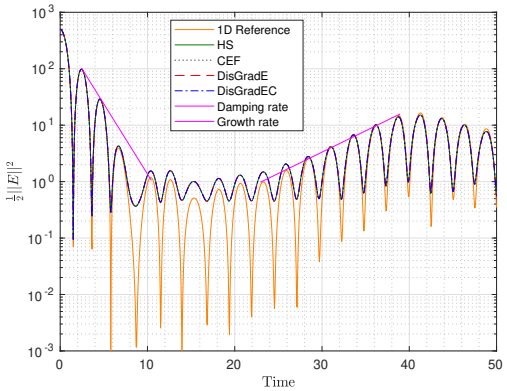

Figure 3 Landau damping on distorted grid: First component of the electric field energy for various integrators with time step $\Delta t = 0.05$ and distortion parameter $\varepsilon = 0.1$ for the coordinate transformation.

Figure 3 shows the first component of the electric energy for various integrators on the distorted grid together with a 1D reference run on the Cartesian grid. All propagators yield similar results, which match the damping and growth rate obtained from the 1D test case in [56], where the damping rate is given as $\gamma_1 = -0.286$ and the growth rate as $\gamma_2 = +0.087$.

Table 1 Landau damping: Maximum error in Gauss' law and in the total energy until time 500 for the semi-explicit and implicit time integrators with time step $\Delta t = 0.05$ and distortion parameter $\varepsilon = 0.1$ for the coordinate transformation.

	Gauss		Energy	
Method	Cartesian	Distorted	Cartesian	Distorted
HS	$3.1 \cdot 10^{-13}$	$5.3 \cdot 10^{-11}$	$1.0 \cdot 10^{-4}$	$1.0 \cdot 10^{-4}$
CEF	$2.9 \cdot 10^{-13}$	$5.3 \cdot 10^{-11}$	$1.0 \cdot 10^{-4}$	$1.0 \cdot 10^{-4}$
DisGradE	$7.4 \cdot 10^{-3}$	$2.9 \cdot 10^{-2}$	$3.1 \cdot 10^{-14}$	$2.5 \cdot 10^{-14}$
DisGradEC	$2.5 \cdot 10^{-13}$	$5.4 \cdot 10^{-11}$	$1.4 \cdot 10^{-13}$	$1.1 \cdot 10^{-12}$

From Table 1 it becomes obvious that the constructed conservation properties are satisfied numerically.

8.3 Weibel Instability

As an electromagnetic test case, we study the Weibel instability [93] as simulated in [56, 21] with the 3D3V initial distribution

$$f_e(\mathbf{x}, \mathbf{v}, t = 0) = (1 + \alpha \cos(\mathbf{k} \cdot \mathbf{x})) \frac{1}{(2\pi)^{\frac{3}{2}} v_{Tx} v_{Ty}^2} \exp\left(-\frac{1}{2} \left(\frac{v_x^2}{v_{Tx}^2} + \frac{v_y^2 + v_z^2}{v_{Ty}^2} \right) \right),$$

where $\mathbf{x} \in [0, L]^3, \mathbf{v} \in \mathbb{R}^3$. The magnetic field is initially set to $\mathbf{B}(\mathbf{x}, t = 0) = \beta \cos(\mathbf{k} \cdot \mathbf{x}) \hat{\mathbf{e}}_z$ and $\mathbf{E}(\mathbf{x}, t = 0)$ is calculated from Poisson's equation. We choose the parameters as $v_{Tx} = \frac{0.02}{\sqrt{2}}, v_{Ty} = \sqrt{12} v_{Tx}, \mathbf{k} = (1.25, 0, 0)^\top, \alpha = 0, L = \frac{2\pi}{1.25}$ and $\beta = 10^{-3}$. For the numerical resolution, we take $800{,}000$ particles, $16 \times 16 \times 2$ grid cells, spline degrees $(3, 3, 1)$ and a time step of $\Delta t = 0.05$ and for the iterative solver a tolerance of 10^{-13}. The tolerance for the non-linear iteration in DisGradEC is set to 10^{-12}. Note that we normalised to dimensionless quantities in terms of the electron Debye length λ_{De} and the electron plasma frequency ω_{pe}.

These parameters are comparable to the 1D2V settings in [56]. However, β is chosen one magnitude larger so that the initial growth of the magnetic field is higher than the effects caused by the particle noise at the chosen resolution.

Remark 8.1. *For the 1D2V Weibel instability, we look only at the waves given by $D_{yy} = 0$ in*

the dispersion relation (18.14). *In dimensionless coordinates, this takes the following form:*

$$D(\omega, k) = \omega^2 - k^2 - 1 + \left(\frac{v_{Ty}}{v_{Tx}}\right)^2 \left[1 + \zeta Z\left(\zeta\right)\right], \zeta = \frac{\omega}{\sqrt{2} k v_{Tx}}.$$

From the dispersion relation the growth rate of the magnetic field is computed as $\gamma = 0.02784$.

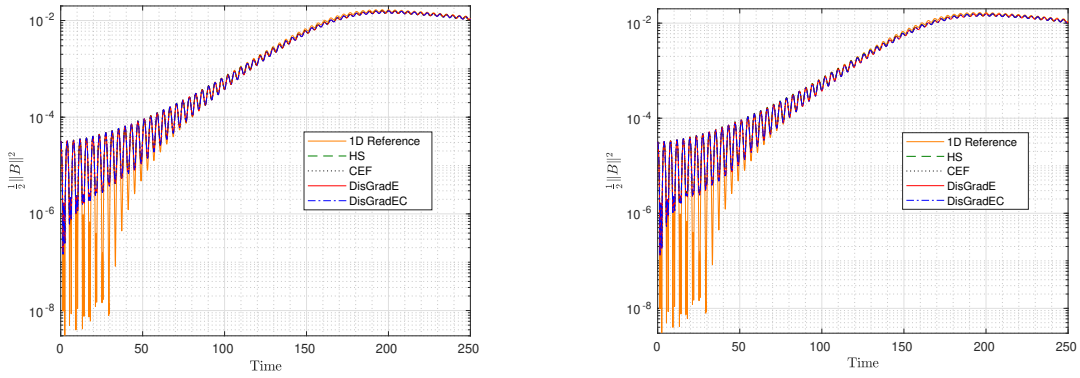

(a) Orthogonal non-uniform grid

(b) Distorted grid

Figure 4 Weibel instability: Magnetic field energy for various integrators with time step $\Delta t = 0.05$ and distortion parameter $\varepsilon = 0.1$ for the coordinate transformation.

Figure 4a shows the magnetic field energy as a function of time for different propagators on the orthogonal non-uniform grid and Figure 4b shows the same quantity on the distorted grid. In both cases, a 1D reference run with an explicit HS on Cartesian coordinates is given for comparison using the 1D Weibel distribution from [56] with $\beta = 10^{-3}$.

Next, we set the wave vector to $\mathbf{k} = (1.25, 1.25, 1.25)^\top$ and $\alpha = 0.1$ so that we have a perturbation in every $\mathbf{x}$-component. For the numerical resolution, we take $1{,}600{,}000$ particles, 8 grid cells in every direction and spline degrees $(3, 3, 3)$. The other parameters remain unchanged.

We run the HS scheme with different distortion parameters ε of the transformation. Therefore, we take $\varepsilon = 0$ as a reference and go from $\varepsilon = 0.01$ up to $\varepsilon = 0.1$ to study the effect of the coordinate transformation. The time step is taken as $\Delta t = 0.01$ to obey the CFL-condition for all choices of ε. The initial distribution is sampled in logical coordinates. Hence, the number of particles per cell is approximately constant. The larger the distortion of the grid, the larger cells appear and parts of the domain become more and more underresolved and the quality of the solution decreases. Note that the considered coordinate transformations are artificial with the goal to validate our method. Problem-specific coordinate systems and sampling methods should be designed such that they yield a resolution that is as homogeneous as possible.

In Figure 5a, we see that for decreasing ε the magnetic field growth rate converges to the scaling case with $\varepsilon = 0$, which coincides with the run without transformation.

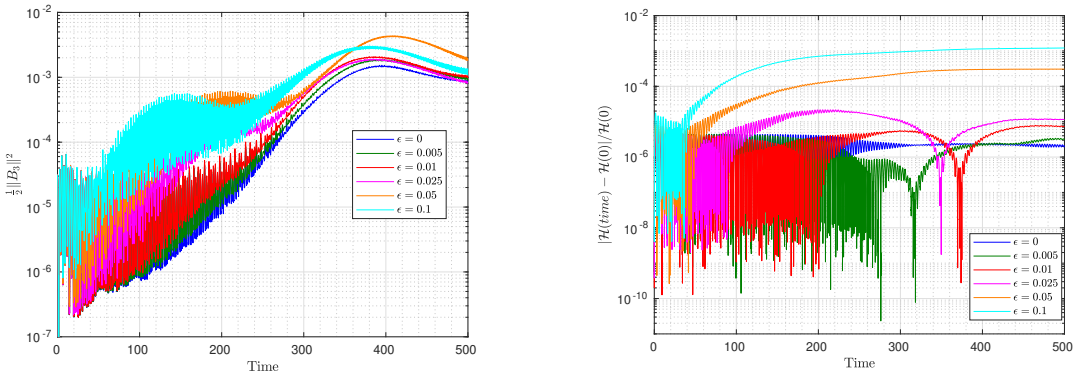

(a) Magnetic field energy

(b) Error in total energy

Figure 5 Weibel instability on distorted grid: Third component of the magnetic field energy and energy error for HS with time step $\Delta t = 0.01$ and different values of the distortion parameter ε for the coordinate transformation.

Last, we look at the conservation properties of our propagators. Therefore, the time step is set to $\Delta t = 0.05$ and the distortion parameter to $\varepsilon = 0.05$ so that all methods run stably. For the fully implicit step in DisGradEC we need on average 4 iterations per time step on the Cartesian grid, 7 on the orthogonal non-uniform grid and 8 on the distorted grid.

Table 2 Weibel instability: Maximum error in Gauss' law and in the total energy until time 500 for the semi-explicit and implicit time integrators with time step $\Delta t = 0.05$ and distortion parameter $\varepsilon = 0.05$ for the coordinate transformation.

	Method	Cartesian	Orthogonal	Distorted
Gauss	HS	$1.9 \cdot 10^{-11}$	$5.9 \cdot 10^{-10}$	$6.8 \cdot 10^{-10}$
	CEF	$1.9 \cdot 10^{-11}$	$5.8 \cdot 10^{-10}$	$6.9 \cdot 10^{-10}$
	DisGradE	$1.1 \cdot 10^{-6}$	$1.7 \cdot 10^{-6}$	$1.6 \cdot 10^{-6}$
	DisGradEC	$3.8 \cdot 10^{-13}$	$6.4 \cdot 10^{-10}$	$8.6 \cdot 10^{-10}$
Energy	HS	$1.1 \cdot 10^{-4}$	$1.8 \cdot 10^{-4}$	$1.6 \cdot 10^{-3}$
	CEF	$1.1 \cdot 10^{-4}$	$1.8 \cdot 10^{-4}$	$1.6 \cdot 10^{-3}$
	DisGradE	$3.2 \cdot 10^{-10}$	$1.4 \cdot 10^{-10}$	$4.2 \cdot 10^{-10}$
	DisGradEC	$6.0 \cdot 10^{-12}$	$1.6 \cdot 10^{-10}$	$4.2 \cdot 10^{-10}$

In Table 2, we see the difference between the energy and the charge conserving methods. As expected, the discrete gradient methods (DisGradE, DisGradEC) conserve the total energy whereas for the HS scheme the energy is not conserved but the error is bounded as can be seen in Figure 5b. As proven in Chapter 4, the charge conserving discrete gradient method (DisGradEC) and the semi-explicit schemes (HS, CEF) conserve Gauss' law. Note that all conservation properties are up to the tolerance of the solver times the condition number of the mass matrices.

8.4 Jean's Instability

8.4.1 Introduction Stellar Dynamics

It is also possible to simulate the dynamics of a stellar system in the GEMPIC framework. Therefore, we consider the dimensionless Vlasov–Ampère system with f representing the distribution function for the stellar particles and $\mathbf{E}$ representing the gravitational energy. The sign in Ampère's law is flipped compared to the plasma physics case because two masses attract each other while charged particles of the same species repel each other,

$$\begin{aligned} \partial_t f + \mathbf{v} \cdot \nabla_{\mathbf{x}} f + \mathbf{E} \cdot \nabla_{\mathbf{v}} f = 0, \\ \dot{\mathbf{E}} = \mathbf{J} - \mathbf{J}_{mean} \end{aligned} \tag{8.2}$$

with $\mathbf{J} = q \int \mathbf{v} f \, \mathrm{d}\mathbf{v}$. To check that we still have a Hamiltonian system, we consider the total energy

$$\mathcal{H} = \frac{m}{2} \int v^2 f(x, \mathbf{v}) \, \mathrm{d}\mathbf{v} \, \mathrm{d}\mathbf{x} - \frac{1}{2} \int \|\mathbf{E}\|^2 \, \mathrm{d}\mathbf{x},$$

which takes the following form at the semi-discrete level:

$$\mathcal{H}_h = \frac{1}{2} \mathbf{V}^\top \mathbb{W}_m \mathbf{V} - \frac{1}{2} \mathbf{e}^\top M_1 \mathbf{e}.$$

Then, its derivative is computed as $D\mathcal{H}_h = (0, \mathbb{W}_m \mathbf{V}, -M_1 \mathbf{e})^\top$ and the discrete Poisson matrix can be written as

$$\mathcal{J} = \begin{pmatrix} 0 & \mathbb{W}_m^{-1} & 0 \\ -\mathbb{W}_m^{-1} & 0 & -\mathbb{W}_{\frac{q}{m}} \mathbf{\Lambda}^1(\mathbf{X}) M_1^{-1} \\ 0 & M_1^{-1} \mathbf{\Lambda}^1(\mathbf{X})^\top \mathbb{W}_{\frac{q}{m}} & 0 \end{pmatrix}.$$

Thus, the equations of motion are given by

$$\begin{aligned} \dot{\mathbf{u}} = \mathcal{J} D\mathcal{H}_h, \\ \begin{pmatrix} \dot{\mathbf{X}} \\ \dot{\mathbf{V}} \\ \dot{\mathbf{e}} \end{pmatrix} = \begin{pmatrix} \mathbf{V} \\ \mathbb{W}_{\frac{q}{m}} \mathbf{\Lambda}^1(\mathbf{X}) \mathbf{e} \\ M_1^{-1} \mathbf{\Lambda}^1(\mathbf{X})^\top \mathbb{W}_q \mathbf{V} \end{pmatrix}. \end{aligned}$$

We discretise in time with the explicit Hamiltonian splitting (HS) scheme and the energy conserving discrete gradient method (DisGradE).

8.4.2 Single Species

As a first 1D test case we consider the Jeans instability from [35, 18] and adapt the setup to our 1D2V GEMPIC code. The initial distribution is given by

$$f_0 = (1 + \alpha \cos(kx)) \frac{1}{\sqrt{2\pi} v_{Tx}} \exp\left(-\frac{v_x^2 + v_y^2}{2 v_{Tx}^2} \right), x \in \left[0, \frac{L}{k}\right], \mathbf{v} \in \mathbb{R}^2$$

with $\alpha = 0.01, v_{Tx} = 1$ and $L = 2\pi$. The first component of the gravitational field, E_1, is computed initially via

$$\begin{aligned} \partial_x^2 \Phi &= \rho - 1, \\ E_1 &= -\partial_x \Phi, \end{aligned} \tag{8.3}$$

where $\rho = q \int f \, \mathrm{d}\mathbf{v}$. E_2 is set to zero initially and stays zero, since J_2 is zero as well. For the weak Jeans instability, we consider the wavenumber $k = 0.8$ and simulate with $N = 64$ grid cells, cubic splines, $N_p = 1{,}000{,}000$ particles and a time step of $\Delta t = 0.05$ until time $T = 100$. The strong instability is computed with the wavenumber $k = 0.1$.

An average current arises from this instability in the Ampère equation, which causes the simulation to become unstable. In the case of a non-zero average current, the Vlasov–Ampère and Vlasov–Poisson system are no longer equivalent. Therefore, we subtract $\mathbf{J}_{mean}$ in (8.2) forcing the average current to stay zero over time in order to guarantee a stable simulation.

The dispersion relation for the stellar Vlasov–Ampère system is taken from [7],

$$D(k, \omega) = \frac{k^2}{k_J^2} - [1 + \xi Z(\xi)] \text{ with } \xi = \frac{\omega}{\sqrt{2} v_{Tx} k}.$$

In the dimensionless case, the Jeans wavenumber is set to $k_J = 1$ so that the Jeans length $\lambda_J = \frac{2\pi}{k_J}$ becomes 2π. From the 1D dispersion relation, we compute a growth rate of 0.304 for the weak Jeans instability and a growth rate of 0.985 for the strong Jeans instability. In Figure

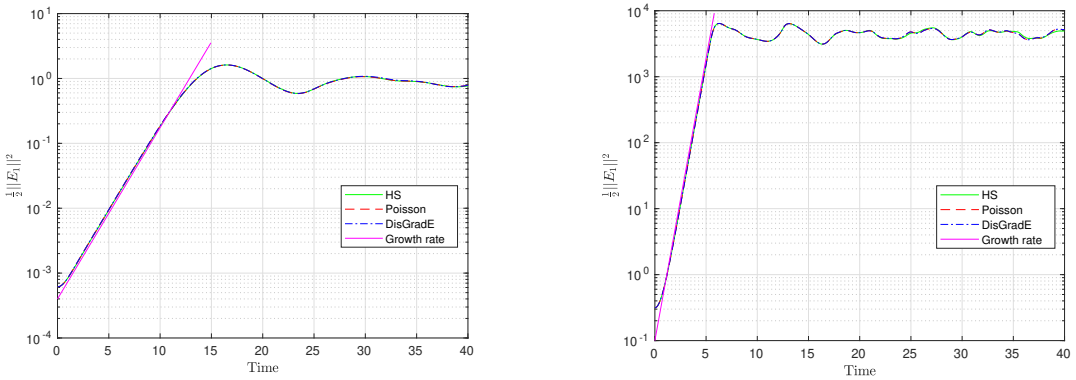

(a) Weak Jeans instability

(b) Strong Jeans instability

Figure 6 Jeans instability: First component of the gravitational energy for various integrators with time step $\Delta t = 0.05$ with analytical growth rates.

6b, we see the gravitational energy together with the analytical growth rates for the weak and the strong Jeans instabilities. In both cases, the ascent of the electric field matches the analytical rate. In Table 3, the Maximum error in Gauss' law and in the total energy are

Table 3 Jeans instability: Maximum error in Gauss' law and in the total energy until time 100 for the semi-explicit and implicit time integrators with time step $\Delta t = 0.05$.

	Gauss		Energy	
Method	Weak	Strong	Weak	Strong
HS	$1.4 \cdot 10^{-15}$	$5.2 \cdot 10^{-14}$	$2.4 \cdot 10^{-5}$	$2.9 \cdot 10^{-2}$
DisGradE	$1.2 \cdot 10^{-3}$	$4.5 \cdot 10^{-2}$	$5.9 \cdot 10^{-14}$	$1.3 \cdot 10^{-11}$

displayed for the explicit HS scheme and the implicit DisGradE method. As expected, the DisGradE method conserves the total energy whereas the HS scheme conserves Gauss' law.

8.4.3 Two Species

Next, we simulate a multispecies test case for hot and cold stellar particles with the same mass. Then, the initial distributions are given by

$$f_{01} = \delta(1 + \alpha \cos(kx) \frac{1}{\sqrt{2\pi} v_{Tx1}} \exp\left(-\frac{v_x^2 + v_y^2}{2v_{Tx1}^2}\right),$$
$$f_{02} = (1-\delta)(1 + \alpha \cos(kx) \frac{1}{\sqrt{2\pi} v_{Tx2}} \exp\left(-\frac{v_x^2 + v_y^2}{2v_{Tx2}^2}\right), x \in \left[0, \frac{L}{k}\right], \mathbf{v} \in \mathbb{R}^2$$

with $\alpha = 0.01, v_{Tx1} = 1, v_{Tx2} = 0.1, \delta \in [0,1]$ and $L = 2\pi$. The first component of the gravitational energy is initially computed by Poisson's equation (8.3) and E_2 is initially zero and stays zero over time. For the weak Jeans instability, we take again a wavenumber of $k = 0.8$. We simulate with $N = 64$ grid cells, cubic splines, $N_p = 1{,}000{,}000$ particles and a time step of $\Delta t = 0.05$ until time $T = 45$. We simulate for $\delta = 0.25, 0.5, 0.75, 0.9, 1.0$ and the dispersion relation is taken again from [7] but adapted to our multispecies simulation with dimensionless coordinates,

$$D(\omega) = 1 - \frac{1}{k^2}\left[\delta\left(1 + \xi_1 Z\left(\xi_1\right)\right) + \frac{v_{Tx1}^2}{v_{Tx2}^2}(1-\delta)\left(1 + \xi_2 Z\left(\xi_2\right)\right)\right]$$

with $\xi_1 = \frac{\omega}{k\sqrt{2} v_{Tx1}}, \xi_2 = \frac{\omega}{k\sqrt{2} v_{Tx2}}$.

Table 4 displays the analytical growth rates computed from the dispersion relation together with the simulated growth rates, which were fitted to the curves of the gravitational energy, for different values of δ. In Figure 7, we see the first component of the gravitational energy for the different values of δ together with the analytical growth rates. As expected, the growth of the gravitational energy matches the analytical rates. Figures 8-11 show the time evolution of

Table 4 Weak Jeans instability: Analytical and simulated growth rates for different values of δ.

δ	Analytical growth rate	Simulated growth rate
0.25	0.83	0.83
0.50	0.73	0.72
0.75	0.60	0.60
0.90	0.47	0.46
1.00	0.30	0.30

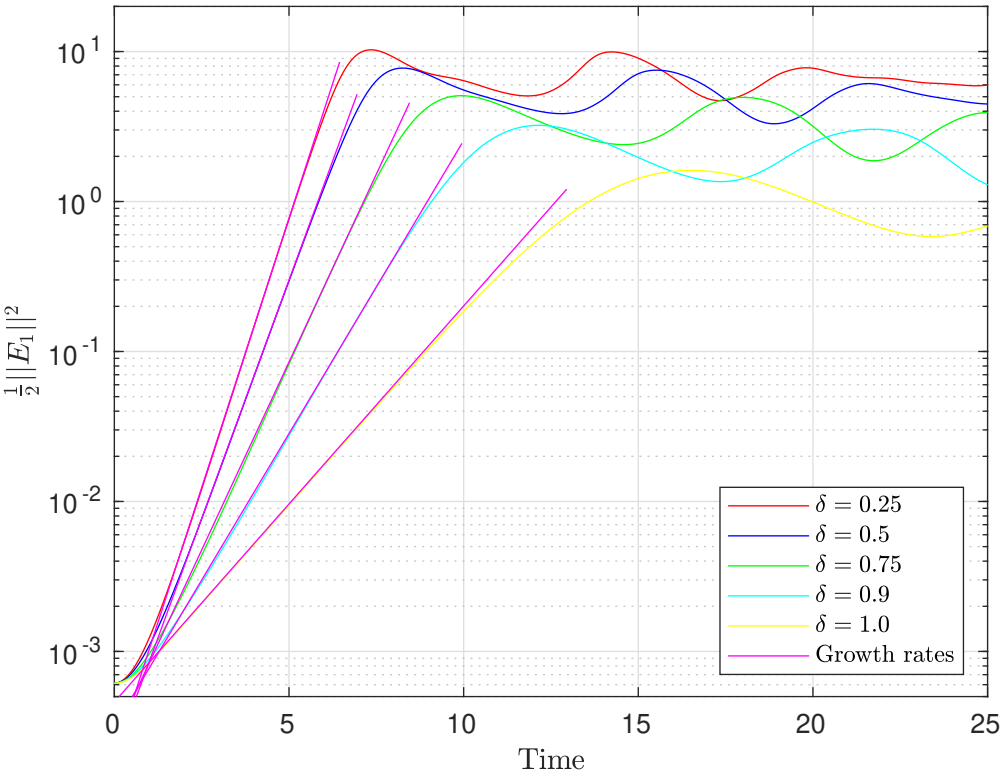

Figure 7 Two species weak Jeans instability: First component of the gravitational energy for HS with time step $\Delta t = 0.05$ for different values of δ together with the analytical growth rates.

the phase space distribution (X, V_1) of the hot particles colored in red and the cold particles colored in blue until $T = 35$.

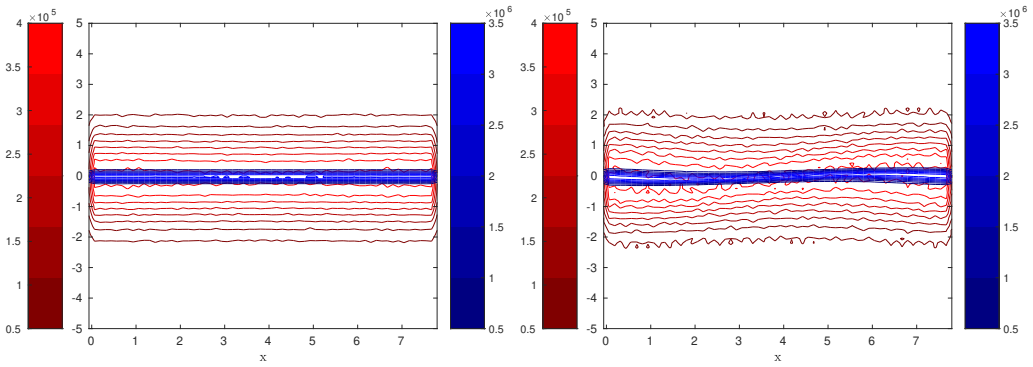

Figure 8 Two species weak Jeans instability with $\delta = 0.75$ at time $T = 0, 5$.

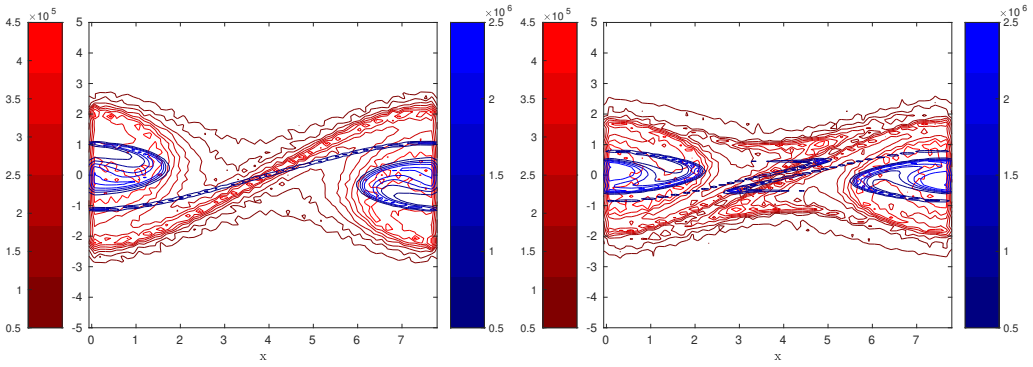

Figure 9 Two species weak Jeans instability with $\delta = 0.75$ at time $T = 10, 15$.

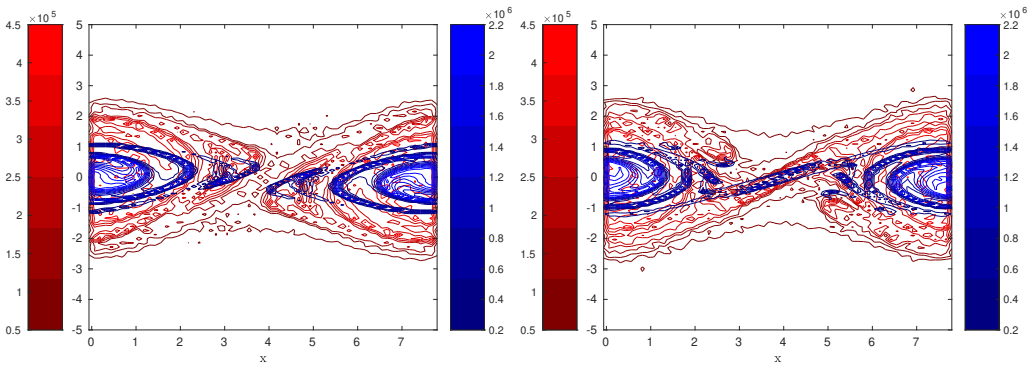

Figure 10 Two species weak Jeans instability with $\delta = 0.75$ at time $T = 20, 25$.

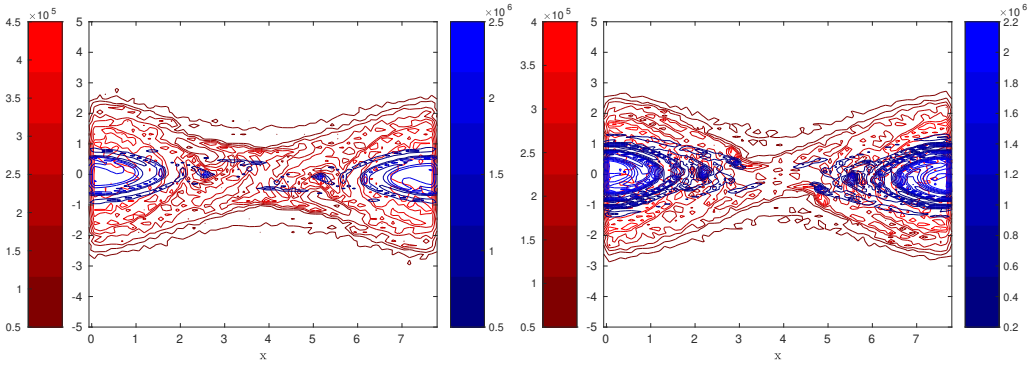

Figure 11 Two species weak Jeans instability with $\delta = 0.75$ at time $T = 30, 35$.

Part II

Boundary Conditions

9 Field Boundary Conditions

In the first part, we have introduced a general coordinate transformation into the structure-preserving GEMPIC framework. However, we assumed periodic boundary conditions, which also limits the coordinate transformation to periodic mappings. In Part II, we extend our system to real boundary conditions enabling the use of radial grids such as a cylindrical or an elliptical grid.

9.1 Weak Formulation of Maxwell's Equations

In the weak formulation of Maxwell's equations in (2.8a) and (2.8c), we have assumed that the boundary terms vanish, which is the case for the chosen periodic boundary conditions. Now, we take a closer look at these natural boundary conditions. Using the cross product form of the Divergence theorem (A.7), Ampère's law tested with $\boldsymbol{\varphi} \in H(\mathrm{curl}, \Omega)$ can be rewritten as

$$\frac{\partial}{\partial t}\int_\Omega \boldsymbol{\varphi}\cdot\mathbf{E}\,\mathrm{d}\mathbf{x} = \int_\Omega \nabla_{\mathbf{x}}\times\boldsymbol{\varphi}\cdot\mathbf{B}\,\mathrm{d}\mathbf{x} + \int_{\partial\Omega}(\mathbf{B}\times\boldsymbol{\varphi})\cdot\mathbf{n}\,\mathrm{d}\sigma - \int_\Omega \boldsymbol{\varphi}\cdot\mathbf{J}\,\mathrm{d}\mathbf{x}.$$

For Gauss' law tested with $\psi \in H^1(\Omega)$ we take the scalar form of the divergence theorem (A.6) to obtain

$$\int_{\partial\Omega}\psi(\mathbf{E}\cdot\mathbf{n})\,\mathrm{d}\sigma - \int_\Omega \nabla\psi\cdot\mathbf{E}\,\mathrm{d}\mathbf{x} = \int_\Omega \psi\rho\,\mathrm{d}\mathbf{x}.$$

Generally, we have to decide between the following two kinds of boundary conditions:

- Dirichlet boundary: $\varphi|_{\partial\Omega} = f$ with a known function f at the boundary $\partial\Omega$,
- Neumann boundary: $(\nabla\varphi\cdot\mathbf{n})|_{\partial\Omega} = f$ with a known function f at the boundary $\partial\Omega$.

For realistic Tokamak geometry, we consider some kind of cylindrical or spherical coordinates with one radial direction and two periodic angles. So without loss of generality, we consider real boundary conditions in the first direction and periodic ones in the other two.

Then, the normal vector to the boundary in logical coordinates is given as $\tilde{\mathbf{n}} = \pm(1,0,0)^\top$. Since the normal vector transforms with the covariant Piola transform (2.14), it takes the following form in physical coordinates:

$$\mathbf{n} = \frac{N(\boldsymbol{\xi})\tilde{\mathbf{n}}}{\|N(\boldsymbol{\xi})\tilde{\mathbf{n}}\|} = \pm\frac{\mathbf{n}_1}{\|\mathbf{n}_1\|}.$$

In the following, we only show the terms for $\tilde{\mathbf{n}} = (1,0,0)^\top$ because in the other case the signs are just flipped. To compute the boundary part of Ampère's law tested with $\boldsymbol{\varphi}$ in curvilinear

coordinates, we insert the Piola transforms for the electromagnetic fields and the test function, (2.14) and (2.15), and use $\mathrm{d}\sigma = \|\mathbf{t}_2 \times \mathbf{t}_3\| \, \mathrm{d}\tilde{\sigma}$,

$$\int_{\partial\tilde{\Omega}} \left(\frac{DF}{J_F} \tilde{\mathbf{B}} \times N\tilde{\boldsymbol{\varphi}} \right) \cdot N\tilde{\mathbf{n}} \frac{\|\mathbf{t}_2 \times \mathbf{t}_3\|}{\|N\tilde{\mathbf{n}}\|} \, \mathrm{d}\tilde{\sigma}.$$

We note that the scalar triple product permutes, $\left(\frac{DF}{J_F} \tilde{\mathbf{B}} \times N\tilde{\boldsymbol{\varphi}} \right) \cdot N\tilde{\mathbf{n}} = (N\tilde{\boldsymbol{\varphi}} \times N\tilde{\mathbf{n}}) \cdot \frac{DF}{J_F} \tilde{\mathbf{B}}$, and insert the notation from Definition 2.1 for the columns of the Jacobian matrix to facilitate the computation of the vector operations,

$$\int_{\partial\tilde{\Omega}} ((\mathbf{n}_1 \tilde{\varphi}_1 + \mathbf{n}_2 \tilde{\varphi}_2 + \mathbf{n}_3 \tilde{\varphi}_3) \times \mathbf{n}_1) \cdot (\mathbf{t}_1 \tilde{B}_1 + \mathbf{t}_2 \tilde{B}_2 + \mathbf{t}_3 \tilde{B}_3) \frac{\|\mathbf{t}_2 \times \mathbf{t}_3\|}{J_F \|\mathbf{n}_1\|} \, \mathrm{d}\tilde{\sigma}.$$

Then, we make use of the vector identities from Proposition 2.2 to obtain

$$\int_{\partial\tilde{\Omega}} \left(-\tilde{\varphi}_2 \frac{\mathbf{t}_3}{J_F} + \tilde{\varphi}_3 \frac{\mathbf{t}_2}{J_F} \right) \cdot (\mathbf{t}_1 \tilde{B}_1 + \mathbf{t}_2 \tilde{B}_2 + \mathbf{t}_3 \tilde{B}_3) \, \mathrm{d}\tilde{\sigma}. \tag{9.1}$$

Using the same formulas for the boundary part of Gauss' law gives us

$$\int_{\partial\tilde{\Omega}} \tilde{\psi} \left(N\tilde{\mathbf{E}} \cdot \frac{\mathbf{n}_1}{\|\mathbf{n}_1\|} \right) \|\mathbf{t}_2 \times \mathbf{t}_3\| \, \mathrm{d}\tilde{\sigma} = \int_{\partial\tilde{\Omega}} \tilde{\psi} \left(\mathbf{n}_1 \tilde{E}_1 + \mathbf{n}_2 \tilde{E}_2 + \mathbf{n}_3 \tilde{E}_3 \right) \cdot \mathbf{n}_1 J_F \, \mathrm{d}\tilde{\sigma}. \tag{9.2}$$

9.2 Poynting Flux

We also have to account for the field energy that crosses the boundary. In Poynting's theorem [74] this dynamic is described.

Theorem 9.1. *The energy balance of the field energy, $\mathcal{H}_{EB}$, is given by*

$$\frac{\mathrm{d}\mathcal{H}_{EB}}{\mathrm{d}t} = -\int_{\partial\Omega} (\mathbf{E} \times \mathbf{B}) \cdot \mathbf{n} \, \mathrm{d}\sigma - \int_{\Omega} \mathbf{J} \cdot \mathbf{E} \, \mathrm{d}\mathbf{x}. \tag{9.3}$$

Proof. The total field energy is defined as $\mathcal{H}_{EB} = \frac{1}{2} \int_{\Omega} \mathbf{E} \cdot \mathbf{E} + \mathbf{B} \cdot \mathbf{B} \, \mathrm{d}\mathbf{x}$ and so the time derivative of this term gives us

$$\frac{\mathrm{d}}{\mathrm{d}t} \mathcal{H}_{EB} = \int_{\Omega} \dot{\mathbf{B}} \cdot \mathbf{B} + \dot{\mathbf{E}} \cdot \mathbf{E} \, \mathrm{d}\mathbf{x}.$$

We insert Ampère's and Faraday's laws,

$$\dot{\mathbf{E}} = \nabla \times \mathbf{B} - \mathbf{J},$$
$$\dot{\mathbf{B}} = -\nabla \times \mathbf{E},$$

to see

$$\begin{aligned}\int_\Omega \dot{\mathbf{B}} \cdot \mathbf{B} + \dot{\mathbf{E}} \cdot \mathbf{E} \,\mathrm{d}\mathbf{x} &= \int_\Omega -(\nabla \times \mathbf{E}) \cdot \mathbf{B} + (\nabla \times \mathbf{B} - \mathbf{J}) \cdot \mathbf{E} \,\mathrm{d}\mathbf{x} \\ &= -\int_\Omega \nabla \cdot (\mathbf{E} \times \mathbf{B}) \,\mathrm{d}\mathbf{x} - \int_\Omega \mathbf{J} \cdot \mathbf{E} \,\mathrm{d}\mathbf{x}.\end{aligned}$$

Then, the result follows from the divergence theorem (A.7). □

Remark 9.2. *The term $\int_{\partial\Omega}(\mathbf{E}\times\mathbf{B})\cdot\mathbf{n}\,\mathrm{d}\sigma$, which gives the field energy crossing the boundary, is called Poynting's flux.*

We transform Poynting's flux to curvilinear coordinates by inserting the Piola transforms for the electromagnetic fields (2.14) and (2.15),

$$\int_{\partial\tilde{\Omega}} \left(N\tilde{\mathbf{E}} \times \frac{DF}{J_F}\tilde{\mathbf{B}} \right) \cdot \frac{\mathbf{n}_1}{\|\mathbf{n}_1\|} \|\mathbf{t}_2 \times \mathbf{t}_3\| \,\mathrm{d}\tilde{\sigma}.$$

Next, we use the permutation property of the scalar triple product and write the equation with the notation from Definition 2.1 for the columns of the Jacobian matrix and its inverse,

$$\int_{\partial\tilde{\Omega}} \Big(\mathbf{n}_1 \times (\mathbf{n}_1\tilde{E}_1 + \mathbf{n}_2\tilde{E}_2 + \mathbf{n}_3\tilde{E}_3) \Big) \cdot (\mathbf{t}_1\tilde{B}_1 + \mathbf{t}_2\tilde{B}_2 + \mathbf{t}_3\tilde{B}_3) \frac{\|\mathbf{t}_2 \times \mathbf{t}_3\|}{J_F\|\mathbf{n}_1\|} \,\mathrm{d}\tilde{\sigma}.$$

Last, we use the vector identities from Proposition 2.2 to obtain

$$\int_{\partial\tilde{\Omega}} \left(\frac{\mathbf{t}_3}{J_F}\tilde{E}_2 - \frac{\mathbf{t}_2}{J_F}\tilde{E}_3 \right) \cdot (\mathbf{t}_1\tilde{B}_1 + \mathbf{t}_2\tilde{B}_2 + \mathbf{t}_3\tilde{B}_3) \,\mathrm{d}\tilde{\sigma}. \tag{9.4}$$

9.3 Spline Boundary Conditions

In this section, we review the construction of spline basis functions with real boundary conditions. First, we review general properties of the basis splines given in [24], which we will use further on.

Let us start with the knot vector $T = \{t_j\}_{1-p\leq j\leq N+p+1}$, which is a non-decreasing sequence of points. In our case, we have chosen the equidistant grid points ξ_j of our N_x cells for the knot sequence so that $\xi_{j+1} - \xi_j = \Delta\xi$.

In Part I, we have worked with basis splines that are defined on a periodic knot sequence, which has the following form:

$$T = \{\xi_{N-p+1}, ..., \xi_N, \xi_1, \xi_2, ..., \xi_{N-1}, \xi_N, \xi_1, ..., \xi_{p+1}\}.$$

From this knot sequence the N splines of degree p are defined according to the following formula:

Definition 9.1. *The j-th basis spline is computed via the recursion formula*

$$S_j^p(\xi) = \frac{\xi - t_j}{t_{j+p} - t_j} S_j^{p-1}(\xi) + \frac{t_{j+p+1} - \xi}{t_{j+p+1} - t_{j+1}} S_{j+1}^{p-1}(x), \tag{9.5}$$

where the spline of degree zero is defined as $S_j^0(x) = \chi_{[t_j, t_{j+1}]}$. Furthermore, the derivative of the j-th spline is calculated as

$$\frac{dS_j^p(\xi)}{\mathrm{d}\xi} = p \left(\frac{S_j^{p-1}(\xi)}{t_{j+p} - t_j} - \frac{S_{j+1}^{p-1}(\xi)}{t_{j+p+1} - t_{j+1}} \right). \tag{9.6}$$

Here, the spline values are collected in a vector as $\mathcal{S}^p(\xi) = (S_1^p(\xi), ..., S_N^p(\xi))$.

Now, for non-periodic boundary conditions, we consider clamped splines. Therefore, we duplicate the outer grid points p times so that they have multiplicity $p+1$. Note that without assuming periodicity we have $N+1$ grid points for N cells. Then, the knot sequence is given by

$$T = \{\xi_1, ..., \xi_1, \xi_2, ..., \xi_N, \xi_{N+1}, ..., \xi_{N+1}\}.$$

From this knot sequence the $N+p$ splines of degree p are defined again via the recursion formula (9.5), where for dimensionality reasons we need to consider an additional first and last zero spline of degree $p-1$.

In our convention, we denote the spline starting in the first cell as S_1^p. Accordingly, the first spline and last spline of degree p are computed via (9.5) as

$$\begin{aligned} S_{1-p}^p(\xi) =& \frac{t_2 - \xi}{t_2 - t_{2-p}} S_{2-p}^{p-1}(\xi) = \frac{\xi_2 - \xi}{\Delta\xi} S_{2-p}^{p-1}(\xi), \\ S_N^p(\xi) =& \frac{\xi - t_N}{t_{N+p} - t_N} S_N^{p-1}(\xi) = \frac{\xi - \xi_N}{\Delta\xi} S_N^{p-1}(\xi). \end{aligned}$$

Since the other splines equal zero at the boundary, we obtain

$$S_j^p(0) = \begin{cases} 1 \text{ when } j = 1-p, \\ 0 \text{ else }, \end{cases} \quad S_j^p(1) = \begin{cases} 1 \text{ when } j = N, \\ 0 \text{ else }. \end{cases}$$

This leads to the following evaluation of the product of two splines at the boundary:

$$[S_i^{p-1} S_j^p]_0^1 = S_i^{p-1}(1) S_j^p(1) - S_i^{p-1}(0) S_j^p(0) = \begin{cases} -1 \text{ when } i = 1-(p-1) \wedge j = 1-p, \\ 1 \text{ when } i = j = N, \\ 0 \text{ else }. \end{cases}$$

We collect the spline values in a vector as $\mathcal{S}^p_\star(\xi) = (S^p_{1-p}(\xi), ..., S^p_N(\xi))$ and write the spline derivative in matrix vector form with the help of the discrete 1D derivative matrix $D_\star$ defined via $\frac{\mathrm{d}}{\mathrm{d}\xi}\mathcal{S}^p_\star(\xi) = \mathcal{S}^{p-1}_\star(\xi)D_\star$. The entries of the matrix are computed using the formula for the spline derivative (9.6),

$$
\begin{aligned}
\frac{\mathrm{d}S^p_{1-p}(\xi)}{\mathrm{d}\xi} &= -\frac{p}{\Delta\xi}S^{p-1}_{2-p}(\xi), \\
\frac{\mathrm{d}S^p_{j-p}(\xi)}{\mathrm{d}\xi} &= \frac{p}{\Delta\xi}\left(\frac{S^{p-1}_{j-p}(\xi)}{j-1} - \frac{S^{p-1}_{j+1-p}(\xi)}{j}\right) \text{ for } 2 \leq j \leq p, \\
\frac{\mathrm{d}S^p_{j}(\xi)}{\mathrm{d}\xi} &= \frac{1}{\Delta\xi}\left(S^{p-1}_{j}(\xi) - S^{p-1}_{j+1}(\xi)\right) \text{ for } 1 \leq j \leq N-p, \\
\frac{\mathrm{d}S^p_{N-j}(\xi)}{\mathrm{d}\xi} &= \frac{p}{\Delta\xi}\left(\frac{S^{p-1}_{N-j}(\xi)}{j+1} - \frac{S^{p-1}_{N-j+1}(\xi)}{j}\right) \text{ for } 1 \leq j \leq p-1, \\
\frac{\mathrm{d}S^p_{N}(\xi)}{\mathrm{d}\xi} &= \frac{p}{\Delta\xi}S^{p-1}_{N}(\xi).
\end{aligned}
$$

Then, the matrix is given by

$$
D_\star \in \mathbb{R}^{(N+p)\times(N+p)}, D_\star = \frac{1}{\Delta\xi}\begin{pmatrix}
0 & 0 & 0 & 0 & 0 & 0 & 0 & 0 & 0 & 0 \\
-\frac{p}{1} & \frac{p}{1} & 0 & 0 & 0 & 0 & 0 & 0 & 0 & 0 \\
0 & \ddots & \ddots & 0 & 0 & 0 & 0 & 0 & 0 & 0 \\
0 & 0 & -\frac{p}{p-1} & \frac{p}{p-1} & 0 & 0 & 0 & 0 & 0 & 0 \\
0 & 0 & 0 & -1 & 1 & 0 & 0 & 0 & 0 & 0 \\
\vdots & \vdots & \vdots & \ddots & \ddots & \ddots & \ddots & \vdots & \vdots & \vdots \\
0 & 0 & 0 & 0 & 0 & -1 & 1 & 0 & 0 & 0 \\
0 & 0 & 0 & 0 & 0 & 0 & -\frac{p}{p-1} & \frac{p}{p-1} & 0 & 0 \\
0 & 0 & 0 & 0 & 0 & 0 & 0 & \ddots & \ddots & 0 \\
0 & 0 & 0 & 0 & 0 & 0 & 0 & 0 & -\frac{p}{1} & \frac{p}{1}
\end{pmatrix},
$$

where the first row accounts for the one spline less we have with degree $p-1$.

The 3D spline basis for differential 0-forms is constructed as a tensor product of the 1D splines,

$$
\tilde{\Lambda}^0(\boldsymbol{\xi}) = \mathcal{S}^p_\star(\xi_1) \otimes \mathcal{S}^p(\xi_2) \otimes \mathcal{S}^p(\xi_3). \tag{9.7}
$$

Without loss of generality, let us assume clamped splines in the first direction and periodic

splines in the other two directions. Then, we build the 3D derivative matrices accordingly,

$$\mathsf{G} = \begin{pmatrix} D_1 \\ D_2 \\ D_3 \end{pmatrix}, \mathsf{C} = \begin{pmatrix} 0 & -D_3 & D_2 \\ D_3 & 0 & -D_1 \\ -D_2 & D_1 & 0 \end{pmatrix}, \mathsf{D} = \mathsf{G}^\top, \tag{9.8}$$

where the block matrices $D_{1,2,3}$ are constructed as the tensor product of 1D derivative matrices via $D_1 = D_\star \otimes \mathbb{I} \otimes \mathbb{I}, D_2 = \mathbb{I} \otimes D \otimes \mathbb{I}, D_3 = \mathbb{I} \otimes \mathbb{I} \otimes D$. Here, $\mathbb{I}$ stands for the identity matrix and the periodic derivative matrix is computed via $\frac{\mathrm{d}}{\mathrm{d}\xi}\mathcal{S}^p(\xi) = \mathcal{S}^{p-1}(\xi)D$,

$$D = \frac{1}{\Delta\xi} \begin{pmatrix} 1 & 0 & ... & 0 & -1 \\ -1 & 1 & 0 & ... & 0 \\ 0 & -1 & 1 & 0 & \vdots \\ \vdots & 0 & \ddots & \ddots & 0 \\ 0 & ... & 0 & -1 & 1 \end{pmatrix}.$$

Then, the 3D spline basis functions for the differential 1-,2- and 3-forms are defined as

$$\tilde{\mathbf{\Lambda}}^1(\boldsymbol{\xi}) = \begin{pmatrix} \tilde{\Lambda}^{1,1}(\boldsymbol{\xi}) & 0 & 0 \\ 0 & \tilde{\Lambda}^{1,2}(\boldsymbol{\xi}) & 0 \\ 0 & 0 & \tilde{\Lambda}^{1,3}(\boldsymbol{\xi}) \end{pmatrix}, \tilde{\mathbf{\Lambda}}^2(\boldsymbol{\xi}) = \begin{pmatrix} \tilde{\Lambda}^{2,1}(\boldsymbol{\xi}) & 0 & 0 \\ 0 & \tilde{\Lambda}^{2,2}(\boldsymbol{\xi}) & 0 \\ 0 & 0 & \tilde{\Lambda}^{2,3}(\boldsymbol{\xi}) \end{pmatrix}, \tag{9.9}$$
$$\tilde{\Lambda}^3(\boldsymbol{\xi}) = \mathcal{S}^{p-1}_\star(\xi_1) \otimes \mathcal{S}^{p-1}(\xi_2) \otimes \mathcal{S}^{p-1}(\xi_3).$$

with

$$\begin{aligned} \tilde{\Lambda}^{1,1}(\boldsymbol{\xi}) &= \mathcal{S}^{p-1}_\star(\xi_1) \otimes \mathcal{S}^p(\xi_2) \otimes \mathcal{S}^p(\xi_3), & \tilde{\Lambda}^{2,1}(\boldsymbol{\xi}) &= \mathcal{S}^p_\star(\xi_1) \otimes \mathcal{S}^{p-1}(\xi_2) \otimes \mathcal{S}^{p-1}(\xi_3), \\ \tilde{\Lambda}^{1,2}(\boldsymbol{\xi}) &= \mathcal{S}^p_\star(\xi_1) \otimes \mathcal{S}^{p-1}(\xi_2) \otimes \mathcal{S}^p(\xi_3), & \tilde{\Lambda}^{2,2}(\boldsymbol{\xi}) &= \mathcal{S}^{p-1}_\star(\xi_1) \otimes \mathcal{S}^p(\xi_2) \otimes \mathcal{S}^{p-1}(\xi_3), \\ \tilde{\Lambda}^{1,3}(\boldsymbol{\xi}) &= \mathcal{S}^p_\star(\xi_1) \otimes \mathcal{S}^p(\xi_2) \otimes \mathcal{S}^{p-1}(\xi_3), & \tilde{\Lambda}^{2,3}(\boldsymbol{\xi}) &= \mathcal{S}^{p-1}_\star(\xi_1) \otimes \mathcal{S}^{p-1}(\xi_2) \otimes \mathcal{S}^p(\xi_3). \end{aligned}$$

Proposition 9.2. *The spline basis functions* $\tilde{\Lambda}^0, \tilde{\mathbf{\Lambda}}^1, \tilde{\mathbf{\Lambda}}^2, \tilde{\Lambda}^3$ *defined in* (9.7) *and* (9.9) *form a*

discrete de Rham sequence with the derivative matrices $\mathsf{G}, \mathsf{C}, \mathsf{D}$ (9.8)*,*

$$\begin{aligned} \nabla_{\boldsymbol{\xi}} \tilde{\Lambda}^0 &= \tilde{\boldsymbol{\Lambda}}^1 \mathsf{G}, \\ \nabla_{\boldsymbol{\xi}} \times \tilde{\boldsymbol{\Lambda}}^1 &= \tilde{\boldsymbol{\Lambda}}^2 \mathsf{C}, \\ \nabla_{\boldsymbol{\xi}} \cdot \tilde{\boldsymbol{\Lambda}}^2 &= \tilde{\Lambda}^3 \mathsf{D}. \end{aligned} \tag{9.10}$$

Proof. Since we defined the derivative matrices to reproduce the partial derivatives of the splines on the level of the degrees of freedom, (9.10) holds by construction. Additionally, we have to check that $\mathsf{CG} = 0$ and $\mathsf{DC} = 0$. We compute the former block-wise as

$$\mathsf{CG} = \begin{pmatrix} -D_3 D_2 + D_2 D_3 \\ D_3 D_1 - D_1 D_3 \\ -D_2 D_1 + D_1 D_2 \end{pmatrix}.$$

Then, the Kronecker product structure of the derivative matrices guarantees that the matrices commute because the identity matrix commutes with every matrix, e.g.

$$D_3 D_1 = (\mathbb{I} \otimes \mathbb{I} \otimes D)(D_\star \otimes \mathbb{I} \otimes \mathbb{I}) = D_\star \otimes \mathbb{I} \otimes D = (D_\star \otimes \mathbb{I} \otimes \mathbb{I})(\mathbb{I} \otimes \mathbb{I} \otimes D) = D_1 D_3.$$

Therefore, the matrix multiplication equals zero. Analogously, we can verify the same result for $\mathsf{DC} = 0$. □

9.4 Boundary Matrices

We insert the spline representation of the magnetic field, (3.7b), into the boundary part of Ampère's law (9.1) and test with the respective spline basis function $\tilde{\boldsymbol{\varphi}} = \tilde{\boldsymbol{\Lambda}}^1$ to obtain

$$\int_{\partial\tilde{\Omega}} \left(0, -\tilde{\Lambda}^{1,2} \frac{\mathbf{t}_3}{J_F}, \tilde{\Lambda}^{1,3} \frac{\mathbf{t}_2}{J_F}\right) \cdot (\mathbf{t}_1 \tilde{\Lambda} 2, 1, \mathbf{t}_2 \tilde{\Lambda}^{2,2}, \mathbf{t}_3 \tilde{\Lambda}^{2,3}) \, \mathrm{d}\tilde{\sigma} \tilde{\mathbf{b}}.$$

Then, we define the boundary matrix

$$\tilde{\mathsf{M}}_b^1 = \int_0^1 \int_0^1 \left(\frac{1}{J_F} \begin{pmatrix} 0 & 0 & 0 \\ -\mathbf{t}_3 \cdot \mathbf{t}_1 \tilde{\Lambda}^{1,2} \tilde{\Lambda}^{2,1} & -\mathbf{t}_3 \cdot \mathbf{t}_2 \tilde{\Lambda}^{1,2} \tilde{\Lambda}^{2,2} & -\mathbf{t}_3 \cdot \mathbf{t}_3 \tilde{\Lambda}^{1,2} \tilde{\Lambda}^{2,3} \\ \mathbf{t}_2 \cdot \mathbf{t}_1 \tilde{\Lambda}^{1,3} \tilde{\Lambda}^{2,1} & \mathbf{t}_2 \cdot \mathbf{t}_2 \tilde{\Lambda}^{1,3} \tilde{\Lambda}^{2,2} & \mathbf{t}_2 \cdot \mathbf{t}_3 \tilde{\Lambda}^{1,3} \tilde{\Lambda}^{2,3} \end{pmatrix} \right) \Bigg|_{\xi_1=0}^1 \mathrm{d}\xi_2 \, \mathrm{d}\xi_3.$$

Analogously, we use the spline representation of the electric field, (3.7a), to rewrite the bound-

ary part of Gauss' law (9.2) and test with the respective spline basis function $\tilde{\psi} = \tilde{\Lambda}^0$,

$$\int_{\partial\tilde{\Omega}} \tilde{\Lambda}^0 \left((\mathbf{n}_1 \tilde{\Lambda}^{1,1}, \mathbf{n}_2 \tilde{\Lambda}^{1,2}, \mathbf{n}_3 \tilde{\Lambda}^{1,3}) \cdot \mathbf{n}_1 \right) J_F \, \mathrm{d}\tilde{\sigma} \tilde{\mathbf{e}}.$$

Then, the 0-form boundary matrix is defined as

$$\tilde{\mathsf{M}}_b^0 = \int_0^1 \int_0^1 \left(\tilde{\Lambda}^0 \left(\mathbf{n}_1 \cdot \mathbf{n}_1 \tilde{\Lambda}^{1,1}, \mathbf{n}_1 \cdot \mathbf{n}_2 \tilde{\Lambda}^{1,2}, \mathbf{n}_1 \cdot \mathbf{n}_3 \tilde{\Lambda}^{1,3} \right) J_F \right) \Big|_{\xi_1=0}^1 \mathrm{d}\xi_2 \, \mathrm{d}\xi_3.$$

Inserting the spline representations of the fields (3.7), the Poynting flux (9.4) takes the following form:

$$\tilde{\mathbf{e}}^\top \int_{\partial\tilde{\Omega}} \frac{1}{J_F} \begin{pmatrix} 0 & 0 & 0 \\ \mathbf{t}_3 \cdot \mathbf{t}_1 \tilde{\Lambda}^{1,2} \tilde{\Lambda}^{2,1} & \mathbf{t}_3 \cdot \mathbf{t}_2 \tilde{\Lambda}^{1,2} \tilde{\Lambda}^{2,2} & \mathbf{t}_3 \cdot \mathbf{t}_3 \tilde{\Lambda}^{1,2} \tilde{\Lambda}^{2,3} \\ -\mathbf{t}_2 \cdot \mathbf{t}_1 \tilde{\Lambda}^{1,3} \tilde{\Lambda}^{2,1} & -\mathbf{t}_2 \cdot \mathbf{t}_2 \tilde{\Lambda}^{1,3} \tilde{\Lambda}^{2,2} & -\mathbf{t}_2 \cdot \mathbf{t}_3 \tilde{\Lambda}^{1,3} \tilde{\Lambda}^{2,3} \end{pmatrix} \mathrm{d}\tilde{\sigma} \tilde{\mathbf{b}} = -\tilde{\mathbf{e}}^\top \tilde{\mathsf{M}}_b^1 \tilde{\mathbf{b}}. \tag{9.11}$$

9.5 Perfect Conductor Boundary Conditions

Looking for a physically meaningful boundary condition, we end up with the perfect conductor boundary condition as described in [41],

$$\tilde{\mathbf{E}} \times \tilde{\mathbf{n}} = 0, \tag{9.12}$$

This also implies that with matching initial conditions

$$\dot{\tilde{\mathbf{B}}} \cdot \tilde{\mathbf{n}} = 0. \tag{9.13}$$

This can be seen by taking the scalar product of Faraday's law (2.17a) with the normal vector,

$$\frac{\partial}{\partial t} \tilde{\mathbf{B}} \cdot \mathbf{n} = -(\nabla_{\boldsymbol{\xi}} \times \tilde{\mathbf{E}}) \cdot \tilde{\mathbf{n}} = -\nabla_{\boldsymbol{\xi}} \cdot (\tilde{\mathbf{E}} \times \tilde{\mathbf{n}}) = 0,$$

since $\tilde{\mathbf{n}}$ is constant in our case. Hence, we have found our pair of boundary conditions for the electromagnetic fields.

Since in our case the normal vector simplifies to $\tilde{\mathbf{n}} = (\pm 1, 0, 0)^\top$, the perfect conductor boundary conditions translate to $(\tilde{\mathbf{E}} \times (\pm 1, 0, 0)^\top)\Big|_{\partial\tilde{\Omega}} = \pm \left((0, \tilde{E}_3(\boldsymbol{\xi}), -\tilde{E}_2(\boldsymbol{\xi}))^\top \right) \Big|_{\partial\tilde{\Omega}} = \mathbf{0}$ and $\left(\frac{\partial \tilde{\mathbf{B}}}{\partial t} \cdot (\pm 1, 0, 0)^\top \right) \Big|_{\partial\tilde{\Omega}} = \pm \dot{\tilde{B}}_1(\boldsymbol{\xi}) \Big|_{\partial\tilde{\Omega}} = 0.$

To satisfy the boundary conditions (9.12), the differential 1-forms have to be in the constrained Sobolev space $H_0(\mathrm{curl}, \tilde{\Omega}) := \{\boldsymbol{\omega} \in L^2(\tilde{\Omega})^3 | \, \mathrm{curl}\, \boldsymbol{\omega} \in L^2(\tilde{\Omega})^3 \wedge (\boldsymbol{\omega} \times \tilde{\mathbf{n}})\Big|_{\partial\tilde{\Omega}} = \mathbf{0}\}$. Additionally, the 2-forms have to be in $H_0(\mathrm{div}, \tilde{\Omega}) := \{\boldsymbol{\omega} \in L^2(\tilde{\Omega})^3 | \, \mathrm{div}\, \boldsymbol{\omega} \in L^2(\tilde{\Omega}) \wedge (\boldsymbol{\omega} \cdot \tilde{\mathbf{n}})\Big|_{\partial\tilde{\Omega}} = 0\}$ to satisfy the derived boundary conditions (9.13).

For our discretisation with spline finite elements, we impose the boundary conditions (9.12) as essential boundary conditions. This yields the following conditions on the spline basis functions:

$$\tilde{\Lambda}^{1,2}(\boldsymbol{\xi})\Big|_{\partial\tilde{\Omega}} = 0, \quad \tilde{\Lambda}^{1,3}(\boldsymbol{\xi})\Big|_{\partial\tilde{\Omega}} = 0, \quad \tilde{\Lambda}^{2,1}(\boldsymbol{\xi})\Big|_{\partial\tilde{\Omega}} = 0. \tag{9.14}$$

Note that the constrained spline finite element spaces resulting from imposed Dirichlet boundary conditions are given in [12, Sec. 3.3].

Consequently, the boundary term from Ampère's equation vanishes for the perfect conductor boundary conditions, since the 1-form boundary matrix equals zero,

$$\tilde{\mathsf{M}}_b^1 = \int_0^1 \int_0^1 \left(\frac{1}{J_F} \begin{pmatrix} 0 & 0 & 0 \\ -\mathbf{t}_3 \cdot \mathbf{t}_1 \tilde{\Lambda}^{1,2} \tilde{\Lambda}^{2,1} & -\mathbf{t}_3 \cdot \mathbf{t}_2 \tilde{\Lambda}^{1,2} \tilde{\Lambda}^{2,2} & -\mathbf{t}_3 \cdot \mathbf{t}_3 \tilde{\Lambda}^{1,2} \tilde{\Lambda}^{2,3} \\ \mathbf{t}_2 \cdot \mathbf{t}_1 \tilde{\Lambda}^{1,3} \tilde{\Lambda}^{2,1} & \mathbf{t}_2 \cdot \mathbf{t}_2 \tilde{\Lambda}^{1,3} \tilde{\Lambda}^{2,2} & \mathbf{t}_2 \cdot \mathbf{t}_3 \tilde{\Lambda}^{1,3} \tilde{\Lambda}^{2,3} \end{pmatrix} \right) \Bigg|_{\partial\tilde{\Omega}} \mathrm{d}\xi_2 \, \mathrm{d}\xi_3 = \mathbf{0}. \tag{9.15}$$

This means that the Poynting flux (9.11) equals zero, too. Therefore, we do not have field energy exchange over the boundary and the system is closed.

In Proposition 9.2, we have proven that the clamped basis splines by construction satisfy a discrete de Rham sequence. Now, we assume perfect conductor boundary conditions (9.14) for the spline basis functions and have to check that (9.10) still holds at the boundary. A compatibility condition is given by the following proposition:

Proposition 9.1. *Assuming perfect conductor boundary conditions, the clamped basis splines constructed in Section 9.3 form a discrete de Rham sequence at the boundary if and only if they satisfy the condition*

$$\mathcal{S}_\star^p(\xi_1)\Big|_{\partial\tilde{\Omega}} = 0. \tag{9.16}$$

Proof. We want to show that the B-splines still form a discrete de Rham sequence as in (9.10). This sequence consists of three lines. We start with the first line stating

$$\nabla_{\boldsymbol{\xi}} \tilde{\Lambda}^0 = \tilde{\boldsymbol{\Lambda}}^1 \mathsf{G}.$$

Then, for a 0-form $\tilde{\Phi} = \tilde{\Lambda}^0(\xi)\tilde{\boldsymbol{\phi}}$, we obtain at the boundary

$$\left(\nabla_{\boldsymbol{\xi}}\tilde{\Lambda}^0(\boldsymbol{\xi})\right)\Big|_{\partial\tilde{\Omega}}\tilde{\boldsymbol{\phi}} = \begin{pmatrix} \partial_{\xi_1}\mathcal{S}^p_\star(\xi_1)\Big|_{\partial\tilde{\Omega}} \otimes \mathcal{S}^p(\xi_2) \otimes \mathcal{S}^p(\xi_3) \\ \mathcal{S}^p_\star(\xi_1)\Big|_{\partial\tilde{\Omega}} \otimes \partial_{\xi_2}\mathcal{S}^p(\xi_2) \otimes \mathcal{S}^p(\xi_3) \\ \mathcal{S}^p_\star(\xi_1)\Big|_{\partial\tilde{\Omega}} \otimes \mathcal{S}^p(\xi_2) \otimes \partial_{\xi_3}\mathcal{S}^p(\xi_3) \end{pmatrix}\tilde{\boldsymbol{\phi}} \overset{!}{=} \begin{pmatrix} \tilde{\Lambda}^{1,1}(\boldsymbol{\xi})\Big|_{\partial\tilde{\Omega}} D_1\boldsymbol{\phi} \\ 0 \\ 0 \end{pmatrix} \overset{(9.14)}{=} \tilde{\boldsymbol{\Lambda}}^1(\boldsymbol{\xi})\Big|_{\partial\tilde{\Omega}}\mathsf{G}\tilde{\boldsymbol{\phi}}.$$

This is satisfied non-trivially if and only if $\mathcal{S}^p_\star(\xi_1)\Big|_{\partial\tilde{\Omega}} = 0$.

Next, for the second line of (9.10), we look at the rotation of a 1-form $\tilde{\mathbf{A}} = \tilde{\boldsymbol{\Lambda}}^1\tilde{\mathbf{a}}$ at the boundary,

$$\begin{aligned}(\nabla_{\boldsymbol{\xi}} \times \tilde{\boldsymbol{\Lambda}}^1)\Big|_{\partial\tilde{\Omega}}\tilde{\mathbf{a}} &= \begin{pmatrix} \mathcal{S}^p_\star(\xi_1)\Big|_{\partial\tilde{\Omega}} \otimes \partial_{\xi_2}\mathcal{S}^p(\xi_2) \otimes \mathcal{S}^{p-1}(\xi_3) - \mathcal{S}^p_\star(\xi_1)\Big|_{\partial\tilde{\Omega}} \otimes \mathcal{S}^{p-1}(\xi_2) \otimes \partial_{\xi_3}\mathcal{S}^p(\xi_3) \\ \mathcal{S}^{p-1}_\star(\xi_1)\Big|_{\partial\tilde{\Omega}} \otimes \mathcal{S}^p(\xi_2) \otimes \partial_{\xi_3}\mathcal{S}^p(\xi_3) - \partial_{\xi_1}\mathcal{S}^p_\star(\xi_1)\Big|_{\partial\tilde{\Omega}} \otimes \mathcal{S}^p(\xi_2) \otimes \mathcal{S}^{p-1}(\xi_3) \\ \partial_{\xi_1}\mathcal{S}^p_\star(\xi_1)\Big|_{\partial\tilde{\Omega}} \otimes \mathcal{S}^{p-1}(\xi_2) \otimes \mathcal{S}^p(\xi_3) - \mathcal{S}^{p-1}_\star(\xi_1)\Big|_{\partial\tilde{\Omega}} \otimes \partial_{\xi_2}\mathcal{S}^p(\xi_2) \otimes \mathcal{S}^p(\xi_3) \end{pmatrix}\tilde{\mathbf{a}} \\ &\overset{!}{=} \begin{pmatrix} 0 \\ \tilde{\Lambda}^{2,2}(\boldsymbol{\xi})\Big|_{\partial\tilde{\Omega}}(D_3\tilde{\mathbf{a}}_1 - D_1\tilde{\mathbf{a}}_3) \\ \tilde{\Lambda}^{2,3}(\boldsymbol{\xi})\Big|_{\partial\tilde{\Omega}}(D_1\tilde{\mathbf{a}}_2 - D_2\tilde{\mathbf{a}}_1) \end{pmatrix} \overset{(9.14)}{=} \tilde{\boldsymbol{\Lambda}}^2(\boldsymbol{\xi})\Big|_{\partial\tilde{\Omega}}\mathsf{C}\tilde{\mathbf{a}}.\end{aligned}$$

This leads again to the compatibility condition $\mathcal{S}^p_\star(\xi_1)\Big|_{\partial\tilde{\Omega}} = 0$.

Since there are no boundary conditions on the differential 3-form basis, the third line of (9.10) is also satisfied at the boundary,

$$\left(\nabla_{\boldsymbol{\xi}} \cdot \tilde{\boldsymbol{\Lambda}}^2(\boldsymbol{\xi})\right)\Big|_{\partial\tilde{\Omega}} = \tilde{\Lambda}^3(\boldsymbol{\xi})\Big|_{\partial\tilde{\Omega}}\mathsf{D},$$

which concludes the proof. □

From this proposition, it follows that also the boundary part from Gauss' law vanishes, since the 0-form boundary matrix equals zero,

$$\tilde{\mathsf{M}}^0_b = \int_0^1\int_0^1 \left(\tilde{\Lambda}^0\left(\mathbf{n}_1 \cdot \mathbf{n}_1\tilde{\Lambda}^{1,1}, \mathbf{n}_1 \cdot \mathbf{n}_2\tilde{\Lambda}^{1,2}, \mathbf{n}_1 \cdot \mathbf{n}_3\tilde{\Lambda}^{1,3}\right)J_F\right)\Big|_{\partial\tilde{\Omega}} \mathrm{d}\xi_2\,\mathrm{d}\xi_3 = 0.$$

We already showed that the initial boundary condition $\tilde{\mathbf{B}} \cdot \tilde{\mathbf{n}} = C$ for the magnetic field is conserved over time because the magnetic field is updated with the curl of the electric field.

Assuming that the basis functions form a de Rham sequence and that $\tilde{\mathbf{B}}$ is computed from the 1-form potential $\tilde{\mathbf{A}}$, we have $\tilde{\mathbf{B}} \cdot \tilde{\mathbf{n}} = 0$, since

$$\begin{aligned}\left(\tilde{\mathbf{B}}(\boldsymbol{\xi}) \cdot \tilde{\mathbf{n}}\right)\Big|_{\partial\tilde{\Omega}} &= \left(\nabla_{\boldsymbol{\xi}} \times \tilde{\boldsymbol{\Lambda}}^1 \cdot \tilde{\mathbf{n}}\right)\Big|_{\partial\tilde{\Omega}} \tilde{\mathbf{a}} \\ &= \mathcal{S}^p_\star(\xi_1)\Big|_{\partial\tilde{\Omega}} \otimes \partial_{\xi_2}\mathcal{S}^p(\xi_2) \otimes \mathcal{S}^p(\xi_3) - \mathcal{S}^p_\star(\xi_1)\Big|_{\partial\tilde{\Omega}} \otimes \mathcal{S}^p(\xi_2) \otimes \partial_{\xi_3}\mathcal{S}^p(\xi_3)\tilde{\mathbf{a}} = 0.\end{aligned}$$

10 Particle Boundary Conditions

10.1 Introduction

When the particle trajectories hit the boundary, we also need to impose some boundary conditions on them. Note that we avoid a possible singularity by excluding the pole on the physical mesh as can be seen exemplarily in Figure 14. Therefore, on the logical mesh, we have an inner boundary at $\xi_1 = 0$ and an outer boundary at $\xi_1 = 1$. Following [17], we consider reflecting boundaries. We make use of the normal vector $\mathbf{n} = N(\boldsymbol{\xi})\tilde{\mathbf{n}} = \mathbf{n}_1$ to compute the reflection at the boundary as

- Inner boundary at $\xi_1 = 0$: $\xi_1 = -\xi_1, \mathbf{v} = \mathbf{v} - 2(\mathbf{n} \cdot \mathbf{v})\frac{\mathbf{n}}{\|\mathbf{n}\|^2} = \mathbf{v} - 2(\mathbf{n}_1 \cdot \mathbf{v})\frac{\mathbf{n}_1}{\|\mathbf{n}_1\|^2}$,
- Outer boundary at $\xi_1 = 1$: $\xi_1 = 2 - \xi_1, \mathbf{v} = \mathbf{v} - 2(\mathbf{n}_1 \cdot \mathbf{v})\frac{\mathbf{n}_1}{\|\mathbf{n}_1\|^2}$.

The particle weight is kept constant. The reflecting boundary prevents heat fluxes and currents at the boundary and ensures exact energy conservation.

In this study, we additionally consider a constant in- and outflow of particles: A particle of identical weight is reinserted at the opposite boundary with the same velocity, which can be considered as periodic particle boundary conditions,

- Inner boundary at $\xi_1 = 0$: $\xi_1 = \xi_1 + 1, \mathbf{v} = \mathbf{v}$,
- Outer boundary at $\xi_1 = 1$: $\xi_1 = \xi_1 - 1, \mathbf{v} = \mathbf{v}$.

This choice again conserves mass, energy and magnetic momentum. This second boundary conditions mimics a periodic behaviour and is considered here as an intermediate step for verification purposes rather than being physically motivated.

10.2 Conservation Properties

10.2.1 Charge Monitoring

In both semi-explicit time discretisation schemes, the charge conservation depends on the exact solution of the particle trajectory in the following part:

$$\tilde{\mathsf{M}}_1 \frac{\tilde{\mathbf{e}}^{n+1} - \tilde{\mathbf{e}}^n}{\Delta t} = -\int_{t^n}^{t^{n+1}} \tilde{\mathbb{\Lambda}}^1(\boldsymbol{\Xi}(\tau))^\top \, \mathrm{d}\tau \mathbb{W}_q \frac{\boldsymbol{\Xi}^{n+1} - \boldsymbol{\Xi}^n}{\Delta t}.$$

Since the particle update is computed iteratively, it is important that we impose the boundary conditions after computing the midpoint $\bar{\boldsymbol{\Xi}} = \frac{\boldsymbol{\Xi}^{n+1} + \boldsymbol{\Xi}^n}{2}$ in (6.4) and (6.6). In the case of a particle trajectory crossing the boundary, we solve this part with a split line integral. First, we compute the point of intersection of the particle trajectory with the boundary and compute the line integral up to that point. Second, we reflect the particle position and velocity at this point and compute the line integral between the point of intersection and the new particle

position.

10.2.2 Energy Monitoring

The energy conservation of the implicit time discretisation methods depends on the solution of the antisymmetric subsystems. Therefore, the DisGradE method stays energy conserving because the particle position is updated independently of the particle velocity and the electromagnetic fields provided that the number of particles is constant.

However, if the position is updated in the same step as the velocity and the electric field, which is the case for the DisGradEC method, it is crucial that the electric and the kinetic energies balance out. So, when a particle crosses the boundary and is reflected back, we need to update the electric field with the new velocity. Solving this system iteratively leads to the problem that the reflection can flip the sign of the particle velocity in iteration, which prevents the convergence. Therefore, the reflection boundary conditions are only implemented for the DisGradE and not for the DisGradEC method.

11 Challenges with Singular Coordinate Transformations

When dealing with a mapping that contains a singularity, there are two main challenges. The first challenge is the construction of smooth basis functions at the pole. However, Toshniwal et al. [87, 86] recently presented an instruction for constructing such basis functions. The second challenge is the evaluation of the electromagnetic fields in an environment around the pole.

Let us consider a radial mapping with a pole at $\xi_1 = 0$ such as the two examples given in (13.2) for $r_0 = 0$. Then, we review a solution for the evaluation of the electric field, which is found in [100]. For a differential 1-form $\mathbf{E}$, the adequate representation is given by the Piola transform (2.14) so that $\mathbf{E}(t, \mathbf{x}) = N(\boldsymbol{\xi})\tilde{\mathbf{E}}(t, \boldsymbol{\xi})$. This holds for all $\xi_1 > 0$ but for $\xi_1 = 0$ the transposed inverse Jacobian matrix becomes singular. Thus, we search for an expression of the electric field in physical coordinates at the pole. Therefore, we rewrite the representation of the electric field by multiplying both sides with the transposed Jacobian matrix, $\tilde{\mathbf{E}}(\boldsymbol{\xi}) = DF^\top(\boldsymbol{\xi})\mathbf{E}(\mathbf{x})$. Componentwise, we can write this out as

$$\begin{aligned}
\tilde{E}_1(\boldsymbol{\xi}) &= \frac{\partial F_1(\boldsymbol{\xi})}{\partial_{\xi_1}} E_1(\mathbf{x}) + \frac{\partial F_2(\boldsymbol{\xi})}{\partial_{\xi_1}} E_2(\mathbf{x}), \\
\tilde{E}_2(\boldsymbol{\xi}) &= \frac{\partial F_1(\boldsymbol{\xi})}{\partial_{\xi_2}} E_1(\mathbf{x}) + \frac{\partial F_2(\boldsymbol{\xi})}{\partial_{\xi_2}} E_2(\mathbf{x}), \\
\tilde{E}_3(\boldsymbol{\xi}) &= L_z E_3(\mathbf{x}).
\end{aligned}$$

At the pole, the third component of the electric field in physical coordinates is given trivially by $E_3(0, 0, z) = \frac{1}{L_z}\tilde{E}_3(0, \xi_2, \xi_3)$. For the first two components of the electric field, we focus on the first line because the partial derivatives in the second line equal zero,

$$\frac{\partial F_1(0, \xi_2)}{\partial_{\xi_2}} = \frac{\partial F_2(0, \xi_2)}{\partial_{\xi_2}} = 0 \quad \forall \xi_2.$$

Thus, we obtain

$$\tilde{E}_1(0, \xi_2, \xi_3) = E_1(0, 0, z)\frac{\partial F_1(0, \xi_2)}{\partial \xi_1} + E_2(0, 0, z)\frac{\partial F_2(0, \xi_2)}{\partial \xi_1}.$$

Then, the components of the electric field in physical coordinates can be calculated from the given field in logical coordinates at the left-hand side for two linear independent angles ξ_2. For the cylindrical coordinates in (13.2), two independent angles would be $\xi_2 = 0$ and $\xi_2 = \frac{1}{4}$ so that the linear system simplifies to

$$\tilde{E}_1(\mathbf{0}) = E_1(\mathbf{0}),\ \tilde{E}_1\left(0, \frac{1}{4}, 0\right) = E_2(\mathbf{0}).$$

We get the same result for every pair of independent angles because the values of the two

components E_1, E_2 need to be constant at the pole. With this expression, we can evaluate the electric field in a small ε-environment around the pole, $\mathbf{x} = \mathbf{0}$. For $\|\mathbf{x}\| < \varepsilon$, we obtain

$$\mathbf{E}(\mathbf{x}) = (1 - \frac{\xi_1}{\varepsilon})\mathbf{E}(0, 0, z) + \frac{\xi_1}{\varepsilon} N(\varepsilon, \xi_2, \xi_3)\tilde{\mathbf{E}}(\varepsilon, \xi_2, \xi_3).$$

Let us transfer this idea to the evaluation of the magnetic field. The magnetic field is transformed by the Piola transform form for 2-forms (2.15), which has the following form:

$$\mathbf{B}(t, \mathbf{x}) = \frac{DF(\boldsymbol{\xi})}{J_F(\boldsymbol{\xi})}\tilde{\mathbf{B}}(t, \boldsymbol{\xi}).$$

At the pole, this representation is not possible because the Jacobian determinant equals zero. Multiplying by the inverse of the Jacobian matrix divided by the Jacobian determinant does not help, since the inverse Jacobian matrix is singular, too.

However, for the magnetic part of the Lorentz force, we only need the cross product of the velocity and the magnetic field,

$$\mathbf{v} \times \mathbf{B} = \mathbf{v} \times \frac{DF}{J_F}\tilde{\mathbf{B}}.$$

This term can be reformulated as in (2.8),

$$\mathbf{v} \times \frac{DF}{J_F}\tilde{\mathbf{B}} = N\left(\tilde{\mathbf{v}} \times \tilde{\mathbf{B}}\right),$$

where we introduced the logical velocity $\tilde{\mathbf{v}} = N^\top(\boldsymbol{\xi})\mathbf{v}$. Finally, we only need a representation of $\tilde{\mathbf{v}}$ at the pole. We can compute the logical velocity as the discrete time derivative of the position, $\tilde{\mathbf{v}}^n = \frac{\boldsymbol{\xi}^{n+1} - \boldsymbol{\xi}^n}{\Delta t}$. However, this works only if there is an analytical inverse of the coordinate transformation, since in this case, we can compute the particle push in physical coordinates avoiding the singularity in the inverse Jacobian matrix, $N^\top(\boldsymbol{\xi})$,

$$\boldsymbol{\xi}^{n+1} = F^{-1}(F(\boldsymbol{\xi}^n) + \Delta t \mathbf{v}^n).$$

Then, we use the same method that we used for the electric field, to obtain

$$\begin{aligned}
\left(\tilde{\mathbf{v}} \times \tilde{\mathbf{B}}(0, \xi_2)\right)_1 &= \frac{\partial x}{\partial \xi_1}(0, \xi_2)(\mathbf{v} \times \mathbf{B})_1(\mathbf{0}) + \frac{\partial y}{\partial \xi_1}(0, \xi_2)(\mathbf{v} \times \mathbf{B})_2(\mathbf{0}), \\
\left(\tilde{\mathbf{v}} \times \tilde{\mathbf{B}}(0, \xi_2)\right)_3 &= (\mathbf{v} \times \mathbf{B}(\mathbf{0}))_3 .
\end{aligned}$$

Subsequently, the Lorentz force in a small ε-environment around the pole is calculated as

$$\frac{q}{m}\left(\left(1 - \frac{\xi_1}{\varepsilon}\right)(\mathbf{E}(0, 0, z) + \mathbf{v} \times \mathbf{B}(0, 0, z)) + \frac{\xi_1}{\varepsilon} N(\varepsilon, \xi_2, \xi_3)(\tilde{\mathbf{E}}(\varepsilon, \xi_2, \xi_3) + \tilde{\mathbf{v}} \times \tilde{\mathbf{B}}(\varepsilon, \xi_2, \xi_3)\right).$$

12 Preconditioner

The condition number of the B-spline finite element mass matrices (3.6) increases exponentially with the degree p of the B-splines as explained in [29]. Therefore, the use of ordinary iterative solvers such as the conjugate gradient (CG) solver becomes computationally expensive and inefficient. Donatelli et al. [29] review several possibilities for fast solvers such as preconditioned conjugate gradient (PCG), h-multigrid or multi-iterative methods. Alternatively, the p-multigrid method is investigated in [85].

In our framework, we use a PCG method to solve the linear equations with the finite element mass matrices $\tilde{\mathsf{M}}_{1,2}$ because there are several options for the preconditioner. Our preconditioner is based on the fact that circulant matrices are diagonal in Fourier space and hence, can be cheaply inverted based on the Fast Fourier Transform (FFT). On a periodic tensor product grid without coordinate transformations, the finite element matrices are circulant so that the linear equation systems can be solved directly after Fourier transformation yielding a very efficient solver compared to iterative solvers in this case. We refer to [55] for a detailed description of this solution strategy. Since the structure of the mass matrices with real boundary conditions is still close enough to a circulant matrix, we choose such an eigenvalue solver, P_{fft}, as preconditioner. Furthermore, its building block is already implemented in the SeLaLib [1].

Observing the structure of the mass matrices for clamped splines of degree p, we notice that only the first and last $p+2$ rows differ from the mass matrix for periodic splines of the same degree. This observation motivates the alternative idea to use the eigenvalues of the periodic matrix only for the middle part that is identical to a periodic mass matrix, except for the periodicity at the boundary, and invert the boundary part, which consists of the first and last $p+2$ rows of the mass matrix, separately.

Figure 12 shows the eigenvalues of the 1D mass matrix with clamped splines for the two preconditioner ideas. We see that both methods improve the distribution of the eigenvalues of the preconditioned matrix. Since we are only interested in the ratio between the lowest and the highest eigenvalue, we decide to use the eigenvalue solver on the whole mass matrix, which has a lower condition number $\kappa = \frac{eigval_{max}}{eigval_{min}}$.

However, in the case of a singular mapping, we need an additional part for the preconditioner to lift the singularity in the mass matrix $\tilde{\mathsf{M}}$ as investigated in [28, Sec. 3.2]. Assuming for instance that the entries of $\tilde{\mathsf{M}}$ are of minimal order $\mathcal{O}\left(\frac{1}{\xi_1}\right)$, we want to precondition with a matrix which has entries of maximal order $\mathcal{O}(\xi_1)$ and is close to an inverse of $\tilde{\mathsf{M}}$.

We start by looking for a matrix whose maximal eigenvalue is similar to the one of $\tilde{\mathsf{M}}$ and that is easily invertible. Two possible choices are the diagonal row lumped mass $(\tilde{\mathsf{M}}^2_{lump})_{ii} = \sum_j \tilde{\mathsf{M}}_{ij}$ or the main diagonal matrix $(\mathsf{D}^2)_{ii} = \tilde{\mathsf{M}}_{ii}$. If the entries of the lumped mass become

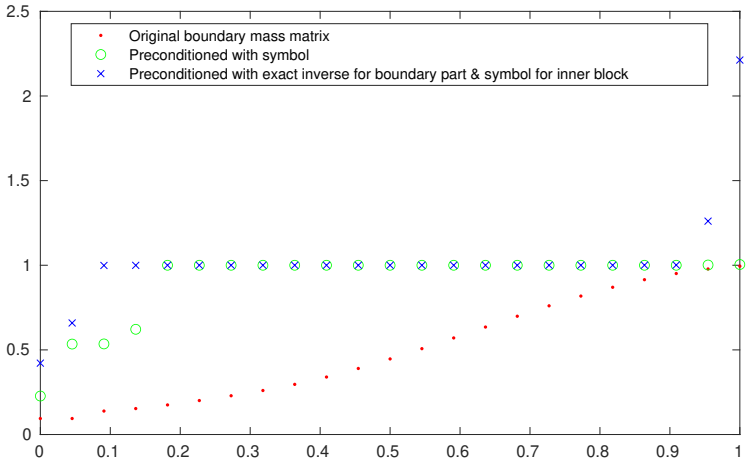

(a) Quadratic spline

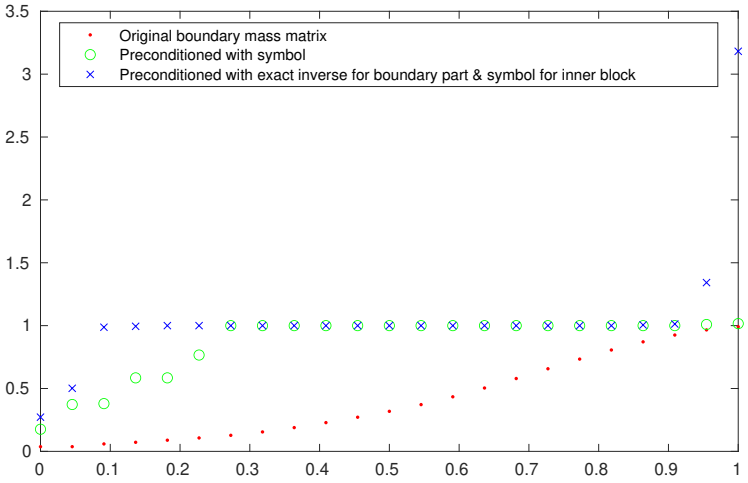

(b) Cubic spline

Figure 12 Analytical eigenvalues of the 1D preconditioned mass matrix for different spline degrees.

very small or even negative, there are two options. Either we define a positive lower limit for the sum of the row or we use the main diagonal matrix instead because the diagonal elements are always positive.

Then, the preconditioner consists of the inverse of the lumped mass or the main diagonal matrix and the eigenvalue preconditioner P_{fft}, which is used on the now uniform system. In order not to destroy the symmetry of the matrix, we construct the preconditioner as

$$\mathsf{P} = \tilde{\mathsf{M}}^{-1}_{lump}\mathsf{P}_{fft}\tilde{\mathsf{M}}^{-1}_{lump} \text{ or } \mathsf{P} = \mathsf{D}^{-1}\mathsf{P}_{fft}\mathsf{D}^{-1},$$

where the entries of the inverse matrices can easily be computed as $(\tilde{\mathsf{M}}^{-1}_{lump})_{ii} = \frac{1}{\sqrt{\sum_j \tilde{\mathsf{M}}_{ij}}}$ and $(\mathsf{D}^{-1})_{ii} = \frac{1}{\sqrt{\tilde{\mathsf{M}}_{ii}}}$.

Table 5 shows the maximum number of iterations for the CG and PCG solver of the mass matrices. The numbers are taken from the simulation of the electromagnetic Weibel instability in Chapter 13 on various grids with a time step of $\Delta t = 0.01$ and a solver tolerance of 10^{-13}. Note that for a lower tolerance the CG solver would not converge without the preconditioner. It can be seen that our preconditioner largely reduces the number of iterations and the iteration count only moderately increases with increasing spline order.

Table 5 Number of iterations for the CG and PCG solver of the mass matrices for spline degree p.

Grid	Number of iterations CG solver			
	$p_x = 2$		$p_x = 3$	
	$N_x = 8$	$N_x = 32$	$N_x = 8$	$N_x = 32$
Cartesian	426	451	740	772
Distorted	498	502	797	818
Cylindrical	1626	2977	2583	4807
Elliptical	2270	2881	3805	4678

Grid	Number of iterations PCG solver			
	$p_x = 2$		$p_x = 3$	
	$N_x = 8$	$N_x = 32$	$N_x = 8$	$N_x = 32$
Cartesian	8	8	11	11
Distorted	18	18	23	22
Cylindrical	10	10	13	14
Elliptical	14	16	21	22

13 Numerical Experiments

13.1 Coordinate Transformation

A new class of mappings is introduced that operate on a deformed domain. For the sinusoidal transformation the mapping is modified to

$$F_{dist}(\boldsymbol{\xi}) = \begin{pmatrix} L_x \left(\xi_1 + \varepsilon \sin(L_p \xi_1) \sin(2\pi\xi_2)\right) \\ L_y \left(\xi_2 + \varepsilon \sin(L_p \xi_1) \sin(2\pi\xi_2)\right) \\ L_z \xi_3 \end{pmatrix}. \tag{13.1}$$

Figure 13 visualises the (x, y)-part of the sinusoidally distorted grid on a square domain with

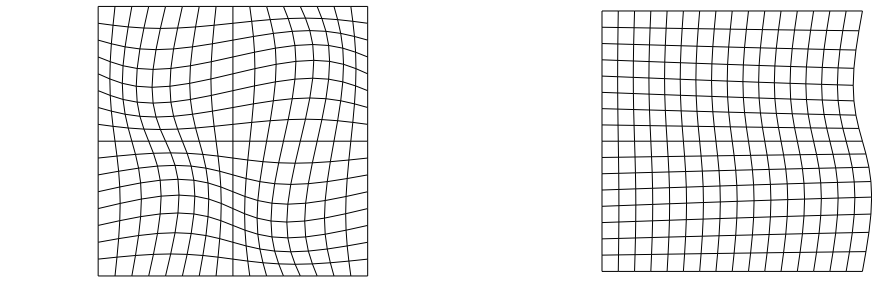

(a) Square domain (b) Deformed domain

Figure 13 Distorted grids on different domains for distortion parameter $\varepsilon = 0.05$.

$L_p = 2\pi$ and on a deformed domain with $L_p = \frac{\pi}{2}$ for the distortion parameter $\varepsilon = 0.05$.

Furthermore, we introduce two radial mappings, a cylindrical and an elliptical transformation,

$$F_{cyl}(\boldsymbol{\xi}) = \begin{pmatrix} (r_0 + L_r \xi_1) \cos(2\pi\xi_2) \\ (r_0 + L_r \xi_1) \sin(2\pi\xi_2) \\ L_z \xi_3 \end{pmatrix}, \quad F_{ell}(\boldsymbol{\xi}) = \begin{pmatrix} L_r \cosh(\xi_1 + r_0) \cos(2\pi\xi_2) \\ L_r \sinh(\xi_1 + r_0) \sin(2\pi\xi_2) \\ L_z \xi_3 \end{pmatrix}. \tag{13.2}$$

Figure 14 visualises the (x, y)-part of the corresponding grids, where the pole is excluded for $r_0 > 0$ avoiding a singularity in the mapping.

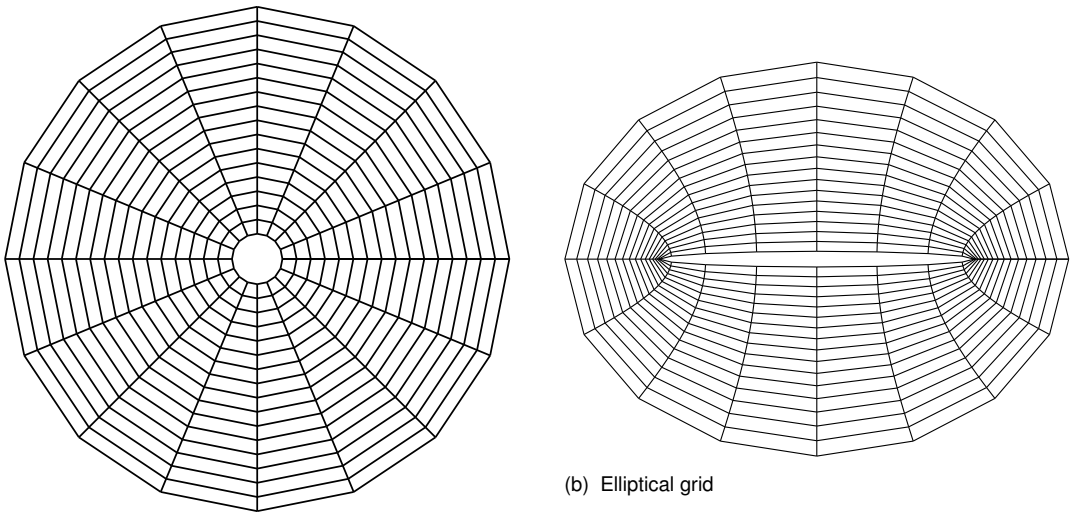

(a) Cylindrical grid

(b) Elliptical grid

Figure 14 Cylindrical grid with $r_0 = 0.5$ and elliptical grid with $r_0 = 0.05$.

13.2 Test case

Motivated by the results in [17], we test the implementation of the perfect conductor boundary and the reflecting particle boundary conditions with a simulation of the Weibel instability [93]. The instability is excited by an anisotropy in the thermal velocity and amplified with the initialisation of the corresponding component of the magnetic field. The initial distribution is given by

$$f(\mathbf{x}, \mathbf{v}, t = 0) = (1 + \alpha \cos(\mathbf{k} \cdot \mathbf{x})) \frac{1}{(2\pi)^{\frac{3}{2}} v_{Tx} v_{Ty} v_{Tz}} \exp\left(-\frac{1}{2} \left(\frac{v_x^2}{v_{Tx}^2} + \frac{v_y^2}{v_{Ty}^2} + \frac{v_z^2}{v_{Tz}^2} \right) \right),$$

where $\mathbf{x} \in [0, L]^3, \mathbf{v} \in \mathbb{R}^3$. We can choose between the following three scenarios that trigger the instability:

- $\mathbf{k} = 1.25\hat{\mathbf{e}}_x, v_{Tx} < v_{Ty,z}$, where we initialise

$$B_2(x) = \beta \cos(k_x x) \text{ or } B_3(x) = \beta \cos(k_x x),$$

- $\mathbf{k} = 1.25\hat{\mathbf{e}}_y, v_{Ty} < v_{Tx,z}$, where we initialise

$$B_1(x, y) = \beta \cos(k_y y) \sin\left(\frac{\pi x}{L_x}\right) \text{ or } B_3(y) = \beta \cos(k_y y),$$

- $\mathbf{k} = 1.25\hat{\mathbf{e}}_z, v_{Tz} < v_{Tx,y}$, where we initialise

$$B_1(x, z) = \beta \cos(k_z z) \sin\left(\frac{\pi x}{L_x}\right) \text{ or } B_2(z) = \beta \cos(k_z z).$$

The remaining two components of the magnetic field are initialised with zero.

We set $v_{Ti} = \frac{0.02}{\sqrt{2}} = \frac{v_{Tj}}{\sqrt{12}} = \frac{v_{Tk}}{\sqrt{12}}$, where $(i,j,k) = (x,y,z),(y,z,x)$ or (z,x,y). To start above the particle noise, we set $\beta = 10^{-3}$ for the initial magnetic field. The initial electric field is calculated from Poisson's equation and the initial perturbation in space is set to zero with $\alpha = 0$.

For the numerical resolution, we take $2{,}048{,}000$ particles, $8\times8\times8$ grid cells, cubic splines and a time step of $\Delta t = 0.1$. The tolerance of the iterative solvers for the DisGradE method is set to 10^{-13} and the tolerance of the PCG solver for the mass matrices is set to 10^{-14}. Note that we normalised to dimensionless quantities in terms of the electron Debye length λ_{De} and the plasma frequency ω_{pe}.

13.2.1 Comparison to Periodic Boundary Conditions

We start by comparing simulation results with the perfect conductor boundary conditions to the simulation results with periodic boundary conditions.

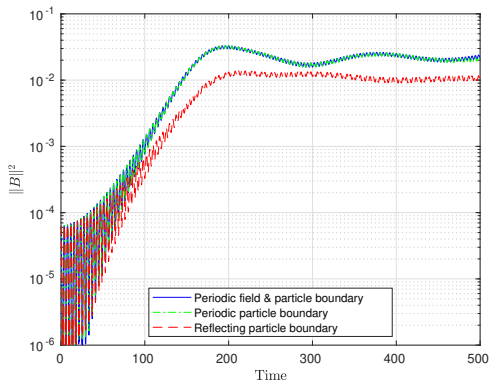

(a) Initialisation of $B_2(x) = \beta\cos(k_x x)$

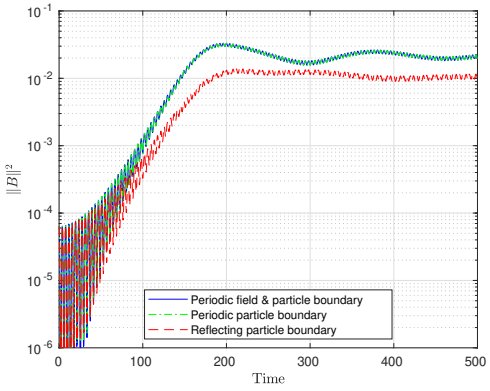

(b) Initialisation of $B_3(x) = \beta\cos(k_x x)$

Figure 15 Weibel instability with $\mathbf{k} = 1.25\hat{\mathbf{e}}_x$: Magnetic field energy for HS with time step $\Delta t = 0.1$ on a Cartesian grid with different boundary conditions.

Figures 15, 16 and 17 show the magnetic field energy on a Cartesian grid for the three different choices of the wave vector $\mathbf{k} = 1.25\hat{\mathbf{e}}_i, i \in \{x,y,z\}$. Additionally, there are two different components of the magnetic field in each scenario that can be initialised to start the Weibel instability right away. Since the results coincide for the three time integrators, we show only the simulation of the semi-explicit HS scheme with a time step of $\Delta t = 0.1$. Displayed are the simulation results for the perfect conductor boundary conditions with periodic or reflecting particle boundaries and a simulation with periodic field and particle boundary conditions for comparison.

When initialising the second and third component of the magnetic field, we see in Figures 15,

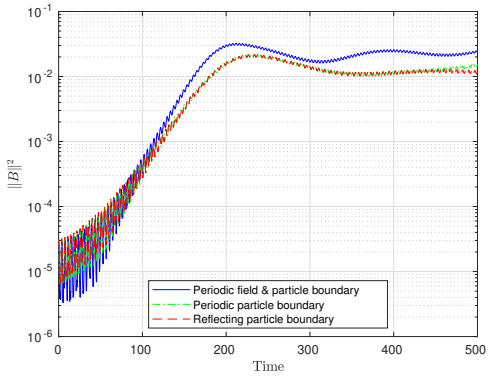

(a) Initialisation of $B_1(x, y) = \beta \sin\left(\frac{\pi x}{L_x}\right) \cos(k_y y)$

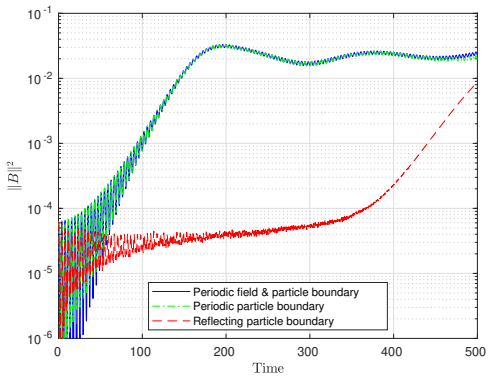

(b) Initialisation of $B_3(y) = \beta \cos(k_y y)$

Figure 16 Weibel instability with $\mathbf{k} = 1.25\hat{\mathbf{e}}_y$: Magnetic field energy for HS with time step $\Delta t = 0.1$ on a Cartesian grid with different boundary conditions.

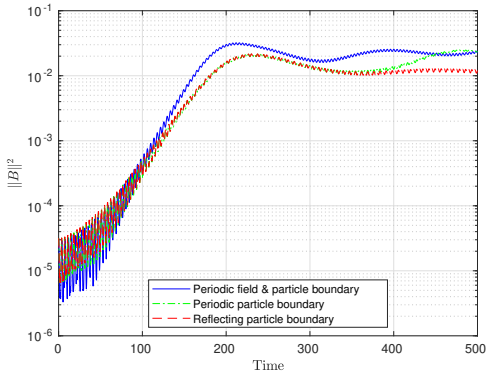

(a) Initialisation of $B_1(x, z) = \beta \sin\left(\frac{\pi x}{L_x}\right) \cos(k_z z)$

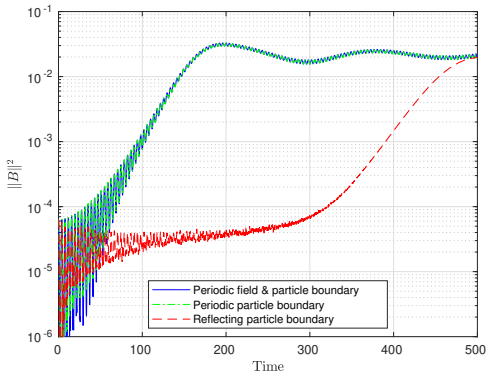

(b) Initialisation of $B_2(z) = \beta \cos(k_z z)$

Figure 17 Weibel instability with $\mathbf{k} = 1.25\hat{\mathbf{e}}_z$: Magnetic field energy for HS with time step $\Delta t = 0.1$ on a Cartesian grid with different boundary conditions.

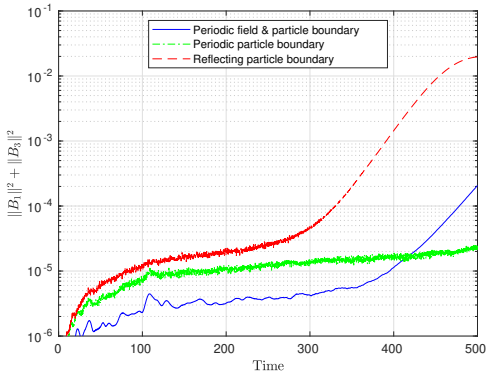

(a) Sum of first and third component of the magnetic field

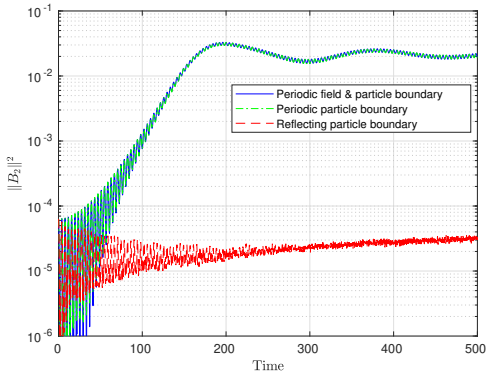

(b) Second component of the magnetic field

Figure 18 Weibel instability with $\mathbf{k} = 1.25\hat{\mathbf{e}}_z$ and initialisation of B_2: Different components of the magnetic field energy for HS with time step $\Delta t = 0.1$ on a Cartesian grid with different boundary conditions.

16b and 17b that the growth of the magnetic field in the simulation with the periodic particle boundary coincides with the growth of the magnetic field in the simulation with periodic field

and particle boundary conditions. However, the reflecting particle boundary leads to a lower growth rate and even delays the beginning of the growth in the magnetic field in the two cases displayed in Figures 16b and 17b. We will try to explain this behaviour exemplarily for the latter case. In Figure 18b, we see that the second component of the magnetic field, which was initialised to start the instability right away, shows no signs of the expected growth for the reflecting boundary conditions. This component is updated as $\dot{B}_2 = \partial_z E_1 - \partial_x E_3$ in Faraday's law (2.8b). Normally, the anisotropy in the velocity causes a discrepancy between the partial derivatives of these two components of the electric field resulting in the growth of the magnetic field. However, the reflecting boundary conditions prevent a current through the boundary, which seems to level the values of the two components of the electric field. Therefore, the growth of the second component of the magnetic field is suppressed. Nevertheless, Figure 18a shows that the instability arises in the first and third component of the magnetic field. However, the growth is delayed, since these two components were not initialised.

On a Cartesian domain, the physical and the logical fields only differ by a constant scaling. Therefore, the perfect conductor boundary conditions on the logical fields ensure E_2, E_3 and B_1 to be zero at the boundary. This is why, we initialise the first component of the magnetic field with $B_1(\mathbf{x}) = \beta \sin\left(\frac{\pi x}{L}\right) \cos(k_y y + k_z z)$. In this case, the growth rates of the periodic and reflecting particle boundary conditions coincide, which are lower than the one with periodic field and particle boundary conditions as can be seen in Figures 16a and 17a.

13.2.2 Domain Deformation

Next, we are interested in the behaviour on a deformed mapped grid. Therefore, we apply the sinusoidal coordinate transformation (13.1) with $L_p = \frac{\pi}{2}$. Again the results for the three time integrators coincide so that we only show the results of the semi-explicit CEF scheme with a time step of $\Delta t = 0.1$.

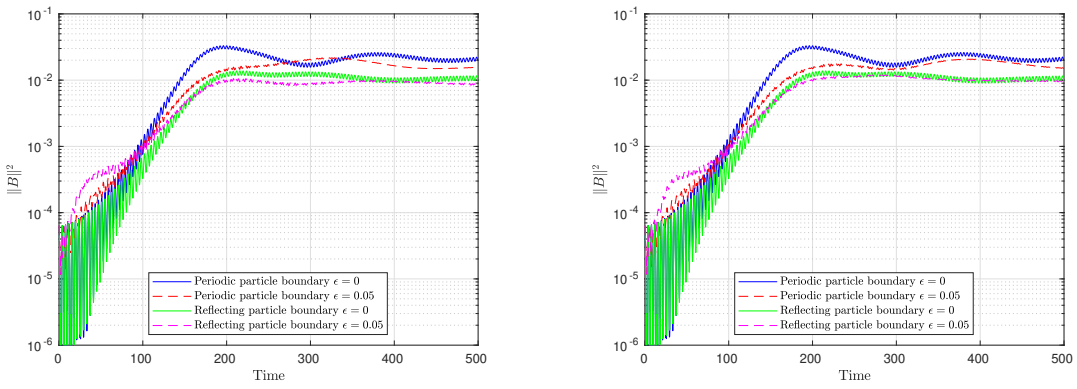

(a) Initialisation of $B_2(x) = \beta \cos(k_x x)$

(b) Initialisation of $B_3(x) = \beta \cos(k_x x)$

Figure 19 Weibel instability with $\mathbf{k} = 1.25\hat{\mathbf{e}}_x$: Magnetic field energy for CEF with time step $\Delta t = 0.1$ on a distorted grid with distortion parameters $\varepsilon = 0, 0.05$ for the coordinate transformation.

Figures 19, 20 and 21 show the magnetic field energy on the distorted grid with distortion

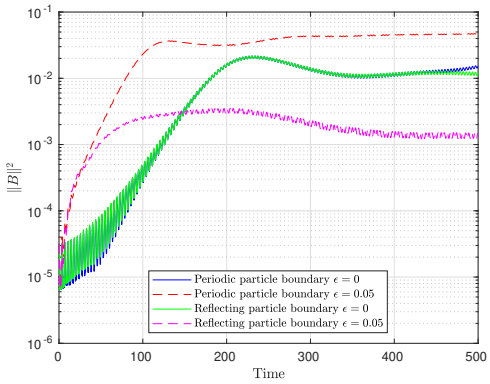

(a) Initialisation of $B_1(x, y) = \beta \sin\left(\frac{\pi x}{L_x}\right) \cos(k_y y)$

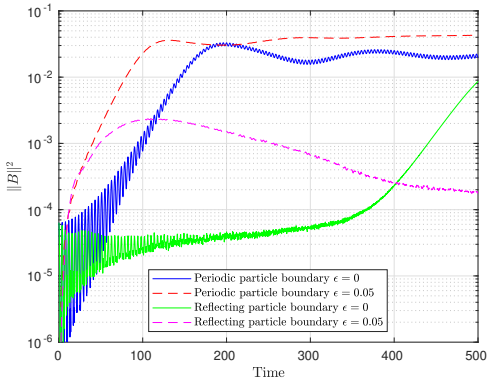

(b) Initialisation of $B_3(y) = \beta \cos(k_y y)$

Figure 20 Weibel instability with $\mathbf{k} = 1.25\hat{\mathbf{e}}_y$: Magnetic field energy for CEF with time step $\Delta t = 0.1$ on a distorted grid with distortion parameters $\varepsilon = 0, 0.05$ for the coordinate transformation.

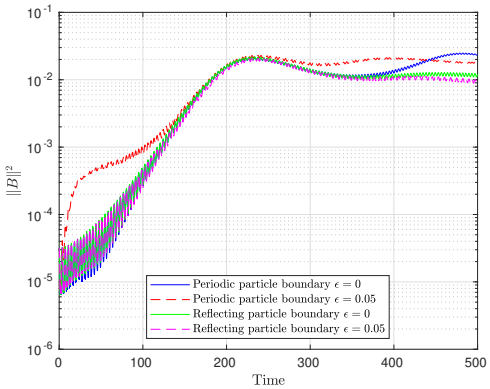

(a) Initialisation of $B_1(x, z) = \beta \sin\left(\frac{\pi x}{L_x}\right) \cos(k_z z)$

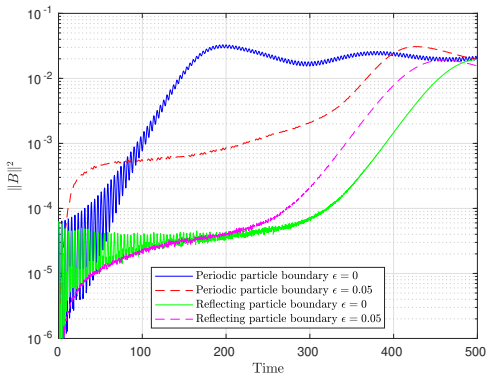

(b) Initialisation of $B_2(z) = \beta \cos(k_z z)$

Figure 21 Weibel instability with $\mathbf{k} = 1.25\hat{\mathbf{e}}_z$: Magnetic field energy for CEF with time step $\Delta t = 0.1$ on a distorted grid with distortion parameters $\varepsilon = 0, 0.05$ for the coordinate transformation.

parameters $\varepsilon = 0$, which is equal to the Cartesian grid, and $\varepsilon = 0.05$ for the three different choices of the wave vector $\mathbf{k} = 1.25\hat{\mathbf{e}}_i, i \in \{x, y, z\}$. Displayed are the simulation results for the perfect conductor boundary conditions with periodic and with reflecting particle boundaries. Figure 19 shows that the domain deformation effects the growth of the magnetic field especially in the beginning. In Figure 20, we see that the coordinate transformation couples the coordinate directions, which leads to the initial steep growth in the magnetic field. In Figure 21b, the reflecting particle boundary still delays the growth of the magnetic field but it starts earlier on the deformed grid. For the periodic particle boundary, the domain deforming transformation leads to a steeper growth in the beginning, which can be seen in Figures 21a and 21b. Figure 21a shows only minor differences for the simulation with a reflecting particle boundary on the Cartesian or on the deformed grid.

Since the coordinate transformation mixes the first two directions of the logical coordinates in the computation of x and y, z is the only periodic coordinate direction left. Therefore, we focus on the scenario with the wave vector $\mathbf{k} = 1.25\hat{\mathbf{e}}_z$. Since the instability is delayed

under coordinate transformation when we initialise the second component of the magnetic field, we look at the case, where the first component of the magnetic field is initialised with $B_1(x,z) = \beta \sin\left(\frac{\pi x}{L_x}\right)\cos(k_z z)$.

As a next step, we investigate the effect of the distortion parameter ε and compare the distorted grid (13.1) on a square mapped grid with $L_p = 2\pi$ to the deformed mapped grid with $L_p = \frac{\pi}{2}$.

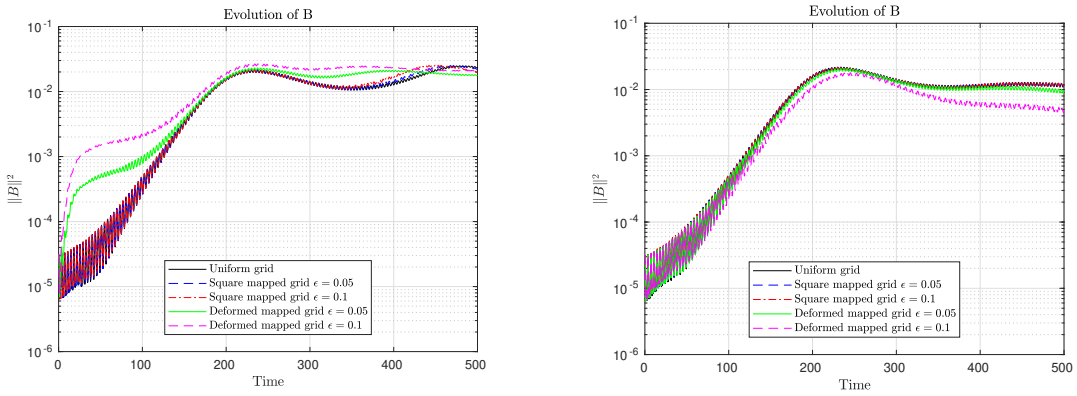

(a) Periodic particle boundary

(b) Reflecting particle boundary

Figure 22 Weibel instability with $\mathbf{k} = 1.25\hat{\mathbf{e}}_z$: Magnetic field energy for CEF with time step $\Delta t = 0.1$ on a distorted grid with different values of the distortion parameter ε for the coordinate transformation.

In Figure 22, the magnetic field energy on the distorted grid is displayed for different values of the distortion parameter ε. We present only the simulation results of the HS scheme with a time step of $\Delta t = 0.1$ because all three schemes show the same behaviour of the magnetic field. We see that for the square mapped grid, the coordinate transformation does not change the growth of the magnetic field even for a high distortion parameter of $\varepsilon = 0.1$. However, for the domain deforming coordinate transformation the higher distortion parameter $\varepsilon = 0.1$ leads to a slightly different growth of the magnetic field. Additionally, after the saturation all the curves drift apart, especially with the periodic particle boundary conditions.

13.2.3 Radial Grids

Let us extend the Weibel instability to the radial grids given by the coordinate transformations in (13.2), where we set $r_0 = 0.01$ to prevent a singularity at $\xi_1 = 0$ and choose $L_r = L - r_0$. From now on, we consider the particles to be reflected at the boundary, since this is an expected physical behaviour. Additionally, we double the resolution in the radial and angular directions to $16\times16\times8$ grid cells in order to see the impact of the time step constraints on the semi-explicit integrators.

Figure 23 shows the first component of the magnetic field energy on a cylindrical and an elliptical grid with reflecting particle boundary conditions. Due to the stability constraints, we

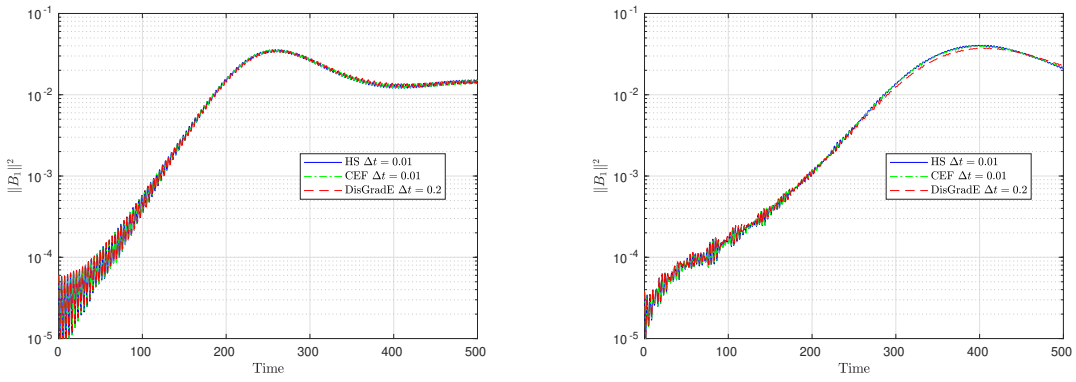

(a) Cylindrical grid

(b) Elliptical grid

Figure 23 Weibel instability with $\mathbf{k} = 1.25\hat{\mathbf{e}}_z$: First component of the magnetic field energy for various integrators with time steps $\Delta t = 0.01, 0.1$ on cylindrical and elliptical grids with $r_0 = 0.01$.

have to choose a lower time step of $\Delta t = 0.01$ for the semi-explicit schemes whereas the implicit method shows comparable results with a time step of $\Delta t = 0.2$ or higher. The stability constraints arise from the smaller cells near the pole, where the semi-explicit schemes have problems, when particles cross too many cells in one time step. Although the semi-implicit DisGradE method takes roughly about seven to ten times longer for a time step than the semi-explicit HS or CEF schemes, it seems that it is more suitable to this type of domain deforming mappings, since its simulation results show the same behaviour of the magnetic field as the semi-explicit schemes while requiring at most one-twentieth of the time steps.

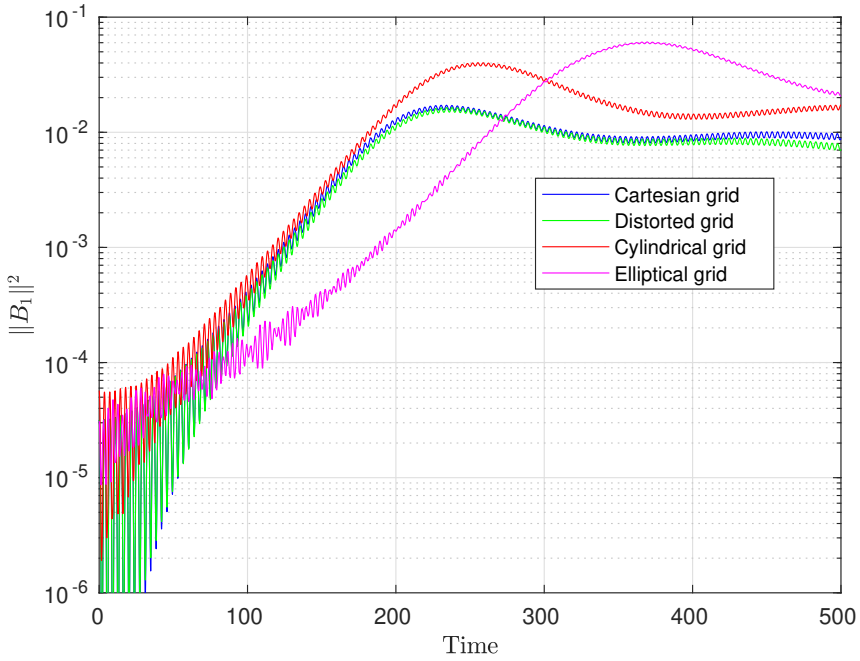

Figure 24 Weibel instability with $\mathbf{k} = 1.25\hat{\mathbf{e}}_z$: First component of the magnetic field energy for DisGradE with time step $\Delta t = 0.1$ for various domain deforming mappings.

In Figure 24, we see the first component of the magnetic field initialised with $B_1(x, z) =$

$\beta \sin\left(\frac{\pi x}{L_x}\right) \cos(k_z z)$ for various domain deforming mappings. The simulation results are obtained by the DisGradE method with a time step of $\Delta t = 0.1$. For all mappings, we see a growth in the magnetic field. However, the growth rates differ as well as the lengths of the linear phase, especially for the elliptical grid, where the saturation happens much later compared to the other cases.

13.2.4 Conservation Properties

Conclusively, let us take a look at the conservation properties of the different time integrators on the deformed mapped grids. Table 6 shows the conservation properties of the three time

Table 6 Weibel instability with perfect conductor boundary conditions: Maximum error in Gauss' law and in the total energy until time 500 for the semi-explicit and implicit time integrators on various grids.

	Method	Cartesian	Distorted	Cylindrical	Elliptical
Gauss	HS	$1.8 \cdot 10^{-11}$	$5.2 \cdot 10^{-10}$	$6.3 \cdot 10^{-10}$	$5.8 \cdot 10^{-10}$
	CEF	$1.8 \cdot 10^{-11}$	$5.2 \cdot 10^{-10}$	$6.4 \cdot 10^{-10}$	$5.6 \cdot 10^{-10}$
	DisGradE	$3.4 \cdot 10^{-4}$	$4.0 \cdot 10^{-4}$	$2.1 \cdot 10^{-3}$	$4.7 \cdot 10^{-3}$
Energy	HS	$1.8 \cdot 10^{-4}$	$1.5 \cdot 10^{-4}$	$1.5 \cdot 10^{-6}$	$2.0 \cdot 10^{-6}$
	CEF	$1.8 \cdot 10^{-4}$	$3.7 \cdot 10^{-3}$	$1.8 \cdot 10^{-6}$	$7.0 \cdot 10^{-7}$
	DisGradE	$2.0 \cdot 10^{-11}$	$9.2 \cdot 10^{-12}$	$5.0 \cdot 10^{-12}$	$1.1 \cdot 10^{-11}$

integrators until $T = 500$ with a time step of $\Delta t = 0.1$ except for the semi-explicit schemes on the radial grids, where stability constraints restrict to a time step of $\Delta t = 0.01$. The distortion parameter is chosen as $\varepsilon = 0.05$. We see the difference between the energy and the charge conserving methods. As expected, the implicit DisGradE method conserves the total energy whereas for the semi-explicit HS and CEF schemes the energy is not conserved. Though, the error is bounded for the semi-explicit schemes. In contrast, the semi-explicit HS and CEF schemes conserve Gauss' law, which is not conserved for the implicit DisGradE method. Note that all conservation properties are up to the tolerance of the solver times the condition number of the mass matrices.

Part III

Quasi-neutral Model

14 Introduction

In several interesting test cases with realistic physical applications, we are only interested in the ion motion, which happens at a time scale about two orders of magnitude greater than the one of the electrons. However, in a full kinetic model, we need to solve for the time scale of the electrons, which requires too much computing power to obtain reasonable results. In this part, we introduce the quasi-neutral model, where we get rid of the stability constraint of the electron time scale by considering a neutralising background density of adiabatic electrons.

In an electrostatic setting, the density of the adiabatic electrons is given by the Maxwell–Boltzmann distribution,

$$n_e(t, \mathbf{x}) = n_{0e}(\mathbf{x}) \mathrm{e}^{\frac{q_e \Phi(t,\mathbf{x})}{T_e(\mathbf{x})}}.$$

Since the exponent is assumed to be small, this can be approximated by

$$n_e(t, \mathbf{x}) = n_{0e}(\mathbf{x}) \left(1 + \frac{q_e \Phi(t, \mathbf{x})}{T_e(\mathbf{x})}\right).$$

Starting from a quasi-neutral setting, where $n_i = n_e$, we obtain

$$\rho = q_e(n_e - n_{0e}) = \frac{q_e^2 n_{0e}}{T_e} \Phi. \tag{14.1}$$

Furthermore, we use the continuity equation to get

$$\frac{\partial \rho}{\partial t} = \frac{q_e^2 n_{0e}}{T_e} \frac{\partial \Phi}{\partial t} = -\nabla \cdot \mathbf{J}. \tag{14.2}$$

Then, the weak form of the quasi-neutrality equations (14.1) and (14.2) tested with $\psi \in H^1(\Omega)$ is given by

$$\begin{aligned} \int_\Omega \frac{q_e^2 n_{0e}}{T_e} \psi \Phi \, \mathrm{d}\mathbf{x} &= \int_\Omega \psi \rho \, \mathrm{d}\mathbf{x}, \\ \frac{\partial}{\partial t} \int_\Omega \frac{q_e^2 n_{0e}}{T_e} \psi \Phi \, \mathrm{d}\mathbf{x} &= \int_\Omega \nabla \psi \cdot \mathbf{J} \, \mathrm{d}\mathbf{x} - \int_{\partial\Omega} \psi (\mathbf{n} \cdot \mathbf{J}) \, \mathrm{d}\sigma. \end{aligned} \tag{14.3}$$

Proposition 14.1. *Under the coordinate transformation $F(\boldsymbol{\xi}) = \mathbf{x}$ the weak formulation of the quasi-neutrality equations* (14.3) *is transformed and discretised as*

$$\tilde{\mathsf{M}}_{0e}\tilde{\boldsymbol{\phi}} = \sum_{p=1}^{N_p} q_p \omega_p \tilde{\Lambda}^0(\boldsymbol{\xi}_p)^\top, \tag{14.4}$$

$$\tilde{\mathsf{M}}_{0e}\dot{\tilde{\boldsymbol{\phi}}} = \mathsf{G}^\top \sum_{p=1}^{N_p} q_p \omega_p \tilde{\boldsymbol{\Lambda}}^1(\boldsymbol{\xi}_p)^\top N(\boldsymbol{\xi}_p)^\top \mathbf{v}_p. \tag{14.5}$$

Proof. First, we insert the coordinate transformation and use the transformation formula (2.16) to obtain

$$\begin{aligned}
\int_{\tilde{\Omega}} \frac{q_e^2 n_{0e}}{T_e} \tilde{\psi}\tilde{\Phi} |J_F(\boldsymbol{\xi})| \,\mathrm{d}\boldsymbol{\xi} &= \int_{\tilde{\Omega}} \tilde{\psi}\tilde{\rho} |J_F(\boldsymbol{\xi})| \,\mathrm{d}\boldsymbol{\xi}, \\
\frac{\partial}{\partial t} \int_{\tilde{\Omega}} \frac{q_e^2 n_{0e}}{T_e} \tilde{\psi}\tilde{\Phi} |J_F(\boldsymbol{\xi})| \,\mathrm{d}\boldsymbol{\xi} &= \int_{\tilde{\Omega}} N \nabla_{\boldsymbol{\xi}} \tilde{\psi} \cdot N\tilde{\mathbf{J}} |J_F(\boldsymbol{\xi})| \,\mathrm{d}\boldsymbol{\xi} - \int_{\partial\tilde{\Omega}} \tilde{\psi}(N\tilde{\mathbf{n}} \cdot N\tilde{\mathbf{J}}) |J_F(\boldsymbol{\xi})| \,\mathrm{d}\tilde{\sigma}.
\end{aligned}$$

Then, we discretise with the finite element method and insert the representation of the scalar potential, which can be written as $\tilde{\Phi} = \tilde{\Lambda}^0(\boldsymbol{\xi})\tilde{\boldsymbol{\phi}}$. Furthermore, we choose the basis function $\tilde{\Lambda}^0 \in \tilde{V}_0$ as test function,

$$\begin{aligned}
\int_{\Omega} \frac{q_e^2 n_{0e}}{T_e} \tilde{\Lambda}^0(\boldsymbol{\xi})^\top \tilde{\Lambda}^0(\boldsymbol{\xi}) \tilde{\boldsymbol{\phi}} |J_F(\boldsymbol{\xi})| \,\mathrm{d}\boldsymbol{\xi} &= \int_{\Omega} \tilde{\Lambda}^0(\boldsymbol{\xi})^\top \tilde{\rho}_h |J_F(\boldsymbol{\xi})| \,\mathrm{d}\boldsymbol{\xi}, \\
\frac{\partial}{\partial t} \int_{\tilde{\Omega}} \frac{q_e^2 n_{0e}}{T_e} \tilde{\Lambda}^0(\boldsymbol{\xi})^\top \tilde{\Lambda}^0(\boldsymbol{\xi}) \tilde{\boldsymbol{\phi}} |J_F(\boldsymbol{\xi})| \,\mathrm{d}\boldsymbol{\xi} &= \int_{\tilde{\Omega}} \left(N(\boldsymbol{\xi}) \nabla_{\boldsymbol{\xi}} \tilde{\Lambda}^0(\boldsymbol{\xi}) \right)^\top N(\boldsymbol{\xi}) \tilde{\mathbf{J}}_h |J_F(\boldsymbol{\xi})| \,\mathrm{d}\boldsymbol{\xi} \\
&\quad - \int_{\partial\tilde{\Omega}} \tilde{\Lambda}^0(\boldsymbol{\xi})(\mathbf{n}_1 \cdot N(\boldsymbol{\xi}) \tilde{\mathbf{J}}_h) |J_F(\boldsymbol{\xi})| \,\mathrm{d}\tilde{\sigma}
\end{aligned}$$

When we assume periodic or perfect conductor boundary conditions as in Section 9.5, the boundary term vanishes.

Next, we use the PIC representation of the transformed densities (3.2b) and (3.2a) and insert the derivative matrix for the gradient (3.4),

$$\begin{aligned}
\int_{\Omega} \frac{q_e^2 n_{0e}}{T_e} \tilde{\Lambda}^0(\boldsymbol{\xi})^\top \tilde{\Lambda}^0(\boldsymbol{\xi}) |J_F(\boldsymbol{\xi})| \,\mathrm{d}\boldsymbol{\xi} \tilde{\boldsymbol{\phi}} &= \int_{\Omega} \tilde{\Lambda}^0(\boldsymbol{\xi})^\top \sum_{p=1}^{N_p} q_p \omega_p \frac{\delta(\boldsymbol{\xi} - \boldsymbol{\xi}_p)}{|J_F(\boldsymbol{\xi})|} |J_F(\boldsymbol{\xi})| \,\mathrm{d}\boldsymbol{\xi}, \\
\int_{\tilde{\Omega}} \frac{q_e^2 n_{0e}}{T_e} \tilde{\Lambda}^0(\boldsymbol{\xi})^\top \tilde{\Lambda}^0(\boldsymbol{\xi}) |J_F(\boldsymbol{\xi})| \,\mathrm{d}\boldsymbol{\xi} \dot{\tilde{\boldsymbol{\phi}}} &= \int_{\tilde{\Omega}} \left(N(\boldsymbol{\xi}) \tilde{\boldsymbol{\Lambda}}^1(\boldsymbol{\xi}) \mathsf{G} \right)^\top \sum_{p=1}^{N_p} q_p \omega_p \frac{\delta(\boldsymbol{\xi} - \boldsymbol{\xi}_p)}{|J_F(\boldsymbol{\xi})|} \mathbf{v}_p |J_F(\boldsymbol{\xi})| \,\mathrm{d}\boldsymbol{\xi}.
\end{aligned}$$

Introducing the mass matrix $\tilde{\mathsf{M}}_{0e} := \int_{\tilde{\Omega}} \frac{q_e^2 n_{0e}}{T_e} \tilde{\Lambda}^0(\boldsymbol{\xi})^\top \tilde{\Lambda}^0(\boldsymbol{\xi}) |J_F(\boldsymbol{\xi})| \,\mathrm{d}\boldsymbol{\xi}$ yields the proposition. □

15 Time Discretisation

We consider a magnetised plasma with a background field $\mathbf{B}_0$ that is constant in time. Then, the equations of motion take the following form:

$$\begin{aligned}\dot{\boldsymbol{\Xi}} &= \mathbb{N}^\top(\boldsymbol{\Xi})\mathbf{V},\\ \dot{\mathbf{V}} &= \mathbb{W}_{\frac{q_i}{m_i}}\mathbb{N}(\boldsymbol{\Xi})\left(-\tilde{\mathbb{\Lambda}}^1(\boldsymbol{\Xi})\mathsf{G}\tilde{\boldsymbol{\phi}} + \tilde{\mathbb{B}}(\boldsymbol{\Xi},\tilde{\mathbf{b}}_0)\mathbb{N}^\top(\boldsymbol{\Xi})\mathbf{V}\right),\\ \tilde{\mathsf{M}}_{0e}\dot{\tilde{\boldsymbol{\phi}}} &= \mathsf{G}^\top\tilde{\mathbb{\Lambda}}^1(\boldsymbol{\Xi})^\top\mathbb{N}^\top(\boldsymbol{\Xi})\mathbb{W}_{q_i}\mathbf{V}.\end{aligned}$$

The Hamiltonian for this electrostatic setting is given by

$$\tilde{\mathcal{H}}_h = \frac{1}{2}\mathbf{V}^\top\mathbb{W}_{m_i}\mathbf{V} + \frac{1}{2}\tilde{\boldsymbol{\phi}}^\top\tilde{\mathsf{M}}_{0e}\tilde{\boldsymbol{\phi}}$$

and the discrete Poisson matrix corresponding to the equations of motion is obtained as

$$\mathbb{J}(\boldsymbol{\Xi},\tilde{\mathbf{b}}_0) = \begin{pmatrix} 0 & \mathbb{N}^\top(\boldsymbol{\Xi})\mathbb{W}_{m_i}^{-1} & 0\\ -\mathbb{W}_{m_i}^{-1}\mathbb{N}(\boldsymbol{\Xi}) & \mathbb{W}_{\frac{q_i}{m_i}}\mathbb{N}(\boldsymbol{\Xi})\tilde{\mathbb{B}}(\boldsymbol{\Xi},\tilde{\mathbf{b}}_0)\mathbb{N}^\top(\boldsymbol{\Xi})\mathbb{W}_{m_i}^{-1} & -\mathbb{W}_{\frac{q_i}{m_i}}\mathbb{N}(\boldsymbol{\Xi})\tilde{\mathbb{\Lambda}}^1(\boldsymbol{\Xi})\mathsf{G}\tilde{\mathsf{M}}_{0e}^{-1}\\ 0 & \tilde{\mathsf{M}}_{0e}^{-1}\mathsf{G}^\top\tilde{\mathbb{\Lambda}}^1(\boldsymbol{\Xi})^\top\mathbb{N}^\top(\boldsymbol{\Xi})\mathbb{W}_{\frac{q_i}{m_i}} & 0\end{pmatrix}.$$

15.1 Hamiltonian Splitting

In this section, we consider a Hamiltonian splitting, where we split the Hamiltonian in two parts $\tilde{\mathcal{H}}_h = \tilde{\mathcal{H}}_p + \tilde{\mathcal{H}}_\Phi$ and denote the corresponding subsystems.

The operator $\tilde{\mathcal{H}}_p$ collects the equations, where the quantities are updated by the particle velocity,

$$\begin{aligned}\dot{\boldsymbol{\Xi}} &= \mathbb{N}^\top(\boldsymbol{\Xi})\mathbf{V},\\ \dot{\mathbf{V}} &= \mathbb{W}_{\frac{q_i}{m_i}}\mathbb{N}(\boldsymbol{\Xi})\tilde{\mathbb{B}}(\boldsymbol{\Xi},\tilde{\mathbf{b}}_0)\mathbb{N}^\top(\boldsymbol{\Xi})\mathbf{V},\\ \tilde{\mathsf{M}}_{0e}\dot{\tilde{\boldsymbol{\phi}}} &= \mathsf{G}^\top\tilde{\mathbb{\Lambda}}^1(\boldsymbol{\Xi})^\top\mathbb{N}^\top(\boldsymbol{\Xi})\mathbb{W}_{q_i}\mathbf{V}.\end{aligned}$$

Then, the system for the operator $\tilde{\mathcal{H}}_\Phi$ consists of the following equation:

$$\dot{\mathbf{V}} = -\mathbb{W}_{\frac{q_i}{m_i}}\mathbb{N}(\boldsymbol{\Xi})\tilde{\mathbb{\Lambda}}^1(\boldsymbol{\Xi})\mathsf{G}\tilde{\boldsymbol{\phi}}. \tag{15.1}$$

As in Subsection 6.1.1, the equations for $\tilde{\mathcal{H}}_p$ are discretised in time with the symplectic mid-

point rule in a fixpoint iteration,

$$\begin{aligned}
\boldsymbol{\Xi}^{n+1} =& \boldsymbol{\Xi}^n + \Delta t \mathbb{N}^\top\left(\overline{\boldsymbol{\Xi}}\right)\overline{\mathbf{V}},\\
\mathbf{V}^{n+1} =& \mathbf{V}^n + \Delta t \mathbb{W}_{\frac{q_i}{m_i}} \mathbb{N}\left(\overline{\boldsymbol{\Xi}}\right)\tilde{\mathbb{B}}\left(\overline{\boldsymbol{\Xi}}, \tilde{\mathbf{b}}_0\right)\mathbb{N}^\top\left(\overline{\boldsymbol{\Xi}}\right)\overline{\mathbf{V}},\\
\tilde{\mathsf{M}}_{0e}\tilde{\boldsymbol{\phi}}^{n+1} =& \tilde{\mathsf{M}}_{0e}\tilde{\boldsymbol{\phi}}^n + \mathsf{G}^\top\int_{t^n}^{t^{n+1}} \tilde{\mathbb{\Lambda}}^1(\boldsymbol{\Xi}(\tau))^\top \mathrm{d}\tau \mathbb{W}_{q_i}\mathbb{N}^\top\left(\overline{\boldsymbol{\Xi}}\right)\overline{\mathbf{V}},
\end{aligned}$$

where $\overline{\boldsymbol{\Xi}} = \frac{\boldsymbol{\Xi}^{n+1}+\boldsymbol{\Xi}^n}{2}, \overline{\mathbf{V}} = \frac{\mathbf{V}^{n+1}+\mathbf{V}^n}{2}$ and $\boldsymbol{\Xi}(\tau) = \frac{(t^{n+1}-\tau)\boldsymbol{\Xi}^n+(\tau-t^n)\boldsymbol{\Xi}^{n+1}}{\Delta t}$. Furthermore, the equation of operator $\tilde{\mathcal{H}}_\Phi$ can be solved explicitly resulting in the charge conserving HS scheme,

$$\mathbf{V}^{n+1} = \mathbf{V}^n - \Delta t \mathbb{W}_{\frac{q_i}{m_i}}\mathbb{N}(\boldsymbol{\Xi}^n)\tilde{\mathbb{\Lambda}}^1(\boldsymbol{\Xi}^n)\mathsf{G}\tilde{\boldsymbol{\phi}}^n.$$

Remark 15.1. *The alternative CEF scheme can be constructed corresponding to Subsection 6.1.2 by computing the velocity update with the static magnetic field in a separate step as in* (6.5).

15.2 Discrete Gradient Method

Splitting the discrete Poisson matrix into three antisymmetric parts leads to the following subsystems:

$$\begin{aligned}
&\text{system 1: } \dot{\boldsymbol{\Xi}} = \mathbb{N}^\top(\boldsymbol{\Xi})\mathbf{V},\\
&\text{system 2: } \dot{\mathbf{V}} = \mathbb{W}_{\frac{q_i}{m_i}}\mathbb{N}(\boldsymbol{\Xi})\tilde{\mathbb{B}}(\boldsymbol{\Xi}, \tilde{\mathbf{b}}_0)\mathbb{N}^\top(\boldsymbol{\Xi})\mathbf{V},\\
&\text{system 3: } \dot{\mathbf{V}} = -\mathbb{W}_{\frac{q_i}{m_i}}\mathbb{N}(\boldsymbol{\Xi})\tilde{\mathbb{\Lambda}}^1(\boldsymbol{\Xi})\mathsf{G}\tilde{\boldsymbol{\phi}}, \quad \tilde{\mathsf{M}}_{0e}\dot{\tilde{\boldsymbol{\phi}}} = \left(\mathbb{N}(\boldsymbol{\Xi})\tilde{\mathbb{\Lambda}}^1(\boldsymbol{\Xi})\mathsf{G}\right)^\top \mathbb{W}_{q_i}\mathbf{V}.
\end{aligned}$$

For the DisGradE method, the first two systems can be discretised as in Section 6.2,

$$\begin{aligned}
&\text{system 1: } \boldsymbol{\Xi}^{n+1} = \boldsymbol{\Xi}^n + \Delta t\frac{\mathbb{N}^\top(\boldsymbol{\Xi}^{n+1}) + \mathbb{N}^\top(\boldsymbol{\Xi}^n)}{2}\mathbf{V}^n,\\
&\text{system 2: } \left(\mathbb{I} - \frac{\Delta t}{2}\mathbb{W}_{\frac{q}{m}}\mathbb{N}\tilde{\mathbb{B}}\mathbb{N}^\top\right)\mathbf{V}^{n+1} = \left(\mathbb{I} + \frac{\Delta t}{2}\mathbb{W}_{\frac{q}{m}}\mathbb{N}\tilde{\mathbb{B}}\mathbb{N}^\top\right)\mathbf{V}^n.
\end{aligned}$$

For system 3, we use the discrete gradient method,

$$\begin{aligned}
\frac{\mathbf{V}^{n+1}-\mathbf{V}^n}{\Delta t} &= -\mathbb{W}_{\frac{q_i}{m_i}}\mathbb{N}(\boldsymbol{\Xi}^n)\tilde{\mathbb{\Lambda}}^1(\boldsymbol{\Xi}^n)\mathsf{G}\frac{\tilde{\boldsymbol{\phi}}^{n+1}+\tilde{\boldsymbol{\phi}}^n}{2},\\
\tilde{\mathsf{M}}_{0e}\frac{\tilde{\boldsymbol{\phi}}^{n+1}-\tilde{\boldsymbol{\phi}}^n}{\Delta t} &= \left(\mathbb{N}(\boldsymbol{\Xi}^n)\tilde{\mathbb{\Lambda}}^1(\boldsymbol{\Xi}^n)\mathsf{G}\right)^\top \mathbb{W}_{q_i}\frac{\mathbf{V}^{n+1}+\mathbf{V}^n}{2}.
\end{aligned}$$

We write this in matrix form as

$$\begin{pmatrix} \mathbb{I} & \frac{\Delta t}{2}\mathbb{W}_{\frac{q_i}{m_i}}\mathbb{N}\tilde{\mathbb{\Lambda}}^1\mathsf{G}, \\ -\frac{\Delta t}{2}(\mathbb{N}\tilde{\mathbb{\Lambda}}^1\mathsf{G})^\top\mathbb{W}_{q_i} & M_{0e} \end{pmatrix} \begin{pmatrix} \mathbf{V}^{n+1} \\ \Phi^{n+1} \end{pmatrix} = \begin{pmatrix} \mathbb{I} & -\frac{\Delta t}{2}\mathbb{W}_{\frac{q_i}{m_i}}\mathbb{N}\tilde{\mathbb{\Lambda}}^1\mathsf{G}, \\ \frac{\Delta t}{2}(\mathbb{N}\tilde{\mathbb{\Lambda}}^1\mathsf{G})^\top\mathbb{W}_{q_i} & M_{0e} \end{pmatrix} \begin{pmatrix} \mathbf{V}^{n} \\ \Phi^{n} \end{pmatrix}$$

and decouple the equations with the Schur complement

$$S_+ = M_{0e} + \frac{\Delta t^2}{4}\mathbb{W}_{q_i}\mathbb{W}_{\frac{q_i}{m_i}}\mathsf{G}^\top(\tilde{\mathbb{\Lambda}}^1)^\top G_m^{-1}\tilde{\mathbb{\Lambda}}^1\mathsf{G}.$$

Then, the inverse of the matrix on the left-hand side can be computed as

$$\begin{pmatrix} \mathbb{I} & \frac{\Delta t}{2}\mathbb{W}_{\frac{q_i}{m_i}}\mathbb{N}\tilde{\mathbb{\Lambda}}^1\mathsf{G}, \\ -\frac{\Delta t}{2}(\mathbb{N}\tilde{\mathbb{\Lambda}}^1\mathsf{G})^\top\mathbb{W}_{q_i} & M_{0e} \end{pmatrix}^{-1} = \begin{pmatrix} \mathbb{I} & -\frac{\Delta t}{2}\mathbb{W}_{\frac{q_i}{m_i}}\mathbb{N}\tilde{\mathbb{\Lambda}}^1\mathsf{G} \\ 0 & \mathbb{I} \end{pmatrix} \begin{pmatrix} \mathbb{I} & 0 \\ 0 & S_+^{-1} \end{pmatrix} \begin{pmatrix} \mathbb{I} & 0 \\ \frac{\Delta t}{2}(\mathbb{N}\tilde{\mathbb{\Lambda}}^1\mathsf{G})^\top\mathbb{W}_{q_i} & \mathbb{I} \end{pmatrix}.$$

Hence, we obtain the decoupled equations,

$$\begin{aligned} \tilde{\boldsymbol{\phi}}^{n+1} &= S_+^{-1}\left(S_-\Phi^n + \Delta t\mathsf{G}^\top\tilde{\mathbb{\Lambda}}^1(\mathbf{\Xi}^n)^\top\mathbb{N}^\top(\mathbf{\Xi}^n)\mathbb{W}_{q_i}\mathbf{V}^n\right), \\ \mathbf{V}^{n+1} &= \mathbf{V}^n - \frac{\Delta t}{2}\mathbb{W}_{\frac{q_i}{m_i}}\mathbb{N}(\mathbf{\Xi}^n)\tilde{\mathbb{\Lambda}}^1(\mathbf{\Xi}^n)\mathsf{G}(\Phi^{n+1}+\Phi^n). \end{aligned}$$

When we solve system 1 and 3 together as in Section 6.3, we get the DisGradEC method with the two subsystems

$$\begin{aligned} &\text{system 1: } \dot{\mathbf{\Xi}} = \mathbb{N}(\mathbf{\Xi})^\top\mathbf{V},\ \dot{\mathbf{V}} = -\mathbb{W}_{\frac{q_i}{m_i}}\mathbb{N}(\mathbf{\Xi})\tilde{\mathbb{\Lambda}}^1(\mathbf{\Xi})\mathsf{G}\tilde{\boldsymbol{\phi}},\ \tilde{\mathsf{M}}_{0e}\dot{\tilde{\boldsymbol{\phi}}} = \left(\mathbb{N}(\mathbf{\Xi})\tilde{\mathbb{\Lambda}}^1(\mathbf{\Xi})\mathsf{G}\right)^\top\mathbb{W}_{q_i}\mathbf{V}, \\ &\text{system 2: } \dot{\mathbf{V}} = \mathbb{W}_{\frac{q_i}{m_i}}\mathbb{N}(\mathbf{\Xi})\tilde{\mathbb{B}}(\mathbf{\Xi},\tilde{\mathbf{b}}_0)\mathbb{N}(\mathbf{\Xi})^\top\mathbf{V}. \end{aligned}$$

While system 2 can be solved as above, we discretise system 1 analogously to (6.10) yielding an energy and charge conserving scheme,

$$\begin{aligned} \frac{\mathbf{\Xi}^{n+1}-\mathbf{\Xi}^n}{\Delta t} &= \frac{\mathbb{N}^\top(\mathbf{\Xi}^{n+1})+\mathbb{N}^\top(\mathbf{\Xi}^n)}{2}\frac{\mathbf{V}^{n+1}+\mathbf{V}^n}{2}, \\ \frac{\mathbf{V}^{n+1}-\mathbf{V}^n}{\Delta t} &= \mathbb{W}_{\frac{q_i}{m_i}}\frac{\mathbb{N}(\mathbf{\Xi}^{n+1})+\mathbb{N}(\mathbf{\Xi}^n)}{2}\frac{1}{\Delta t}\int_{t^n}^{t^{n+1}}\tilde{\mathbb{\Lambda}}^1(\mathbf{\Xi}(\tau))\,\mathrm{d}\tau\mathsf{G}\,\frac{\tilde{\boldsymbol{\phi}}^{n+1}+\tilde{\boldsymbol{\phi}}^n}{2}, \\ \frac{\tilde{\mathsf{M}}_{0e}\tilde{\boldsymbol{\phi}}^{n+1}-\tilde{\mathsf{M}}_{0e}\tilde{\boldsymbol{\phi}}^n}{\Delta t} &= -\frac{1}{\Delta t}\mathsf{G}^\top\int_{t^n}^{t^{n+1}}\tilde{\mathbb{\Lambda}}^1(\mathbf{\Xi}(\tau))^\top\,\mathrm{d}\tau\frac{\mathbb{N}^\top(\mathbf{\Xi}^{n+1})+\mathbb{N}^\top(\mathbf{\Xi}^n)}{2}\mathbb{W}_{q_i}\frac{\mathbf{V}^{n+1}+\mathbf{V}^n}{2}. \end{aligned}$$

15.3 Linearised δf Method

The quasi-neutral model induces major problems with particle noise. Therefore, we rely on noise reduction techniques to obtain satisfying results even though we loose the conservation properties.

In [84, 83], a linear δf method for the quasi-neutral Vlasov system is described based on the linearised electrostatic Vlasov equation for ions,

$$\frac{\mathrm{d}}{\mathrm{d}t}\delta\tilde{f}_i = \frac{\partial\delta\tilde{f}_i}{\partial t} + N^\top(\boldsymbol{\xi})\mathbf{v}\cdot\nabla_{\boldsymbol{\xi}}\delta\tilde{f}_i + \frac{q_i}{m_i}\mathbf{v}\times\mathbf{B}_0\cdot\nabla_{\mathbf{v}}\delta f_i = -\frac{q_i}{m_i}N(\boldsymbol{\xi})\delta\tilde{\mathbf{E}}\cdot\nabla_{\mathbf{v}}f_{0i},$$

with the equilibrium function

$$\tilde{f}_{0i}(\boldsymbol{\xi},\mathbf{v}) = \frac{n_{0i}}{(\sqrt{2\pi}v_{Tx})^3}\exp\left(-\frac{v_x^2+v_y^2+v_z^2}{2v_{Tx}^2}\right).$$

So, the unperturbed particle characteristics are given as

$$\begin{aligned}\dot{\boldsymbol{\xi}}_p &= N(\boldsymbol{\xi}_p)\mathbf{v}_p,\\ \dot{\mathbf{v}}_p &= \frac{q_i}{m_i}\mathbf{v}_p\times\mathbf{B}_0\end{aligned}$$

and the weights for the linear $\delta\tilde{f}$ method, $w_p(\boldsymbol{\xi}_p,\mathbf{v}_p,t) = \frac{\delta\tilde{f}_i(\boldsymbol{\xi}_p,\mathbf{v}_p,t)}{\tilde{f}_{0i}(\boldsymbol{\xi}_p,\mathbf{v}_p)}J_F(\boldsymbol{\xi}_p)$, are updated as

$$\frac{\mathrm{d}w_p}{\mathrm{d}t} = \frac{\mathrm{d}}{\mathrm{d}t}\frac{\delta\tilde{f}_i}{\tilde{f}_{0i}}J_F(\boldsymbol{\xi}_p) = -\frac{q_i}{m_i}N(\boldsymbol{\xi}_p)\delta\tilde{\mathbf{E}}(\boldsymbol{\xi}_p)\cdot\nabla_{\mathbf{v}_p}\tilde{f}_{0i}(\boldsymbol{\xi}_p,\mathbf{v}_p)\frac{J_F(\boldsymbol{\xi}_p)}{\tilde{f}_{0i}(\boldsymbol{\xi}_p,\mathbf{v}_p)}. \tag{15.2}$$

The scalar potential and with it the electric field are still advanced by the quasi-neutrality equation (14.2).

The linear $\delta\tilde{f}$ method can be simply integrated in the semi-explicit time stepping schemes given in Section 15.1 by replacing (15.1) in operator $\tilde{\mathcal{H}}_\Phi$ with equation (15.2). In this case, the weight update can be discretised explicitly in time. In the implicit schemes given in Section 15.2, the use of the linear δf method would break down the antisymmetric structure of the system leading to a different discretisation of the equations of motion. Therefore, we only use the linear δf method for the semi-explicit schemes.

16 Numerical Experiments

16.1 Ion Acoustic Wave

In [84], the setup for a periodic ion acoustic wave is given. This is an electrostatic test case with constant external magnetic field, $\mathbf{B} = B_0 \hat{\mathbf{e}}_z$, and the following initial distribution:

$$f_i(\mathbf{x}, \mathbf{v}, t = 0) = (1 + \alpha \cos(\mathbf{k} \cdot \mathbf{x})) \frac{1}{(2\pi)^{\frac{3}{2}} v_{Ti}^3} \exp\left(-\frac{1}{2}\left(\frac{v^2}{v_{Ti}^2}\right)\right), \mathbf{x} \in [0, \mathbf{L}], \mathbf{v} \in \mathbb{R}^3.$$

The scalar potential at initial time, $\Phi(\mathbf{x}, t = 0)$, is calculated from the quasi-neutrality equation (14.4). We choose the parameters as $B_0 = 1, \alpha = 0.5, T_e = 5, v_{Ti} = \sqrt{\frac{T_i}{m_i}} = \sqrt{\frac{1}{1}} = 1$, $\mathbf{k} = \left(0, 0.3, \frac{2\pi}{1000}\right)^\top, L_x = L_y = \frac{2\pi}{0.3}$ and $L_z = 1000$. For the numerical resolution, we take $1{,}024{,}000$ particles, $2 \times 8 \times 16$ grid cells, spline degrees $(1, 3, 3)$ and a time step of $\Delta t = 0.1$. The tolerance of the iterative solvers for the DisGradE method is set to 10^{-13} and the tolerance of the PCG solver for the mass matrices is set to 10^{-14}. The tolerance for the non-linear iteration in DisGradEC is set to 10^{-10}. Note that we normalised to dimensionless quantities in terms of the ion gyroradius ρ_i and the ion cyclotron frequency ω_{ci}.

Adapting the dispersion relation from (18.22) to this test case and introducing the dimensionless quantities yields

$$D(\mathbf{k}, \omega) = 1 + \frac{T_e}{T_i} \frac{\omega}{\sqrt{2} k_z v_{Ti}} \left[1 + \sum_{n=-\infty}^{\infty} Z\left(\frac{\omega - n}{\sqrt{2} k_z v_{Ti}}\right) \Lambda_n\left(\left(\frac{k_y v_{Ti} m_i}{B_0 q_i}\right)^2\right)\right].$$

For our parameters, we obtain on the one hand $\omega = 0.0168 - 0.0024i$ and on the other hand $\omega = 1.1859 + 0.0i$. The former represents an ion acoustic wave with a a damping rate of $\gamma = -0.0024$ and a wave period of $T = \frac{2\pi}{0.0168} = 373.86$ whereas the latter stands for an undamped Bernstein wave with a period of $T = \frac{2\pi}{1.1859} = 5.2982$.

In Figure 25, we see that the damping rate computed by the dispersion relation is only matched in the beginning. Afterwards, the constant Bernstein wave suppresses further damping, which is also observed in the paper of Sturdevant et al. [84].

Table 7 Ion acoustic wave: Maximum error in Gauss' law and in the total energy until time 1000 for the semi-explicit and implicit time integrators with time step $\Delta t = 0.1$.

	Gauss	Energy
HS	$7.0 \cdot 10^{-12}$	$6.3 \cdot 10^{-4}$
CEF	$7.5 \cdot 10^{-12}$	$3.8 \cdot 10^{-4}$
DisGradE	5.1	$1.9 \cdot 10^{-12}$
DisGradEC	$6.1 \cdot 10^{-12}$	$1.2 \cdot 10^{-8}$

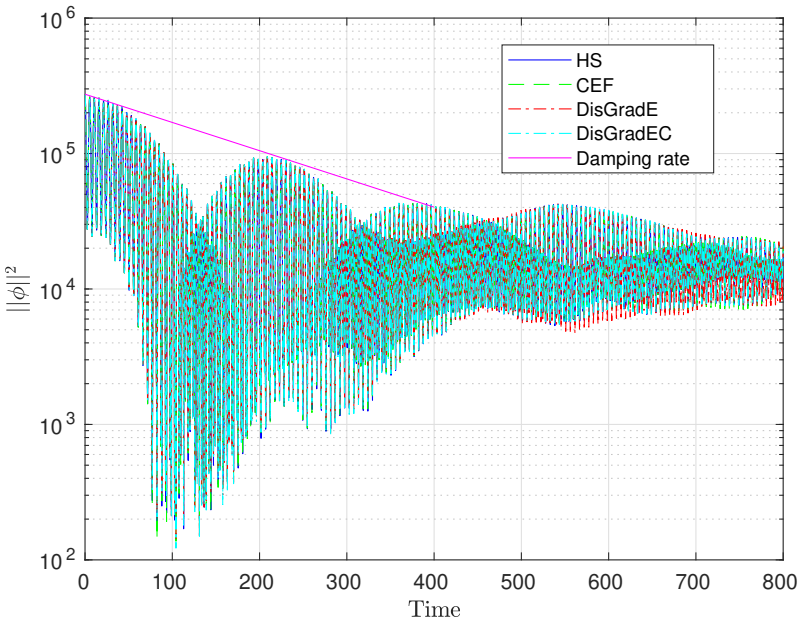

Figure 25 Ion acoustic wave: Scalar potential energy for various integrators with time step $\Delta t = 0.1$ and analytical damping rate.

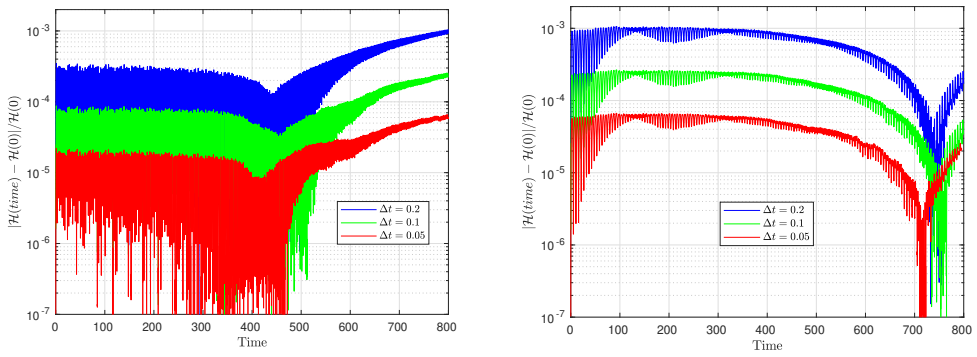

(a) HS scheme

(b) CEF scheme

Figure 26 Ion acoustic wave: Energy error for the semi-explicit time integrators with various time steps.

We have started with this periodic 2D test case embedded in 3D on the one hand to compare to the test case in [84] and on the other hand to show the compatibility of the ansatz with adiabatic electrons with the structure-preserving framework. In Table 7, we see the maximum error in Gauss' law and in the total energy for the different time integrators. As expected, the semi-explicit HS and CEF schemes as well as the fully implicit DisGradEC method conserve Gauss' law whereas the implicit DisGradE and DisGradEC methods conserve the total energy. We check the error in the total energy and Gauss' law for different time steps Δt to see if the errors are bounded by the time step size. Figure 26 shows the maximum error in the total energy for the semi-explicit schemes HS and CEF whereas Figure 27b shows the maximum error in Gauss' law for the implicit DisGradE scheme. For the DisGradEC method, the energy error depends on the tolerance of the non-linear iteration and on the time step as can be seen in Figure 27a.

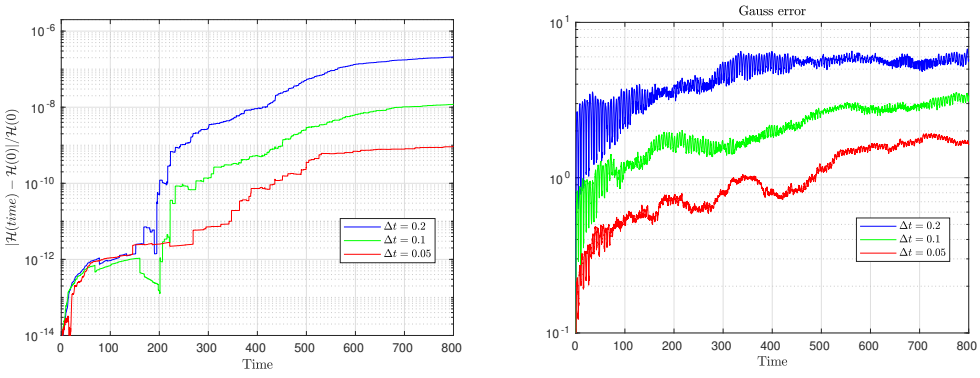

(a) Energy error for DisGradEC method

(b) Gauss' law error for DisGradE method

Figure 27 Ion acoustic wave: Energy and Gauss' law error for the implicit time integrators with various time steps.

16.2 Ion Temperature Gradient Instability

The test case for an ion temperature gradient instability (ITG) in slab geometry is taken from [83]. However, we consider a 3D setting with perfect conductor boundary conditions for the fields and reflecting particle boundary conditions. In this case, we have to use the linear δf method reviewed in Section 15.3 to reduce the particle noise. Additionally, we introduce the field-line-following coordinate $\mathbf{R} = \left(x + \frac{m_i v_y}{q_i B_0}, y - \frac{m_i v_x}{q_i B_0}, z\right)^\top$ to obtain an initial steady state solution of the electrostatic Vlasov equation, where the external magnetic field is given by $\mathbf{B} = B_0 \hat{\mathbf{e}}_z$.

Then, the initial distribution with a gyrotrope initial perturbation takes the following form:

$$f_i(\mathbf{R}, \mathbf{x}, \mathbf{v}) = \left[1 + \alpha \sin\left(\frac{\pi x}{L_x}\right)\left(\cos(\mathbf{k}\cdot\mathbf{R}) + \frac{1}{2}\cos(\mathbf{k}\cdot\mathbf{x})\exp\left(-\frac{T_i(R_x) m_i (k_x^2 + k_y^2)}{2}\right)\right)\right] f_{0i}(R_x, \mathbf{v}),$$

$$f_{0i}(R_x, \mathbf{v}) = \frac{1}{\left(\sqrt{2\pi \frac{T_i(R_x)}{m_i}}\right)^3} \exp\left(-\frac{m_i v^2}{2T_i(R_x)}\right), \mathbf{x} \in [0, \mathbf{L}], \mathbf{v} \in \mathbb{R}^3.$$

The initial scalar potential $\Phi(\mathbf{x}, t = 0)$ is computed from the quasi-neutrality equation (14.4). We choose the parameters as $\alpha = 0.1, T_e = 4, m_i = 1, \mathbf{k} = (0, 0.2, 0.002)^\top$, $L_x = L_y = \frac{2\pi}{k_y}$ and $L_z = \frac{2\pi}{k_z}$. For the numerical resolution, we take $N_p = 8{,}192{,}000$ particles, $N_x = 8{\times}8{\times}16$ grid cells, cubic splines and a time step of $\Delta t = 0.125$. The tolerance of the PCG solver for the mass matrices is set to 10^{-14}. Note that we normalised to dimensionless quantities in terms of the ion gyroradius $\rho_{i0} = \frac{\sqrt{k_B \bar{T}_i m_i}}{q_i B_0}$ and the ion cyclotron frequency $\omega_{ci0} = \frac{q_i B_0}{m_i}$.

Since Sturdevant et al. refer to [76] for the test case, we assume the ion temperature profile and its gradient to be given as

$$T_i(R_x) = \bar{T}_i \left[1 - \kappa_{T_i} \omega_{T_i} L_x \tanh\left(\frac{R_x}{\omega_{T_i} L_x}\right)\right], \tag{16.1a}$$

$$T_i'(R_x) = -\frac{\bar{T}_i \kappa_{T_i}}{\cosh^2\left(\frac{R_x}{\omega_{T_i} L_x}\right)}, \tag{16.1b}$$

where $\bar{T}_i = 1$ and $\omega_{T_i}, \kappa_{T_i}$ are varied. Note that we have to choose ω_{T_i} in such a way that the temperature profile stays positive. Figure 28 shows the temperature profile and gradient for various values of κ_{T_i} and ω_{Ti}.

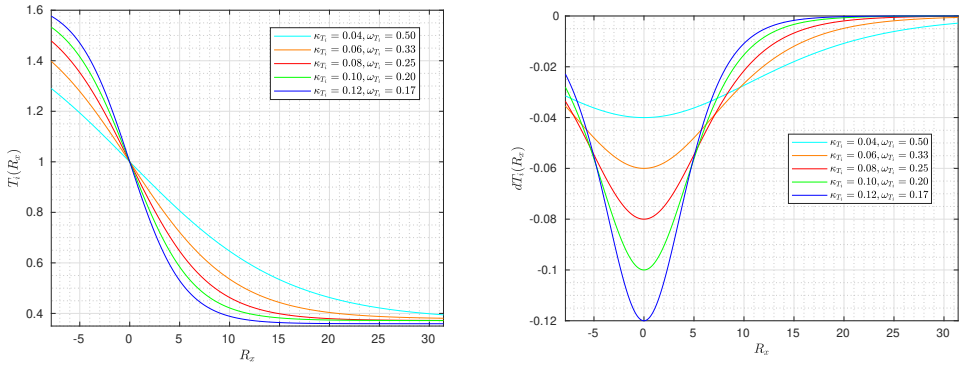

(a) Temperature profile

(b) Temperature gradient

Figure 28 Temperature profile and gradient for various values of κ_{T_i} and ω_{Ti}.

The velocity gradient of the initial distribution function f_{0i}, which is used in the linear δf method, can be computed as

$$\nabla_{\mathbf{v}} f_{0i} = \left(-\frac{m_i \mathbf{v}}{T_i(R_x)} + \hat{\mathbf{e}}_y \frac{m_i}{q_i B_0} \left(\frac{m_i v^2}{2T_i(R_x)} - \frac{3}{2} \right) \frac{T_i'(R_x)}{T_i(R_x)} \right) f_{0i}.$$

Following [83], we start by approximating the temperature and its gradient with the constant values at $R_x = 0$, $T_i(R_x = 0) = \bar{T}_i = 1$ and $T_i'(R_x = 0) = -\kappa_{T_i} \bar{T}_i$ so that the velocity gradient simplifies to

$$\nabla_{\mathbf{v}} f_{0i} = \left(-\frac{m_i \mathbf{v}}{\bar{T}_i} - \hat{\mathbf{e}}_y \frac{m_i}{q_i B_0} \left(\frac{m_i v^2}{2\bar{T}_i} - \frac{3}{2} \right) \kappa_{T_i} \right) f_{0i}.$$

Furthermore, these are the same approximations used in Chapter 18 to derive the dispersion relation (18.22). Then, we compute the growth rates for various choices of κ_{T_i} from this dispersion relation,

$$\begin{aligned} D =& 1 + \frac{T_e}{\bar{T}_i} \left[1 + \zeta_0 \sum_{n=-\infty}^{\infty} (Z(\zeta_n)\Lambda_n(\xi) - \right. \\ & \left. \frac{k_y \kappa_{T_i}}{2B_0 \omega} [Z(\zeta_n)\Lambda_n(\xi) - 2\zeta_n(1 + \zeta_n Z(\zeta_n))\Lambda_n(\xi) - 2\xi Z(\zeta_n)\Lambda_n'(\xi)] \right) \Bigg], \end{aligned}$$

where $\xi = \frac{m_i k_y^2 \bar{T}_i}{q_i^2 B_0^2}, \zeta_n = \frac{\omega - n}{\sqrt{2} k_z \sqrt{\frac{\bar{T}_i}{m_i}}}$.

In Table 8, we see the analytical growth rates computed from the dispersion relation above together with the ones obtained from the simulations by fitting growth rates to the curves during the linear phase. Figure 29 shows the simulation results of the ITG in slab geometry for the different values of κ_{T_i} together with the analytical growth rates. All runs are computed

Table 8 Ion temperature gradient instability in slab geometry: Analytical and simulated growth rates for the approximated and varying temperature profiles and gradients for different values of κ_{T_i}.

κ_{T_i}	Analytical growth rate	Simulated growth rate	
	constant profile	constant profile	varying profile
0.12	$4.3 \cdot 10^{-3}$	$4.4 \cdot 10^{-3}$	$3.9 \cdot 10^{-3}$
0.10	$3.9 \cdot 10^{-3}$	$3.9 \cdot 10^{-3}$	$3.7 \cdot 10^{-3}$
0.08	$3.4 \cdot 10^{-3}$	$3.4 \cdot 10^{-3}$	$3.2 \cdot 10^{-3}$
0.06	$2.8 \cdot 10^{-3}$	$2.7 \cdot 10^{-3}$	$2.2 \cdot 10^{-3}$
0.04	$2.0 \cdot 10^{-3}$	$1.9 \cdot 10^{-3}$	$1.3 \cdot 10^{-3}$

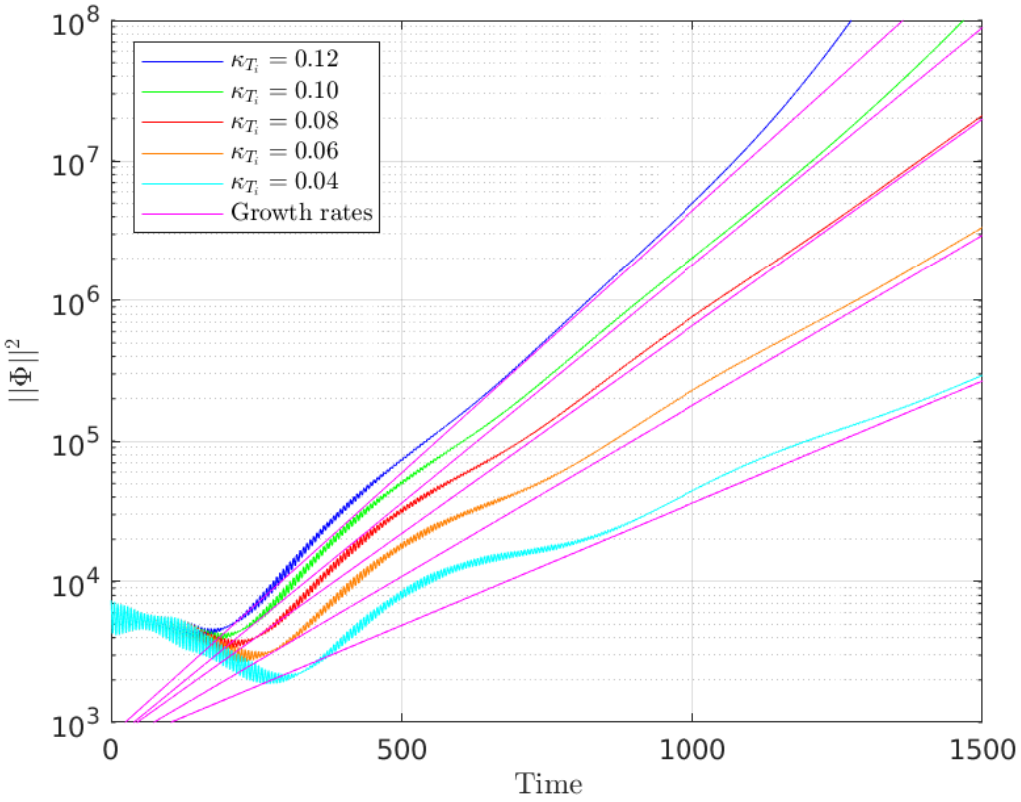

Figure 29 Ion temperature gradient instability in slab geometry: Scalar potential energy for CEF with time step $\Delta t = 0.125$ for various values of κ_{T_i} with approximated temperature profiles and gradients and analytical growth rates.

with the linear δf method for the approximated temperature profiles and gradients. We show only the simulation results of the alternative Hamiltonian splitting scheme CEF, since the HS scheme yields comparable results. The computed growth rates are matched in the linear phase. However, for values of $\kappa_{T_i} \geq 0.1$, we see the beginning of a steeper growth after $T = 1200$. This can be explained by the interaction with higher modes.

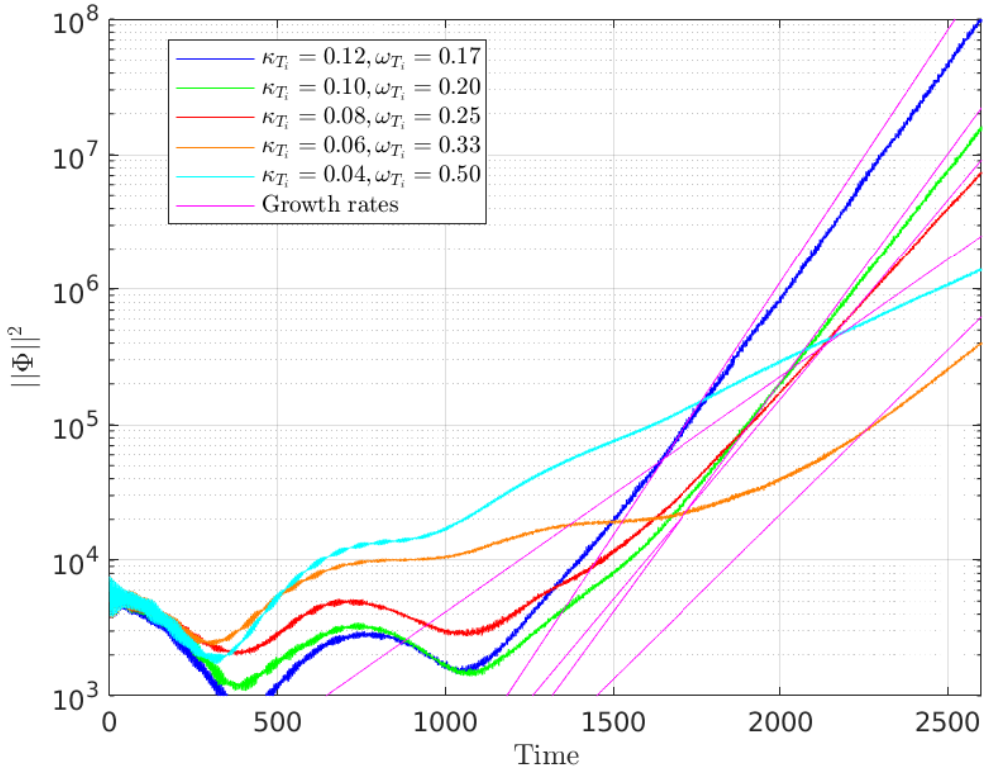

Figure 30 Ion temperature gradient instability in slab geometry: Scalar potential energy for CEF with time step $\Delta t = 0.125$ for various values of κ_{T_i} and ω_{Ti} with varying temperature profiles and gradients and analytical growth rates.

While the simulations with approximated temperature profiles and gradients yield good results compared to the dispersion relation that used the same approximations, we are also interested in the results with varying temperature profiles. Figure 30 shows the simulation of the ITG in slab geometry with the temperature profiles and gradients given in (16.1a) and (16.1b). All simulations are performed with the linear δf method for the CEF method. We see that the instability starts later and the growth rate is lower when we use the varying profiles.

As a next step, we want to simulate the ITG on a cylindrical grid. The test case is taken from [60], where the MEDIUM test case from [20] is simulated, and adapted to our framework. We still consider an constant external magnetic field in $z-$direction, $\mathbf{B} = B_0 \hat{\mathbf{e}}_z$, and the initial distribution is given by

$$f(r, \theta, z, \mathbf{v}, t = 0) = \left[1 + \alpha \sin\left(\frac{\pi(r - r_0)}{r_1 - r_0}\right) \cos\left(m\theta + \frac{n}{R_0} z\right)\right] f_{0i}(R_x, \mathbf{v}),$$
$$(r, \theta, z) \in [r_0, r_1] \times [0, 2\pi] \times [0, 2\pi R_0], \mathbf{v} \in \mathbb{R}^3$$

with the equilibrium Maxwellian

$$f_{0i}(R_x, \mathbf{v}) = \frac{n_{0i}(R_x)}{\left(\sqrt{2\pi \frac{T_i(R_x)}{m_i}}\right)^3} \exp\left(-\frac{m_i v^2}{2T_i(R_x)}\right).$$

The parameters are chosen as $\alpha = 0.1, T_e = T_i, m_i = 1, (m,n) = (15,1), r_0 = 0.1, r_1 = 14.5, R_0 = 239.8081535$ and $B_0 = 1$. For the numerical resolution, we take $N_p = 8{,}192{,}000$ particles, $N_x = 8\times16\times16$ grid cells, cubic splines and a time step of $\Delta t = 0.1$. The tolerance of the PCG solver for the mass matrices is set to 10^{-14} and the normalisation to dimensionless quantities is still in terms of the ion gyroradius ρ_{i0} and the ion cyclotron frequency ω_{ci0}.

The profiles for the temperature and the density are given as

$$T_s(r) = \bar{T}_s \exp\left(-\kappa_{T_s}\omega_{T_s}\tanh\left(\frac{r-\bar{r}}{\omega_{T_s}}\right)\right), s \in \{i,e\},$$
$$n_0(r) = \bar{n}_0 \exp\left(-\kappa_{n_0}\omega_{n_0}\tanh\left(\frac{r-\bar{r}}{\omega_{n_0}}\right)\right),$$

where $\bar{r} = \frac{r_0+r_1}{2}$ and the parameters are chosen as $\bar{T}_i = 1.0, \kappa_{T_i} = 0.27586, \omega_{T_i} = 1.45, \bar{n}_0 = \frac{r_1-r_0}{\int_{r_0}^{r_1}\exp\left(-\kappa_{n_0}\omega_{n_0}\tanh\left(\frac{r-\bar{r}}{\omega_{n_0}}\right)\right)dr} \approx 0.99, \kappa_{n_0} = 0.055, \omega_{n_0} = 2.9.$

The velocity gradient of the initial distribution function f_{0i} can be computed as

$$\nabla_{\mathbf{v}} f_{0i} = \left(-\frac{m_i\mathbf{v}}{T_i(R_x)} + \hat{\mathbf{e}}_y\frac{m_i}{q_iB_0}\left[\frac{n_{0i}'(R_x)}{n_{0i}(R_x)} + \left(\frac{m_iv^2}{2T_i(R_x)} - \frac{3}{2}\right)\frac{T_i'(R_x)}{T_i(R_x)}\right]\right) f_{0i}.$$

Analogously to the test case in slab geometry, we approximate the profiles and their gradients with constant values at $r = \bar{r}$, $T_i(r=\bar{r}) = \bar{T}_i = 1$, $n_0(r=\bar{r}) = \bar{n}_0 \approx 0.99$, $T_i'(r=\bar{r}) = -\kappa_{T_i}\bar{T}_i = 0.27586$, $n_0'(r=\bar{r}) = -\kappa_{n_0}\bar{n}_0 \approx 0.054$. These approximations are necessary to use the linear δf method, since we lack a representation of the field-line-following coordinate R_x in the cylindrical geometry. Figures 31 and 32 show the density and temperature profiles together with these approximations.

Then, the velocity gradient of the initial distribution function simplifies to

$$\nabla_{\mathbf{v}} f_{0i} = \left(-\frac{m_i\mathbf{v}}{\bar{T}_i} - \hat{\mathbf{e}}_y\frac{m_i}{q_iB_0}\left[\kappa_{n_0} + \left(\frac{m_iv^2}{2\bar{T}_i} - \frac{3}{2}\right)\kappa_{T_i}\right]\right) f_{0i}.$$

In Figure 33, we see the simulation results of the semi-explicit time integrators with time step $\Delta t = 0.1$. Both simulations are performed with the linear δf method. Fitting a linear growth rate to the curves yields a growth rate of $\gamma \approx 0.02$ whereas in [60] a growth rate of $\gamma \approx 3.8\cdot10^{-3}$ is computed. This shows that the constant approximations of the density and temperature profiles and their gradients lead to a higher growth rate.

Since the linear δf simulations of the ITG instability lack conservation properties, the next goal would be going to full f simulations that yield the conservation properties of our structure-

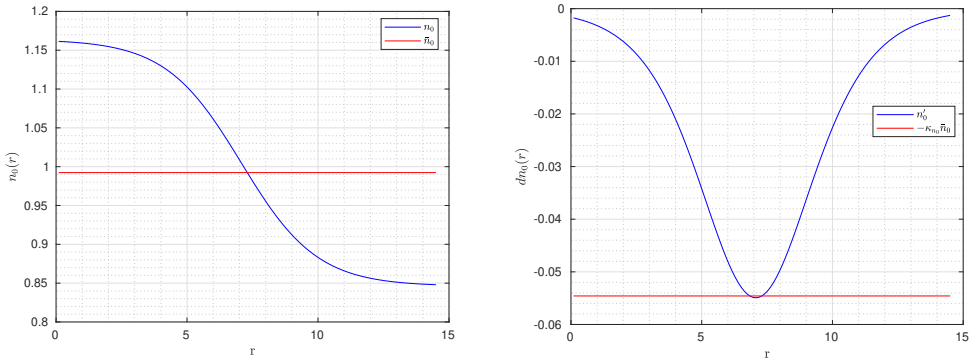

(a) Density profile

(b) Density gradient

Figure 31 Density profile and gradient for the ITG simulation in cylindrical geometry.

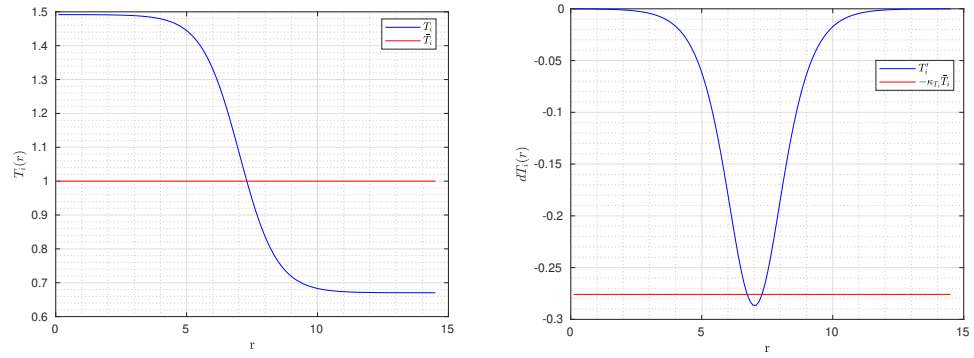

(a) Temperature profile

(b) Temperature gradient

Figure 32 Temperature profile and gradient for the ITG simulation in cylindrical geometry.

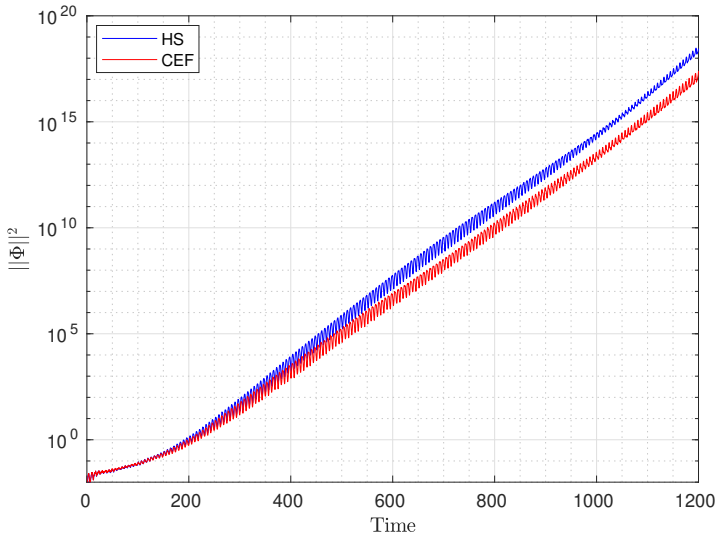

Figure 33 Ion temperature gradient instability in cylindrical geometry: Scalar potential energy for the semi-explicit time integrators with time step $\Delta t = 0.1$ with approximated density and temperature profiles and gradients.

preserving framework. Therefore, we have to deal with the following challenges:

- First, we need to investigate different temperature profiles for the ITG in slab geometry. For example, variation of the parameter ω_{T_i} leads to different growth rates.
- Second, we want to verify the growth rates that follow from the varying temperature profiles. However, the alterations for the dispersion relation to deal with a varying temperature profile are not trivial. One solution could be to compare to reference simulations made with gyrokinetic codes, where dispersion relations already exist for simplified models.
- Last, the problems with the particle noise imply that we need a huge amount of particles to get the necessary resolution for the instability to happen. We have to try out different amounts of particles unless we find a way to verify the conservation properties with δf methods.

For the ITG in cylindrical geometry, the additional problem arises that we need to find a field-line-following coordinate R_x so that $f_0(R_x, \mathbf{v})$ is an steady state solution of the Vlasov equation. A solution for the δf method is described in [44, Sec.5], where an extra source term is used to account for the case when f_0 is not an kinetic equilibrium. Moreover, we lack a dispersion relation for cylindrical coordinates so that we rely on reference solutions and the computed growth rates of gyrokinetic models.

Part IV

Physical Units and Dispersion Relation

17 Normalisation

17.1 Vlasov–Maxwell Equations in SI Units

In SI units the Vlasov equation for particle species s is given as

$$\partial_t f_s + \mathbf{v} \cdot \nabla_{\mathbf{x}} f_s + \frac{q_s}{m_s} (\mathbf{E} + \mathbf{v} \times \mathbf{B}) \cdot \nabla_{\mathbf{v}} f_s = 0 \tag{17.1}$$

and Maxwell's equations as

$$\nabla \times \mathbf{E} = -\frac{\partial \mathbf{B}}{\partial t}, \tag{17.2a}$$

$$\nabla \times \mathbf{B} = \mu_0 \left(\mathbf{J} + \varepsilon_0 \frac{\partial \mathbf{E}}{\partial t} \right), \tag{17.2b}$$

$$\nabla \cdot \mathbf{E} = \frac{\rho}{\varepsilon_0}, \tag{17.2c}$$

$$\nabla \cdot \mathbf{B} = 0. \tag{17.2d}$$

The equations are coupled by the source terms, namely the charge

$$\rho = \sum_s q \int f_s \, \mathrm{d}\mathbf{v}$$

and the current

$$\mathbf{J} = \sum_s q \int \mathbf{v} f_s \, \mathrm{d}\mathbf{v}.$$

The total energy of the system is given by the Hamiltonian in SI units,

$$\mathcal{H} = \sum_s \frac{m_s}{2} \int |\mathbf{v}|^2 f_s \, \mathrm{d}\mathbf{x} \, \mathrm{d}\mathbf{v} + \frac{\varepsilon_0}{2} \int \|\mathbf{E}\|^2 \, \mathrm{d}\mathbf{x} + \frac{1}{2\mu_0} \int \|\mathbf{B}\|^2 \, \mathrm{d}\mathbf{x}. \tag{17.3}$$

17.2 Physical Parameters of a Plasma

In the following, we use a number of physical constants:

- Vacuum permeability $\mu_0 = 1.2566370621219 * 10^{-6} \frac{N}{A^2}$,
- Vacuum permittivity $\varepsilon_0 = 8.854187812813 * 10^{-12} \frac{As}{Vm}$,
- Boltzmann constant $\kappa_B = 1.380649 * 10^{-23} \frac{J}{K}$,
- Elementary charge $q = 1.602176634 * 10^{-19} C$,
- Electron mass $m_e = 9.109383701528 * 10^{-31} kg$,
- Proton mass $m_p = 1.6726219236951 * 10^{-27} kg$,

- Neutron mass $m_n = 1.6749274980495 * 10^{-27} kg$.

A plasma, which consist of ionised particles, is characterised by the temperature T, density n and mass m of the negative charged electrons and the positive charged ion kernels. Mostly, we consider electrons and ions with the same temperature and density, $T_i = T_e = T_K, n_e = n_i = n$. Although the SI unit for the temperature T_k is Kelvin, we usually give the energy T_E instead, which is calculated from the temperature via the formula $T_E = T_k k_B$. Furthermore, the energy is often given in electron volt, which has the value of the elementary charge, $1ev = 1.602176634 * 10^{-19} J$.

Since the plasma in the fusion reactor consists of Deuterium and Tritium, we assume that the ion mass is given by the sum of the mass of one proton and one neutron, which build the kernel of Deuterium. It is quite common not to use the real mass ratio from electrons and ions, which is denoted as $M = m_i/m_e = 3670.5$, but to set an artificial value, for example $M = 200$. We will see the practicality of this setting later on.

Additionally, we need the initial magnetic field B to compute the following simulation parameters:

- Thermal velocity $\left[\frac{m}{s}\right] : v_{Ts} = \sqrt{\frac{k_B T_s}{m_s}}$,
- Plasma frequency $\left[s^{-1}\right] : \omega_{ps} = \sqrt{\frac{n_s q_s^2}{\varepsilon_0 m_s}}$,
- Debye length $[m] : \lambda_{Ds} = \frac{v_{Te}}{\omega_{ps}} = \sqrt{\frac{\varepsilon_0 k_B T_s}{n_s q_s^2}}$,
- Cyclotron frequency $\left[s^{-1}\right] : \omega_{cs} = \frac{|q_s|B}{m_s}$,
- Gyroradius $[m] : \rho_s = \frac{v_{Ts}}{\omega_{cs}} = \frac{\sqrt{k_B T_s m_s}}{|q_s|B}$,
- Plasma beta $\left[\frac{NJ}{A^2 m^3 T^2}\right] : \beta_s = \frac{\mu_0 n_s T_s k_B}{B^2}$.

In Table 9, we state the parameters from above for the specific settings of different fusion devices.

17.3 Dimensionless Parameters

For numerical simulations, the equations are normalised such that the resulting dimensionless quantities are of order one. For the normalisation, the following quantities are fixed: n_{ref}, T_{ref}, m_{ref}, q_{ref} and ω_{ref} or L_{ref}. First, the species, ions or electrons, is chosen and then, the frequency or length such as the cyclotron frequency and the gyroradius or the plasma frequency and the Debye length.

From these initial values, we define the following quantities:

- The reference velocity $v_{\mathrm{ref}} = \sqrt{\frac{T_{\mathrm{ref}} k_B}{m_{\mathrm{ref}}}}$,

Table 9 Parameters for different fusion devices.

Devices		Wendelstein 7x	Asdex Upgrade	ITER
Major radius	$R_0[m]$	5.5	1.6	6.2
Minor radius	$a[m]$	0.53	0.8	2.0
Magnetic field	$B[T]$	2.5	3.9	5.3
Average particle density	$n[m^{-3}]$	$1.89 \cdot 10^{20}$	$2.0 \cdot 10^{20}$	$1.0 \cdot 10^{20}$
Average thermal energy	$T[keV]$	5.0	8.7	$8.8, 8.0$
Thermal velocity	$v_{Te}[ms^{-1}]$	$3 \cdot 10^7$	$3.9 \cdot 10^7$	$3.9 \cdot 10^7$
	$v_{Ti}[ms^{-1}]$	$4.9 \cdot 10^5$	$6.5 \cdot 10^5$	$6.2 \cdot 10^5$
Larmor radius	$\rho_e[m]$	$6.7 \cdot 10^{-5}$	$5.7 \cdot 10^{-5}$	$4.0 \cdot 10^{-5}$
	$\rho_i[m]$	$4.1 \cdot 10^{-3}$	$3.5 \cdot 10^{-3}$	$2.4 \cdot 10^{-3}$
Cyclotron frequency	$\omega_{ce}[s^{-1}]$	$4.4 \cdot 10^{11}$	$6.9 \cdot 10^{11}$	$9.3 \cdot 10^{11}$
	$\omega_{ci}[s^{-1}]$	$1.2 \cdot 10^8$	$1.9 \cdot 10^8$	$2.5 \cdot 10^8$
Debye length	$\lambda_{De}[m]$	$3.8 \cdot 10^{-5}$	$4.9 \cdot 10^{-5}$	$7.0 \cdot 10^{-5}$
	$\lambda_{Di}[m]$	$3.8 \cdot 10^{-5}$	$4.9 \cdot 10^{-5}$	$6.6 \cdot 10^{-5}$
Plasma frequency	$\omega_{pe}[s^{-1}]$	$7.8 \cdot 10^{11}$	$8.0 \cdot 10^{11}$	$5.6 \cdot 10^{11}$
	$\omega_{pi}[s^{-1}]$	$1.3 \cdot 10^{10}$	$1.3 \cdot 10^{10}$	$9.3 \cdot 10^9$

- The reference length or frequency $L_{\text{ref}} = \frac{v_{\text{ref}}}{\omega_{\text{ref}}}, \omega_{\text{ref}} = \frac{v_{\text{ref}}}{L_{\text{ref}}}$,
- The reference epsilon $\varepsilon_{\text{ref}} = \frac{q_{\text{ref}}^2 n_{\text{ref}}}{\omega_{\text{ref}}^2 m_{\text{ref}}}$,
- The reference beta $\beta_{\text{ref}} = \mu_0 \varepsilon_0 v_{\text{ref}}^2$.

There are two obvious choices for the reference frequency, either the plasma frequency or the gyrofrequency. For the choice $\omega_{\text{ref}} = \omega_{ps}$, we get $\varepsilon_{\text{ref}} = \frac{q_s^2 n_s}{\omega_{ps}^2 m_s} = \varepsilon_0$ and it follows that $\beta_{\text{ref}} = \frac{\mu_0 v_{Ts}^2 q_s n_s}{\omega_{ps}^2 m_s}, s = e, i$. On the other hand, if we choose $\omega_{\text{ref}} = \omega_{cs}$, we get $\beta_{\text{ref}} = \frac{\mu_0 k_B T_s n_s}{B^2} = \beta_s, s = e, i$, which is the definition of the plasma beta.

Based on the reference values, we define the following rescaled quantities:

- $\hat{T}_s = \frac{k_B T_s}{T_{\text{ref}}}$, $\hat{q}_s = \frac{q_s}{q_{\text{ref}}}$, $\hat{m}_s = \frac{m_s}{m_{\text{ref}}}$, $\hat{n}_s = \frac{n_s}{n_{\text{ref}}}$, $s = i, e$,
- $\hat{t} = t\omega_{\text{ref}}$, $\hat{L} = \frac{L}{L_{\text{ref}}}$, $\hat{\mathbf{x}} = \frac{\mathbf{x}}{L_{\text{ref}}}$, $\hat{k} = kL_{\text{ref}}$, $\hat{\mathbf{v}} = \frac{\mathbf{v}}{v_{\text{ref}}}$,
- $\hat{f} = \frac{v_{\text{ref}}^3}{n_{\text{ref}}} f$, $\hat{\rho} = \frac{\rho}{q_{\text{ref}} n_{\text{ref}}}$, $\hat{\mathbf{J}} = \frac{\mathbf{J}}{n_{\text{ref}} v_{\text{ref}} q_{\text{ref}}}$,

- $\hat{\phi} = \frac{q_{\text{ref}}}{T_{\text{ref}}}\phi$, $\hat{\mathbf{E}} = \frac{L_{\text{ref}}}{v_{\text{ref}}^2}\frac{q_{\text{ref}}}{m_{\text{ref}}}\mathbf{E}$, $\hat{\mathbf{B}} = \frac{L_{\text{ref}}}{v_{\text{ref}}}\frac{q_{\text{ref}}}{m_{\text{ref}}}\mathbf{B}$,
- $\hat{\mathcal{H}} = \frac{\omega_{\text{ref}}^3}{m_{\text{ref}} v_{\text{ref}}^5 n_{\text{ref}}}\mathcal{H}$.

17.3.1 Vlasov-Maxwell System

Proposition 17.1. *The dimensionless Vlasov–Maxwell system takes the following form:*

$$\partial_{\hat{t}}\hat{f}_s + \hat{\mathbf{v}}\cdot\nabla_{\hat{\mathbf{x}}}\hat{f}_s + \frac{\hat{q}}{\hat{m}}\left(\hat{\mathbf{E}} + \hat{\mathbf{v}}\times\hat{\mathbf{B}}\right)\cdot\nabla_{\hat{\mathbf{v}}}\hat{f}_s = 0,$$

$$\begin{aligned}
\frac{\partial\hat{\mathbf{B}}}{\partial\hat{t}} &= -\nabla_{\hat{\mathbf{x}}}\times\hat{\mathbf{E}}, & \nabla_{\hat{\mathbf{x}}}\cdot\hat{\mathbf{E}} &= \frac{\varepsilon_{\text{ref}}}{\varepsilon_0}\hat{\rho},\\
\frac{\partial\hat{\mathbf{E}}}{\partial\hat{t}} &= \frac{1}{\beta_{\text{ref}}}\nabla_{\hat{\mathbf{x}}}\times\hat{\mathbf{B}} - \frac{\varepsilon_{\text{ref}}}{\varepsilon_0}\hat{\mathbf{J}}, & \nabla_{\hat{\mathbf{x}}}\cdot\hat{\mathbf{B}} &= 0
\end{aligned}$$

with the source terms

$$\hat{\rho} = \sum_s \hat{q}_s\int\hat{f}_s\,\mathrm{d}\hat{\mathbf{v}}, \quad \hat{\mathbf{J}} = \sum_s\hat{q}_s\int\hat{\mathbf{v}}\hat{f}_s\,\mathrm{d}\hat{\mathbf{v}}.$$

Proof. First, we rescale the Vlasov equation in SI units (17.1) with the dimensionless quantities. Note that we can approximate the partial derivatives as

$$\frac{\partial g}{\partial t} = \frac{g^{n+1}-g^n}{\Delta t}, \quad \nabla_{\mathbf{x}} g = \frac{g^{n+1}-g^n}{\Delta\mathbf{x}}, \quad \nabla_{\mathbf{v}} g = \frac{g^{n+1}-g^n}{\Delta\mathbf{v}},$$

which leads to the scaling $\partial_t = \partial_{\hat{t}}\omega_{\text{ref}}, \nabla_{\mathbf{x}} = \nabla_{\hat{\mathbf{x}}}L_{\text{ref}}^{-1}, \nabla_{\mathbf{v}} = \nabla_{\hat{\mathbf{v}}}v_{\text{ref}}^{-1}$. Then, the Vlasov equation can be written as

$$\frac{n_{\text{ref}}\omega_{\text{ref}}}{v_{\text{ref}}^3}\partial_{\hat{t}}\hat{f}_s + \frac{n_{\text{ref}}v_{\text{ref}}}{v_{\text{ref}}^3 L_{\text{ref}}}\hat{\mathbf{v}}\cdot\nabla_{\hat{\mathbf{x}}}\hat{f}_s + \frac{n_{\text{ref}}}{v_{\text{ref}}^3 v_{\text{ref}}}\frac{q_{\text{ref}}}{m_{\text{ref}}}\frac{\hat{q}_s}{\hat{m}_s}\left(\frac{v_{\text{ref}}^2}{L_{\text{ref}}}\frac{m_{\text{ref}}}{q_{\text{ref}}}\hat{\mathbf{E}} + v_{\text{ref}}\frac{v_{\text{ref}}}{L_{\text{ref}}}\frac{m_{\text{ref}}}{q_{\text{ref}}}\hat{\mathbf{v}}\times\hat{\mathbf{B}}\right)\cdot\nabla_{\hat{\mathbf{v}}}\hat{f}_s = 0.$$

Next, we multiply the equation with $\frac{v_{\text{ref}}^3}{n_{\text{ref}}\omega_{\text{ref}}}$ and use the definition $\omega_{\text{ref}} = \frac{v_{\text{ref}}}{L_{\text{ref}}}$ to get the dimensionless Vlasov equation

$$\partial_{\hat{t}}\hat{f}_s + \hat{\mathbf{v}}\cdot\nabla_{\hat{\mathbf{x}}}\hat{f}_s + \frac{\hat{q}_s}{\hat{m}_s}\left(\hat{\mathbf{E}} + \hat{\mathbf{v}}\times\hat{\mathbf{B}}\right)\cdot\nabla_{\hat{\mathbf{v}}}\hat{f}_s = 0.$$

Additionally, we review the definition of the source terms,

$$\rho = \sum_s q_{\text{ref}}\hat{q}_s\int\frac{n_{\text{ref}}}{v_{\text{ref}}^3}\hat{f}_s v_{\text{ref}}^3\,\mathrm{d}\hat{\mathbf{v}}, \quad \mathbf{J} = \sum_s q_{\text{ref}}\hat{q}_s\int v_{\text{ref}}\frac{n_{\text{ref}}}{v_{\text{ref}}^3}\hat{\mathbf{v}}\hat{f}_s\,\mathrm{d}\hat{\mathbf{v}}.$$

We see that the definition of the dimensionless source terms as $\hat{\rho} = \frac{1}{q_{\mathrm{ref}} n_{\mathrm{ref}}} \rho$, $\hat{\mathbf{J}} = \frac{1}{q_{\mathrm{ref}} n_{\mathrm{ref}} v_{\mathrm{ref}}} \mathbf{J}$ is the obvious choice.

Second, we consider the electric Gauss law (17.2b) with dimensionless variables,

$$\frac{v_{\mathrm{ref}}^2 m_{\mathrm{ref}}}{L_{\mathrm{ref}}^2 q_{\mathrm{ref}}} \nabla_{\hat{\mathbf{x}}} \cdot \hat{\mathbf{E}} = \frac{q_{\mathrm{ref}} n_{\mathrm{ref}}}{\varepsilon_0} \hat{\rho}.$$

In this case, we use $\varepsilon_{\mathrm{ref}} = \frac{q_{\mathrm{ref}}^2 n_{\mathrm{ref}}}{\omega_{\mathrm{ref}}^2 m_{\mathrm{ref}}}$ and are left with the factor $\frac{\varepsilon_{\mathrm{ref}}}{\varepsilon_0}$,

$$\nabla_{\hat{\mathbf{x}}} \cdot \hat{\mathbf{E}} = \frac{q_{\mathrm{ref}}^2 n_{\mathrm{ref}}}{\omega_{\mathrm{ref}}^2 m_{\mathrm{ref}} \varepsilon_0} \hat{\rho} = \frac{\varepsilon_{\mathrm{ref}}}{\varepsilon_0} \hat{\rho}.$$

Since the right-hand side of the magnetic Gauss law (17.2d) equals zero, this equation scales perfectly,

$$\begin{aligned} L_{\mathrm{ref}}^{-1} \frac{v_{\mathrm{ref}}}{L_{\mathrm{ref}}} \frac{m_{\mathrm{ref}}}{q_{\mathrm{ref}}} \nabla_{\hat{\mathbf{x}}} \cdot \hat{\mathbf{B}} &= 0 \\ \Leftrightarrow \nabla_{\hat{\mathbf{x}}} \cdot \hat{\mathbf{B}} &= 0. \end{aligned}$$

In Faraday's law (17.2c) the partial time and position derivatives cancel out together with the normalisation factors of the electric and magnetic field,

$$L_{\mathrm{ref}}^{-1} \frac{v_{\mathrm{ref}}^2}{L_{\mathrm{ref}}} \frac{m_{\mathrm{ref}}}{q_{\mathrm{ref}}} \nabla_{\hat{\mathbf{x}}} \times \hat{\mathbf{E}} = -\omega_{\mathrm{ref}} \frac{v_{\mathrm{ref}}}{L_{\mathrm{ref}}} \frac{m_{\mathrm{ref}}}{q_{\mathrm{ref}}} \frac{\partial \hat{\mathbf{B}}}{\partial \hat{t}}.$$

We multiply both sides with $\frac{q_{\mathrm{ref}} L_{\mathrm{ref}}^2}{m_{\mathrm{ref}} v_{\mathrm{ref}}^2}$ and obtain

$$\nabla_{\hat{\mathbf{x}}} \times \hat{\mathbf{E}} = -\frac{\partial \hat{\mathbf{B}}}{\partial \hat{t}}.$$

Last, we insert the dimensionless quantities in Ampère's law (17.2a),

$$\left(\frac{v_{\mathrm{ref}} m_{\mathrm{ref}}}{L_{\mathrm{ref}}^2 q_{\mathrm{ref}}} \right) \nabla_{\hat{\mathbf{x}}} \times \hat{\mathbf{B}} = \mu_0 \left(n_{\mathrm{ref}} v_{\mathrm{ref}} q_{\mathrm{ref}} \hat{\mathbf{J}} + \varepsilon_0 \frac{v_{\mathrm{ref}}^2 m_{\mathrm{ref}} \omega_{\mathrm{ref}}}{L_{\mathrm{ref}} q_{\mathrm{ref}}} \frac{\partial \hat{\mathbf{E}}}{\partial \hat{t}} \right).$$

We multiply both sides with $\frac{L_{\mathrm{ref}}^2 q_{\mathrm{ref}}}{v_{\mathrm{ref}}^2 m_{\mathrm{ref}}}$ and use the $\varepsilon_{\mathrm{ref}}$ and ω_{ref} definitions from above to get

$$\begin{aligned} \nabla_{\hat{\mathbf{x}}} \times \hat{\mathbf{B}} &= \left(\frac{L_{\mathrm{ref}}^2 q_{\mathrm{ref}}}{v_{\mathrm{ref}} m_{\mathrm{ref}}} \right) \mu_0 \left(\varepsilon_{\mathrm{ref}} \frac{v_{\mathrm{ref}}^3 m_{\mathrm{ref}}}{L_{\mathrm{ref}}^2 q_{\mathrm{ref}}} \hat{\mathbf{J}} + \varepsilon_0 \frac{v_{\mathrm{ref}}^3 m_{\mathrm{ref}}}{L_{\mathrm{ref}}^2 q_{\mathrm{ref}}} \frac{\partial \hat{\mathbf{E}}}{\partial \hat{t}} \right) \\ \Leftrightarrow \nabla_{\hat{\mathbf{x}}} \times \hat{\mathbf{B}} &= \mu_0 v_{\mathrm{ref}}^2 \varepsilon_0 \left(\frac{\varepsilon_{\mathrm{ref}}}{\varepsilon_0} \hat{\mathbf{J}} + \frac{\partial \hat{\mathbf{E}}}{\partial \hat{t}} \right). \end{aligned}$$

Then, we solve for the time derivative of the electric field and introduce the reference beta $\beta_{\text{ref}} = \mu_0 \varepsilon_0 v_{\text{ref}}^2$,

$$\frac{1}{\beta_{\text{ref}}} \nabla_{\hat{\mathbf{x}}} \times \hat{\mathbf{B}} - \frac{\varepsilon_{\text{ref}}}{\varepsilon_0} \hat{\mathbf{J}} = \frac{\partial \hat{\mathbf{E}}}{\partial \hat{t}}.$$

□

Proposition 17.2. *The dimensionless Hamiltonian takes the following form:*

$$\hat{\mathcal{H}} = \sum_s \frac{\hat{m}_s}{2} \int |\hat{\mathbf{v}}|^2 \hat{f}_s \, \mathrm{d}\hat{\mathbf{x}} \, \mathrm{d}\hat{\mathbf{v}} + \frac{\varepsilon_0}{\varepsilon_{\text{ref}}} \frac{1}{2} \int \|\hat{\mathbf{E}}\|^2 \, \mathrm{d}\hat{\mathbf{x}} + \frac{1}{\mu \varepsilon_{\text{ref}} v_{\text{ref}}^2} \frac{1}{2} \int \|\hat{\mathbf{B}}\|^2 \, \mathrm{d}\hat{\mathbf{x}}.$$

Proof. We insert the dimensionless quantities in the Hamiltonian in SI units (17.3),

$$\begin{aligned} \mathcal{H} = &\sum_s \frac{m_{\text{ref}} \hat{m}_s}{2} \int v_{\text{ref}}^2 |\hat{\mathbf{v}}|^2 \frac{n_{\text{ref}}}{v_{\text{ref}}^3} \hat{f}_s L_{\text{ref}}^3 \, \mathrm{d}\hat{\mathbf{x}} v_{\text{ref}}^3 \, \mathrm{d}\hat{\mathbf{v}} \\ &+ \frac{\varepsilon_0}{2} \int \left(\frac{v_{\text{ref}}^2 m_{\text{ref}}}{L_{\text{ref}} q_{\text{ref}}} \right)^2 \|\hat{\mathbf{E}}\|^2 L_{\text{ref}}^3 \, \mathrm{d}\mathbf{x} + \frac{1}{2\mu_0} \int \left(\frac{v_{\text{ref}} m_{\text{ref}}}{L_{\text{ref}} q_{\text{ref}}} \right)^2 \|\hat{\mathbf{B}}\|^2 L_{\text{ref}}^3 \, \mathrm{d}\hat{\mathbf{x}}. \end{aligned}$$

Multiplying the equation with $\frac{\omega_{\text{ref}}^3}{m_{\text{ref}} v_{\text{ref}}^5 n_{\text{ref}}}$ yields

$$\begin{aligned} \hat{\mathcal{H}} = &\sum_s \frac{\omega_{\text{ref}}^3}{m_{\text{ref}} v_{\text{ref}}^5 n_{\text{ref}}} m_{\text{ref}} L_{\text{ref}}^3 v_{\text{ref}}^2 n_{\text{ref}} \frac{\hat{m}_s}{2} \int |\hat{\mathbf{v}}|^2 \hat{f}_s \, \mathrm{d}\hat{\mathbf{x}} \, \mathrm{d}\hat{\mathbf{v}} \\ &+ \frac{\omega_{\text{ref}}^3}{m_{\text{ref}} v_{\text{ref}}^5 n_{\text{ref}}} \frac{\varepsilon_0 v_{\text{ref}}^4 L_{\text{ref}} m_{\text{ref}}^2}{q_{\text{ref}}^2} \frac{1}{2} \int \|\hat{\mathbf{E}}\|^2 \, \mathrm{d}\mathbf{x} + \frac{\omega_{\text{ref}}^3}{m_{\text{ref}} v_{\text{ref}}^5 n_{\text{ref}}} \frac{v_{\text{ref}}^2 L_{\text{ref}} m_{\text{ref}}^2}{\mu_0 q_{\text{ref}}^2} \frac{1}{2} \int \|\hat{\mathbf{B}}\|^2 \, \mathrm{d}\hat{\mathbf{x}}. \end{aligned}$$

Last, we use the definition of ω_{ref} and ε_{ref} to obtain

$$\hat{\mathcal{H}} = \sum_s \frac{\hat{m}_s}{2} \int |\hat{\mathbf{v}}|^2 \hat{f}_s \, \mathrm{d}\hat{\mathbf{x}} \, \mathrm{d}\hat{\mathbf{v}} + \frac{\varepsilon_0}{\varepsilon_{\text{ref}}} \frac{1}{2} \int \|\hat{\mathbf{E}}\|^2 \, \mathrm{d}\hat{\mathbf{x}} + \frac{1}{\mu \varepsilon_{\text{ref}} v_{\text{ref}}^2} \frac{1}{2} \int \|\hat{\mathbf{B}}\|^2 \, \mathrm{d}\hat{\mathbf{x}}.$$

□

17.3.2 Quasi-neutral Vlasov System

Proposition 17.3. *The coupling of the Vlasov equation* (17.1) *with the quasi-neutrality equations* (14.1) *and* (14.2) *rescales perfectly to dimensionless quantities.*

Proof. We have already shown that the Vlasov equation rescales perfectly. Hence, we only consider the quasi-neutrality equations and its Hamiltonian. Let us start with the quasi-neutrality equations in SI units,

$$\frac{q^2 n_e}{T_e} \phi = \rho - q n_e, \quad \frac{q^2 n_e}{T_e} \partial_t \phi = -\nabla_x \cdot \mathbf{J}.$$

When we insert the dimensionless variables, we see that both equations scale perfectly,

$$\begin{aligned}\frac{q_{\mathrm{ref}}^2 n_{\mathrm{ref}}}{T_{\mathrm{ref}}}\frac{T_{\mathrm{ref}}}{q_{\mathrm{ref}}}\frac{\hat{q}^2\hat{n}_e}{\hat{T}_e}\hat{\phi} &= q_{\mathrm{ref}} n_{\mathrm{ref}}\hat{\rho} - \hat{q} q_{\mathrm{ref}}\hat{n}_e n_{\mathrm{ref}},\\ \Leftrightarrow \frac{\hat{q}^2\hat{n}_e}{\hat{T}_e}\hat{\phi} &= \hat{\rho} - \hat{q}\hat{n}_e,\end{aligned}$$

$$\begin{aligned}\frac{q_{\mathrm{ref}}^2 n_{\mathrm{ref}}}{T_{\mathrm{ref}}}\frac{T_{\mathrm{ref}}}{q_{\mathrm{ref}}}\omega_{\mathrm{ref}}\frac{\hat{q}^2\hat{n}_e}{\hat{T}_e}\partial_{\hat{t}}\hat{\phi} &= -L_{\mathrm{ref}}^{-1} n_{\mathrm{ref}} v_{\mathrm{ref}} q_{\mathrm{ref}}\nabla_{\hat{\mathbf{x}}}\cdot\hat{\mathbf{J}},\\ \Leftrightarrow \frac{\hat{q}^2\hat{n}_e}{\hat{T}_e}\partial_{\hat{t}}\hat{\phi} &= -\nabla_{\hat{\mathbf{x}}}\cdot\hat{\mathbf{J}}.\end{aligned}$$

Then, we look at the total energy for the system and insert the dimensionless quantities,

$$\begin{aligned}\mathcal{H} &= \sum_s \frac{m_s}{2}\int |\mathbf{v}|^2 f_s \,\mathrm{d}\mathbf{x}\,\mathrm{d}\mathbf{v} + \frac{1}{2}\int \frac{q^2 n_e}{T_e}\|\Phi\|^2\,\mathrm{d}\mathbf{x}\\ &= \sum_s \frac{m_{\mathrm{ref}}\hat{m}_s}{2}\int v_{\mathrm{ref}}^2|\hat{\mathbf{v}}|^2\frac{n_{\mathrm{ref}}}{v_{\mathrm{ref}}^3}\hat{f}_s L_{\mathrm{ref}}^3\,\mathrm{d}\hat{\mathbf{x}} v_{\mathrm{ref}}^3\,\mathrm{d}\hat{\mathbf{v}} + \frac{1}{2}\int \frac{q_{\mathrm{ref}}^2 n_{\mathrm{ref}}}{T_{\mathrm{ref}}}\frac{\hat{q}^2\hat{n}_e}{\hat{T}_e}\frac{T_{\mathrm{ref}}^2}{q_{\mathrm{ref}}^2}\|\hat{\phi}\|^2 L_{\mathrm{ref}}^3\,\mathrm{d}\hat{\mathbf{x}}.\end{aligned}$$

We multiply the equation with $\frac{\omega_{\mathrm{ref}}^3}{m_{\mathrm{ref}} v_{\mathrm{ref}}^5 n_{\mathrm{ref}}}$ and use the definition of ω_{ref} and $\hat{\mathcal{H}}$ from above as well as the fact that we can write T_{ref} as $v_{\mathrm{ref}}^2 m_{\mathrm{ref}}$ to obtain

$$\begin{aligned}\hat{\mathcal{H}} &= \sum_s \frac{\omega_{\mathrm{ref}}^3}{m_{\mathrm{ref}} v_{\mathrm{ref}}^5 n_{\mathrm{ref}}} m_{\mathrm{ref}} L_{\mathrm{ref}}^3 v_{\mathrm{ref}}^2 n_{\mathrm{ref}}\frac{\hat{m}_s}{2}\int |\hat{\mathbf{v}}|^2\hat{f}_s\,\mathrm{d}\hat{\mathbf{x}}\,\mathrm{d}\hat{\mathbf{v}} + \frac{\omega_{\mathrm{ref}}^3}{m_{\mathrm{ref}} v_{\mathrm{ref}}^5 n_{\mathrm{ref}}} n_{\mathrm{ref}} T_{\mathrm{ref}} L_{\mathrm{ref}}^3\int \frac{\hat{q}^2\hat{n}_e}{\hat{T}_e}\|\hat{\phi}\|^2 d\hat{\mathbf{x}}\\ &= \sum_s \frac{\hat{m}_s}{2}\int |\hat{\mathbf{v}}|^2\hat{f}_s\,\mathrm{d}\hat{\mathbf{x}}\,\mathrm{d}\hat{\mathbf{v}} + \frac{1}{2}\int \frac{\hat{q}^2\hat{n}_e}{\hat{T}_e}\|\hat{\phi}\|^2 d\hat{\mathbf{x}}.\end{aligned}$$

□

18 Dispersion Relation

18.1 Linearised Vlasov Equation

In this section, we search for analytical solutions of a simplified Vlasov–Maxwell system.

Proposition 18.1. *The linearised Vlasov equation takes the following form:*

$$\frac{\partial \delta f}{\partial t} + \mathbf{v} \cdot \nabla_{\mathbf{x}} \delta f + \frac{q}{m}(\mathbf{E}_0 + \mathbf{v} \times \mathbf{B}_0) \cdot \nabla_{\mathbf{v}} \delta f = -\frac{q}{m}(\delta \mathbf{E} + \mathbf{v} \times \delta \mathbf{B}) \cdot \nabla_{\mathbf{v}} f_0. \tag{18.1}$$

Proof. We look for a normalised steady state solution $f_0(\mathbf{x}, \mathbf{v})$ of the collisionless Vlasov equation,

$$\begin{aligned} &\frac{\partial f_0}{\partial t} + \mathbf{v} \cdot \nabla_{\mathbf{x}} f_0 + \frac{q}{m}(\mathbf{E}_0 + \mathbf{v} \times \mathbf{B}_0) \cdot \nabla_{\mathbf{v}} f_0 = 0 \\ &\quad \Leftrightarrow \mathbf{v} \cdot \nabla_{\mathbf{x}} f_0 = -\frac{q}{m}(\mathbf{E}_0 + \mathbf{v} \times \mathbf{B}_0) \cdot \nabla_{\mathbf{v}} f_0. \end{aligned}$$

Lemma 18.2. *Assuming zero steady state fields, a Maxwellian distribution in $\mathbf{v}$ is an equilibrium function for the Vlasov equation,*

$$f_0(\mathbf{v}) = \frac{n_0}{(\sqrt{2\pi})^3 v_{Tx} v_{Ty} v_{Tz}} \exp\left(-\frac{1}{2}\left(\frac{(v_x - \bar{v}_x)^2}{v_{Tx}^2} + \frac{(v_y - \bar{v}_y)^2}{v_{Ty}^2} + \frac{(v_z - \bar{v}_z)^2}{v_{Tz}^2}\right)\right). \tag{18.2}$$

Proof. The steady state electric field satisfies Gauss' law,

$$\nabla \cdot \mathbf{E}_0 = q\left(\int f_0 \, \mathrm{d}\mathbf{v} - n_0\right) = 0,$$

where $n_0 = \int f_0 \, \mathrm{d}\mathbf{v}$. Hence, $\mathbf{E}_0$ is a constant and we have chosen it to be zero. Since we assumed that the magnetic field $\mathbf{B}_0$ equals zero as well, it follows that $\mathbf{v} \cdot \nabla_{\mathbf{x}} f_0 = 0$. Therefore, the equilibrium function only depends on $\mathbf{v}$. Last, we want f_0 to be normalised in the sense that $\int f_0(\mathbf{v}) \, \mathrm{d}\mathbf{v} = 1$. Thus, the Maxwellian distribution is a feasible choice for the steady state solution of the Vlasov equation. □

Lemma 18.3. *Considering only a magnetic steady state field, the equilibrium function can be written as*

$$f_0(v_\perp, v_\parallel) = \frac{n_0}{\left(\sqrt{2\pi}\right)^3 v_{T_\perp}^2 v_{T_\parallel}} \exp\left(-\frac{v_\perp^2}{2v_{T_\perp}^2} - \frac{v_\parallel^2}{2v_{T_\parallel}^2}\right). \tag{18.3}$$

Proof. Without loss of generality, we assume that the background field lies in z-direction,

$\mathbf{B}_0 = \hat{\mathbf{e}}_z B_0$. Then, we choose the following cylindrical coordinates for the velocity:

$$\mathbf{v} = (v_\perp \sin(\theta), v_\perp(\cos(\theta), v_\parallel)^\top$$

and compute

$$(\mathbf{v} \times \mathbf{B}_0) \cdot \nabla f_0(v_\perp, v_\parallel) = \begin{pmatrix} v_\perp \cos\theta \\ -v_\perp \sin\theta \\ 0 \end{pmatrix} \cdot \begin{pmatrix} -\frac{v_\perp \sin\theta}{v_{T_\perp}} \\ -\frac{v_\perp \cos\theta}{v_{T_\perp}} \\ -\frac{v_\parallel}{v_{T_\parallel}} \end{pmatrix} B_0 f_0 = \mathbf{0}.$$

Consequently, we have

$$\mathbf{v} \cdot \nabla_{\mathbf{x}} f_0 = \mathbf{v} \times \mathbf{B}_0 \cdot \nabla_{\mathbf{v}} f_0 = 0,$$

which shows that $f_0(v_\perp, v_\parallel)$ is a steady state solution of the Vlasov equation. □

Lemma 18.4. *When the density, $N(R_x)$, or the temperature, $T(R_x)$, are position dependent, an equilibrium function is given by*

$$f_0(N, T, K) = \frac{N(R_x)}{\left(\sqrt{2\pi \frac{T(R_x)}{m_i}}\right)^3} \exp\left(-\frac{K(\mathbf{v})}{T(R_x)}\right). \tag{18.4}$$

Proof. Assuming that the electric field $\mathbf{E}_0$ still equals zero, we obtain from the steady state equation that

$$\mathbf{v} \cdot \nabla_{\mathbf{x}} f_0 = -\frac{q}{m} \mathbf{v} \times \mathbf{B}_0 \cdot \nabla_{\mathbf{v}} f_0.$$

Without loss of generality, we assume that the magnetic field lies in the z-direction, $\mathbf{B}_0 = \hat{\mathbf{e}}_z B_0$. Let us introduce the kinetic energy $K = \frac{mv^2}{2}$ and the new field-line-following coordinate $\mathbf{R} = (x + \frac{v_y}{\Omega_0}, y - \frac{v_x}{\Omega_0}, z)^\top$, where $\Omega_0 = \frac{qB_0}{m}$ denotes the gyrofrequency of the background field. Note that for $B_0 \to \infty$ this system converges to the guiding centre model.

Then, we perform a linear Taylor expansion of f_0 in x,

$$f_0(R_x, \mathbf{v}) = f_0(x, \mathbf{v}) + \frac{v_y}{\Omega_0} \frac{\partial f_0(x, \mathbf{v})}{\partial x} + \mathcal{O}\left(\left(\frac{v_y}{\Omega_0}\right)^2\right),$$

to show that the Maxwellian is still normalised,

$$\int f_0(R_x, \mathbf{v}) \, \mathrm{d}\mathbf{v} = \int f_0(x, \mathbf{v}) \, \mathrm{d}\mathbf{v} + \int \frac{v_y}{\Omega_0} \frac{\partial f_0(x, \mathbf{v})}{\partial x} \, \mathrm{d}\mathbf{v} = n_0(x).$$

The partial derivatives of the distribution function are computed as

$$\begin{aligned}
\partial_{v_x} f_0(R_x, K) &= -\frac{v_x m}{T(x)} f_0(x, \mathbf{v}), \quad \partial_{v_z} f_0(R_x, K) = -\frac{v_z m}{T(x)} f_0(x, \mathbf{v}), \\
\partial_{v_y} f_0(R_x, K) &= -\frac{v_y m}{T(x)} f_0(x, \mathbf{v}) + \frac{\partial_x f_0(x, \mathbf{v})}{\Omega_0}, \\
\partial_x f_0(x, \mathbf{v}) &= \frac{\partial f_0}{\partial N}\frac{\partial N}{\partial x} + \frac{\partial f_0}{\partial T}\frac{\partial T}{\partial x} = \left[\frac{\frac{\mathrm{d}}{\mathrm{d}x} n_0(x)}{n_0(x)} + \left(\frac{mv^2}{2T(x)} - \frac{3}{2}\right)\frac{\frac{\mathrm{d}}{\mathrm{d}x} T(x)}{T(x)}\right] f_0(x).
\end{aligned}$$

Next, we insert the computed derivatives into the condition for the steady state solution and obtain

$$\begin{aligned}
v_x \partial_x f_0(x, \mathbf{v}) =& \mathbf{v} \cdot \nabla_{\mathbf{x}} f_0(R_x, K) = -\frac{q}{m} \mathbf{v} \times \mathbf{B}_0 \cdot \nabla_{\mathbf{v}} f_0(R_x, K) = -\frac{q}{m}(v_y B_0 \partial_{v_x} f_0 - v_x B_0 \partial_{v_y} f_0) \\
=& \frac{q}{m}\left(\frac{v_x m v_y B_0}{T(x)} f_0(x, \mathbf{v}) - \frac{v_y m v_x B_0}{T(x)} f_0(x, \mathbf{v}) + v_x B_0 \frac{\partial_x f_0(x, \mathbf{v})}{\Omega_0}\right) = v_x \partial_x f_0(x, \mathbf{v}).
\end{aligned}$$

□

Let us consider a small perturbation of the equilibrium state for the fields and the particle distribution function, $f = f_0 + \varepsilon \delta f, \mathbf{E} = \mathbf{E}_0 + \varepsilon \delta \mathbf{E}, \mathbf{B} = \mathbf{B}_0 + \varepsilon \delta \mathbf{B}$ and insert this representation into the Vlasov equation,

$$\frac{\partial (f_0 + \varepsilon \delta f)}{\partial t} + \mathbf{v} \cdot \nabla_{\mathbf{x}} (f_0 + \varepsilon \delta f) + \frac{q}{m}((\mathbf{E}_0 + \varepsilon \delta \mathbf{E}) \mathbf{v} \times (\mathbf{B}_0 + \varepsilon \delta \mathbf{B}) \cdot \nabla_{\mathbf{v}} (f_0 + \delta f) = 0.$$

Then, we use the fact that f_0 is a steady state solution and expand the terms to

$$\begin{aligned}
\varepsilon \left(\frac{\partial \delta f}{\partial t} + \mathbf{v} \cdot \nabla_{\mathbf{x}} \delta f + \frac{q}{m}(\mathbf{E}_0 + \mathbf{v} \times \mathbf{B}_0) \cdot \nabla_{\mathbf{v}} \delta f + \varepsilon \frac{q}{m}(\delta \mathbf{E} + \mathbf{v} \times \delta \mathbf{B}) \cdot \nabla_{\mathbf{v}} \delta f\right) \\
= -\varepsilon \frac{q}{m}(\delta \mathbf{E} + \mathbf{v} \times \delta \mathbf{B}) \cdot \nabla_{\mathbf{v}} f_0.
\end{aligned}$$

Keeping only linear terms in ε leads to (18.1). □

18.2 Transformed Field Equations

Proposition 18.1. *The Fourier–Laplace transformed Maxwell equations take the following form:*

$$\widehat{\delta \mathbf{B}} = \frac{\mathbf{k} \times \widehat{\delta \mathbf{E}}}{\omega}, \tag{18.5a}$$

$$\mu_0 \varepsilon_0 \omega^2 \widehat{\delta \mathbf{E}} - k^2 \widehat{\delta \mathbf{E}} + \mathbf{k}(\mathbf{k} \cdot \widehat{\delta \mathbf{E}}) = -i \mu_0 \omega \widehat{\delta \mathbf{J}}, \tag{18.5b}$$

$$\mathbf{k} \cdot \widehat{\delta \mathbf{E}} = -i \frac{\widehat{\delta \rho}}{\varepsilon_0},$$

$$\mathbf{k} \cdot \widehat{\delta \mathbf{B}} = 0,$$

Proof. Let us take a look at Maxwell's equations,

$$\mu_0\varepsilon_0\frac{\partial \mathbf{E}}{\partial t} = \nabla_{\mathbf{x}} \times \mathbf{B} - \mu_0\mathbf{J}, \qquad \nabla_{\mathbf{x}} \cdot \mathbf{E} = \frac{\rho}{\varepsilon_0},$$
$$\frac{\partial \mathbf{B}}{\partial t} = -\nabla_{\mathbf{x}} \times \mathbf{E}, \qquad \nabla_{\mathbf{x}} \cdot \mathbf{B} = 0.$$

We linearise Maxwell's equations and take the Fourier–Laplace ansatz from (A.1) for the perturbed fields,

$$\delta\mathbf{E}(\mathbf{x},t) = \int \widehat{\delta\mathbf{E}}(\mathbf{k},\omega)\exp\left(-i\omega t + i\mathbf{k}\cdot\mathbf{x}\right)\,\mathrm{d}\mathbf{k}\,\mathrm{d}\omega,$$
$$\delta\mathbf{B}(\mathbf{x},t) = \int \widehat{\delta\mathbf{B}}(\mathbf{k},\omega)\exp\left(-i\omega t + i\mathbf{k}\cdot\mathbf{x}\right)\,\mathrm{d}\mathbf{k}\,\mathrm{d}\omega.$$

Inserting this ansatz into the linearised equations leads to

$$\omega\widehat{\delta\mathbf{B}} = \mathbf{k}\times\widehat{\delta\mathbf{E}}, \tag{18.6a}$$
$$\mu_0\varepsilon_0\omega\widehat{\delta\mathbf{E}} = -\mathbf{k}\times\widehat{\delta\mathbf{B}} - i\mu_0\widehat{\delta\mathbf{J}}, \tag{18.6b}$$
$$\mathbf{k}\cdot\widehat{\delta\mathbf{E}} = -i\frac{\widehat{\delta\rho}}{\varepsilon_0},$$
$$\mathbf{k}\cdot\widehat{\delta\mathbf{B}} = 0.$$

We use Faraday's equation (18.6a) to cancel out $\widehat{\delta\mathbf{B}}$ in the Ampère equation (18.6b). This gives us

$$\mu_0\varepsilon_0\omega\widehat{\delta\mathbf{E}} = -\mathbf{k}\times\frac{1}{\omega}(\mathbf{k}\times\widehat{\delta\mathbf{E}}) - i\mu_0\widehat{\delta\mathbf{J}},$$
$$\Leftrightarrow \mu_0\varepsilon_0\omega^2\widehat{\delta\mathbf{E}} - k^2\widehat{\delta\mathbf{E}} + \mathbf{k}(\mathbf{k}\cdot\widehat{\delta\mathbf{E}}) = -i\mu_0\omega\widehat{\delta\mathbf{J}},$$

where we denote $\mathbf{k}\cdot\mathbf{k}$ as k^2.

The source terms are defined as

$$\widehat{\delta\mathbf{J}} = q\int \mathbf{v}\widehat{\delta f}\mathbf{v}, \quad \widehat{\delta\rho} = q\int \widehat{\delta f}\mathbf{v}.$$

□

Proposition 18.2. *The transformed Poisson equation is given by*

$$k^2\widehat{\delta\Phi} = \frac{\widehat{\delta\rho_s}}{\varepsilon_0}. \tag{18.7}$$

Proof. The Poisson equation for one species s has the following form:

$$-\nabla \cdot \nabla \Phi = \frac{q_s}{\varepsilon_0} \left(\int \delta f_s \, \mathrm{d}\mathbf{v} - n_0 \right).$$

It is linearised as

$$k^2 \widehat{\delta\Phi} = \frac{q_s}{\varepsilon_0} \int \widehat{\delta f}_s \, \mathrm{d}\mathbf{v},$$

where we inserted the Fourier–Laplace ansatz from (A.1) for the scalar potential and the distribution function,

$$\begin{aligned} f_s(\mathbf{x}, t) &= \int \widehat{\delta f}_s(\mathbf{k}, \omega) \exp\left(-i\omega t + i\mathbf{k} \cdot \mathbf{x}\right) \, \mathrm{d}\mathbf{k} \, \mathrm{d}\omega, \\ \delta\Phi(\mathbf{x}, t) &= \int \widehat{\delta\Phi}(\mathbf{k}, \omega) \exp\left(-i\omega t + i\mathbf{k} \cdot \mathbf{x}\right) \, \mathrm{d}\mathbf{k} \, \mathrm{d}\omega. \end{aligned}$$

Here, the charge density term is defined as

$$\widehat{\delta\rho}_s = q_s \int \widehat{\delta f}_s \mathbf{v}. \tag{18.8}$$

□

Proposition 18.3. *The transformed quasi-neutrality equations are given by*

$$\begin{aligned} \frac{q^2 n_{0e} \widehat{\delta\Phi}}{T_e} &= \widehat{\delta\rho}_i, \\ \omega \frac{q^2 n_{0e} \widehat{\delta\Phi}}{T_e} &= \mathbf{k} \cdot \widehat{\delta\mathbf{J}}_i. \end{aligned} \tag{18.9}$$

Proof. The quasi-neutrality equations have the following form:

$$\begin{aligned} \frac{q^2 n_{0e} \Phi}{T_e} &= q_i \int f_i \, \mathrm{d}\mathbf{v} + q_e n_{0e}, \\ \frac{q^2 n_{0e}}{T_e} \frac{\partial \Phi}{\partial t} &= -\nabla \cdot \left(q_i \int \mathbf{v} f_i \, \mathrm{d}\mathbf{v} \right), \end{aligned}$$

where we assume $n_{0e} = n_{0i} = n_0$.

For the background potential, we obtain

$$\Phi_0 = \frac{T_e}{q n_0} \left(\int f_0 \, \mathrm{d}\mathbf{v} - n_0 \right) = 0.$$

Then, the linearised quasi-neutrality equations take the following form:

$$\frac{q^2 n_0 \widehat{\delta\Phi}}{T_e} = q_i \int \widehat{\delta f}_i \,\mathrm{d}\mathbf{v},$$
$$-i\omega \frac{q^2 n_0 \widehat{\delta\Phi}}{T_e} = -i\mathbf{k} \cdot \left(q_i \int \mathbf{v} \widehat{\delta f}_i \,\mathrm{d}\mathbf{v} \right),$$

where we used the Fourier–Laplace ansatz from (A.1),

$$f_i(\mathbf{x}, t) = \int \widehat{\delta f}_i(\mathbf{k}, \omega) \exp\left(-i\omega t + i\mathbf{k} \cdot \mathbf{x}\right) \,\mathrm{d}\mathbf{k}\,\mathrm{d}\omega,$$
$$\delta\Phi(\mathbf{x}, t) = \int \widehat{\delta\Phi}(\mathbf{k}, \omega) \exp\left(-i\omega t + i\mathbf{k} \cdot \mathbf{x}\right) \,\mathrm{d}\mathbf{k}\,\mathrm{d}\omega.$$

The source terms are defined as

$$\widehat{\delta\mathbf{J}}_i = q_i \int \mathbf{v} \widehat{\delta f}_i \mathbf{v}, \quad \widehat{\delta\rho}_i = q_i \int \widehat{\delta f}_i \mathbf{v}.$$

□

18.3 1D Dispersion Relation

In this chapter, we consider a one dimensional (1D) plasma wave without background fields, i.e. $\mathbf{E}_0 = \mathbf{B}_0 = 0$. Without loss of generality we assume $\mathbf{k} = (k, 0, 0)^\top$. For the perturbed quantities we consider the Fourier and Laplace transformations introduced in (A.1),

$$\delta f(x, t) = \int \widehat{\delta f}(k, \omega) \exp\left(-i\omega t + ikx\right) \,\mathrm{d}k\,\mathrm{d}\omega,$$
$$\delta\Phi(x, t) = \int \widehat{\delta\Phi}(k, \omega) \exp\left(-i\omega t + ikx\right) \,\mathrm{d}k\,\mathrm{d}\omega,$$
$$\delta\mathbf{E}(x, t) = \int \widehat{\delta\mathbf{E}}(k, \omega) \exp\left(-i\omega t + ikx\right) \,\mathrm{d}k\,\mathrm{d}\omega,$$
$$\delta\mathbf{B}(x, t) = \int \widehat{\delta\mathbf{B}}(k, \omega) \exp\left(-i\omega t + ikx\right) \,\mathrm{d}k\,\mathrm{d}\omega.$$

Inserting this representation into (18.1) and solving for $\widehat{\delta f}$ leads to

$$\widehat{\delta f} = i\frac{q}{m} \frac{\widehat{\delta\mathbf{E}} + \mathbf{v} \times \widehat{\delta\mathbf{B}}}{kv_x - \omega} \cdot \nabla_{\mathbf{v}} f_0. \tag{18.10}$$

18.3.1 Electrostatic Dispersion

A general formulation of this setting can be found in [78, Sec. 3.3].

Proposition 18.1. *In an electrostatic setting, the linearised 1D charge density for a species*

s is computed as

$$\widehat{\delta\rho}_s = -\widehat{\delta\Phi}\frac{q^2 n_{0s}}{m_s v_{Ts}^2}\left[1 + \zeta_s Z(\zeta_s)\right], \tag{18.11}$$

where $\zeta_s = \frac{\omega - k\bar{v}_x}{k\sqrt{2}v_{Ts}}$.

Proof. We consider an electrostatic setting, where $\delta\mathbf{B} = 0$ and $\delta\mathbf{E} = -\nabla_{\mathbf{x}}\delta\Phi$. For the Fourier–Laplace coefficients, this gives us

$$\widehat{\delta\mathbf{E}} = -i\mathbf{k}\widehat{\delta\Phi}.$$

Then, the representation of $\widehat{\delta f}$ in (18.10) simplifies to

$$\widehat{\delta f} = \frac{q}{m}\frac{k\widehat{\delta\Phi}}{kv_x - \omega}\partial_{v_x} f_0.$$

Inserting this representation into (18.8) yields the linearised charge density,

$$\widehat{\delta\rho}_s = \frac{q^2}{m_s}\int \frac{k\widehat{\delta\Phi}}{kv_x - \omega}\partial_{v_x} f_0 \,\mathrm{d}\mathbf{v}.$$

Next, we insert the equilibrium function $f_{0s}(\mathbf{v})$ from (18.2) adapted to 1D,

$$\widehat{\delta\rho}_s = -\widehat{\delta\Phi}\frac{q^2 n_{0s}}{m_s v_{Ts}^2}\int \frac{k(v_x - \bar{v}_x)}{kv_x - \omega}\frac{1}{\sqrt{2\pi}v_{Ts}}\exp\left(-\frac{(v_x - \bar{v}_x)^2}{2v_{Ts}^2}\right)\mathrm{d}v_x.$$

Afterwards, we substitute $v_x - \bar{v}_x = \sqrt{2}v_{Ts}\sigma$,

$$\widehat{\delta\rho}_s = -\widehat{\delta\Phi}\frac{q^2 n_{0s}}{m_s v_{Ts}^2}\frac{1}{\sqrt{\pi}}\int \frac{\sigma}{\sigma - \frac{\omega - k\bar{v}_x}{k\sqrt{2}v_{Ts}}}\exp\left(-\sigma^2\right)\mathrm{d}\sigma.$$

Finally, we set $\zeta_s = \frac{\omega - k\bar{v}_x}{k\sqrt{2}v_{Ts}}$ and expand the integral to

$$\widehat{\delta\rho}_s = -\widehat{\delta\Phi}\frac{q^2 n_{0s}}{m_s v_{Ts}^2}\left[1 + \zeta_s\frac{1}{\sqrt{\pi}}\int \frac{\exp\left(-\sigma^2\right)}{\sigma - \zeta_s}\mathrm{d}\sigma\right].$$

Then, we use Definition A.2 of the Zeta function to obtain the proposition. □

Corrolary 18.2. *The dispersion relation of the 1D Vlasov–Poisson system for a species s*

takes the following form with $\zeta_s = \frac{\omega - k\bar{v}_x}{k\sqrt{2}v_{Ts}}$*:*

$$D(k,\omega) = 1 + \frac{\omega_{ps}^2}{k^2 v_{Ts}^2}\left[1 + \zeta_s Z(\zeta_s)\right]. \tag{18.12}$$

Proof. In this case, we couple the electrostatic Vlasov equation to the Poisson equation. Thus, we insert the representation of $\widehat{\delta\rho}_s$ given by (18.11) into the linearised Poisson equation (18.10),

$$k^2\widehat{\delta\Phi} = -\widehat{\delta\Phi}\frac{q^2 n_{0s}}{\varepsilon_0 m_s v_{Ts}^2}\left[1 + \zeta_s Z(\zeta_s)\right].$$

Then, we solve for the form $D(k,\omega)\widehat{\delta\Phi} = 0$ and use the definition of the plasma frequency, $\omega_{ps} = \sqrt{\frac{q^2 n_{0s}}{m_s \varepsilon_0}}$, to obtain

$$\left(1 + \frac{\omega_{ps}^2}{k^2 v_{Ts}^2}\left[1 + \zeta_s Z(\zeta_s)\right]\right)\widehat{\delta\Phi} = 0.$$

□

Corrolary 18.3. *The multispecies dispersion relation of the 1D Vlasov–Poisson system is given by*

$$D(k,\omega) = 1 + \frac{\omega_{pe}^2}{k^2 v_{Te}^2}\left[1 + \zeta_e Z(\zeta_e)\right] + \frac{\omega_{pi}^2}{k^2 v_{Ti}^2}\left[1 + \zeta_i Z(\zeta_i)\right]$$

with $\zeta_e = \frac{\omega - k\bar{v}_x}{k\sqrt{2}v_{Te}}, \zeta_i = \frac{\omega - k\bar{v}_x}{k\sqrt{2}v_{Ti}}$*.*

Proof. We take the dispersion relation for one species (18.12) and set $f = f_e + f_i$. □

Corrolary 18.4. *The dispersion relation of the 1D quasi-neutral Vlasov system takes the following form with* $\zeta_i = \frac{\omega - k\bar{v}_i}{k\sqrt{2}v_{Ti}}$*:*

$$D(k,w) = 1 + \frac{T_e n_{0i}}{T_i n_{0e}}\left[1 + \zeta_i Z(\zeta_i)\right]. \tag{18.13}$$

Proof. For this system, we couple the electrostatic Vlasov equation for ions with the quasi-neutrality equations. Therefore, we insert the representation of $\widehat{\delta\rho}_i$ taken from (18.11) into the linearised quasi-neutrality equation (18.9),

$$\frac{q^2 n_{0e}\widehat{\delta\Phi}}{T_e} = -\widehat{\delta\Phi}\frac{q^2 n_{0i}}{m_i v_{Ti}^2}\left[1 + \zeta_i Z(\zeta_i)\right].$$

Then, we solve for the form $D(k,\omega)\widehat{\delta\Phi} = 0$,

$$\left(1 + \frac{T_e n_{0i}}{T_i n_{0e}} \left[1 + \zeta_i Z(\zeta_i)\right]\right) \widehat{\delta\Phi} = 0.$$

□

18.3.2 Electromagnetic Dispersion

Proposition 18.5. *The dispersion relation of the 1D Vlasov–Maxwell system takes the following form:*

$$\det\left(D(k,\omega)\right) = D_{xx}(k,\omega) D_{yy}(k,\omega) D_{zz}(k,\omega) \tag{18.14}$$

with $\zeta = \frac{\omega_x}{k\sqrt{2}v_{Tx}}$ *and*

$$\begin{aligned}
D_{xx}(k,\omega) &= 1 + 2\frac{\omega_p^2}{\omega^2}\zeta^2[1 + \zeta Z(\zeta)], \\
D_{yy}(k,\omega) &= 1 - \frac{k^2}{\mu_0\varepsilon_0\omega^2} + \frac{\omega_p^2}{\omega^2}\left(\frac{v_{Ty}^2}{v_{Tx}^2}[1 + \zeta Z(\zeta)] - 1\right), \\
D_{zz}(k,\omega) &= 1 - \frac{k^2}{\mu_0\varepsilon_0\omega^2} + \frac{\omega_p^2}{\omega^2}\left(\frac{v_{Tz}^2}{v_{Tx}^2}[1 + \zeta Z(\zeta)] - 1\right).
\end{aligned}$$

Proof. We couple the Vlasov equation to Maxwell's equations via the source terms

$$\boldsymbol{\rho} = \sum_s q_s \int f \,\mathrm{d}\mathbf{v}, \; \mathbf{J} = \sum_s q_s \int f\mathbf{v} \,\mathrm{d}\mathbf{v}.$$

First, we substitute $\widehat{\delta\mathbf{B}}$ in (18.10) via (18.5a),

$$\widehat{\delta f} = i\frac{q}{m}\frac{\widehat{\delta\mathbf{E}} + \mathbf{v} \times \frac{\mathbf{k}\times\widehat{\delta\mathbf{E}}}{\omega}}{kv_x - \omega} \cdot \nabla_{\mathbf{v}} f_0.$$

Second, we insert this representation of δf into the linearised Ampère equation (18.5b),

$$(\mu_0\varepsilon_0\omega^2 - k^2)\widehat{\delta\mathbf{E}} + \mathbf{k}(\mathbf{k}\cdot\widehat{\delta\mathbf{E}}) - \omega\mu_0\frac{q^2}{m}\int \frac{\widehat{\delta\mathbf{E}} + \mathbf{v} \times \frac{\mathbf{k}\times\widehat{\delta\mathbf{E}}}{\omega}}{kv_x - \omega} \cdot \nabla_{\mathbf{v}} f_0 \mathbf{v} \,\mathrm{d}\mathbf{v} = 0.$$

Then, we reformulate $\mathbf{v} \times \frac{\mathbf{k}\times\widehat{\delta\mathbf{E}}}{\omega}$ as $(\mathbf{v}\cdot\widehat{\delta\mathbf{E}})\frac{\mathbf{k}}{\omega} - (\mathbf{v}\cdot\mathbf{k})\frac{\widehat{\delta\mathbf{E}}}{\omega}$ and insert our choice for the wave

vector, $\mathbf{k} = (k, 0, 0)^\top$,

$$\begin{pmatrix} \omega^2 \widehat{\delta E}_x \\ \left(\omega^2 - \frac{k^2}{\mu_0 \varepsilon_0}\right) \widehat{\delta E}_y \\ \left(\omega^2 - \frac{k^2}{\mu_0 \varepsilon_0}\right) \widehat{\delta E}_z \end{pmatrix} - \frac{\omega}{k} \frac{q^2}{m \varepsilon_0} \int \frac{\mathbf{v}}{v_x - \frac{\omega}{k}} \begin{pmatrix} \widehat{\delta E}_x + \frac{k}{\omega}(v_y \widehat{\delta E}_y + v_z \widehat{\delta E}_z) \\ (1 - \frac{k}{\omega} v_x) \widehat{\delta E}_y \\ (1 - \frac{k}{\omega} v_x) \widehat{\delta E}_z \end{pmatrix} \cdot \begin{pmatrix} \partial_{v_x} f_0 \\ \partial_{v_y} f_0 \\ \partial_{v_z} f_0 \end{pmatrix} \mathrm{d}\mathbf{v} = 0.$$

The system can be written as

$$D(k, \omega) \widehat{\delta \mathbf{E}} = 0.$$

Thus, we need to compute the determinant of the matrix $D(k, \omega)$ to find a solution for k and ω. To simplify the expression, we assume $\bar{\mathbf{v}} = \mathbf{0}$ and introduce the representation of the equilibrium function $f_0(\mathbf{v})$ from (18.2) to compute the velocity gradient in the matrix entries,

$$\begin{aligned}
D_{xx} &= \omega^2 + \frac{\omega}{k} \omega_p^2 \int \frac{v_x}{v_x - \frac{\omega}{k}} \frac{v_x}{v_{Tx}^2} \frac{\mathrm{e}^{-\frac{1}{2}\left(\frac{v_x^2}{v_{Tx}^2} + \frac{v_y^2}{v_{Ty}^2} + \frac{v_z^2}{v_{Tz}^2}\right)}}{(\sqrt{2\pi})^3 v_{Tx} v_{Ty} v_{Tz}} \mathrm{d}\mathbf{v}, \\
D_{xy} &= \frac{\omega}{k} \omega_p^2 \int \frac{v_x}{v_x - \frac{\omega}{k}} \left(\frac{\frac{k}{\omega} v_x}{v_{Tx}^2} + \frac{1 - \frac{k}{\omega} v_x}{v_{Ty}^2} \right) v_y \frac{\mathrm{e}^{-\frac{1}{2}\left(\frac{v_x^2}{v_{Tx}^2} + \frac{v_y^2}{v_{Ty}^2} + \frac{v_z^2}{v_{Tz}^2}\right)}}{(\sqrt{2\pi})^3 v_{Tx} v_{Ty} v_{Tz}} \mathrm{d}\mathbf{v}, \\
D_{xz} &= \frac{\omega}{k} \omega_p^2 \int \frac{v_x}{v_x - \frac{\omega}{k}} \left(\frac{\frac{k}{\omega} v_x}{v_{Tx}^2} + \frac{1 - \frac{k}{\omega} v_x}{v_{Tz}^2} \right) v_z \frac{\mathrm{e}^{-\frac{1}{2}\left(\frac{v_x^2}{v_{Tx}^2} + \frac{v_y^2}{v_{Ty}^2} + \frac{v_z^2}{v_{Tz}^2}\right)}}{(\sqrt{2\pi})^3 v_{Tx} v_{Ty} v_{Tz}} \mathrm{d}\mathbf{v}, \\
D_{yx} &= \frac{\omega}{k} \omega_p^2 \int \frac{v_y}{v_x - \frac{\omega}{k}} \frac{v_x}{v_{Tx}^2} \frac{\mathrm{e}^{-\frac{1}{2}\left(\frac{v_x^2}{v_{Tx}^2} + \frac{v_y^2}{v_{Ty}^2} + \frac{v_z^2}{v_{Tz}^2}\right)}}{(\sqrt{2\pi})^3 v_{Tx} v_{Ty} v_{Tz}} \mathrm{d}\mathbf{v}, \\
D_{yy} &= \omega^2 - \frac{k^2}{\mu_0 \varepsilon_0} + \frac{\omega}{k} \omega_p^2 \int \frac{v_y^2}{v_x - \frac{\omega}{k}} \left(\frac{\frac{k}{\omega} v_x}{v_{Tx}^2} + \frac{1 - \frac{k}{\omega} v_x}{v_{Ty}^2} \right) \frac{\mathrm{e}^{-\frac{1}{2}\left(\frac{v_x^2}{v_{Tx}^2} + \frac{v_y^2}{v_{Ty}^2} + \frac{v_z^2}{v_{Tz}^2}\right)}}{(\sqrt{2\pi})^3 v_{Tx} v_{Ty} v_{Tz}} \mathrm{d}\mathbf{v}, \\
D_{yz} = D_{zy} &= \frac{\omega}{k} \omega_p^2 \int \frac{v_y}{v_x - \frac{\omega}{k}} \left(\frac{\frac{k}{\omega} v_x}{v_{Tx}^2} + \frac{1 - \frac{k}{\omega} v_x}{v_{Tz}^2} \right) v_z \frac{\mathrm{e}^{-\frac{1}{2}\left(\frac{v_x^2}{v_{Tx}^2} + \frac{v_y^2}{v_{Ty}^2} + \frac{v_z^2}{v_{Tz}^2}\right)}}{(\sqrt{2\pi})^3 v_{Tx} v_{Ty} v_{Tz}} \mathrm{d}\mathbf{v}, \\
D_{zx} &= \frac{\omega}{k} \omega_p^2 \int \frac{v_z}{v_x - \frac{\omega}{k}} \frac{v_x}{v_{Tx}^2} \frac{\mathrm{e}^{-\frac{1}{2}\left(\frac{v_x^2}{v_{Tx}^2} + \frac{v_y^2}{v_{Ty}^2} + \frac{v_z^2}{v_{Tz}^2}\right)}}{(\sqrt{2\pi})^3 v_{Tx} v_{Ty} v_{Tz}} \mathrm{d}\mathbf{v}, \\
D_{zz} &= \omega^2 - \frac{k^2}{\mu_0 \varepsilon_0} + \frac{\omega}{k} \omega_p^2 \int \frac{v_z^2}{v_x - \frac{\omega}{k}} \left(\frac{\frac{k}{\omega} v_x}{v_{Tx}^2} + \frac{1 - \frac{k}{\omega} v_x}{v_{Tz}^2} \right) \frac{\mathrm{e}^{-\frac{1}{2}\left(\frac{v_x^2}{v_{Tx}^2} + \frac{v_y^2}{v_{Ty}^2} + \frac{v_z^2}{v_{Tz}^2}\right)}}{(\sqrt{2\pi})^3 v_{Tx} v_{Ty} v_{Tz}} \mathrm{d}\mathbf{v}.
\end{aligned}$$

Using (A.5b), we compute

$$\int_{-\infty}^{\infty} v_y \frac{\mathrm{e}^{-\frac{1}{2}\left(\frac{v_x^2}{v_{Tx}^2}+\frac{v_y^2}{v_{Ty}^2}+\frac{v_z^2}{v_{Tz}^2}\right)}}{(\sqrt{2\pi})^3 v_{Tx}v_{Ty}v_{Tz}}\,\mathrm{d}v_y = \int_{-\infty}^{\infty} v_z \frac{\mathrm{e}^{-\frac{1}{2}\left(\frac{v_x^2}{v_{Tx}^2}+\frac{v_y^2}{v_{Ty}^2}+\frac{v_z^2}{v_{Tz}^2}\right)}}{(\sqrt{2\pi})^3 v_{Tx}v_{Ty}v_{Tz}}\,\mathrm{d}v_z = 0$$

to see that all off-diagonal entries of the matrix equal zero. Therefore, the determinant of the matrix breaks down to the product of the diagonal entries,

$$\det\left(D(k,\omega)\right) = D_{xx}(k,\omega)D_{yy}(k,\omega)D_{zz}(k,\omega) = 0.$$

Then, we use (A.5c) to compute

$$\int_{-\infty}^{\infty} v_y^2 \frac{\mathrm{e}^{-\frac{1}{2}\frac{v_y^2}{v_{Ty}^2}}}{(\sqrt{2\pi})v_{Ty}}\,\mathrm{d}v_y = v_{Ty}^2,$$
$$\int_{-\infty}^{\infty} v_z^2 \frac{\mathrm{e}^{-\frac{1}{2}\frac{v_z^2}{v_{Tz}^2}}}{(\sqrt{2\pi})v_{Tz}}\,\mathrm{d}v_z = v_{Tz}^2$$

and obtain the following diagonal entries:

$$D_{xx}(k,\omega) = \omega^2 + \frac{\omega}{k}\omega_p^2 \int \frac{v_x^2}{v_x - \frac{\omega}{k}} \frac{1}{v_{Tx}^2} \frac{\mathrm{e}^{-\frac{1}{2}\frac{v_x^2}{v_{Tx}^2}}}{\sqrt{2\pi}v_{Tx}}\,\mathrm{d}v_x,$$
$$D_{yy}(k,\omega) = \omega^2 - \frac{k^2}{\mu_0\varepsilon_0} + \omega_p^2 \int \frac{1}{v_x - \frac{\omega}{k}} \left(\frac{v_x}{v_{Tx}^2} + \frac{\frac{\omega}{k} - v_x}{v_{Ty}^2}\right) v_{Ty}^2 \frac{\mathrm{e}^{-\frac{1}{2}\frac{v_x^2}{v_{Tx}^2}}}{\sqrt{2\pi}v_{Tx}}\,\mathrm{d}v_x,$$
$$D_{zz}(k,\omega) = \omega^2 - \frac{k^2}{\mu_0\varepsilon_0} + \omega_p^2 \int \frac{1}{v_x - \frac{\omega}{k}} \left(\frac{v_x}{v_{Tx}^2} + \frac{\frac{\omega}{k} - v_x}{v_{Tz}^2}\right) v_{Tz}^2 \frac{\mathrm{e}^{-\frac{1}{2}\frac{v_x^2}{v_{Tx}^2}}}{\sqrt{2\pi}v_{Tx}}\,\mathrm{d}v_x.$$

Next, we substitute $v_x = \sqrt{2}v_{Tx}\sigma$ to solve the integral over v_x,

$$D_{xx}(k,\omega) = \omega^2 + 2\frac{\omega}{k\sqrt{2}v_{Tx}}\omega_p^2 \int \frac{\sigma^2}{\sigma - \frac{\omega}{k\sqrt{2}v_{Tx}}} \frac{\mathrm{e}^{-\sigma^2}}{\sqrt{\pi}}\,\mathrm{d}\sigma$$
$$D_{yy}(k,\omega) = \omega^2 - \frac{k^2}{\mu_0\varepsilon_0} + \omega_p^2 v_{Ty}^2 \int \frac{1}{\sigma - \frac{\omega}{k\sqrt{2}v_{Tx}}} \left(\frac{\sigma}{v_{Tx}^2} + \frac{\frac{\omega}{k\sqrt{2}v_{Tx}} - \sigma}{v_{Ty}^2}\right) \frac{\mathrm{e}^{-\sigma^2}}{\sqrt{\pi}}\,\mathrm{d}\sigma,$$
$$D_{zz}(k,\omega) = \omega^2 - \frac{k^2}{\mu_0\varepsilon_0} + \omega_p^2 v_{Tz}^2 \int \frac{1}{\sigma - \frac{\omega}{k\sqrt{2}v_{Tx}}} \left(\frac{\sigma}{v_{Tx}^2} + \frac{\frac{\omega}{k\sqrt{2}v_{Tx}} - \sigma}{v_{Tz}^2}\right) \frac{\mathrm{e}^{-\sigma^2}}{\sqrt{\pi}}\,\mathrm{d}\sigma.$$

Last, we expand these integrals and introduce $\zeta = \frac{\omega}{k\sqrt{2}v_{Tx}}$,

$$
\begin{aligned}
D_{xx}(k,\omega) &= \omega^2 + 2\zeta\omega_p^2 \left[0 + \zeta\left(1 + \frac{\zeta}{\sqrt{\pi}}\int \frac{\mathrm{e}^{-\sigma^2}}{\sigma-\zeta}\,\mathrm{d}\sigma\right)\right] \\
D_{yy}(k,\omega) &= \omega^2 - \frac{k^2}{\mu_0\varepsilon_0} + \omega_p^2 \left[\frac{v_{Ty}^2}{v_{Tx}^2}\left(1 + \frac{\zeta}{\sqrt{\pi}}\int \frac{\mathrm{e}^{-\sigma^2}}{\sigma-\zeta}\,\mathrm{d}\sigma\right)\right. \\
&\quad \left. + \left(\frac{\zeta}{\sqrt{\pi}}\int \frac{\mathrm{e}^{-\sigma^2}}{\sigma-\zeta}\,\mathrm{d}\sigma - \left(1 + \frac{\zeta}{\sqrt{\pi}}\int \frac{\mathrm{e}^{-\sigma^2}}{\sigma-\zeta}\,\mathrm{d}\sigma\right)\right)\right], \\
D_{zz}(k,\omega) &= \omega^2 - \frac{k^2}{\mu_0\varepsilon_0} + \omega_p^2 \left[\frac{v_{Tz}^2}{v_{Tx}^2}\left(1 + \frac{\zeta}{\sqrt{\pi}}\int \frac{\mathrm{e}^{-\sigma^2}}{\sigma-\zeta}\,\mathrm{d}\sigma\right)\right. \\
&\quad \left. + \left(\frac{\zeta}{\sqrt{\pi}}\int \frac{\mathrm{e}^{-\sigma^2}}{\sigma-\zeta}\,\mathrm{d}\sigma - \left(1 + \frac{\zeta}{\sqrt{\pi}}\int \frac{\mathrm{e}^{-\sigma^2}}{\sigma-\zeta}\,\mathrm{d}\sigma\right)\right)\right],
\end{aligned}
$$

where we used (A.5a) and (A.5b).

Inserting the Zeta-function (A.2) leads to

$$
\begin{aligned}
D_{xx}(k,\omega) &= \omega^2 + 2\omega_p^2\zeta^2\left(1 + \zeta Z(\zeta)\right), \\
D_{yy}(k,\omega) &= \omega^2 - \frac{k^2}{\mu_0\varepsilon_0} + \omega_p^2\left(\frac{v_{Ty}^2}{v_{Tx}^2}\left(1 + \zeta Z(\zeta)\right) - 1\right), \\
D_{zz}(k,\omega) &= \omega^2 - \frac{k^2}{\mu_0\varepsilon_0} + \omega_p^2\left(\frac{v_{Tz}^2}{v_{Tx}^2}\left(1 + \zeta Z(\zeta)\right) - 1\right).
\end{aligned}
$$

Dividing the determinant by ω^2 yields (18.14). □

18.4 2D Dispersion Relation

The general procedure is taken from [22] whereas the treatment of the temperature gradient is reviewed in [11]. Since we want to use the dispersion relations for a curvilinear setting, where we only have two periodic coordinate directions, we focus on a two dimensional wave vector. Conventionally, we consider the second and third coordinate directions as periodic angles. Thus, without loss of generality, we assume that $\mathbf{k} = (0, k_\perp, k_z)^\top$.

Let us consider an external electric that equals zero, $\mathbf{E}_0 = 0$, a constant external magnetic field $\mathbf{B}_0 = \hat{\mathbf{e}}_z B_0$ and an equilibrium function $f_0(\mathbf{x}, v_\perp, v_z)$, where $v_\perp = \sqrt{v_x^2 + v_y^2}$. We can write the linearised Vlasov equation (18.1) as the total time derivative of δf with a source term on the right-hand side,

$$
\frac{\mathrm{d}}{\mathrm{d}t}\delta f = \left(\partial_t + \mathbf{v}\cdot\nabla_{\mathbf{x}} + \frac{q}{m}(\mathbf{v}\times\mathbf{B}_0)\cdot\nabla_{\mathbf{v}}\right)\delta f = -\frac{q}{m}(\delta\mathbf{E} + \mathbf{v}\times\delta\mathbf{B})\cdot\nabla_{\mathbf{v}} f_0.
$$

With the method of characteristics, which is described in the appendix A, we solve for δf by

integrating along the particle characteristics,

$$\delta f = -\frac{q}{m}\int (\delta\mathbf{E}(\mathbf{x}',t') + \mathbf{v}'(t')\times\delta\mathbf{B}(\mathbf{x}',t'))\cdot\nabla_{\mathbf{v}'}f_0(\mathbf{v}')\,\mathrm{d}t'. \tag{18.15}$$

We consider the unperturbed particle characteristics

$$\begin{aligned}\dot{\mathbf{x}}'(t') &= \mathbf{v}'(t'),\\ \dot{\mathbf{v}}'(t') &= \mathbf{v}'(t')\times\mathbf{B}_0\end{aligned}$$

with the initial conditions $\mathbf{x}'(t)=\mathbf{x}, \mathbf{v}'(t)=\mathbf{v}$.

These trajectories are integrated as

$$\mathbf{x}'(t') = \mathbf{x} + \begin{pmatrix} -\frac{v_\perp}{\Omega_0}\left(\cos(\theta+\Omega_0(t'-t))-\cos\theta\right)\\ \frac{v_\perp}{\Omega_0}\left(\sin(\theta+\Omega_0(t'-t))-\sin\theta\right)\\ v_z(t'-t)\end{pmatrix}, \tag{18.16}$$

$$\mathbf{v}'(t') = \begin{pmatrix} v_\perp\sin(\theta+\Omega_0(t'-t))\\ v_\perp\cos(\theta+\Omega_0(t'-t))\\ v_z\end{pmatrix}, \tag{18.17}$$

where $\Omega_0 = \frac{qB_0}{m}$ is the gyrofrequency of the magnetic background field. For the perturbed quantities, we make an ansatz with a Fourier–Laplace transformation as in (A.1),

$$\begin{aligned}\delta f(\mathbf{x},t) &= \int \widehat{\delta f}(k_\perp,k_z,\omega)\exp\left(-i\omega t + i(k_\perp y + k_z z)\right)\,\mathrm{d}k_\perp\,\mathrm{d}k_z\,\mathrm{d}\omega,\\ \delta\mathbf{E}(\mathbf{x},t) &= \int \widehat{\delta\mathbf{E}}(k_\perp,k_z,\omega)\exp\left(-i\omega t + i(k_\perp y + k_z z)\right)\,\mathrm{d}k_\perp\,\mathrm{d}k_z\,\mathrm{d}\omega,\\ \delta\mathbf{B}(\mathbf{x},t) &= \int \widehat{\delta\mathbf{B}}(k_\perp,k_z,\omega)\exp\left(-i\omega t + i(k_\perp y + k_z z)\right)\,\mathrm{d}k_\perp\,\mathrm{d}k_z\,\mathrm{d}\omega.\end{aligned}$$

First, we insert the Fourier–Laplace representation into (18.15) and solve for $\widehat{\delta f}$,

$$\widehat{\delta f} = -\frac{q}{m}\int_{-\infty}^{t}(\widehat{\delta\mathbf{E}} + \mathbf{v}'\times\widehat{\delta\mathbf{B}})\cdot\nabla_{\mathbf{v}'}f_0\exp(i(k_\perp(y'-y)+k_z(z'-z))-\omega(t'-t))\,\mathrm{d}t'.$$

Second, we substitute $\tau = (t'-t)$ to use the solution of the particle position characteristics (18.16),

$$\widehat{\delta f} = -\frac{q}{m}\int_{-\infty}^{0}\left(\widehat{\delta\mathbf{E}} + \mathbf{v}'\times\widehat{\delta\mathbf{B}}\right)\cdot\nabla_{\mathbf{v}'}f_0\exp\left(\frac{ik_\perp v_\perp}{\Omega_0}\left(\sin(\theta+\Omega_0\tau)-\sin(\theta)\right)+i(k_z v_z-\omega)\tau\right)\,\mathrm{d}\tau. \tag{18.18}$$

Furthermore, we transform the velocity derivative and insert the solution of the velocity trajectory (18.17). Therefore, we assume an equilibrium function f_0 as in (18.4), where we approximate the temperature and density profiles and their gradients with constant values for simplification,

$$\frac{\partial f_0}{\partial_{v_x'}} = \frac{\partial f_0}{\partial_{v_\perp}} \frac{\partial v_\perp}{\partial v_x'} = \partial_{v_\perp} f_0 \frac{v_x'}{v_\perp} = \sin(\theta + \Omega_0 \tau) \partial_{v_\perp} f_0,$$
$$\frac{\partial f_0}{\partial_{v_y'}} = \frac{1}{\Omega_0} \frac{\partial f_0}{\partial x} + \frac{\partial f_0}{\partial v_\perp} \frac{\partial v_\perp}{\partial v_y'} = \frac{\partial_x f_0}{\Omega_0} + \partial_{v_\perp} f_0 \frac{v_y'}{v_\perp} = \frac{\partial_x f_0}{\Omega_0} + \cos(\theta + \Omega_0 \tau) \partial_{v_\perp} f_0.$$

Then, we rearrange the integral using the definition of the Bessel function (A.3). Additionally, we use the exponential representations of cosine and sinus,

$$\cos(\theta + \Omega_0 \tau) = \frac{\mathrm{e}^{i(\theta+\Omega_0\tau)} + \mathrm{e}^{-i(\theta+\Omega_0\tau)}}{2},$$
$$\sin(\theta + \Omega_0 \tau) = \frac{\mathrm{e}^{i(\theta+\Omega_0\tau)} - \mathrm{e}^{-i(\theta+\Omega_0\tau)}}{2i},$$

to calculate the following terms:

$$\begin{aligned}
&\cos(\theta + \Omega_0 \tau) \exp\left(\frac{i k_\perp v_\perp}{\Omega_0} \left(\sin(\theta + \Omega_0 \tau) - \sin(\theta) \right) \right) \\
=& \frac{\mathrm{e}^{i(\theta+\Omega_0\tau)} + \mathrm{e}^{-i(\theta+\Omega_0\tau)}}{2} \sum_{n,n'=-\infty}^{\infty} J_n\left(\frac{k_\perp v_\perp}{\Omega_0} \right) J_{n'}\left(\frac{k_\perp v_\perp}{\Omega_0} \right) \mathrm{e}^{i(n-n')\theta + in\Omega_0\tau} \\
=& \sum_{n,n'=-\infty}^{\infty} J_n\left(\frac{k_\perp v_\perp}{\Omega_0} \right) J_{n'}\left(\frac{k_\perp v_\perp}{\Omega_0} \right) \frac{\mathrm{e}^{i((n+1)-n')\theta + i(n+1)\Omega_0\tau} + \mathrm{e}^{i((n-1)-n')\theta + i(n-1)\Omega_0\tau}}{2} \\
=& \sum_{n,n'=-\infty}^{\infty} \frac{J_{n-1}\left(\frac{k_\perp v_\perp}{\Omega_0} \right) + J_{n+1}\left(\frac{k_\perp v_\perp}{\Omega_0} \right)}{2} J_{n'}\left(\frac{k_\perp v_\perp}{\Omega_0} \right) \mathrm{e}^{i(n-n')\theta + in\Omega_0\tau},
\end{aligned}$$

$$\begin{aligned}
&\sin(\theta + \Omega_0 \tau) \exp\left(\frac{i k_\perp v_\perp}{\Omega_0} \left(\sin(\theta + \Omega_0 \tau) - \sin(\theta) \right) \right) \\
=& \frac{\mathrm{e}^{i(\theta+\Omega_0\tau)} - \mathrm{e}^{-i(\theta+\Omega_0\tau)}}{2i} \sum_{n,n'=-\infty}^{\infty} J_n\left(\frac{k_\perp v_\perp}{\Omega_0} \right) J_{n'}\left(\frac{k_\perp v_\perp}{\Omega_0} \right) \mathrm{e}^{i(n-n')\theta + in\Omega_0\tau} \\
=& \sum_{n,n'=-\infty}^{\infty} J_n\left(\frac{k_\perp v_\perp}{\Omega_0} \right) J_{n'}\left(\frac{k_\perp v_\perp}{\Omega_0} \right) \frac{\mathrm{e}^{i((n+1)-n')\theta + i(n+1)\Omega_0\tau} - \mathrm{e}^{i((n+1)-n')\theta + i(n+1)\Omega_0\tau}}{2i} \\
=& \sum_{n,n'=-\infty}^{\infty} \frac{J_{n-1}\left(\frac{k_\perp v_\perp}{\Omega_0} \right) - J_{n+1}\left(\frac{k_\perp v_\perp}{\Omega_0} \right)}{2i} J_{n'}\left(\frac{k_\perp v_\perp}{\Omega_0} \right) \mathrm{e}^{i(n-n')\theta + in\Omega_0\tau}.
\end{aligned}$$

Last, we set $b = \frac{k_\perp v_\perp}{\Omega_0}$ and use the identities (A.3) and (A.2) to obtain

$$\cos(\theta + \Omega_0\tau) \exp\left(\frac{ik_\perp v_\perp}{\Omega_0}\left(\sin(\theta + \Omega_0\tau) - \sin(\theta)\right)\right) = \sum_{n,n'=-\infty}^{\infty} \frac{n}{b} J_n(b) J_{n'}(b)\, \mathrm{e}^{i(n-n')\theta + in\Omega_0\tau},$$

$$\sin(\theta + \Omega_0\tau) \exp\left(\frac{ik_\perp v_\perp}{\Omega_0}\left(\sin(\theta + \Omega_0\tau) - \sin(\theta)\right)\right) = \sum_{n,n'=-\infty}^{\infty} i\frac{d}{db} J_n(b) J_{n'}(b)\, \mathrm{e}^{i(n-n')\theta + in\Omega_0\tau}.$$

Then, we insert the result into the integral term (18.18),

$$\widehat{\delta f} = -\frac{q}{m}\int_{-\infty}^{0} \sum_{n,n'=-\infty}^{\infty} \left(\widehat{\delta\mathbf{E}} + \mathbf{v}' \times \widehat{\delta\mathbf{B}}\right) \cdot \begin{pmatrix} \frac{\partial f_0}{\partial v_\perp} i\frac{d}{db} J_n(b) \\ (\frac{\partial_x f_0}{\Omega_0} + \frac{\partial f_0}{\partial v_\perp}\frac{n}{b}) J_n(b) \\ \frac{\partial f_0}{\partial v_z} J_n(b) \end{pmatrix} J_{n'}(b)\, \mathrm{e}^{i(n-n')\theta + i(n\Omega_0 + k_z v_z - \omega)\tau}\, \mathrm{d}\tau. \tag{18.19}$$

18.4.1 Electrostatic Dispersion

Proposition 18.1. *In an electrostatic setting, the linearised charge density for a species s is computed as*

$$\widehat{\delta\rho}_s = -\widehat{\delta\Phi}\frac{q^2 N}{m_s^2 v_{Ts}^2}\left(1 + \left(1 - \frac{\omega_T'}{\omega}\right)\zeta_0 \sum_{n=-\infty}^{\infty} Z(\zeta_n)\Lambda_n(\xi)\right), \tag{18.20}$$

where $\zeta_n = \frac{\omega - n\Omega_0}{k_z\sqrt{2}v_{Ts}}$ and $\xi = \frac{k_\perp^2 v_{Ts}^2}{\Omega_0^2}$.

Proof. Let us assume an electrostatic system. Therefore, we set $\widehat{\delta\mathbf{B}} = 0$ and the electric field is computed as $\mathbf{E} = -\nabla\Phi$, from which follows $\widehat{\delta\mathbf{E}} = -i\mathbf{k}\widehat{\delta\Phi}$.

Then, we can solve the time integral from (18.19),

$$\begin{aligned}\widehat{\delta f} &= -\frac{q}{m}\sum_{n,n'=-\infty}^{\infty} -i\mathbf{k}\widehat{\delta\Phi} \cdot \begin{pmatrix} \frac{\partial f_{0s}}{\partial v_\perp} i\frac{d}{db} J_n(b) \\ (\frac{\partial_x f_{0s}}{\Omega_0} + \frac{\partial f_{0s}}{\partial v_\perp}\frac{n}{b}) J_n(b) \\ \frac{\partial f_{0s}}{\partial v_z} J_n(b) \end{pmatrix} J_{n'}(b)\, \frac{\mathrm{e}^{i(n-n')\theta}}{i(n\Omega_0 + k_z v_z - \omega)} \\ &= \frac{q}{m}\sum_{n,n'=-\infty}^{\infty} \left(\frac{k_\perp}{\Omega_0}\frac{\partial f_{0s}}{\partial x} + \frac{k_\perp n}{b}\frac{\partial f_{0s}}{\partial v_\perp} + k_z\frac{\partial f_{0s}}{\partial v_z}\right) \frac{J_n(b) J_{n'}(b) \mathrm{e}^{i(n-n')\theta}}{n\Omega_0 + k_z v_z - \omega}\widehat{\delta\Phi}.\end{aligned}$$

We compute the linearised charge density from (18.8) by inserting the representation of $\widehat{\delta f}$,

$$\widehat{\delta\rho}_s = \frac{q^2}{m_s}\widehat{\delta\Phi}\int \sum_{n,n'=-\infty}^{\infty}\left(\frac{k_\perp}{\Omega_0}\frac{\partial f_{0s}}{\partial_x} + \frac{k_\perp n}{b}\frac{\partial f_{0s}}{\partial_{v_\perp}} + k_z\frac{\partial f_{0s}}{\partial_{v_z}}\right)\frac{J_n(b)J_{n'}(b)\mathrm{e}^{i(n-n')\theta}}{n\Omega_0 + k_z v_z - \omega}\,\mathrm{d}\mathbf{v}.$$

To solve the velocity integral, first, we insert the initial distribution f_{0s} from (18.4) with the constant approximations of the temperature and density profiles and their gradients and compute the partial velocity derivatives,

$$\widehat{\delta\rho} = \widehat{\delta\Phi}\frac{q^2}{m_s}\int \sum_{n,n'=-\infty}^{\infty}\left(\frac{m_s}{T_s}\omega'_{Ts}f_{0s} - \frac{k_\perp n}{b}\frac{m_s v_\perp}{T_s}f_{0s} - k_z\frac{m v_z}{T_s}f_{0s}\right)\frac{J_n(b)J_{n'}(b)\mathrm{e}^{i(n-n')\theta}}{n\Omega_0 + k_z v_z - \omega}\,\mathrm{d}\mathbf{v},$$

where $\omega'_{Ts} = \frac{k_\perp T_s}{q_s B_0}\left(\frac{\mathrm{d}N}{\mathrm{d}x}\partial_N + \frac{\mathrm{d}T}{\mathrm{d}x}\partial_T\right)$. Second, we transform the velocity integral to cylindrical coordinates via

$$\int_{\mathbb{R}^3}\mathrm{d}\mathbf{v} = \int_0^\infty\int_0^{2\pi}\int_{-\infty}^{\infty} v_\perp\,\mathrm{d}v_\perp\,\mathrm{d}\theta\,\mathrm{d}v_z.$$

The double sum breaks down due to the integral

$$\int_0^{2\pi}\exp(i(n-n')\theta)\,\mathrm{d}\theta = 2\pi\delta_{n,n'}$$

and setting $v_{Ts} = \sqrt{\frac{T_s}{m_s}}$ we obtain

$$\widehat{\delta\rho} = -\widehat{\delta\Phi}\frac{q^2}{m_s^2 v_{Ts}^2}\int\sum_{n=-\infty}^{\infty} J_n^2\left(\frac{k_\perp v_\perp}{\Omega_0}\right)\frac{n\Omega_0 - \omega'_T + k_z v_z}{n\Omega_0 + k_z v_z - \omega}\frac{2\pi v_\perp N}{\left(\sqrt{2\pi}v_{Ts}\right)^3}\mathrm{e}^{-\frac{(v_\perp^2+v_z^2)}{2v_{Ts}^2}}\,\mathrm{d}v_\perp\,\mathrm{d}v_z.$$

For the integral over v_z, we substitute $\frac{v_z}{\sqrt{2}v_{Ts}} = \tau$ and for the integral over $v_\perp$, $\frac{v_\perp}{\sqrt{2}v_{Ts}} = \sigma$, which leads to

$$\widehat{\delta\rho} = -\widehat{\delta\Phi}\frac{2q^2N}{m_s^2 v_{Ts}^2\sqrt{\pi}}\sum_{n=-\infty}^{\infty}\int_0^\infty \sigma\mathrm{e}^{-\sigma^2}J_n^2\left(\frac{k_\perp\sqrt{2}v_{Ts}\sigma}{\Omega_0}\right)\mathrm{d}\sigma\int_{-\infty}^{\infty}\frac{n\Omega_0 - \omega'_T + k_z\sqrt{2}v_{Ts}\tau}{n\Omega_0 + k_z\tau\sqrt{2}v_{Ts} - \omega}\mathrm{e}^{-\tau^2}\,\mathrm{d}\tau.$$

Then, the integral over σ is computed with (A.4a) as

$$\int\sigma\mathrm{e}^{-\sigma^2}J_n^2\left(\frac{k_\perp\sqrt{2}v_{Ts}\sigma}{\Omega_0}\right)\mathrm{d}\sigma = \frac{1}{2}\Lambda_n\left(\xi\right),$$

where $\xi = \frac{k_\perp^2 v_{Ts}^2}{\Omega_0^2}$ and $\Lambda_n(\xi)$ is the modified Bessel function of the first kind. Next, we define

$\zeta_n = \frac{\omega - n\Omega_0}{k_z\sqrt{2}v_{Ts}}$ and compute the integral over τ as

$$\begin{aligned}\int_{-\infty}^{\infty} \frac{n\Omega_0 - \omega_T' + k_z\sqrt{2}v_{Ts}\tau}{n\Omega_0 + k_z\sqrt{2}v_{Ts}\tau - \omega} \mathrm{e}^{-\tau^2}\,\mathrm{d}\tau &= \int_{-\infty}^{\infty} \frac{\tau + \frac{n\Omega_0 - \omega_T'}{k_z\sqrt{2}v_{Ts}}}{\tau - \frac{\omega - n\Omega_0}{k_z\sqrt{2}v_{Ts}}} \mathrm{e}^{-\tau^2}\,\mathrm{d}\tau \\ &= \int_{-\infty}^{\infty} \mathrm{e}^{-\tau^2}\,\mathrm{d}\tau + \frac{\omega - \omega_T'}{k_z\sqrt{2}v_{Ts}} \int_{-\infty}^{\infty} \frac{\mathrm{e}^{-\tau^2}}{\tau - \frac{\omega - n\Omega_0}{k_z\sqrt{2}v_{Ts}}}\,\mathrm{d}\tau \\ &= \sqrt{\pi}\left(1 + \left(1 - \frac{\omega_T'}{\omega}\right)\zeta_0 Z(\zeta_n)\right).\end{aligned}$$

Putting these results together, we obtain

$$\widehat{\delta\rho} = -\widehat{\delta\Phi}\frac{q^2 N}{m_s^2 v_{Ts}^2} \sum_{n=-\infty}^{\infty} \left(1 + \left(1 - \frac{\omega_T'}{\omega}\right)\zeta_0 Z(\zeta_n)\right)\Lambda_n(\xi).$$

Observing that $\sum_{n=-\infty}^{\infty} \Lambda_n(\xi) = 1\ \forall \xi \in \mathbb{R}$ yields the proposition. □

Corrolary 18.2. *The dispersion relation of the electrostatic Vlasov–Poisson system for one species s takes the following form with $\zeta_n = \frac{\omega - n\Omega_0}{k_z\sqrt{2}v_{Ts}}$ and $\xi = \frac{k_\perp^2 v_{Ts}^2}{\Omega_0^2}$:*

$$D = k_\perp^2 + k_z^2 + \frac{\omega_{ps}^2}{v_{Ts}^2}\left(1 + \left(1 - \frac{\omega_T'}{\omega}\right)\zeta_0 \sum_{n=-\infty}^{\infty} Z(\zeta_n)\Lambda_n(\xi)\right). \tag{18.21}$$

Proof. We couple the electrostatic collisionless Vlasov equation with the Poisson equation. Thus, we insert the representation of $\widehat{\delta\rho}$ from (18.20) into the linearised Poisson equation (18.7),

$$k^2\widehat{\delta\Phi} = -\widehat{\delta\Phi}\frac{q^2 N}{\varepsilon_0 m_s^2 v_{Ts}^2}\left(1 + \left(1 - \frac{\omega_T'}{\omega}\right)\zeta_0 \sum_{n=-\infty}^{\infty} Z(\zeta_n)\Lambda_n(\xi)\right).$$

We solve the equation for $\widehat{\delta\Phi}$ and get the form $D(\mathbf{k}, \omega, x)\widehat{\delta\Phi} = 0$ with

$$D(\mathbf{k}, \omega, x) = k^2 + \frac{\omega_{ps}^2}{v_{Ts}^2}\left(1 + \left(1 - \frac{\omega_T'}{\omega}\right)\zeta_0 \sum_{n=-\infty}^{\infty} Z(\zeta_n)\Lambda_n(\xi)\right).$$

□

Corrolary 18.3. *The dispersion relation of the quasi-neutral Vlasov system can be written as*

$$D(k_\perp, k_z, \omega) = \frac{N}{T_e} + \frac{N}{T_i}\left(1 + \left(1 - \frac{\omega_T'}{\omega}\right)\zeta_0 \sum_{n=-\infty}^{\infty} Z(\zeta_n)\Lambda_n(\xi)\right), \tag{18.22}$$

where $\zeta_n = \frac{\omega - n\Omega_0}{k_z\sqrt{\frac{2T_i}{m_i}}}$ *and* $\xi = \frac{k_\perp^2 T_i}{\Omega_0^2 m_i}$.

Proof. We couple the electrostatic collisionless Vlasov equation for ions with the quasi-neutrality equations. Therefore, we insert the representation of $\widehat{\delta\rho}_i$ from (18.20) into the linearised quasi-neutrality equation (18.9),

$$\frac{q^2 N \widehat{\delta\Phi}}{T_e} = -\widehat{\delta\Phi}\frac{q^2 N}{T_i}\left(1 + \left(1 - \frac{\omega_T'}{\omega}\right)\zeta_0 \sum_{n=-\infty}^{\infty} Z(\zeta_n)\Lambda_n(\xi)\right).$$

We solve this for $\widehat{\delta\Phi}$ and get the form $D(\mathbf{k}, \omega, x)\widehat{\delta\Phi} = 0$, which leads to (18.22). □

Remark 18.4. *We can expand the dispersion relation to*

$$D(k_\perp, k_z, \omega) = \frac{N}{T_e} + \frac{N}{T_i}\left[1 + \zeta_0 \sum_{n=-\infty}^{\infty}\left(Z(\zeta_n)\Lambda_n(\xi) - \frac{k_\perp T_i \kappa_{T_i}}{q_i B_0 \omega}\partial_{T_i}(\zeta_0 Z(\zeta_n)\Lambda_n(\xi))\right)\right],$$

where we assume $\frac{\mathrm{d}N}{\mathrm{d}t} = 0$ *and the temperature derivative is computed as*

$$\partial_{T_i}\left(\zeta_0 Z(\zeta_n)\Lambda_n(\xi)\right) = -\frac{\zeta_0}{2T_i}\left[\left(Z(\zeta_n) + \zeta_n Z'(\zeta_n)\right)\Lambda_n(\xi) - 2\xi Z(\zeta_n)\Lambda_n'(\xi)\right].$$

This leads to

$$\begin{aligned} D = \frac{N}{T_e} + \frac{N}{T_i}\Bigg[1 + \zeta_0 \sum_{n=-\infty}^{\infty} &(Z(\zeta_n)\Lambda_n(\xi) \\ &+ \frac{k_\perp}{2q_i B_0 \omega}\frac{\mathrm{d}T_i}{\mathrm{d}x}[(Z(\zeta_n) + \zeta_n Z'(\zeta_n))\Lambda_n(\xi) - 2\xi Z(\zeta_n)\Lambda_n'(\xi)]\Big)\Bigg]. \end{aligned}$$

We insert the derivative of the Zeta function to obtain

$$\begin{aligned} D = \frac{N}{T_e} + \frac{N}{T_i}\Bigg[1 + \zeta_0 \sum_{n=-\infty}^{\infty} &(Z(\zeta_n)\Lambda_n(\xi) \\ &+ \frac{k_\perp}{2q_i B_0 \omega}\frac{\mathrm{d}T_i}{\mathrm{d}x}[Z(\zeta_n)\Lambda_n(\xi) - 2\zeta_n(1 + \zeta_n Z(\zeta_n))\Lambda_n(\xi) - 2\xi Z(\zeta_n)\Lambda_n'(\xi)]\Big)\Bigg]. \end{aligned}$$

For a small argument $\xi \ll 1$*, the sum is dominated by the* $0-$*th Bessel function* Λ_0*. Therefore, we break down the sum to* $n = 0$*. Additionally, we have*

$$\lim_{\xi \to 0}\Lambda_0(\xi) = 1 - \xi.$$

This leads to the following simplified dispersion relation:

$$D = \frac{N}{T_e} + \frac{N}{T_i}\left(1 + \zeta_0 Z(\zeta_0) + \frac{k_\perp}{2q_i B_0 \omega}\frac{\mathrm{d}T_i}{\mathrm{d}x}\zeta_0\left[Z(\zeta_0) - 2\zeta_0(1+\zeta_0 Z(\zeta_0))\right]\right).$$

18.4.2 Electromagnetic Dispersion

Proposition 18.5. *For a constant temperature and density, the current has the following entries*

$$\begin{aligned}
J_{xx} =& -i\varepsilon_0\omega_{ps}^2 \sum_{n=-\infty}^{\infty} \frac{\zeta_0}{\omega} Z(\zeta_n)\left(-2G(n-1,n+1,3,\sqrt{2\xi})\right.\\
&\left.\times \frac{\xi}{4}\left[\Lambda_{n+2}(\xi) + \left(\frac{4}{\sqrt{2\xi}} - 2\right)\Lambda_{n+1}(\xi) + 2\Lambda_n(\xi) + \left(\frac{4}{\sqrt{2\xi}} - 2\right)\Lambda_{n-1}(\xi) + \Lambda_{n-2}(\xi)\right]\right),\\
J_{xy} =& -\varepsilon_0\omega_{ps}^2 \sum_{n=-\infty}^{\infty} \frac{\sqrt{2}n\Omega_0}{v_{T_\perp}k_\perp}\frac{\zeta_0}{\omega} Z(\zeta_n)\left(G(n-1,n,2,\sqrt{2\xi}) - G(n+1,n,2,\sqrt{2\xi})\right),\\
J_{xz} =& -\varepsilon_0\omega_{ps}^2 \sum_{n=-\infty}^{\infty} \frac{2v_{T_\perp}}{v_{Tz}}\frac{\zeta_0}{\omega}[1+\zeta_n Z(\zeta_n)]\left(G(n-1,n,2,\sqrt{2\xi}) - G(n+1,n,2,\sqrt{2\xi})\right),\\
J_{yx} =& -J_{xy},\\
J_{yy} =& -i\varepsilon_0\omega_{ps}^2 \sum_{n=-\infty}^{\infty} \frac{n^2\Omega_0^2}{\omega v_{T_\perp}^2 k_\perp^2}\Lambda_n(\xi)\zeta_0 Z(\zeta_n),\\
J_{yz} =& -i\varepsilon_0\omega_{ps}^2 \sum_{n=-\infty}^{\infty} \frac{n\Omega_0}{v_{Tz}^2 k_z k_\perp}\Lambda_n(\xi)[1+\zeta_n Z(\zeta_n)],\\
J_{zx} =& -\frac{v_{Tz}^2}{v_{T_\perp}^2}J_{xz},\\
J_{zy} =& \frac{v_{Tz}^2}{v_{T_\perp}^2}J_{yz},\\
J_{zz} =& -i2\varepsilon_0\omega_{ps}^2 \sum_{n=-\infty}^{\infty} \Lambda_n(\xi)\frac{\zeta_0}{\omega}\zeta_n[1+\zeta_n Z(\zeta_n)],
\end{aligned}$$

where $\xi = \frac{k_\perp^2 v_{T_\perp}^2}{\Omega_0^2}$ *and* $\zeta_n = \frac{\omega - n\Omega_0}{k_z\sqrt{2}v_{Tz}}$.

Proof. Let us assume that the temperature and density profiles are constant. This leads to $\partial_x f_0 = 0$ and

$$\widehat{\delta f} = -\frac{q}{m}\int_{-\infty}^{0}\sum_{n,n'=-\infty}^{\infty}\left(\widehat{\delta\mathbf{E}} + \mathbf{v}'\times\widehat{\delta\mathbf{B}}\right)\cdot\begin{pmatrix}\frac{\partial f_0}{\partial v_\perp} i\frac{dJ_n(b)}{db}\\ \frac{\partial f_0}{\partial v_\perp}\frac{n}{b}J_n(b)\\ \frac{\partial f_0}{\partial v_z}J_n(b)\end{pmatrix} J_{n'}(b)\,\mathrm{e}^{i(n-n')\theta + i(n\Omega_0 + k_z v_z - \omega)\tau}\,\mathrm{d}\tau.$$

In the Lorentz force, we can substitute the magnetic field for the electric field via (18.5a) and solve for it,

$$\begin{aligned}\widehat{\delta f} = &- \frac{q}{m} \sum_{n,n'=-\infty}^{\infty} J_{n'}(b) \mathrm{e}^{i(n-n')\theta} \int_{-\infty}^{0} \mathrm{e}^{i(n\Omega_0 + k_z v_z - \omega)\tau} \, \mathrm{d}\tau \\ &\left(iJ_n'(b) \left[\partial_{v_\perp} f_0 + \frac{k_z}{\omega} (v_\perp \partial_{v_z} f_0 - v_z \partial_{v_\perp} f_0) \right] \widehat{E}_x \right. \\ &+ \frac{n}{b} J_n(b) \left[\partial_{v_\perp} f_0 + \frac{k_z}{\omega} \left(v_\perp \partial_{v_z} f_0 - v_z \partial_{v_\perp} f_0 \right) \right] \widehat{E}_y \\ &\left. + \, J_n(b) \left[\partial_{v_z} f_0 - \frac{n k_\perp}{b\omega} (v_\perp \partial_{v_z} f_0 - v_z \partial_{v_\perp} f_0) \right] \widehat{E}_z \right).\end{aligned}$$

Then, we solve the time integral and obtain

$$\begin{aligned}\widehat{\delta f} = &- \frac{q}{m} \sum_{n,n'=-\infty}^{\infty} J_{n'}\left(b\right) \frac{\mathrm{e}^{i(n-n')\theta}}{i(n\Omega_0 + k_z v_z - \omega)} \\ &\left(iJ_n'(b) \left[\partial_{v_\perp} f_0 + \frac{k_z}{\omega} (v_\perp \partial_{v_z} f_0 - v_z \partial_{v_\perp} f_0) \right] \widehat{E}_x \right. \\ &+ \frac{n}{b} J_n(b) \left[\partial_{v_\perp} f_0 + \frac{k_z}{\omega} \left(v_\perp \partial_{v_z} f_0 - v_z \partial_{v_\perp} f_0 \right) \right] \widehat{E}_y \\ &\left. + \, J_n(b) \left[\partial_{v_z} f_0 - \frac{n k_\perp}{b\omega} (v_\perp \partial_{v_z} f_0 - v_z \partial_{v_\perp} f_0) \right] \widehat{E}_z \right).\end{aligned}$$

Now, we are able to compute the source term $\widehat{\delta \mathbf{J}}$ for Ampère's equation. Therefore, we transform the integral over $\mathbf{v}$ into the integral over $v_\perp, \theta, v_z$,

$$\widehat{\delta \mathbf{J}} = q \int_{\mathbb{R}^3} \mathbf{v} \widehat{\delta f} \, \mathrm{d}\mathbf{v} = q \int_0^\infty \int_0^{2\pi} \int_{-\infty}^{\infty} \mathbf{v} \widehat{\delta f} v_\perp \, \mathrm{d}v_\perp \, \mathrm{d}\theta \, \mathrm{d}v_z.$$

As before, we write the velocity in cylindrical coordinates and use the identity

$$\sum_{n'=-\infty}^{\infty} J_{n'}(b) \int_0^{2\pi} \mathrm{e}^{i(n-n')\theta} \begin{pmatrix} v_\perp \sin\theta \\ v_\perp \cos\theta \\ v_z \end{pmatrix} \mathrm{d}\theta = 2\pi \sum_{n=-\infty}^{\infty} \begin{pmatrix} -iv_\perp J_n'(b) \\ \frac{n v_\perp}{b} J_n(b) \\ v_z J_n(b) \end{pmatrix}$$

given in [22] to obtain

$$\begin{aligned}\widehat{\delta\mathbf{J}} =& i\frac{q^2}{m}\int_0^\infty\int_{-\infty}^\infty\sum_{n=-\infty}^\infty \frac{2\pi}{n\Omega_0 + k_z v_z - \omega}\begin{pmatrix} -iv_\perp J_n'(b) \\ \frac{nv_\perp}{b}J_n(b) \\ v_z J_n(b)\end{pmatrix} \\ &\left(iJ_n'(b)\left[\partial_{v_\perp} f_0 + \frac{k_z}{\omega}(v_\perp\partial_{v_z} f_0 - v_z\partial_{v_\perp} f_0)\right]\widehat{E}_x\right. \\ &+ \frac{n}{b}J_n(b)\left[\partial_{v_\perp} f_0 + \frac{k_z}{\omega}\left(v_\perp\partial_{v_z} f_0 - v_z\partial_{v_\perp} f_0\right)\right]\widehat{E}_y \\ &\left.+\ J_n(b)\left[\partial_{v_z} f_0 - \frac{n\Omega_0}{v_\perp\omega}(v_\perp\partial_{v_z} f_0 - v_z\partial_{v_\perp} f_0)\right]\widehat{E}_z\right) v_\perp\,\mathrm{d}v_\perp\,\mathrm{d}v_z.\end{aligned}$$

Assuming an equilibrium function as in (18.3), we can compute the velocity gradient as

$$\begin{aligned}\partial_{v_\perp} f_0 &= -\frac{v_\perp}{v_{T_\perp}^2} f_0, \\ \partial_{v_z} f_0 &= -\frac{v_z}{v_{Tz}^2} f_0\end{aligned}$$

and following from that:

$$v_\perp\partial_{v_z} f_0 - v_z\partial_{v_\perp} f_0 = 0.$$

In this case, the current simplifies to

$$\begin{aligned}\widehat{\delta\mathbf{J}} =& -i\frac{q^2}{m}\int_0^\infty\int_{-\infty}^\infty\sum_{n=-\infty}^\infty \frac{2\pi}{n\Omega_0 + k_z v_z - \omega}\begin{pmatrix} -iv_\perp J_n'(b) \\ \frac{nv_\perp}{b}J_n(b) \\ v_z J_n(b)\end{pmatrix} \\ &\left(\frac{v_\perp}{v_{T_\perp}^2} iJ_n'(b)\widehat{E}_x + \frac{v_\perp}{v_{T_\perp}^2}\frac{n}{b}J_n(b)\widehat{E}_y + \frac{v_z}{v_{Tz}^2}J_n(b)\widehat{E}_z\right) f_0 v_\perp\,\mathrm{d}v_\perp\,\mathrm{d}v_z.\end{aligned}$$

We write this as the matrix vector product $\widehat{\delta\mathbf{J}} = J\widehat{\delta\mathbf{E}}$ with the matrix entries

$$
\begin{aligned}
J_{xx} =& -i\frac{q^2 2\pi}{m v_{T_\perp}^2}\int_0^\infty\int_{-\infty}^\infty\sum_{n=-\infty}^\infty \frac{v_\perp^3}{n\Omega_0 + k_z v_z - \omega} J_n'(b)^2 f_0 \,\mathrm{d}v_\perp \,\mathrm{d}v_z,\\
J_{xy} =& -J_{yx} = -\frac{q^2 2\pi}{m v_{T_\perp}^2}\int_0^\infty\int_{-\infty}^\infty\sum_{n=-\infty}^\infty \frac{n\Omega_0}{k_\perp}\frac{v_\perp^2}{n\Omega_0 + k_z v_z - \omega} J_n'(b) J_n(b) f_0 \,\mathrm{d}v_\perp \,\mathrm{d}v_z,\\
J_{xz} =& -\frac{v_{T_\perp}^2}{v_{Tz}^2}J_{zx} = -\frac{q^2 2\pi}{m v_{Tz}^2}\int_0^\infty\int_{-\infty}^\infty\sum_{n=-\infty}^\infty \frac{v_z v_\perp^2}{n\Omega_0 + k_z v_z - \omega} J_n'(b) J_n(b) f_0 \,\mathrm{d}v_\perp \,\mathrm{d}v_z,\\
J_{yy} =& -i\frac{q^2 2\pi}{m v_{T_\perp}^2}\int_0^\infty\int_{-\infty}^\infty\sum_{n=-\infty}^\infty \frac{n^2\Omega_0^2}{k_\perp^2}\frac{v_\perp}{n\Omega_0 + k_z v_z - \omega} J_n(b)^2 f_0 \,\mathrm{d}v_\perp \,\mathrm{d}v_z,\\
J_{yz} =& \frac{v_{T_\perp}^2}{v_{Tz}^2}J_{zy} = -i\frac{q^2 2\pi}{m v_{Tz}^2}\int_0^\infty\int_{-\infty}^\infty\sum_{n=-\infty}^\infty \frac{n\Omega_0}{k_\perp}\frac{v_\perp v_z}{n\Omega_0 + k_z v_z - \omega} J_n(b)^2 f_0 \,\mathrm{d}v_\perp \,\mathrm{d}v_z,\\
J_{zz} =& -i\frac{q^2 2\pi}{m v_{Tz}^2}\int_0^\infty\int_{-\infty}^\infty\sum_{n=-\infty}^\infty \frac{v_z^2 v_\perp}{n\Omega_0 + k_z v_z - \omega} J_n(b)^2 f_0 \,\mathrm{d}v_\perp \,\mathrm{d}v_z.
\end{aligned}
$$

Inserting f_0 from (18.3) yields

$$
\begin{aligned}
J_{xx} =& -i\frac{n_0 q^2 2\pi}{m v_{T_\perp}^2}\sum_{n=-\infty}^\infty\int_0^\infty \frac{v_\perp^3}{2\pi v_{T_\perp}^2}\mathrm{e}^{-\frac{v_\perp^2}{2v_{T_\perp}^2}} J_n'(b)^2 \,\mathrm{d}v_\perp \int_{-\infty}^\infty \frac{\mathrm{e}^{-\frac{v_z^2}{2v_{Tz}^2}}}{\sqrt{2\pi}v_{Tz}}\frac{1}{k_z v_z - \omega + n\Omega_0}\,\mathrm{d}v_z,\\
J_{xy} =& -\frac{n_0 q^2 2\pi}{m v_{T_\perp}^2}\sum_{n=-\infty}^\infty\frac{n\Omega_0}{k_\perp}\int_0^\infty \frac{v_\perp^2}{2\pi v_{T_\perp}^2}\mathrm{e}^{-\frac{v_\perp^2}{2v_{T_\perp}^2}} J_n'(b) J_n(b) \,\mathrm{d}v_\perp \int_{-\infty}^\infty \frac{\mathrm{e}^{-\frac{v_z^2}{2v_{Tz}^2}}}{\sqrt{2\pi}v_{Tz}}\frac{1}{k_z v_z - \omega + n\Omega_0}\,\mathrm{d}v_z,\\
J_{xz} =& -\frac{n_0 q^2 2\pi}{m v_{Tz}^2}\sum_{n=-\infty}^\infty\int_0^\infty \frac{v_\perp^2}{2\pi v_{T_\perp}^2}\mathrm{e}^{-\frac{v_\perp^2}{2v_{T_\perp}^2}} J_n'(b) J_n(b) \,\mathrm{d}v_\perp \int_{-\infty}^\infty \frac{\mathrm{e}^{-\frac{v_z^2}{2v_{Tz}^2}}}{\sqrt{2\pi}v_{Tz}}\frac{v_z}{k_z v_z - \omega + n\Omega_0}\,\mathrm{d}v_z,\\
J_{yy} =& -i\frac{n_0 q^2 2\pi}{m v_{T_\perp}^2}\sum_{n=-\infty}^\infty\int \frac{n^2\Omega_0^2}{2\pi v_{T_\perp}^2 k_\perp^2}v_\perp \mathrm{e}^{-\frac{v_\perp^2}{2v_{T_\perp}^2}} J_n(b)^2 \,\mathrm{d}v_\perp \int \frac{\mathrm{e}^{-\frac{v_z^2}{2v_{Tz}^2}}}{\sqrt{2\pi}v_{Tz}}\frac{1}{k_z v_z - \omega + n\Omega_0}\,\mathrm{d}v_z,\\
J_{yz} =& -i\frac{n_0 q^2 2\pi}{m v_{Tz}^2}\frac{n\Omega_0}{k_\perp}\sum_{n=-\infty}^\infty\int_0^\infty \frac{v_\perp}{2\pi v_{T_\perp}^2}\mathrm{e}^{-\frac{v_\perp^2}{2v_{T_\perp}^2}} J_n(b)^2 \,\mathrm{d}v_\perp \int_{-\infty}^\infty \frac{\mathrm{e}^{-\frac{v_z^2}{2v_{Tz}^2}}}{\sqrt{2\pi}v_{Tz}}\frac{v_z}{k_z v_z - \omega + n\Omega_0}\,\mathrm{d}v_z,\\
J_{zz} =& -i\frac{n_0 q^2 2\pi}{m v_{Tz}^2}\sum_{n=-\infty}^\infty\int_0^\infty \frac{v_\perp}{2\pi v_{T_\perp}^2}\mathrm{e}^{-\frac{v_\perp^2}{2v_{T_\perp}^2}} J_n(b)^2 \,\mathrm{d}v_\perp \int_{-\infty}^\infty \frac{\mathrm{e}^{-\frac{v_z^2}{2v_{Tz}^2}}}{\sqrt{2\pi}v_{Tz}}\frac{v_z^2}{k_z v_z - \omega + n\Omega_0}\,\mathrm{d}v_z.
\end{aligned}
$$

We substitute $\frac{v_z}{\sqrt{2}v_{Tz}} = \tau$ and $\frac{v_\perp}{\sqrt{2}v_{T_\perp}} = \sigma$ and insert the recursion formula for the derivative

of the Bessel function (A.3) to get

$$
\begin{aligned}
J_{xx} =& -i\frac{n_0 q^2}{m}\sum_{n=-\infty}^{\infty}\int_0^\infty \sigma^3 \mathrm{e}^{-\sigma^2}\left(J_{n-1}(\beta\sigma)^2 + J_{n+1}(\beta\sigma)^2 - 2J_{n-1}(\beta\sigma)J_{n+1}(\beta\sigma)\right)\mathrm{d}\sigma \\
&\times \frac{1}{k_z\sqrt{2}v_{Tz}}\int_{-\infty}^{\infty}\frac{\mathrm{e}^{-\tau^2}}{\sqrt{\pi}}\frac{1}{\tau - \frac{\omega - n\Omega_0}{k_z\sqrt{2}v_{Tz}}}\,\mathrm{d}\tau, \\
J_{xy} =& -\frac{n_0 q^2}{m}\sum_{n=-\infty}^{\infty}\frac{\sqrt{2}n\Omega_0}{k_\perp v_{T_\perp}}\int_0^\infty \sigma^2 \mathrm{e}^{-\sigma^2}(J_{n-1}(\beta\sigma) - J_{n+1}(\beta\sigma))J_n(\beta\sigma)\,\mathrm{d}\sigma \\
&\times \frac{1}{k_z\sqrt{2}v_{Tz}}\int_{-\infty}^{\infty}\frac{\mathrm{e}^{-\tau^2}}{\sqrt{\pi}}\frac{1}{\tau - \frac{\omega - n\Omega_0}{k_z\sqrt{2}v_{Tz}}}\,\mathrm{d}\tau, \\
J_{xz} =& -\frac{n_0 q^2}{m}\sum_{n=-\infty}^{\infty}\frac{2v_{T_\perp}}{v_{Tz}}\int_0^\infty \sigma^2 \mathrm{e}^{-\sigma^2}(J_{n-1}(\beta\sigma) - J_{n+1}(\beta\sigma))J_n(\beta\sigma)\,\mathrm{d}\sigma \\
&\times \frac{1}{k_z\sqrt{2}v_{Tz}}\int_{-\infty}^{\infty}\frac{\mathrm{e}^{-\tau^2}}{\sqrt{\pi}}\frac{\tau}{\tau - \frac{\omega - n\Omega_0}{k_z\sqrt{2}v_{Tz}}}\,\mathrm{d}\tau, \\
J_{yy} =& -i\frac{n_0 q^2}{m}\sum_{n=-\infty}^{\infty}\frac{2n^2\Omega_0^2}{k_\perp^2 v_{T_\perp}^2}\int_0^\infty \sigma \mathrm{e}^{-\sigma^2}J_n(\beta\sigma)^2\,\mathrm{d}\sigma\frac{1}{k_z\sqrt{2}v_{Tz}}\int_{-\infty}^{\infty}\frac{\mathrm{e}^{-\tau^2}}{\sqrt{\pi}}\frac{1}{\tau - \frac{\omega - n\Omega_0}{k_z\sqrt{2}v_{Tz}}}\,\mathrm{d}\tau, \\
J_{yz} =& -i\frac{n_0 q^2}{m}\sum_{n=-\infty}^{\infty}\frac{2\sqrt{2}n\Omega_0}{v_{Tz}k_\perp}\int_0^\infty \sigma \mathrm{e}^{-\sigma^2}J_n(\beta\sigma)^2\,\mathrm{d}\sigma\frac{1}{k_z\sqrt{2}v_{Tz}}\int_{-\infty}^{\infty}\frac{\mathrm{e}^{-\tau^2}}{\sqrt{\pi}}\frac{\tau}{\tau - \frac{\omega - n\Omega_0}{k_z\sqrt{2}v_{Tz}}}\,\mathrm{d}\tau, \\
J_{zz} =& -i\frac{n_0 q^2}{m}\sum_{n=-\infty}^{\infty}4\int_0^\infty \sigma \mathrm{e}^{-\sigma^2}J_n(\beta\sigma)^2\,\mathrm{d}\sigma\frac{1}{k_z v_{Tz}\sqrt{2}}\int_{-\infty}^{\infty}\frac{\mathrm{e}^{-\tau^2}}{\sqrt{\pi}}\frac{\tau^2}{\tau - \frac{\omega - n\Omega_0}{k_z\sqrt{2}v_{Tz}}}\,\mathrm{d}\tau,
\end{aligned}
$$

where $\beta = \frac{k_\perp\sqrt{2}v_{T_\perp}}{\Omega_0}$.

Next, we define $\xi = \frac{k_\perp^2 v_{T_\perp}^2}{\Omega_0^2}$ and $\zeta_n = \frac{\omega - n\Omega_0}{k_z\sqrt{2}v_{Tz}}$ and use the integral formulas for the Bessel functions (A.4a), (A.4b) and (A.4c) as well as the definition of the Zeta function A.2 to obtain the proposition.

□

From the linearised Ampère equation (18.5b), we obtain

$$
\left[\begin{pmatrix} \omega^2 - \frac{k_\perp^2 + k_z^2}{\mu_0\varepsilon_0} & 0 & 0 \\ 0 & \omega^2 - \frac{k_z^2}{\mu_0\varepsilon_0} & \frac{k_\perp k_z}{\mu_0\varepsilon_0} \\ 0 & \frac{k_\perp k_z}{\mu_0\varepsilon_0} & \omega^2 - \frac{k_\perp^2}{\mu_0\varepsilon_0} \end{pmatrix} + i\frac{\omega}{\mu_0\varepsilon_0}\,J\right]\widehat{\delta\mathbf{E}} = 0.
$$

Then, the dispersion relation is obtained by computing the determinant of

$$D(k_\perp, k_z, \omega) = \begin{pmatrix} \omega^2 - \frac{k_\perp^2 + k_z^2}{\mu_0 \varepsilon_0} + i\frac{\omega}{\mu_0 \varepsilon_0} J_{xx} & i\frac{\omega}{\mu_0 \varepsilon_0} J_{xy} & i\frac{\omega}{\mu_0 \varepsilon_0} J_{xz} \\ i\frac{\omega}{\mu_0 \varepsilon_0} J_{yx} & \omega^2 - \frac{k_z^2}{\mu_0 \varepsilon_0} + i\frac{\omega}{\mu_0 \varepsilon_0} J_{yy} & \frac{k_\perp k_z}{\mu_0 \varepsilon_0} + i\frac{\omega}{\mu_0 \varepsilon_0} J_{yz} \\ i\frac{\omega}{\mu_0 \varepsilon_0} J_{zx} & \frac{k_\perp k_z}{\mu_0 \varepsilon_0} + i\frac{\omega}{\mu_0 \varepsilon_0} J_{zy} & \omega^2 - \frac{k_\perp^2}{\mu_0 \varepsilon_0} + i\frac{\omega}{\mu_0 \varepsilon_0} J_{zz} \end{pmatrix}.$$

19 Summary and Outlook

In this thesis, we have derived a geometric particle-in-cell method on mapped grids based on a discretisation of the fields with finite element exterior calculus [3]. After examining different representations of the particle trajectories, we have decided to use a hybrid particle pusher. Our formulation yields a semi-discrete Poisson system that satisfies the Jacobi identity. For the discretisation in time, we have constructed charge conserving schemes based on a Hamiltonian splitting as well as energy conserving schemes based on an antisymmetric splitting of the Poisson matrix and the discrete gradient method.

In the first part, we have restricted ourselves to test problems with periodic boundary conditions in order to investigate the influence of the coordinate transformation in an easier setting. This has also limited the coordinate transformations to the class of periodic mappings. For our standard test cases, we have shown numerical results matching the analytical growth and damping rates and verified the expected conservation properties of the different time integrators.

In the second part, we have investigated the natural boundary conditions of the weak formulation of Maxwell's equations and constructed new basis functions from clamped basis splines that form a discrete de Rham sequence. Furthermore, we have presented a fast and efficient preconditioner based on a Fourier solver for the conjugate gradient solvers of the boundary mass matrices. Then, we have applied perfect conductor boundary conditions for the fields and reflecting boundary conditions for the particles enabling the use of domain deforming coordinate transformations such as cylindrical or elliptical mappings. As a last point, we have reviewed the challenges arising from singular mappings and proposed an idea on how to handle the transformation of the Lorentz force near a singularity. In a simulation of the Weibel instability, which was inspired by a similar approach in [17], we have studied the effect of the deformed mapped grids and verified the compatibility of the boundary conditions with the conservation properties of the structure preserving discretisations.

Following the recent publication of Toshniwal & Hughes [86], as future work, it would be possible to construct smooth spline basis functions that form a de Rham complex at the pole. The implementation of such basis functions for the GEMPIC framework would enable the use of radial grids with a singularity.

In the third part, we have introduced the quasi-neutrality ansatz with adiabatic electrons into the GEMPIC framework. This ansatz allows us to choose time steps at the time scale of the ion motion, which makes it possible to simulate ion driven instabilities such as the ion temperature gradient instability. After discretising the quasi-neutrality equations in time with the established charge or energy conserving methods, we have verified their conservation properties in a simulation of an ion acoustic wave. For the ion temperature gradient instability, test cases from Sturdevant et al. [83] in a slab geometry and from Latu et al. [60] in a cylinder

have been adapted to our framework. We have used the linear δ f method to reduce the particle noise and matched the numerical results with the growth rates computed by the dispersion relation.

For future work, it would be interesting to go to non-linear δf and full f simulations with varying temperature gradients extending the approximations we used for the linear δf method. The overall goal should be the comparison of simulations with the full kinetic code to reference simulations by gyrokinetic codes such as Gysela [39] or Gygles [34].

A Appendix

Method of Characteristics

The method of characteristics is among others described in [33]. In our case, we start with a differential equation of the following form:

$$\frac{\partial f(t,\mathbf{x},\mathbf{v})}{\partial t} + P(t,\mathbf{x},\mathbf{v})\nabla_{\mathbf{x}} f(t,\mathbf{x},\mathbf{v}) + Q(t,\mathbf{x},\mathbf{v})\nabla_{\mathbf{v}} f(t,\mathbf{x},\mathbf{v}) = 0,$$

where $\mathbf{x}(t), \mathbf{v}(t)$ are time dependent. Then, we use the chain rule to write this as

$$\frac{\mathrm{d}f}{\mathrm{d}t} = \frac{\partial f}{\partial t} + \frac{\partial f}{\partial \mathbf{x}}\frac{\partial \mathbf{x}}{\partial t} f + \frac{\partial f}{\partial \mathbf{v}}\frac{\partial \mathbf{v}}{\partial t} = 0.$$

In this case, we obtain the characteristics

$$\begin{aligned}\frac{\partial \mathbf{x}}{\partial t} &= P(t,\mathbf{x},\mathbf{v}),\\ \frac{\partial \mathbf{v}}{\partial t} &= Q(t,\mathbf{x},\mathbf{v}),\end{aligned}$$

along which f stays constant, since $\frac{\mathrm{d}f}{\mathrm{d}t} = 0$ for this choice of P and Q. This defines a solution of the differential equation for f.

For the Vlasov equation this leads to the well known particle equations of motion with

$$P = \mathbf{v},\ Q = \frac{q}{m}\left(\mathbf{E} + \mathbf{v}\times\mathbf{B}\right).$$

Fourier and Laplace Transformation

Proposition A.1. *A space and time dependent function $f(\mathbf{x},t)$ that has a periodic domain in space, can be represented with a Fourier transformation in space and a Laplace transformation in time in the following form:*

$$f(\mathbf{x},t) = \int \widehat{f}(\mathbf{k},\omega)\exp\left(-i\omega t + i\mathbf{k}\cdot\mathbf{x}\right)\,\mathrm{d}\mathbf{k}\,\mathrm{d}\omega. \tag{A.1}$$

Zeta Function

Definition A.2. *The Zeta function is defined as*

$$Z(\zeta) = \frac{1}{\sqrt{\pi}}\int \frac{\exp(-x^2)}{x-\zeta}\,\mathrm{d}x = \sqrt{\pi}\exp(-\zeta^2)[i - \mathrm{erfi}(\zeta)],$$

where the derivative is given by

$$Z'(\zeta) = -2(1+\zeta Z(\zeta)).$$

Bessel Function

The formulas are taken from the fifth edition of [38, Sec.6.633] and are adapted for our purpose.

Definition A.3. *The Bessel functions are defined as*

$$\exp(ib\sin(a)) = \sum_{n=-\infty}^{\infty} J_n(b)\exp(ina).$$

It follows that the Bessel function can be expressed as

$$\frac{n}{x}J_n(x) = \frac{J_{n-1}(x) + J_{n+1}(x)}{2}, \tag{A.2}$$

and the derivative can be written as

$$\frac{\mathrm{d}J_n(x)}{\mathrm{d}x} = \frac{J_{n-1}(x) - J_{n+1}(x)}{2}. \tag{A.3}$$

The Bessel functions can be integrated via the following formulas:

$$\int_0^\infty x\mathrm{e}^{-x^2}J_n^2(\beta x)\,\mathrm{d}x = \frac{1}{2}\mathrm{e}^{-\frac{\beta^2}{2}}I_n\left(\frac{\beta^2}{2}\right) = \frac{1}{2}\Lambda_n\left(\frac{\beta^2}{2}\right), \tag{A.4a}$$

$$\int_0^\infty x^3\mathrm{e}^{-x^2}J_n^2(\beta x)\,\mathrm{d}x = \frac{\beta^2}{8}\left[\Lambda_{n+1}\left(\frac{\beta^2}{2}\right) + \left(\frac{4}{\beta^2} - 2\right)\Lambda_n\left(\frac{\beta^2}{2}\right) + \Lambda_{n-1}\left(\frac{\beta^2}{2}\right)\right], \tag{A.4b}$$

$$\int_0^\infty x^p\mathrm{e}^{-x^2}J_q(\beta x)J_r(\beta x)\,\mathrm{d}x = 2^{-(q+r+1)}\beta^{q+r}\frac{\Gamma\left(\frac{p+q+r+1}{2}\right)}{\Gamma(q+1)\Gamma(r+1)} \tag{A.4c}$$
$$\times\ {}_3F_3\left[\frac{q+r+1}{2}, \frac{q+r+2}{2}, \frac{p+q+r+1}{2}; q+1, r+1, q+r+1; -\beta^2\right]$$

where the scaled Bessel function is defined as $\Lambda_n(\xi) = I_n(\xi)\exp(-\xi)$ and its derivative is given by $\Lambda_n'(\xi) = -\Lambda_n(\xi) + \frac{\Lambda_{n+1}(\xi)+\Lambda_{n-1}(\xi)}{2}$. The general hypergeometric function can be written as

$${}_3F_3(a_1, a_2, a_3; b_1, b_2, b_3; z) = \sum_{k=0}^{\infty}\prod_{i=1}^{3}\frac{\Gamma(k+a_i)}{\Gamma(a_i)}\prod_{j=1}^{3}\frac{\Gamma(b_j)}{\Gamma(k+b_j)}\frac{z^k}{k!} =: G(q, r, p, \beta).$$

Useful Integrals

For the computation of the dispersion relation in Chapter 18, we use the following integrals:

$$\int_{-\infty}^{\infty} \frac{\mathrm{e}^{-\frac{\sigma^2}{\alpha^2}}}{\sqrt{\pi}\alpha}\,\mathrm{d}\sigma = 1, \tag{A.5a}$$

$$\int_{-\infty}^{\infty} \sigma\frac{\mathrm{e}^{-\frac{\sigma^2}{\alpha^2}}}{\sqrt{\pi}\alpha}\,\mathrm{d}\sigma = 0, \tag{A.5b}$$

$$\int_{-\infty}^{\infty} \sigma^2\frac{\mathrm{e}^{-\frac{\sigma^2}{\alpha^2}}}{\sqrt{\pi}\alpha}\,\mathrm{d}\sigma = \frac{\alpha^2}{2}. \tag{A.5c}$$

Divergence Theorem

Proposition A.4. *For the integration by parts, we use the divergence theorem in the following forms:*

- *The standard form for a scalar function g and a vector field $\mathbf{F}$,*

$$\int_\Omega \nabla\cdot(\mathbf{F}g)\,\mathrm{d}\mathbf{x} = \int_\Omega g(\nabla\cdot\mathbf{F})\,\mathrm{d}\mathbf{x} = -\int_\Omega \nabla g\cdot\mathbf{F}\,\mathrm{d}\mathbf{x} + \int_{\partial\Omega} g(\mathbf{F}\cdot\mathbf{n})\,\mathrm{d}\sigma, \tag{A.6}$$

- *The cross product form for vector fields, $\mathbf{F},\mathbf{G}$,*

$$\int_\Omega \nabla\times(\mathbf{F}\cdot\mathbf{G})\,\mathrm{d}\mathbf{x} = \int_\Omega \mathbf{G}\cdot(\nabla\times\mathbf{F})\,\mathrm{d}\mathbf{x} - \int_\Omega (\nabla\times\mathbf{G})\cdot\mathbf{F}\,\mathrm{d}\mathbf{x} = \int_{\partial\Omega}(\mathbf{F}\times\mathbf{G})\cdot\mathbf{n}\,\mathrm{d}\sigma. \tag{A.7}$$

Equations of Motion in Cylindrical Coordinates

Let us exemplarily take a look at the equations of motion in cylindrical coordinates. Therefore, we use the following mapping:

$$F(\boldsymbol{\xi}) = \begin{pmatrix} L_r \xi_1 \cos(2\pi\xi_2) \\ L_r \xi_1 \sin(2\pi\xi_2) \\ L_z \xi_3 \end{pmatrix}, \; DF(\boldsymbol{\xi}) = \begin{pmatrix} L_r \cos(2\pi\xi_2) & -2\pi L_r \xi_1 \sin(2\pi\xi_2) & 0 \\ L_r \sin(2\pi\xi_2) & 2\pi L_r \xi_1 \cos(2\pi\xi_2) & 0 \\ 0 & 0 & L_z \end{pmatrix},$$

$$F^{-1}(\mathbf{x}) = \begin{pmatrix} \frac{\sqrt{x_1^2+x_2^2}}{L_r} \\ \operatorname{atan2}(x_2, x_1) \\ \frac{x_3}{L} \end{pmatrix}, \; DF^{-1}(\boldsymbol{\xi}) = \begin{pmatrix} \frac{\cos(2\pi\xi_2)}{L_r} & \frac{\sin(2\pi\xi_2)}{L_r} & 0 \\ -\frac{\sin(2\pi\xi_2)}{2\pi L_r \xi_1} & \frac{\cos(2\pi\xi_2)}{2\pi L_r \xi_1} & 0 \\ 0 & 0 & \frac{1}{L} \end{pmatrix},$$

$$G_m(\boldsymbol{\xi}) = \begin{pmatrix} L_r^2 & 0 & 0 \\ 0 & 4\pi^2 L_r^2 \xi_1^2 & 0 \\ 0 & 0 & L_z^2 \end{pmatrix}, \; G_m^{-1}(\boldsymbol{\xi}) = \begin{pmatrix} \frac{1}{L_r^2} & 0 & 0 \\ 0 & \frac{1}{4\pi^2 L_r^2 \xi_1^2} & 0 \\ 0 & 0 & \frac{1}{L_z^2} \end{pmatrix}, J_F(\boldsymbol{\xi}) = L_z 2\pi L_r^2 \xi_1.$$

The cylindrical coordinate transformation is an orthogonal mapping so that the metric is a diagonal matrix and the mass matrices are block diagonal,

$$\begin{aligned} \tilde{\mathsf{M}}_1 &= \operatorname{diag}\left(\tilde{\mathsf{M}}_{11}, \tilde{\mathsf{M}}_{12}, \tilde{\mathsf{M}}_{13}\right) \\ &= \operatorname{diag}\left(\int \tilde{\Lambda}_1^1(\boldsymbol{\xi})^\top \tilde{\Lambda}_1^1(\boldsymbol{\xi}) 2\pi L_z \xi_1 \, \mathrm{d}\boldsymbol{\xi}, \int \tilde{\Lambda}_2^1(\boldsymbol{\xi})^\top \tilde{\Lambda}_2^1(\boldsymbol{\xi}) \frac{L_z}{2\pi\xi_1} \, \mathrm{d}\boldsymbol{\xi}, \int \tilde{\Lambda}_3^1(\boldsymbol{\xi})^\top \tilde{\Lambda}_3^1(\boldsymbol{\xi}) \frac{2\pi L_r^2 \xi_1}{L_z} \, \mathrm{d}\boldsymbol{\xi}\right), \\ \tilde{\mathsf{M}}_2 &= \operatorname{diag}\left(\tilde{\mathsf{M}}_{21}, \tilde{\mathsf{M}}_{22}, \tilde{\mathsf{M}}_{23}\right) \\ &= \operatorname{diag}\left(\int \tilde{\Lambda}_1^2(\boldsymbol{\xi})^\top \tilde{\Lambda}_1^2(\boldsymbol{\xi}) \frac{1}{L_z 2\pi\xi_1} \, \mathrm{d}\boldsymbol{\xi}, \int \tilde{\Lambda}_2^2(\boldsymbol{\xi})^\top \tilde{\Lambda}_2^2(\boldsymbol{\xi}) \frac{2\pi\xi_1}{L_z} \, \mathrm{d}\boldsymbol{\xi}, \int \tilde{\Lambda}_3^2(\boldsymbol{\xi})^\top \tilde{\Lambda}_3^2(\boldsymbol{\xi}) \frac{L_z}{2\pi L_r^2 \xi_1} \, \mathrm{d}\boldsymbol{\xi}\right). \end{aligned}$$

We write out the equations for the following particle pushers, where the derivative matrices $D_i, i = 1, 2, 3$ are taken from (9.8):

- Hybrid particle pushing with the velocity $\mathbf{v}$ in physical coordinates,

$$
\begin{pmatrix} \dot{\xi}_1 \\ \dot{\xi}_2 \\ \dot{\xi}_3 \end{pmatrix} = \begin{pmatrix} \frac{\cos(2\pi\xi_2)}{L_r} v_x + \frac{\sin(2\pi\xi_2)}{L_r} v_y \\ -\frac{\sin(2\pi\xi_2)}{2\pi L_r \xi_1} v_x + \frac{\cos(2\pi L_r \xi_2)}{2\pi\xi_1} v_y \\ \frac{v_z}{L_z} \end{pmatrix} =: \begin{pmatrix} \tilde{v}_1 \\ \tilde{v}_2 \\ \tilde{v}_3 \end{pmatrix},
$$

$$
\begin{pmatrix} \dot{v}_x \\ \dot{v}_y \\ \dot{v}_z \end{pmatrix} = \frac{q}{m} \begin{pmatrix} \frac{\cos(2\pi\xi_2)}{L_r} & -\frac{\sin(2\pi\xi_2)}{2\pi L_r \xi_1} & 0 \\ \frac{\sin(2\pi\xi_2)}{L_r} & \frac{\cos(2\pi\xi_2)}{2\pi L_r \xi_1} & 0 \\ 0 & 0 & \frac{1}{L_z} \end{pmatrix} \begin{pmatrix} \tilde{\Lambda}^1_1(\boldsymbol{\xi})\tilde{e}_1 + \tilde{v}_2\tilde{\Lambda}^2_3(\boldsymbol{\xi})\tilde{b}_3 - \tilde{v}_3\tilde{\Lambda}^2_2(\boldsymbol{\xi})\tilde{b}_2 \\ \tilde{\Lambda}^1_2(\boldsymbol{\xi})\tilde{e}_2 + \tilde{v}_3\tilde{\Lambda}^2_1(\boldsymbol{\xi})\tilde{b}_1 - \tilde{v}_1\tilde{\Lambda}^2_3(\boldsymbol{\xi})\tilde{b}_3 \\ \tilde{\Lambda}^1_3(\boldsymbol{\xi})\tilde{e}_3 + \tilde{v}_1\tilde{\Lambda}^2_2(\boldsymbol{\xi})\tilde{b}_2 - \tilde{v}_2\tilde{\Lambda}^2_1(\boldsymbol{\xi})\tilde{b}_1 \end{pmatrix},
$$

$$
\begin{pmatrix} \dot{\tilde{e}}_1 \\ \dot{\tilde{e}}_2 \\ \dot{\tilde{e}}_3 \end{pmatrix} = \begin{pmatrix} \tilde{\mathsf{M}}^{-1}_{11} \left(\mathsf{D}_3^\top \tilde{\mathsf{M}}_{22} \tilde{b}_2 - \mathsf{D}_2^\top \tilde{\mathsf{M}}_{23} \tilde{b}_3 - q \tilde{\Lambda}^1_1(\boldsymbol{\xi})^\top \tilde{v}_1 \right) \\ \tilde{\mathsf{M}}^{-1}_{12} \left(\mathsf{D}_1^\top \tilde{\mathsf{M}}_{23} \tilde{b}_3 - \mathsf{D}_3^\top \tilde{\mathsf{M}}_{21} \tilde{b}_1 - q \tilde{\Lambda}^1_2(\boldsymbol{\xi})^\top \tilde{v}_2 \right) \\ \tilde{\mathsf{M}}^{-1}_{13} \left(\mathsf{D}_2^\top \tilde{\mathsf{M}}_{21} \tilde{b}_1 - \mathsf{D}_1^\top \tilde{\mathsf{M}}_{22} \tilde{b}_2 - q \tilde{\Lambda}^1_3(\boldsymbol{\xi})^\top \tilde{v}_3 \right) \end{pmatrix},
$$

$$
\begin{pmatrix} \dot{\tilde{b}}_1 \\ \dot{\tilde{b}}_2 \\ \dot{\tilde{b}}_3 \end{pmatrix} = - \begin{pmatrix} -D_3\tilde{e}_2 + D_2\tilde{e}_3 \\ D_3\tilde{e}_1 - D_1\tilde{e}_3 \\ -D_2\tilde{e}_1 + D_1\tilde{e}_2 \end{pmatrix}.
$$

- Logical particle pushing for the contravariant components of the velocity, $\tilde{\mathbf{v}}$,

$$
\begin{aligned}
\begin{pmatrix} \dot{\xi}_1 \\ \dot{\xi}_2 \\ \dot{\xi}_3 \end{pmatrix} &= \begin{pmatrix} \tilde{v}_1 \\ \tilde{v}_2 \\ \tilde{v}_3 \end{pmatrix}, \\
\begin{pmatrix} \dot{\tilde{v}}_1 \\ \dot{\tilde{v}}_2 \\ \dot{\tilde{v}}_3 \end{pmatrix} &= \begin{pmatrix} \frac{q}{m}(\tilde{\Lambda}^1_1(\boldsymbol{\xi})\tilde{e}_1 + \tilde{v}_2\tilde{\Lambda}^2_3(\boldsymbol{\xi})\tilde{b}_3 - \tilde{v}_3\tilde{\Lambda}^2_2(\boldsymbol{\xi})\tilde{b}_2) + \tilde{v}_2^2\xi_1 \\ \frac{q}{m}\frac{\tilde{\Lambda}^1_2(\boldsymbol{\xi})\tilde{e}_2+\tilde{v}_3\tilde{\Lambda}^2_1(\boldsymbol{\xi})\tilde{b}_1-\tilde{v}_1\tilde{\Lambda}^2_3(\boldsymbol{\xi})\tilde{b}_3}{4\pi^2\xi_1^2} - 2\frac{\tilde{v}_1\tilde{v}_2}{\xi_1} \\ \frac{q}{m}\frac{\tilde{\Lambda}^1_3(\boldsymbol{\xi})\tilde{e}_3+\tilde{v}_1\tilde{\Lambda}^2_2(\boldsymbol{\xi})\tilde{b}_2-\tilde{v}_2\tilde{\Lambda}^2_1(\boldsymbol{\xi})\tilde{b}_1}{L_z^2} \end{pmatrix}, \\
\begin{pmatrix} \dot{\tilde{e}}_1 \\ \dot{\tilde{e}}_2 \\ \dot{\tilde{e}}_3 \end{pmatrix} &= \begin{pmatrix} \tilde{\mathsf{M}}^{-1}_{11}\left(D_3^\top\tilde{\mathsf{M}}_{22}\tilde{b}_2 - D_2^\top\tilde{\mathsf{M}}_{23}\tilde{b}_3 - q\tilde{\Lambda}^1_1(\boldsymbol{\xi})^\top\tilde{v}_1\right) \\ \tilde{\mathsf{M}}^{-1}_{12}\left(D_1^\top\tilde{\mathsf{M}}_{23}\tilde{b}_3 - D_3^\top\tilde{\mathsf{M}}_{21}\tilde{b}_1 - q\tilde{\Lambda}^1_2(\boldsymbol{\xi})^\top\tilde{v}_2\right) \\ \tilde{\mathsf{M}}^{-1}_{13}\left(D_2^\top\tilde{\mathsf{M}}_{21}\tilde{b}_1 - D_1^\top\tilde{\mathsf{M}}_{22}\tilde{b}_2 - q\tilde{\Lambda}^1_3(\boldsymbol{\xi})^\top\tilde{v}_3\right) \end{pmatrix}, \\
\begin{pmatrix} \dot{\tilde{b}}_1 \\ \dot{\tilde{b}}_2 \\ \dot{\tilde{b}}_3 \end{pmatrix} &= - \begin{pmatrix} -D_3\tilde{e}_2 + D_2\tilde{e}_3 \\ D_3\tilde{e}_1 - D_1\tilde{e}_3 \\ -D_2\tilde{e}_1 + D_1\tilde{e}_2 \end{pmatrix}.
\end{aligned}
$$

- Logical particle pushing for the covariant components of the velocity $\hat{\mathbf{v}}$,

$$
\begin{aligned}
\begin{pmatrix} \dot{\xi}_1 \\ \dot{\xi}_2 \\ \dot{\xi}_3 \end{pmatrix} &= \begin{pmatrix} \hat{v}_1 \\ \frac{1}{4\pi^2 L_r^2 \xi_1^2} \hat{v}_2 \\ \frac{\hat{v}_3}{L_z^2} \end{pmatrix}, \\
\begin{pmatrix} \dot{\hat{v}}_1 \\ \dot{\hat{v}}_2 \\ \dot{\hat{v}}_3 \end{pmatrix} &= \frac{q}{m} \begin{pmatrix} \tilde{\Lambda}_1^1(\boldsymbol{\xi}) \tilde{e}_1 + \frac{\hat{v}_2}{4\pi^2 L_r^2 \xi_1^2} \tilde{\Lambda}_3^2(\boldsymbol{\xi}) \tilde{b}_3 - \frac{\hat{v}_3}{L_z^2} \tilde{\Lambda}_2^2(\boldsymbol{\xi}) \tilde{b}_2 \frac{m \hat{v}_2^2}{q 4\pi^2 L_r^2 \xi_1^3} \\ \tilde{\Lambda}_2^1(\boldsymbol{\xi}) \tilde{e}_2 + \frac{\hat{v}_3}{L_z^2} \tilde{\Lambda}_1^2(\boldsymbol{\xi}) \tilde{b}_1 - \hat{v}_1 \tilde{\Lambda}_3^2(\boldsymbol{\xi}) \tilde{b}_3 \\ \tilde{\Lambda}_3^1(\boldsymbol{\xi}) \tilde{e}_3 + \hat{v}_1 \tilde{\Lambda}_2^2(\boldsymbol{\xi}) \tilde{b}_2 - \frac{\hat{v}_2}{4\pi^2 L_r^2 \xi_1^2} \tilde{\Lambda}_1^2(\boldsymbol{\xi}) \tilde{b}_1 \end{pmatrix}, \\
\begin{pmatrix} \dot{\tilde{e}}_1 \\ \dot{\tilde{e}}_2 \\ \dot{\tilde{e}}_3 \end{pmatrix} &= \begin{pmatrix} \tilde{\mathsf{M}}_{11}^{-1} \left(D_3^\top \tilde{\mathsf{M}}_{22} \tilde{b}_2 - D_2^\top \tilde{\mathsf{M}}_{23} \tilde{b}_3 - q \tilde{\Lambda}_1^1(\boldsymbol{\xi})^\top \hat{v}_1 \right) \\ \tilde{\mathsf{M}}_{12}^{-1} \left(D_1^\top \tilde{\mathsf{M}}_{23} \tilde{b}_3 - D_3^\top \tilde{\mathsf{M}}_{21} \tilde{b}_1 - \frac{q \tilde{\Lambda}_2^1(\boldsymbol{\xi})^\top \hat{v}_2}{4\pi^2 L_r^2 \xi_1^2} \right) \\ \tilde{\mathsf{M}}_{13}^{-1} \left(D_2^\top \tilde{\mathsf{M}}_{21} \tilde{b}_1 - D_1^\top \tilde{\mathsf{M}}_{22} \tilde{b}_2 - q \tilde{\Lambda}_3^1(\boldsymbol{\xi})^\top \frac{1}{L_z^2} \hat{v}_3 \right) \end{pmatrix}, \\
\begin{pmatrix} \dot{\tilde{b}}_1 \\ \dot{\tilde{b}}_2 \\ \dot{\tilde{b}}_3 \end{pmatrix} &= - \begin{pmatrix} -D_3 \tilde{e}_2 + D_2 \tilde{e}_3 \\ D_3 \tilde{e}_1 - D_1 \tilde{e}_3 \\ -D_2 \tilde{e}_1 + D_1 \tilde{e}_2 \end{pmatrix}.
\end{aligned}
$$

  As mentioned in Section 6.1, the latter equations of motion with the covariant components of the velocity $\hat{\mathbf{v}}$ yield an explicit Hamiltonian splitting because the velocity directions are decoupled.

Acknowledgements

I would like to thank my supervisor Eric Sonnendrücker for keeping the overview and proposing new approaches and my mentor Katharina Kormann for helping me with all sort of problems that came up during my PhD, from simple coding bugs to major comprehension problems. Next, I would like to thank Philip J. Morrison for taking care of me during my stay in Austin and for the detailed explanation of the physical background of GEMPIC. Furthermore, I would like to thank Roman Hatzky, Irene Garnelo, Michael Kraus, Stefan Possanner, Mario Räth, Florian Holderied, Eero Hirvijoki and Hendrik Speleers for all the helpful discussions.

The numerical simulations presented in this thesis have been performed mostly on the extension cluster DRACO of the high-performance computing system of the Max Planck Computing and Data Facility.

This work has been carried out within the framework of the EUROfusion consortium and has received funding from the Euratom research and training programme 2014-2018 and 2019-2020 under grant agreement No 633053. The views and opinions expressed herein do not necessarily reflect those of the European Commission.

Additionally, this work has been supported by Deutsche Forschungsgemeinschaft (DFG) through the TUM International Graduate School of Science and Engineering (IGSSE).

List of Publications

Part I has been partially published in:

- B. Perse, K. Kormann, and E. Sonnendrücker. Geometric particle-in-cell simulations of the Vlasov–Maxwell system in curvilinear coordinates. SIAM Journal on Scientific Computing, 43(1):B194–B218, 2021.

Part II has been partially published in:

- B. Perse, K. Kormann, E. Sonnendrücker. Perfect Conductor Boundary Conditions for Geometric Particle-in-Cell Simulations of the Vlasov-Maxwell System in Curvilinear Coordinates. arXiv:2111.08342, 2021

Bibliography

[1] SeLaLib. https://github.com/selalib/selalib, 2021.

[2] J. Ameres. *Stochastic and Spectral Particle Methods for Plasma Physics*. PhD thesis, TU Munich, 2018.

[3] D. N. Arnold, R. S. Falk, and R. Winther. Finite element exterior calculus, homological techniques, and applications. *Acta Numer.*, 15:1–155, 2006.

[4] V. Artigues, K. Kormann, M. Rampp, and K. Reuter. Evaluation of performance portability frameworks for the implementation of a particle-in-cell code. *Concurrency Computat. Pract. Exper.*, page e5640, 2019.

[5] S. Asmussen and P. W. Glynn. *Stochastic simulation: algorithms and analysis*, volume 57. Springer Science & Business Media, 2007.

[6] D. Bachman. *A geometric approach to differential forms*. Springer, 2012.

[7] G. Bertin. *Dynamics of galaxies*. Cambridge University Press, 2014.

[8] C. K. Birdsall and A. B. Langdon. Plasma Physics via Computer Simulation, MacGraw-Hill. *New York*, 1985.

[9] A. Bossavit. Differential geometry for the student of numerical methods in electromagnetism, 1990. *Lecture notes, École Supérieure d'Electricité*, 1991.

[10] A. J. Brizard. *Introduction To Lagrangian Mechanics, An*. World Scientific Publishing Company, 2014.

[11] S. Brunner. Waves and instabilities in inhomogeneous plasmas. *3d circle course at Centre de Recherches en Physique des Plasmas, Association Euratom-Confédération Suisse, Ecole Polytechnique Feédérale de Lausanne, Switzerland, https://crppwww. epfl. ch/brunner/inhomoplasma. pdf (entered 01.06. 2018)*, 2014.

[12] A. Buffa, G. Sangalli, and R. Vazquez. Isogeometric analysis in electromagnetics: B-splines approximation. *Comput. Methods Appl. M.*, 199(17):1143 – 1152, 2010.

[13] M. Campos Pinto, J. Ameres, K. Kormann, and E. Sonnendrücker. On Geometric Fourier Particle In Cell Methods. *arXiv e-prints*, pages arXiv–2102, 2021.

[14] M. Campos Pinto, K. Kormann, and E. Sonnendrücker. Variational Framework for

Structure-Preserving Electromagnetic Particle-In-Cell Methods. *arXiv e-prints*, pages arXiv–2101, 2021.

[15] E. Celledoni, V. Grimm, R. I. McLachlan, D. I. McLaren, D. O'Neale, B. Owren, and G. R. W. Quispel. Preserving energy resp. dissipation in numerical PDEs using the "Average Vector Field" method. *J. Comput. Phys.*, 231(20):6770–6789, 2012.

[16] L. Chacón and G. Chen. A curvilinear, fully implicit, conservative electromagnetic PIC algorithm in multiple dimensions. *J. Comput. Phys.*, 316:578–597, 2016.

[17] L. Chacón and G. Chen. Energy-conserving perfect-conductor boundary conditions for an implicit, curvilinear Darwin particle-in-cell algorithm. *J. Comput. Phys.*, 391:216–225, 2019.

[18] Y. Cheng and I. M. Gamba. Numerical study of one-dimensional Vlasov–Poisson equations for infinite homogeneous stellar systems. *Commun. Nonlinear Sci.*, 17(5):2052–2061, 2012.

[19] P. Colella, M. R. Dorr, J. A. F. Hittinger, and D. F. Martin. High-order, finite-volume methods in mapped coordinates. *J. Comput. Phys.*, 230(8):2952–2976, 2011.

[20] D. Coulette and N. Besse. Numerical comparisons of gyrokinetic multi-water-bag models. *J. Comput. Phys.*, 248:1–32, 2013.

[21] N. Crouseilles, L. Einkemmer, and E. Faou. Hamiltonian splitting for the Vlasov–Maxwell equations. *J. Comput. Phys.*, 283:224–240, 2015.

[22] R. C. Davidson. *Kinetic waves and instabilities in a uniform plasma*. MIT Plasma Science and Fusion Center, 1981.

[23] J. M. Dawson. Particle simulation of plasmas. *Rev. Mod. Phys.*, 55(2):403, 1983.

[24] C. De Boor. On calculating with B-splines. *J. Approx. Theory*, 6(1):50–62, 1972.

[25] G. L. Delzanno, E. Camporeale, J. D. Moulton, J. E. Borovsky, E. A. MacDonald, and M. F. Thomsen. CPIC: a curvilinear particle-in-cell code for plasma–material interaction studies. *IEEE T. Plasma Sci.*, 41(12):3577–3587, 2013.

[26] M. Desbrun, A. N. Hirani, M. Leok, and J. E. Marsden. Discrete exterior calculus. *arXiv preprint math/0508341*, 2005.

[27] W. D. D'Haeseleer, W. N. G. Hitchon, J. D. Callen, and J. Shohet. *Flux coordinates*

and magnetic field structure: a guide to a fundamental tool of plasma theory. Springer, 2012.

[28] M. Donatelli, C. Garoni, C. Manni, S. Serra-Capizzano, and H. Speleers. Robust and optimal multi-iterative techniques for IgA collocation linear systems. *Comput. Methods Appl. Mech. Eng.*, 284:1120–1146, 2015.

[29] M. Donatelli, C. Garoni, C. Manni, S. Serra-Capizzano, and H. Speleers. Robust and optimal multi-iterative techniques for IgA Galerkin linear systems. *Comput. Methods Appl. Mech. Eng.*, 284:230–264, 2015.

[30] J. W. Eastwood, W. Arter, N. J. Brealey, and R. W. Hockney. Body-fitted electromagnetic PIC software for use on parallel computers. *Comput. Phys. Commun.*, 87(1-2):155–178, 1995.

[31] E. G. Evstatiev and B. A. Shadwick. Variational formulation of particle algorithms for kinetic plasma simulations. *J. Comput. Phys.*, 245:376–398, 2013.

[32] C. A. Fichtl, J. M. Finn, and K. L. Cartwright. An arbitrary curvilinear-coordinate method for particle-in-cell modeling. *Comput. Sci. Discov.*, 5(1):014011, 2012.

[33] H. Fischer and H. Kaul. *Mathematik für Physiker*. Springer, 1988.

[34] M. Fivaz, S. Brunner, G. De Ridder, O. Sauter, T. Tran, J. Vaclavik, L. Villard, and K. Appert. Finite element approach to global gyrokinetic particle-in-cell simulations using magnetic coordinates. *Comput. Phys. Commun.*, 111(1-3):27–47, 1998.

[35] T. Fujiwara. Vlasov simulations of stellar systems-infinite homogeneous case. *Publications of the Astronomical Society of Japan*, 33:531, 1981.

[36] O. Gonzalez. Time integration and discrete Hamiltonian systems. *J. Nonlinear Sci.*, 6(5):449, Sep 1996.

[37] D. Gonzalez-Herrero, A. Micera, E. Boella, J. Park, and G. Lapenta. ECsim-CYL: Energy Conserving Semi-Implicit particle in cell simulation in axially symmetric cylindrical coordinates. *Comput. Phys. Commun.s*, 236:153–163, 2019.

[38] I. S. Gradshteyn and I. M. Ryzhik. *Table of integrals, series, and products*. Academic press, 1994.

[39] V. Grandgirard, J. Abiteboul, J. Bigot, T. Cartier-Michaud, N. Crouseilles, G. Dif-Pradalier, C. Ehrlacher, D. Esteve, X. Garbet, P. Ghendrih, et al. A 5d gyrokinetic

full-f global semi-lagrangian code for flux-driven ion turbulence simulations. *Comput. Phys. Commun.s*, 207:35–68, 2016.

[40] Y. N. Grigoryev, V. A. Vshivkov, and M. P. Fedoruk. *Numerical "particle-in-cell" Methods: Theory and Applications*. Walter de Gruyter, 2002.

[41] Y. Guo. Global weak solutions of the Vlasov-Maxwell system with boundary conditions. *Commun. Math. Phys.*, 154(2):245–263, 1993.

[42] E. Hairer, C. Lubich, and G. Wanner. *Geometric numerical integration: structure-preserving algorithms for ordinary differential equations*, volume 31. Springer, 2006.

[43] A. Hamiaz, M. Mehrenberger, H. Sellama, and E. Sonnendrücker. The semi-Lagrangian method on curvilinear grids. *Commun. Appl. Ind. Math.*, 7(3):99–137, 2016.

[44] R. Hatzky, R. Kleiber, A. Könies, A. Mishchenko, M. Borchardt, A. Bottino, and E. Sonnendrücker. Reduction of the statistical error in electromagnetic gyrokinetic particle-in-cell simulations. *Journal of Plasma Physics*, 85(1), 2019.

[45] Y. He, H. Qin, Y. Sun, J. Xiao, R. Zhang, and J. Liu. Hamiltonian time integrators for Vlasov-Maxwell equations. *Phys. Plasmas*, 22(12):124503, 2015.

[46] Y. He, Y. Sun, H. Qin, and J. Liu. Hamiltonian particle-in-cell methods for Vlasov–Maxwell equations. *Phys. Plasmas*, 23(9):092108, 2016.

[47] R. Hiptmair. Finite elements in computational electromagnetism. *Acta Numer.*, 11:237–339, 2002.

[48] E. Hirvijoki. Charge-conserving, variational particle-in-cell method for the drift-kinetic Vlasov-Maxwell system. *arXiv preprint arXiv:1910.03441*, 2019.

[49] E. Hirvijoki. Structure-preserving marker-particle discretizations of Coulomb collisions for particle-in-cell codes. *Plasma Physics and Controlled Fusion*, 2021.

[50] E. Hirvijoki, M. Kraus, and J. W. Burby. Metriplectic particle-in-cell integrators for the Landau collision operator. *arXiv preprint arXiv:1802.05263*, 2018.

[51] R. W. Hockney and J. W. Eastwood. *Computer simulation using particles*. crc Press, 1988.

[52] F. Holderied, S. Possanner, and X. Wang. MHD-kinetic hybrid code based on structure-preserving finite elements with particles-in-cell. *J. Comput. Phys.*, 433:110143, 2021.

[53] T. Itoh and K. Abe. Hamiltonian-conserving discrete canonical equations based on variational difference quotients. *J. Comput. Phys.*, 76(1):85–102, 1988.

[54] X. Jianyuan and Q. Hong. Explicit structure-preserving geometric particle-in-cell algorithm in curvilinear orthogonal coordinate systems and its applications to whole-device 6d kinetic simulations of tokamak physics. *Plasma Sci. Technol.*, 23(5):055102, 2021.

[55] K. Kormann and E. Sonnendrücker. Energy-conserving time propagation for a structure-preserving particle-in-cell Vlasov–Maxwell solver. *J. Comput. Phys.*, 425:109890, 2021.

[56] M. Kraus, K. Kormann, P. J. Morrison, and E. Sonnendrücker. GEMPIC: Geometric electromagnetic particle-in-cell methods. *J. Plasma Phys.*, 83(4), 2017.

[57] M. Kraus and T. M. Tyranowski. Variational integrators for stochastic dissipative Hamiltonian systems. *IMA Journal of Numerical Analysis*, 2019.

[58] J. Kreeft, A. Palha, and M. Gerritsma. Mimetic framework on curvilinear quadrilaterals of arbitrary order. *arXiv preprint arXiv:1111.4304*, 2011.

[59] G. Lapenta. Exactly energy conserving semi-implicit particle in cell formulation. *J. Comput. Phys.*, 2017.

[60] G. Latu, M. Mehrenberger, Y. Güçlü, M. Ottaviani, and E. Sonnendrücker. Field-aligned interpolation for semi-Lagrangian gyrokinetic simulations. *Journal of Scientific Computing*, 74(3):1601–1650, 2018.

[61] H. R. Lewis. Energy-conserving numerical approximations for Vlasov plasmas. *J. Comput. Phys.*, 6(1):136–141, 1970.

[62] H. R. Lewis. Variational algorithms for numerical simulation of collisionless plasma with point particles including electromagnetic interactions. *J. Comput. Phys.*, 10(3):400–419, 1972.

[63] V. D. Liseikin. *Grid generation methods*, volume 1. Springer, 1999.

[64] F. E. Low. A Lagrangian Formulation of the Boltzmann-Vlasov Equation for Plasmas. In *Proc. R. Soc. A*, volume 248, pages 282–287, 1958.

[65] J. E. Marsden and A. Weinstein. The Hamiltonian structure of the Maxwell-Vlasov equations. *Physica D: Nonlinear Phenomena*, 4(3):394 – 406, 1982.

[66] P. McCorquodale, M. R. Dorr, J. A. F. Hittinger, and P. Colella. High-order finite-volume methods for hyperbolic conservation laws on mapped multiblock grids. *J. Comput. Phys.*, 288:181–195, 2015.

[67] R. I. McLachlan and G. R. W. Quispel. Discrete gradient methods have an energy conservation law. *Discrete Cont. Dyn.-A*, 34:1099, 2014.

[68] R. I. McLachlan, G. R. W. Quispel, and N. Robidoux. Geometric integration using discrete gradients. *Philosophical Transactions of the Royal Society of London. Series A: Mathematical, Physical and Engineering Sciences*, 357(1754):1021–1045, 1999.

[69] P. J. Morrison. The Maxwell–Vlasov equations as a continuous Hamiltonian system. *Phys. Lett. A*, 80(5–6):383–386, 1980.

[70] P. J. Morrison. Poisson brackets for fluids and plasmas. In *AIP Conference proceedings*, volume 88, pages 13–46. American Institute of Physics, 1982.

[71] P. J. Morrison. Structure and structure-preserving algorithms for plasma physics. *Phys. Plasmas*, 24(5):055502, 2017.

[72] B. Perse. Energy-conserving Implicit Time Discretisation for the GEMPIC Framework. Master's thesis, TU Munich, 2017.

[73] B. Perse, K. Kormann, and E. Sonnendrücker. Geometric Particle-in-Cell Simulations of the Vlasov–Maxwell System in Curvilinear Coordinates. *SIAM J. Sci. Comput.*, 43(1):B194–B218, 2021.

[74] J. H. Poynting. On the transfer of energy in the electromagnetic field. *Proc. R. Soc. Lond.*, 36(228-231):186–187, 1883.

[75] G. R. W. Quispel and G. S. Turner. Discrete gradient methods for solving ODEs numerically while preserving a first integral. *J. Phys. A-Math. Gen.*, 29(13):L341, 1996.

[76] D. Schnack, J. Cheng, D. Barnes, and S. Parker. Comparison of kinetic and extended magnetohydrodynamics computational models for the linear ion temperature gradient instability in slab geometry. *Phys. Plasmas*, 20(6):062106, 2013.

[77] B. A. Shadwick, A. B. Stamm, and E. G. Evstatiev. Variational formulation of macroparticle plasma simulation algorithms. *Phys. Plasmas*, 21(5):055708, 2014.

[78] E. Sonnendrücker. Numerical methods for the Vlasov–Maxwell equations. *Lecture notes WS2012/13*, 2012.

[79] E. Sonnendrücker and A. Ratnani. Advanced finite element methods. *Lecture notes WS2016/17*, 2016.

[80] E. Sonnendrücker, A. Wacher, R. Hatzky, and R. Kleiber. A split control variate scheme for pic simulations with collisions. *J. Comput. Phys.*, 295:402–419, 2015.

[81] J. Squire, H. Qin, and W. M. Tang. Geometric integration of the Vlasov–Maxwell system with a variational particle-in-cell scheme. *Phys. Plasmas*, 19:084501, 2012.

[82] A. B. Stamm, B. A. Shadwick, and E. G. Evstatiev. Variational formulation of macroparticle models for electromagnetic plasma simulations. *IEEE Transactions on Plasma Science*, 42(6):1747–1758, 2014.

[83] B. Sturdevant, Y. Chen, and S. Parker. Low frequency fully kinetic simulation of the toroidal ion temperature gradient instability. *Phys. Plasmas*, 24(8):081207, 2017.

[84] B. J. Sturdevant, S. E. Parker, Y. Chen, and B. B. Hause. An implicit δf particle-in-cell method with sub-cycling and orbit averaging for Lorentz ions. *J. Comput. Phys.*, 316:519–533, 2016.

[85] R. Tielen, M. Möller, and C. Vuik. Efficient p-multigrid based solvers for isogeometric analysis on multipatch geometries. In H. van Brummelen, C. Vuik, M. Möller, C. Verhoosel, B. Simeon, and B. Jüttler, editors, *Isogeometric Analysis and Applications 2018*, pages 209–225, Cham, 2021. Springer International Publishing.

[86] D. Toshniwal and T. J. Hughes. Isogeometric discrete differential forms: Non-uniform degrees, Bézier extraction, polar splines and flows on surfaces. *Comput. Methods Appl. Mech. Eng.*, 376, 2021.

[87] D. Toshniwal, H. Speleers, R. R. Hiemstra, and T. J. Hughes. Multi-degree smooth polar splines: A framework for geometric modeling and isogeometric analysis. *Comput. Methods Appl. Mech. Eng.*, 316:1005–1061, 2017.

[88] T. M. Tyranowski. Stochastic variational principles for the collisional Vlasov-Maxwell and Vlasov-Poisson equations. *arXiv preprint arXiv:2102.09611*, 2021.

[89] G. Vogman, U. Shumlak, and P. Colella. Conservative fourth-order finite-volume Vlasov–Poisson solver for axisymmetric plasmas in cylindrical (r, v_r, v_θ) phase space coordinates. *J. Comput. Phys.*, 373:877–899, 2018.

[90] J. Wang, D. Kondrashov, P. C. Liewer, and S. R. Karmesin. Three-dimensional

deformable-grid electromagnetic particle-in-cell for parallel computers. *J. Plasma Phys.*, 61(3):367–389, 1999.

[91] Z. Wang, H. Qin, B. Sturdevant, and C.-S. Chang. Geometric electrostatic particle-in-cell algorithm on unstructured meshes. *J. Plasma Phys.*, 87(4), 2021.

[92] K. F. Warnick, R. H. Selfridge, and D. V. Arnold. Teaching electromagnetic field theory using differential forms. *IEEE Transactions on education*, 40(1):53–68, 1997.

[93] E. S. Weibel. Spontaneously growing transverse waves in a plasma due to an anisotropic velocity distribution. *Phys. Rev. Lett.*, 2(3):83, 1959.

[94] A. Weinstein and P. J. Morrison. Comments on: The Maxwell-Vlasov equations as a continuous Hamiltonian system. *Phys. Lett. A*, 86(4):235–236, 1981.

[95] H. Whitney. Geometric Integration Theory Princeton Univ. *Press, Princeton, NJ*, 1957.

[96] J. Xiao, H. Qin, and J. Liu. Structure-preserving geometric particle-in-cell methods for Vlasov-Maxwell systems. *Plasma Sci. Technol.*, 20(11):110501, 2018.

[97] J. Xiao, H. Qin, J. Liu, Y. He, R. Zhang, and Y. Sun. Explicit high-order non-canonical symplectic particle-in-cell algorithms for Vlasov–Maxwell systems. *Phys. Plasmas*, 22:112504, 2015.

[98] J. Xiao, H. Qin, J. Liu, and R. Zhang. Local energy conservation law for a spatially-discretized Hamiltonian Vlasov-Maxwell system. *Phys. Plasmas*, 24(6):062112, 2017.

[99] E. Zoni. *Theoretical and numerical studies of gyrokinetic models for shaped Tokamak plasmas*. PhD thesis, TU Munich, 2019.

[100] E. Zoni and Y. Güçlü. Solving hyperbolic-elliptic problems on singular mapped disk-like domains with the method of characteristics and spline finite elements. *J. Comput. Phys.*, 398:108889, 2019.